ELECTROSPINNING OF POLYACRYLONITRILE NANOFIBRES WITH ADDITIVES:

STUDY OF ORIENTATION AND CRYSTALLINITY

Thesis presented in partial fulfillment of the requirements for a Doctorate of Science (PhD) Degree

University of Stellenbosch

Department of Chemistry and Polymer Science

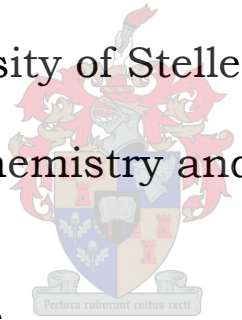

Submitted by PhD Candidate

Corinne Jean Greyling **March 2010**

Accepted by Promoter

Prof. Ronald D Sanderson **March 2010**

DECLARATION

By submitting this dissertation electronically, I declare that the entirety of the work contained therein is my own, original work, that I am the owner of the copyright thereof (unless to the extent explicitly otherwise stated) and that I have not previously in its entirety or in part submitted it for obtaining any qualification.

March 2010

Dedicated to:

The most influential people in my life

My Hero and Loving Father,
Johannes Frederikus Wilhelmus Greyling

My Angel Mother,
Sheila Olive Greyling (Neé Strauch)

My Cousin, The Boytjie from Benoni,
Prof Glen Elder, Dean at UVM, USA

And my friends,
Dearest George Aspeling

Johan Bonthuys and Dr Frank Reinecke

And my Rotweiler Mutt – too many missed walkies
"Rocky Boy"

Who all passed on during the compilation of this thesis

ABSTRACT

Polyacrylonitrile, (PAN), polymers are of interest due to their many unique characteristics in comparison to most other fibre forming polymers. The focus of this study was the effect of electrospinning variables and additives on their unusual thermal properties and internal molecular morphology with the objective of improving the performance of this fibre in industrial application, or at least contributing to the understanding of how the fibre processing variables affect the thermal performance.

The process of electrospinning was used to process samples of PAN fibres with additives in order to determine their effect on the molecular orientation and crystallinity of the resultant nano- and micron-sized fibres. The effect of additives in the forms of low molecular weight oligomers, blends of conductive polymers and nanoparticles and conductive salts (mainly copper and lithium based) on the molecular structure and thermal properties is reported. In addition the effect of certain electrospinning processing variables such as the PAN polymer grade, the type of solvent, the temperature, the spinning voltage and the spinning distance were evaluated in terms of their effect on the resultant fibre molecular structure.

The crystallinity and molecular orientation are quantified using various analytical techniques including: Fourier-Transform Infra-Red Spectroscopy (FTIR); Differential Scanning Colorimetry; (DSC) Thermal Gravimetric Analysis, TGA, Scanning and Transmission Electron Microscopy; Wide-Angle X-ray Diffractometry, XRD, Small-angle Neutron Scattering; SANS, Solid-state ^{13}C Nuclear Magnetic Resonance Spectroscopy; NMR, and Electron-spin Resonance Spectroscopy, ESR.

The researcher has ascertained in this study that the orientation of electrospun PAN is comparable to that in commercial wet-spun fibres when the electrospinning field strength is greater than 0,75 kV per cm. The process of electrospinning leads to chemical degradation of the PAN polymer only previously noted by other fibre scientists after heating PAN fibres to more than 280 °C. This is due to the high mechanical stress on the high surface area electospun fibres spun into an oxygen rich air atmosphere.

The addition of certain salts, particularly lithium chloride and copper nitrate, to the PAN electrospinning dope by the researchers produced fibres with improved thermal stability in comparison to the control PAN samples with no additives. In addition these salts lower the endotherm for the production of carbonized fibres from PAN fibres and will therefore make more structured, stronger, high tenacity carbon fibres. The XRD revealed that through the addition of certain salts to disrupt the dipole interations in PAN, that fibres with a 2D hexagonal crystal structure can be electrospun and have a structure similar to wet spun PAN. It is shown that fibres in a non-aligned electrospun mat have a 3D crystal structure and lower molecular orientation that wet spun fibres. Some industrial applications of electrospinning using PAN fibres are developed and reported.

OPSOMMING

Polyakrilonitrielpolimere (PAN) is van belang weens die baie unieke eienskappe wat hulle het in vergelyking met die meeste ander vesel-vormende polimere. Die fokus van hierdie studie op die effek van verskeie veranderlikes en byvoegmiddels op hul buitengewone termiese eienskappe en interne molekulêre morfologie, met die doel om die werksverrigting van hierdie vesel in industriële toepassings te verbeter, of ten minste by te dra tot die begrip van hoe die vesel-prosesveranderlikes die termiese werksverrigting beïnvloed.

Die elektrospinproses is gebruik om monsters van PAN met bymiddels te prosesseer om vas te stel wat die effek sou wees op die molekulêre oriëntering en kristalliniteit van die gelewerde nano- en mikron-grootte vesels. Verslag word gelewer oor die effek van bymiddels in die vorm van oligomere met ‘n lae molekulêre gewig, mengsels van geleidende polimere en verskillende nano-partikels en geleidende soute (meestal koper- en litium-gebaseerd). Die effek van sekere veranderlikes in die elektro-spinproses, soos die PAN polimeer-graad, die temperatuur, die tipe oplosmiddel, die spin-spanning en spin-afstand, is geëvalueer in terme van hulle effek op die vesels wat gelewer word.

Die kristalliniteit en molekulêre oriëntering word gekwantifiseer deur verskeie analitiese tegnieke te gebruik, onder meer: Fourier-Transform Infrarooispektroskopie; Differensiële Skandeerkolorimetrie; Termiese Gravimetriese Ontleding; Skandeeringelektronmikroskopie; Transmissie Elektron Mikroskopie; Wye-hoek X-straal Diffraktometrie; Klein-hoek Neutronstrooiing; Vaste-toestand ^{13}C Kern Magnetiese Resonansiespektroskopie; en Elektronspin Resonansiespektroskopie.

Dit is in hierdie studie vasgestel dat die oriëntering van elektro-gespinde PAN vergelykbaar is met kommersiële nat-gespinde vesels as die elektro-spin veldsterkte groter is as 0,75 kV per cm. Die elektro-spin proses lei tot chemiese degradasie van die PAN polimeer, wat voorheen slegs deur ander vesel-wetenskaplikes waargeneem is nadat PAN tot meer as 280°C verhit is. Dit word veroorsaak deur die hoë meganiese spanning op die hoë-oppervlakarea vesels wat in ‘n suurstofryke lug-atmosfeer gespin word.

Die byvoeging van sekere soute, veral litiumchloried en kopernitraat, by die PAN elektro-spin spinlak (dope) deur die navorser het vesels gelewer met verbeterde termiese stabiliteit in vergelyking met die kontrole PAN-monsters sonder bymiddels. Verder verlaag hierdie soute die endoterm vir die produksie van gekarboniseerde vesels uit PAN-vesels, en dit sal daarom meer gestruktureerde, sterker koolstofvesels met hoë taaiheid lewer. X-straaldiffraksieanalise het gewys dat gewone elekrospin vesels ’n driedimensionele struktuur het maar as gevolg van die byvoeging van sekere soute, wat die dipoolinteraksies in PAN opbreek, dat vesels wat 'n soortgelyke tweedimensionele struktuur het as dié van groot skaalse kommersiële nat-spin vesels, maklik d.m.v. die elektrospinproses berei kan word. Enkele nywerheidstoepassings van elektrospin is ontwikkel, en beskryf.

ACKNOWLEDGEMENTS

Dr Bernd Huber, and **Jon Shifferdecker** of Kelheim Faserwerk, Germany, for the supply of the polyacrylonitrile Dolanit® chemicals and information.

David Service and Steve Amos, of Acordis Fibres, Grimsby, UK for supply of the 120k PAN.

Otto Stökl of Beier Industries, Pinetown, RSA, for textile testing and for being a friend.

Jason Hawke and "Sir" **Clifford Andrews** of Andrew Textile Industries, Bury, UK for the supply of non-woven PAN needlefelt and information and discussions of biomedical applications of ES and friendship.

Peter Shultz and **Bernd Ebener** of Tomas Josef Heimbach GmbH, Filtration Division, Duren, Germany for the filtration efficiency testing.

Dr Herbert Griesser and **Rudolf Hemelmayr**, Lenzing Plastics, Austria for the supply of raw materials and information.

Dr Wim van der Goes of Montefibre, Milan, Italy for the supply of Ricem® PAN powder and fibres.

Miranda Waldron and Mohammed Jaffer, UCT Microscopy Unit for excellent service in microscopy.

Ullrich Buttner, University of Stellenbosch, Electronic Engineering Department for electrical engineering advice and modifications, design of the experimental electrospinning set-up, design and manufacture of the rotating grounded electrode, carbonization facilities, CuO laser vapour deposition and brilliant advice and motivation.

Leon Baidjurak and **Andrew Twyford**, Howden Africa, Gauteng, RSA for information of electrospun industrial filtration and flue gas catalysis applications.

Eskom for funding the industrial electrospinning research and many discussions; Uncle Rod Hansen, the hero Joe Strydom, Irish Phiri, Gerhard Gericke and Kammy Dhaver.

Prof Klaus Koch, University of Stellenbosch, Analytical Chemistry for the supply of the Chemisorb® Oligomer and information. **Prof Andrew Crouch,** (now WITS) and **Dr Mosidi Makgae**, (now PBMR), ex Univ. of Stellenbosch, Analytical Chemistry, for Cyclic Voltammetry measurements.

Prof Frank Ko, Drexel University, Philadelphia, PA, USA for an informative working visit and his students; Hoa Lam, Ashraf Ali and Jason Lyons for assistance with laboratory electrospinning.

Prof Yuris Dzenis, University of Lincoln Nebraska, Nebraska, USA for an introduction to Electrospinning, an informative visit and also to his student, Jingxin Wei.

Prof Joachim Wendorff and **Prof. Andreas Greiner**; Fabreich Chemie, University of Marburg for a valuable working visit; and all their wonderful students especially Roland Dersch, Martin Graesser,

Martin Steinhart, Markus Rudisile and Michael Bognitski for assistance with spinning in Marburg. A special appreciation to Dr Bernd Brandl for XRD assistance and translation skills.

Dr Gunnar Jeschke, **Dr Ingo Schnell**, **Dr Anke Hoffmann**, Max Plank Institute for Polymers, Mainz, Germany for a great visit and expertise in solid state NMR and ESR measurements.

Dr Deon Bezuidenhout., Cape Heart Academy, UCT Medical School for funding and discussions on electrospun tissue scaffolds and collagen chemistry and friendship.

Derek McAuley, **Yolande Koen**, **Yaseen Hoosain** and **Valeska Cloete** whilst based at the Polymer Science Facilities in Stellenbosch for expert assistance with thermal analysis, rheology, FTIR and sonication respectively.

Johan Bonthuys (expert without "portfolio") now departed, **Calvin Maart, Erinda Cooper** and **Oom Hennie**, the technical service backbone of the Polymer facilities, University of Stellenbosch. **Dr Frank Reinecke**, now departed, University of Stellenbosch, Polymer Science, for advice and many teas.

Dr Robbie Luckay for his excellent Chauffer Services and constant chemical consultation.

Tannie Truida Prekel, my other Mum, **Prof Heinz Prekel**, wise advisors and for personal support.

WAC, for the "never-a dull-moment', friendship and for introducing me to a new thought paradigm.

The Funders: NRF, Eskom, US International Office, Harry Crosseley Bursary, Department of Chemistry & Polymer Science, US Analytical Chemistry, UCT Cape Heart Academy.

My brilliant assistant for 2 years **Ebrahim "Einstein" Vesamian,** The bald Irishman, **Chris Laffin,** for assistance with aligned electrospinning and constant bad Irish jokes.

Prof HG Raubenheimer for wise advice and unending support in my darkest days.

Prof Vincent Mathot (Belgium), Dr Matthew Tonge (Australia).

Aymeric Sallin, the Master Jedi**,** for mentoring.

Rallston Richards, for assistance with the development of the high voltage insulator, editing the thesis and assistance with all – the very best assistant in the world.

Thanks to my sister, **Adv. DA Greyling** for helping keep a roof over my head.

Dr Remy Bucher for excellent XRD service at iThemba Labs.

TABLE OF CONTENTS

LIST OF FIGURES

LIST OF TABLES

LIST OF ABBREVIATIONS

AA	**Acrylic acid**
AES-ICP	**Atomic emission spectroscopy**
AFM	**Atomic force microscopy**
BET	**Emmett Teller**
CN	**Nitrile group**
CV	**Cyclic voltametry**
DMAc	**Di-methyl acetamide**
DMF	**Di-methyl formamide**
DMSO	**Di-methyl sulphoxide**
DSC	**Differential scanning colorimetry**
EDAX	**Energy dispersive X-ray analysis**
ES	**Electrospinning / electrospun**
ESR	**Electron spin resonance spectroscopy**
FESEM	**Environmental scanning electron microscope**
FFESS	**Flow- limited field-injection electrostatic spraying**
FTIR	**Fourier transform infra-red spectroscopy**
HFIP	**Hexafluoro isopropanol**
HRTEM	**High resolution transmission electron microscope**
IA	**Itaconic acid**
IR	**Infra-red**
k	**Thousands**
LVD	**Laser vapor deposition**
MA	**Methyl acrylate**
MW	**Molecular weight**
MWNT, SWNT	**Multi-walled and single-walled carbon nanotubes**

NMR	**Nuclear magnetic resonance spectroscopy**
OEM	**Original equipment manufacturer**
OF	**Orientation factor**
PAN	**Polyacrylonitrile**
PANi	**Polyaniline**
PBI	**Polybenzimidasole**
PLA	**Polylactic acid**
PVP	**Polyvinyl pyrollidone**
SAF	**Activated carbon fabric**
SEM	**Scanning electron microscopy**
SERS	**Surface enhanced Raman scattering**
TEM	**Transmission electron microscopy**
TEOS	**Tetra-ethyl-ortho-silicate**
TGA	**Thermal gravimetric analysis**
TMA	**Thermal mechanical analysis**
UMASS	**University of Massachusetts**
Uni	**University**
UV	**Ultraviolet**
UHMW	**Ultra high molecular weight**
VA	**Vinyl acetate**
Xc . Xa	**Weight fraction of crystalline or amourphous regions**
XRD	**X-ray diffraction spectroscopy**

CHAPTER 1

INTRODUCTION AND OBJECTIVES

1.1 INTRODUCTION

Electrospinning is used in this study to make polyacrylonitrile, (PAN), fibers with various copper additives and systematically change and study some variables which affect fibre crystallinity and molecular orientation in PAN fibres. The electrospun PAN fibres are in the nanometer diameter range. The resultant fibres / fabrics could be used, in numerous applications, including the filtration of nanoparticles, catalyst immobilization, as electrodes, in biomedical applications and in composites to improve crack resistance *etc.*. A distinct disadvantage of electrospun fibres, however, is the poor mechanical properties, assumed due to the low diameter and maybe also the different internal molecular orientation - as opposed to high tenacity conventional wet-spun PAN fibres. The structure of electrospun fibres has been found to be similar to melt spun fibres only for Nylon (Dersch et al. 2002) but the crystallinity and molecular orientation of PAN electrospun fibres, with additives, are investigated further in this study, and compared to commercial wet-spun technical grade PAN fibres.

PAN is used commercially as a fibre-forming polymer and as the pre-cursor for carbon fibres. It is an interesting polymer to study since the typical crystallinity models proposed for most commercial polymeric fibres cannot define the PAN fibre crystal structure. Polypropylene, polyester or polyamide fibres are defined as semi-crystalline containing distinctive crystalline and amorphous domains ordered along the fibre length. PAN fibre has been described as “quasi-crystalline”, containing regions of “more ordered” and “less ordered” molecular orientation and, thus is claimed as the only polymer with two distinct glass transition temperatures (Masson 1995).

The primary polymer structure of PAN is the reason for the different polymorphic structures in PAN fibres (hexagonal and orthorhombic packing and planar and zig-zag conformations). The highly polar pendant nitrile groups undergo anti-parallel bonding between adjacent polymer molecular chains. This interaction prevents an “extended chain conformation” in the spinning dope solution and high crystallinity in the resultant fibre, yet affords an ultimate high tenacity fibre due to the secondary Van Der Waal’s bonding forces.

PAN polymers are of interest due to their many unique characteristics in comparison to most other fibre forming polymers. In this study, the unusual thermal properties and internal molecular morphology of PAN are discussed in detail. The effect of additives on the molecular packing in the form of low molecular weight oligomers, blends of conductive polymers and different PAN grades, nanoparticles and conductive salts are reported.

Some investigations (Masson 1995; Qin 2004) have shown that iron and lithium salts are able to disrupt the anti-parallel nitrile bonding sufficiently to allow the extended chain conformation of

PAN in solution, and thus increase the molecular orientation and crystallinity in the resultant wet spun fibres and thereby increase the thermal and chemical resistance of the PAN fibres. Only a few researchers have recently included additives in electrospun PAN fibres. Most of the numerous articles on electrospinning do not report on the crystallinity and / or molecular orientation of the polymer chain packing in the resultant fibres in relation to changes in either the electrospinning processing variables or due to additives.

1.2 ELECTROSPINNING OF POLYACRYLONITRILE

This research project focuses on the electrospinning of PAN. There are numerous potential applications of PAN spun fibres and the carbonized and activated carbon fibre derivatives within industry. Polyacrylonitrile fibres in the micrometer diameter range (0,9 to 8,0 dtex) are used commercially for hot gas filtration, as outdoor awning material, for yacht sails and as concrete reinforcement. In the carbonized form they are used as reinforcement in lightweight composites and in the activated form as absorbents.

In 1934, Anton Formhals (US Patent, 1,975,504) patented the electrospinning process. An experimental set-up was described for the production of micron diameter polymer filaments using an electrostatic force. A high voltage is used to create an electrically charged jet of polymer solution or melt, which dries or solidifies to yield a polymer fibre. The process allows for control of the fibre diameter and structure as well as the mat morphology by altering the nature of the polymer and the processing variables. Early research was from a single spinneret (pipette) onto a static grounded electrode. The process has been modified by many researchers to include spinning from multiple spinnerets to increase the productivity and the use of various types of take-up devices to form aligned fibres with improved mechanical properties. Electrospinning research is thus now a multidisciplinary field requiring expertise from scientists and engineers. Electrospinning can with ease produce smaller diameter fibres than conventional wet spinning methods. Electrospinning is a non-mechanical and inexpensive process relative to conventional wet spinning but the molecular orientation has not been studied in depth.

1.3 MOTIVATION (Improving the properties of PAN fibres)

The main aim of this Ph.D research is; “to investigate ways to increase the crystallinity and orientation and thereby the thermal and chemical resistance of polyacrylonitrile fibres” or at least, to contribute to the understanding of the effect of various spinning processing variables and additives using the facile electrospinning technique. The results can be potentially applied to improve the chemical and thermal resistance of commercial wet spun PAN fibres, for example, for application in hot gas filtration. Various avenues are pursued in efforts to achieve this as discussed briefly below.

The author's M.Sc thesis (Greyling 2000) outlines the problems with polyacrylonitrile homopolymer in certain hot gas filtration applications. Degradation is initiated in the less ordered "amorphous" regions of the commercial free radical polymerized (Fe^{2+}/ Fe^{3+}/ AIBN) PAN fibres that have a polydispersity of greater than 2,5.

Controlled "living radical polymerization" of acrylonitrile could be one possible route to improving the thermal and chemical degradation; by decreasing the size of the "amorphous" domains and increasing the packing density, crystallinity, in the more ordered domains of the PAN fibre. Atom transfer radical polymerization, ATRP, using a bipyridine / Cu based initiator and redox system was attempted as a way to reduce the number of very short and very long chains and thereby reduce the polydispersity and size / proportion of the amorphous domains (Matyjaszewski 1997). The maximum, M_w, achieved before catalyst inactivation was 28 000 Daltons, polydispersity of 1,03. This M_W is not high enough for sufficient entanglements for fibre formation. The results are not presented or discussed further in this document. Subsequently electrospinning, using commercial PAN grades, was considered as a method by which one could rapidly produce fibres from small quantities of the PAN.

The possibility of changing the tacticity of the PAN to create increased crystallinity and chemical and thermal resistance has been investigated. Work in Japan using the urea-clathrate canal polymerization technique has produced a PAN with an 82% degree of crystallinity. This small-scale production method using gamma radiation is not viable for up scaling but studies of the crystalline homopolymer PAN structures are of academic interest (Minagawa et al. 2001). Normally free radical polymerization yields a totally atactic polymer. In Japan, researchers have also obtained highly syndiotactic polyacrylate polymers, produced via a free radical mechanism, in highly fluorinated solvents, such as toxic hexafluoro-isopropanol (Isobe et al. 1999). In addition, researchers have used the effect of a high molecular weight and a two-stage draw ratio as a means to increase the molecular orientation and crystallinity of PAN fibres (Yamane 1997).

An interest in the effect of copper salts on the spinning of PAN fibres was inspired by three factors:

- Firstly it is known that in order to conduct useful GPC analysis of PAN one must add a small quantity of LiCl to the solution to ensure an extended chain conformation by disrupting the inter and intramolecular nitrile dipole interactions. (Masson 1995) Thus, , fibres spun from such a solution could have a higher degree of molecular orientation.
- The incorporation of AgCl in PAN fibres was shown to induce an ordered graphitic structure even at room temperature (Wang et al. 2005; Qin 2004).
- Thirdly, the effect of the remnant Cu^{2+}/Cu^{+} catalyst residues from the ATRP process, on the structure of PAN fibres was of interest and concern. It has been shown previously that the addition of metal ions to the PAN spinning dope yielded fibres with increased tenacity (Bajaj et al. 1998).

The author's interest in the relationship between copper salts and PAN fibres was further encouraged by the possibility of converting the copper salts to either nano-sized copper oxide particles, a potential commercial nanocatalyst for various industrial processes.

The mechanical properties are of importance in industrial applications of fibres but are not addressed directly here. The strength and toughness of aligned electrospun PAN has been studied intensely by other research groups using the AFM. The degree of molecular orientation is directly proportional to the strength but difficult to measure on a single nanofibre in a random mat and is thus motivation for the assessment of molecular orientation and crystallinity. Measurement of the strength of nanofibres and modified electrospun and wet-spun PAN fibres is recommended as future research.

1.4 OBJECTIVES

1.4.1 To study the effect of the electrospinning process such that the process of electrospinning produces fibres with repeatable mat geometry and properties and define the operating parameters for reproducible electrospinning of uniform PAN fibres.

1.4.2 To contribute to understanding the effect of various electrospinning variables on the degree of crystallinity and molecular orientation and resultant thermal properties of PAN and use the advantage of being able to electrospin small quantities of polymer into fibre form to assess the effect of additives in the form of nanoparticles, polymer blends, different grades of PAN, short chain oligomers and conductive copper salts on the crystallinity, molecular orientation and thermal properties of the electrospun fibres.

1.4.3 To compare the internal morphology, crystallinity and orientation of solution electrospun PAN with other commercial wet spun PAN fibres of the exact same polymer grades.

1.4.4 To assess the potential use of electrospun mats in certain industrial applications

1.5 METHODOLOGY AND LAYOUT OF THE THESIS

The process of electrospinning is used to study the effect of changes in certain variables on the resultant crystallinity and molecular orientation of the electrospun PAN fibres. These are compared with the structure and orientation of wet spun PAN fibres from exactly the same starting materials as wet spun PAN fibres. The polymer variables include different grades of PAN with small amounts of comonomers, the molecular weight of the PAN, the concentration (viscosity) and the solvent type. The processing variables studied include the spinning voltage, the spinning temperature and the spinning distance.

The crystallinity is studied by Differential Scanning Colorimetry, (DSC) and X-ray Diffractometry, (XRD). The orientation is assessed by an FTIR technique specific to PAN fibres and also by

Nuclear Magnetic Resonance Spectroscopy (NMR), Electron Spin Resonance Spectroscopy, (ESR) and XRD. In addition Microscopy, (SEM and TEM) and Thermal Analyses (TGA) are utilised.

Much research on electrospun PAN has been reported in recent years, so in Chapter 3 only a few unique findings on changes in the electrospinning variables are reported. New techniques to describe the mat uniformity are presented. In Chapter 4 the effect of the systematic addition of various additives on the PAN is studied in-depth using a range of solid-state, analytical techniques and data is presented at far higher resolution than normally used. In Chapter 5, certain potential applications of electrospun nanofibres are reported. Chapter 6 presents the overall conclusions, drawn from the range of analyses and a new theory for an additional crystalline phase is proposed to explain the small, yet, persistent peaks in the expanded solid-state FTIR, DSC and XRD results. Recommended future related research is discussed in Chapter 7.

1.6 **REFERENCES**

Bajaj, D. K., Paliwal, A. K. & Gupta, 1998. Influence of Metal Ions on Structure and Properties of Acrylic Fibers. *Journal of Applied Polymer Science***,** 67, p.1647-59.

Dersch, R., Liu, T., Schaper, A.K., Greiner, A & J. H. Wendorff. J.H., 2003. Electrospun Nanofibers: Internal Structure and Intrinsic Orientation. *Journal of Polymer Science: Part A: Polymer Chemistry,* 41, p.545–553.

Greyling, C.J., 2000, Optimisation of Methods to Evaluate Pulse-jet Fabric Filters, University of Stellenbosch, M.Sc Thesis.

Isobe, Y., Yamada, K., & Okamoto, Y., 1999. Stereospecific free-radical polymerization of methacrylates using fluoroalcohols as solvents. *Macromolecules,* 32, p.5979-981.

Masson, J., 1995. *Acrylic Fibre Technology and Applications*. NY, Marcel Dekker.

Matyjaszewski, K., 1997. Synthesis of well-defined polyacrylonitrile by atom transfer radical polymerization. *Macromolecules*, 30, p.6398-400.

Minagawa, M., Taira, T., Yabuta, Y., Nozaki, K. & Yoshii, F., 2001. An anomalous tacticity-crystallinity relationship: a WAXD study of stereoregular isotactic (83-25%) poly(acrylonitrile) powder prepared by urea clathrate polymerization. *Macromolecules*, 34, p.3679-683.

Qin, X., 2004. The effect of LiCl on electrospinning of PAN polymer solution: theoretical analysis and experimental verification. *Polymer*, 45, p.6409-413.

Yamane, A. & Sawai, D., 1997. Development of ductility and tensile properties upon two-stage draw of ultrahigh molecular weight poly(acrylonitrile), *Macromolecules*, 30, p.4170-178.

Wang, Y., Aponte, M., Leon, N., Ramos, I., Furlan, R., Evoy, S. & Santiago-Avilė, J., 2005. Preparation of silver nanoparticles dispersed in polyacrylonitrile nanofiber film spun by electrospinning. *Materials Letters*, 59, p.3046-049.

CHAPTER 2

LITERATURE SURVEY

2.1 ELECTROSPINNING

2.1.1. Introduction to the literature review

This literature review is expansive to include critical analysis on proposed fibre molecular structure models and spinning processes, various grades of uniquely performing polyacrylonitrile polymers and polymer salt complexes, as well as, the use of solid state analytical techniques to measure molecular orientation and fibre crystallinity, using less conventional experimental methodology and data handling.

A critical summary of the literature review is given in Section 2.4. The gaps in related similar studies and the new contributions to filling these gaps are presented in Section 6.3.

The process of electrospinning was first published in 1934. The early patents include: Formhals, A., US Patent, 1,975,504 (1934), Formhals, A., US Patent, 2,160,962 (1939) and Formhals, A., US Patent, 2,187, 306 (1940). In the electrospinning process a high voltage is used to create an electrically charged jet of polymer solution or melt, which dries or solidifies to leave a polymer fibre. One electrode is placed into the spinning solution / melt and the other attached to a collector. An electric field is subjected to the end of the capillary tube that contains the polymer fluid held by its surface tension. This induces a charge on the surface of the liquid. Mutual charge repulsion causes a force directly opposite to the surface tension. As the intensity of the electric field is increased, the hemispherical surface of the fluid at the tip of the capillary tube elongates to form a conical shape known as the Taylor cone. With increasing field strength, a critical value is attained when the repulsive electrostatic force overcomes the surface tension and a charged jet of fluid is ejected from the tip of the Taylor cone.

The discharged polymer solution jet undergoes a series of whipping instability processes wherein the solvent evaporates, leaving behind a charged polymer fibre, which is laid on a grounded collecting electrode. In the case of the melt spinning the discharged jet solidifies when it travels in the air and is collected on the grounded metal screen. The instabilities result in small diameter fibres being produced. An example of a experimental set up used for electrospinning is shown in Figure 2.1. he polymer solution or melt is contained in a glass tube, usually a pipette or a syringe. A metering pump or gravity is used as the feed. A high voltage generator through a metal wire immersed in the polymer solution provides the driving force. The high voltage source can typically generate up to 30 kV, and the set-up can be AC or DC, run on either positive or negative polarity.

The above description of the process allows for control of the fibre diameter and structure as well as the mat morphology. Both the nature of the polymer and the processing variables can be readily altered.

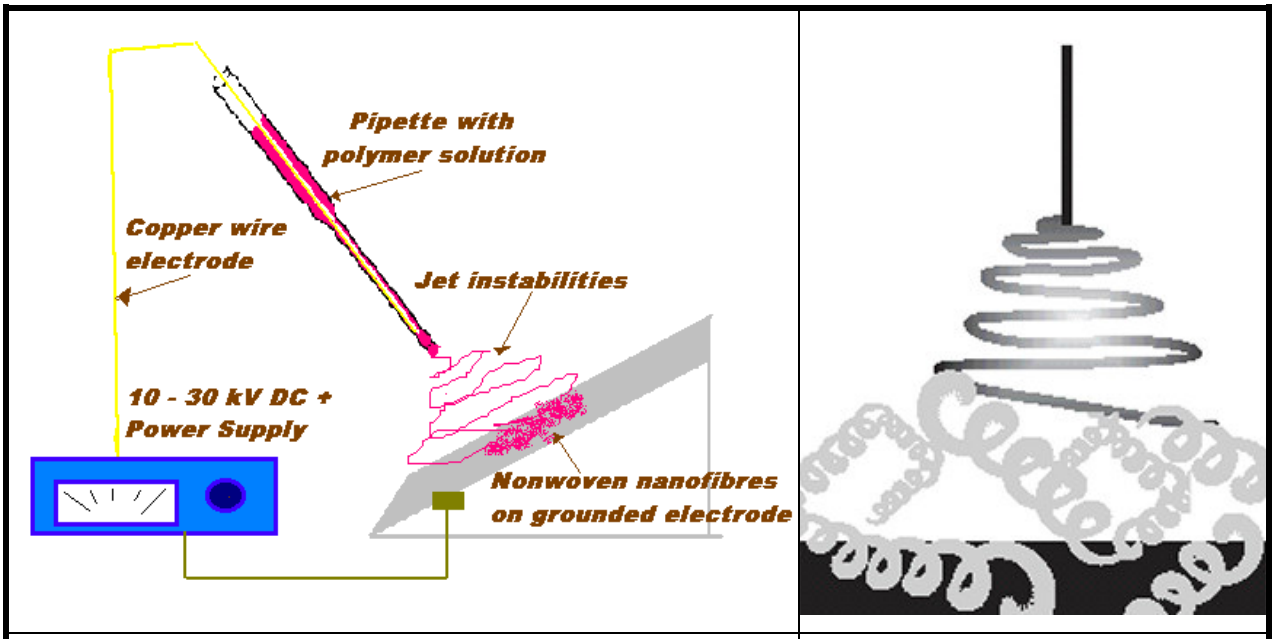

a) Cartoon of the full setup | b) Jet stages I, II and III

Figure 2.1 Schematic of the basic electrospinning set-up used in this research.

The advantages of electrospinning include:

- The production of nano-meter diameter fibres.
- The production of lightweight, easily processable, conducting polymeric fibres. Fibre spinning variables can be changed and the effects thereof characterised rapidly.
- The fibres can be spun directly into a non-woven mat, as is the case in the production of geotextile materials, using micrometer diameter size fibres. The fibres are charged and repel each other at the grounded electrode to form a random mat.
- Fibres can be spun from a few milligrams of polymer. About 5 kg polymer is needed to spin a fibre using commercial wet-spinning fibre processing equipment. There is little waste material and specialty fibres for trial purposes are spun quickly and easily.
- The resultant fibres have a narrow diameter size distribution and as a result the porosity of the formed non-woven is even and can be controlled. Electrospinning is a non-mechanical process, yet, despite the cost of electricity consumption, it still has a lower cost than the costs of conventional wet and dry spinning fibre production techniques.

- Nanometer diameter fibres, stretched up to a draw ratio of 300 000 can be produced within a distance of about 20 cm in less than a second whilst, for example, small decitex commercial PAN fibres require spinning and drawing production lines of about 100 m.
- A suitable, stable 30 kV DC generator costs about ZAR 10 000,00, which is significantly less than a lab-scale wet spinning rig. After the capital, the cost of operation is minimal.
- The formation of polymeric fibres, which cannot form fibres by other spinning techniques i.e. atactic polystyrene and butadiene.

Since the late 1990's the number of publications and spending on related research is growing exponentially each year as depicted in the graphic Figure 2.2 below extracted from http//www.sciencedirect.com in October 2009 using keywords; electrospinning and / or PAN and / or electrospinning and PAN and orientation.

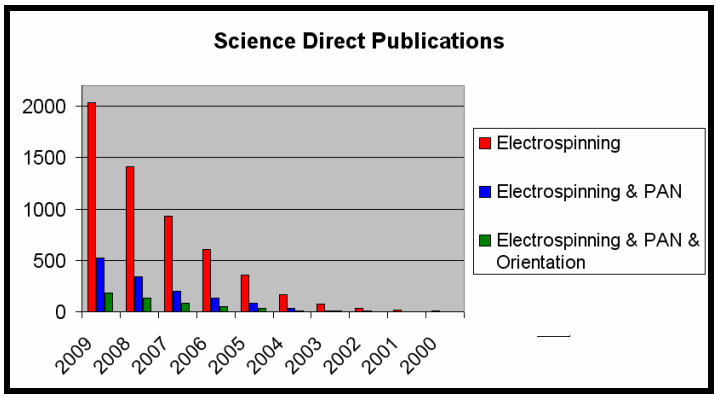

Figure 2.2 Growth in electrospinning related publications.

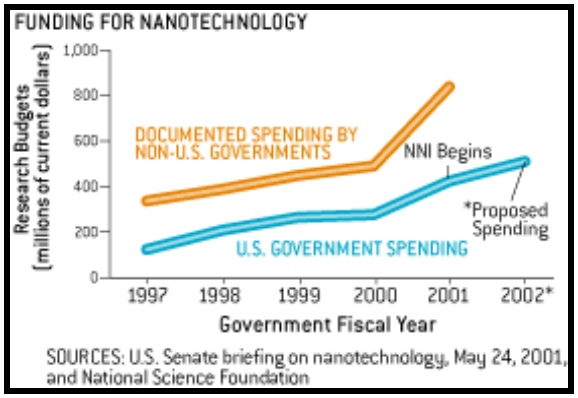

Figure 2.3 Growth in nanotechnology spending in the USA.

Some of the more recent electrospinning related patents include:

USP 2004012357 Polymer, polymer microfiber, polymer nanofiber and applications including filter structures; Chung, Hoo Y. (US), Hall, John R. B. (US), Gogins, Mark A. (US), Crofoot, Douglas G. (US), Weik, Thomas M. (US)*;* 2004; Donaldson Company, Incorporated, USA.

WO0151690; Electrospinning ultrafine conductive polymeric fibers; MacDiarmid AG, Ko FK, Lec RM, Noris ID, Shaker M; 2001; Uni. of Pennsylvania and Drexel University, USA.

US6110590; Synthetically spun silk nanofibers and a process for making the same; Reneker DH, Eby RK, Ertley D, Hudson SD, Zarkoob S.; 2000; University of Akron, USA.

WO 2001027365; Electrospun fibers and an apparatus therefore; Smith, Daniel; Reneker, Darrell; Mcanus, Albert; Schreuder-Gibson, Heidi; Mello, Charlene; Sennet, Michael; Gibson, Phillip; 2001, University of Akron, USA.

Table 2.1. Electrospinning review articles

1st Author	Institution	Description
Chronakis (2005)	Swedish Institute for Polymer and Fiber Research, Sweden	Ceramic and composite nanofibers by electrospinning. Encapsulation, alignment, organic – inorganic hybrid fibers. (11 pages, 66 references)
Fong, (2001)	University of Akron, Akron, OH, USA	Process, properties and applications. (22 pages, 45 references)
Frenot, (2003)	Swedish Institute for Fiber and Polymer Research, Sweden	Process, variables, morphology and applications. (12 pages, 65 references)
Greiner, (2007)	Philipps-Universität Marburg, TransMIT Centre for Polymer Research, Germany	Process, structure formation in fibres and non-wovens, mechanical properties and applications. (23 pages, 465 references)
Huang, (2003)	Tongji University, PR China	Process, electrode configuration, polymer /solvents; applications, characterization, modeling. (31 pages, 169 references)
Li, (2004)	University of Washington, Seattle, USA	Process, modifications to apparatus, control, polymer type, inorganics, encapsulation, modification, core-shell, applications. (20 pages, 90 references)
Subbiah, (2005)	Texas Tech University; Lubbock, Texas, USA	History, equipment, process variables, solvents, properties, applications (13 pages, 78 references)

The Huang review includes a list of the types of polymers, the conditions of processing and the potential applications from 169 reference articles on electrospinning and applications. The review of Greiner includes a list of the biomedical applications.

Of note are the electrospinning publications in some highly reputable popular science magazines. In 2004 in The National Geographic electrospinning is discussed in an article on Textiles for potential application in military uniforms for protection in chemical and biological warfare, (Newman 2003); in 2000 in the Scientific American as a wound dressing which can form tissue scaffolds and minimize scarring on burn victims (Martindale 2000) and in 2004, is discussed in general in the journal Science (Dzenis 2004).

The fibres from electrospinning with a diameter of around 100 nm but as high as 1 μm are referred to as nanofibres. Such fibres are often quoted in references on "Nanotechnology". However, The National Science Foundation, (NSF), in the USA has defined "Nanotechnology", as the study of components where at least one of the dimensions should be less than 100 nm. This is only rarely true for electrospun fibres. However fibres with a diameter as small as 3 nm have been electrospun. In such a case there are only about 40 molecules across the diameter, of which about half the molecules are on the surface {Lyons (2004)}.

The variables, which affect the spinning process, are listed below. They have been discussed at length in literature and excellent descriptions are available in the review articles listed in Table 2.1 above.

The effect of some of these variables specifically on the spinning of PAN fibres is reported in Chapter 3.

The basics of the electrospinning process are explained earlier in this chapter of this document.

This literature review will therefore focus only specifically on more recent publications from the year 2004 and also on the effect of the variables of specific relevance to this research project; i.e. the spinning of various grades of PAN and the addition of nanoparticles and salts to the spinning dope and in addition post-spinning treatments of the nanofibres.

A literature review on the use of sol-gel processing with electrospun polymeric and inorganic fibres is available. Further literature is discussed in Chapter 5 as relevant to each application.

2.1.2. Polymer and processing variables in the electrospinning process

In principal, nearly all soluble or fusible polymers can be processed into fibers by electrospinning, provided that the molecular parameters (such as solubility, glass-transition temperature, melting point, crystallization velocity, molecular weight, molecular-weight distribution, entanglement density, solvent vapor pressure, and pH value) and process parameters (i.e. concentration, electrical conductivity, surface tension, feed rate, electrode separation / geometry, temperature, and relative humidity) are correctly set (Greiner & Wendorff, 2007).

Polymer variables

- Molecular weight, molecular weight distribution and co-monomer content
- The architecture (branched, linear), tacticity and thus degree of crystallinity of the polymer
- Solution properties (viscosity / rheology, conductivity and surface tension)

Other variables, which affect the electrospinning process:

- Electrical field, flow rate, polymer concentration and solvent type
- Distance between the capillary and collection electrode
- Ambient parameters (temperature, humidity and air velocity in the chamber)
- The electrode geometry, number of spinnerets and the motion of target screen

The effect of the processing variables are discussed in depth in the excellent review articles of Fong, Huang, Li, Lyons and Subbiah as referenced in Table 2.1.

At Drexel University, an interesting concept of a dimensionless Berry number, (Be), was developed whereby the viscosity and molecular weight can be correlated with electrospun fibre diameter. This then relates the degree of entanglements in solution as depicted in Figure 2.4 (Lam 2004).

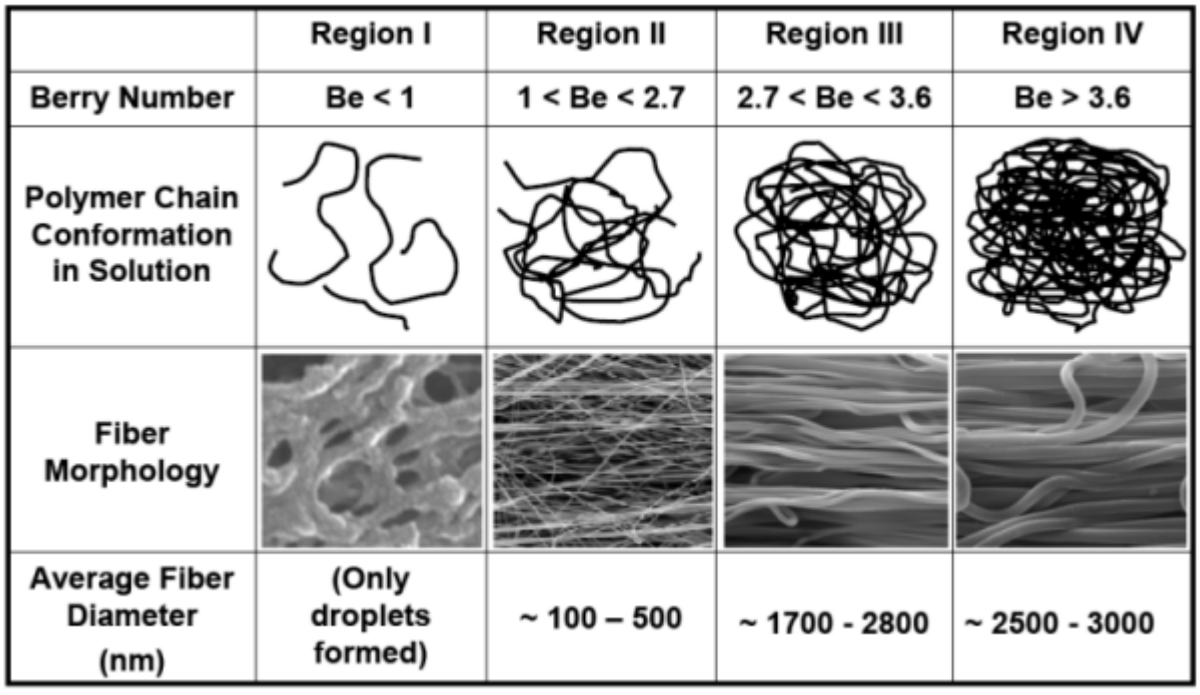

Figure 2.4 Polymer chain conformation to the four regions of the "Berry Number" (Lam 2004).

The Berry Number is the product of the intrinsic viscosity and the concentration. The results for electrospun polylactic acid (PLA) are presented in Table 2.2.

Table 2.2 Berry number versus average diameter for electrospun PLA (Ali 2003)

Polylactic Acid, PLA	
Berry Number	**Diameter in μm**
1	0.1
1.8	0.2
2.3	0.5
2.6	0.5
2.9	1.8
3.1	2.2
3.6	2.8
4.4	2.6
4.6	2.7

2.1.3 Process of nanofibre formation

The process by which the polymer jet exiting the spinneret becomes a nanofibre was until 1999 ascribed to the splitting of the initial single electrified jet (Reneker & Chun 1996). In 2000, the working group of Prof. D. Reneker at The University of Akron and the group of Prof Rutledge at UMASS and MIT used high-frame-rate videotography to observe the electrified jet as shown in Figure 2.5 (b). They found that the thinning of the jet from the Taylor cone (Taylor 1969), is mainly caused by the bending instability. The jet is initially a straight line, which undergoes instabilities, and the single thread undergoes a whipping action, forming a spiraling loop. Some splitting of the jet may also occur (Li & Xia 2004). This is seen visually in real time as a conical envelope in Figure 2.5 (a).

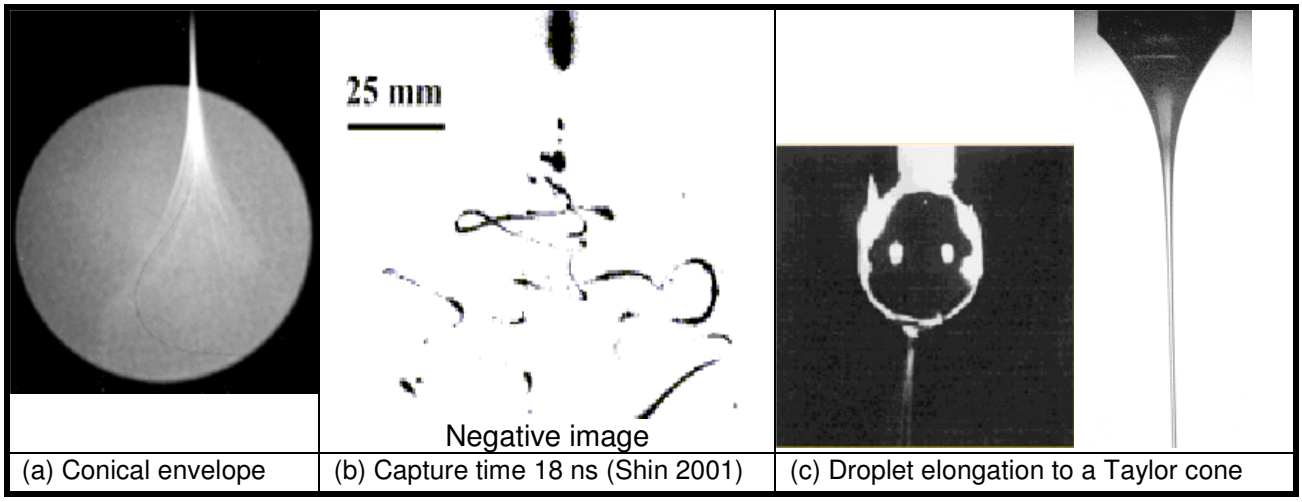

(a) Conical envelope | (b) Capture time 18 ns (Shin 2001) | (c) Droplet elongation to a Taylor cone

Figure 2.5 Photographs of the single electrospinning thread.

Hohman, Shin, Rutledge and Brenner (2001) studied the electrically forced jet and instabilities. They proposed a stability theory for electrified fluid jets. They have demonstrated that an essential

mechanism of electrospinning is a rapidly whipping fluid jet. An asymptotic approximation of the equations of electrohydrodynamics was developed so that quantitative comparisons with experiments can be carried out. The approximation governs both long wavelength asymmetric distortions of the jet, as well as long wavelength oscillations of the centerline of the jet. First, a method for calculating the shape and charge density of a steady jet as it thins from the nozzle was presented and was shown to capture quantitative features of the experiments. Then, this information was combined with the stability analysis to predict scaling laws for the jet behaviour and to produce operating diagrams for when electrospinning occurs, both as a function of experimental parameters. Predictions how electrospinning changes as a function of the fluid conductivity and viscosity were also presented.

Electromechanical coupling, nonlinear rheology and unusual jet instabilities complicate analysis of the electrospinning process. Steady-state spinning was modeled in the nonlinear rheologic regime important for polymer jets. Experimental observations and modeling of bending (or whipping) instability produced a major breakthrough in process analysis. It has been suggested that bending instabilities constitute a major mechanism responsible for the rapid jet thinning in this process. These instabilities are also responsible for the resulting random nanofiber orientation.

2.1.4 Electrospun PAN and carbon nanofibres

The literature citing the electrospinning of PAN and carbon fibres to-date is summarized in Table 2.3.

Table 2.3 Electrospinning literature of PAN and carbon fibres

1st Author	Institution and Analytical Techniques	PAN grade	Comments and applications
Agend (2007)	Malekashtar Uni. of Techn. Tehran, Iran. SEM, electrical, thermal, conductivity of AC	8% 150 000 $g.mol^{-1}$ in DMF Aldrich	Conductivity versus pyrolysis temperature. 500 to 1100 °C in N_2 for 1 hr.
Baumgarten (1971)	University of Wilmington, Delaware, USA.	Commercial grade	Voltage of a PAN in DMF showed fibre diameter influenced by viscosity: $d = \eta^{0.5}$. Increasing field strength first gives small diameter, then the diameter increases.
Chen (2008)	Shanxi Uni. Taiwan.	MW = 86 000 9% in DMF	$AgNO_3$ (10 to 69%) / PAN / PPy
Drew	UMASS Lowell, USA.	MW = 86 200	Collected on aluminium foil.

(2003)	SEM, TEM, EDAX	7,5% PAN in DMF	Solution deposition of continuous thin coatings of titanium dioxide (TiO_2) and tin dioxide (SnO_2), 80 nm thick. Catalysis, sensors.
Fennessey (2004)	UMASS, Amherst, USA. FESEM, XRD, FTIR dichroism, birefringence	MW= 200 000 10% PAN in DMF	Rotating grounded electrode Aligned carbon fibre precursors.
Ge (2006)	Univ. of Akron, Ohio, USA & Marburg. SEM, TEM, AFM, TMA, EDAX, UV, XRD, TGA	MW = 86 000 7% PAN in DMF 10% MWNT	The degree of orientation for the surface-oxidized MWNTs (f = 0.90) >PAN crystals (f = 0.62). UV / vis show charge transfer complexes between MWNTs and PAN. Increases the electrical conductivity and thermal stability.
Gu (2005)	Tongji University, China. Factorial experiment	6, 8 10 & 12% PAN in DMF	The effect of variables on the diameter using SEM.
Hou (2005)	Jiangxi Normal Unversity, China. Akron and Marburg. SEM, AFM, TEM FTIR, XRD, Raman	MW = 86 000 7% PAN in DMF 2 to 35% MWNT	Moving collector Improved modulus and less shrinkage on oxidative stabilization 220 °C in air for 2 hrs. Then 220 to 850 °C at a rate of 2°C.min^{-1} in Ar.
Kalayci (2005)	UMASS, Dartmouth, MA, USA. Charge / mass web, SEM, modeling	PAN in DMF, 333 and 2800 cP	Charge consequences in electrospun polyacylonitrile (PAN) nanofibers; deposition time vs. charge, effect of pos. or neg. charge. Charge via an O-ring electrode = ionized field charging.
Kim (2003)	Chonnam National University, Korea. SEM, BET, CV	10% PAN in DMF	Stabilized; 1 °C.min^{-1} up to 280 °C, for 1 hr under airflow. Then 5°C.min^{-1} up to 700, 750, and 800°C and activated for 30 min 30 vol.% of steam in N_2. Battery electrodes.
Kim (2005)	Chonnam National University, Korea. SEM, BET, CV Impedance spectroscopy	20% PBI in DMAc	Heated to 700, 750, 800 or 850 °C at 5°C.min^{-1} in N_2. Activated by 30% steam in N_2 for 30 min. Supercapacitor application.

Ko (2003)	Drexel University, USA. Raman, AFM, SEM, TEM	SWNT in PLA and PAN	Nanocomposite yarns by co-electrospinning.
Lam (2004)	Drexel University, USA. SEM, Raman, HRTEM, tensile	MW = 150 000 SWNT DWNT	Stabilised at 200°C, carbonized at 700°C, graphitized at 1600°C in Ar. Reinforcement of composites
Lee (2005)	Inha University, South Korea. SEM, conductivity	MW = 150 000 7% PAN in DMF	0,05 to 0,5 wt % $AgNO_3$ reduced to Ag nanoparticles 5,8 nm. One step process where DMF is the reducing agent.
Mack (2005)	Drexel University, USA. AFM nanohardness.	MW = 150 000 7%PAN in DMF	1 to 4 % graphite nanoplatelets.
Mironov (2003)	Moscow State University, Russia.	11% PAN-AA in DMF	The effect of variables on the diameter using AFM.
Park (2005)	Hanyang University, Republic of Korea. XRD, Raman, SEM, TEM, conductivity	10% PAN in DMAc Iron acetyl acetonate	Syringe pump feed Heating at 1°Cmin^{-1} up to 260 °C, holding for 2 hrs in air. Carbonization at 900 to 1500 °C for 1 hour in N_2, 2°Cmin^{-1}.
Qin (2004)	Donghua University, China Modeling, jet diameter	MW=75 000, 10% PAN in DMF 1 and 4% LiCl	Li:CN = 1:20 to 1:5 The effect of conductivity on the spinning jet diameter.
Vaisman (2007)	Weismann Inst. Of Science, Israel XRD and FTIR	MW = 150 000 0,1 & 2% MCNT's	Ethylene carbonate as plasticizer / additive. **New phase identified**. Solution and electrospun from DMF
Wang (2004)	UPenn, USA. DTA-TGA, SEM, Raman	6% PAN in DMF	Stationary screen electrode. Pyrolyzed at 837, 1073, 1273 and 1474 K for 30 min in vacuum 10^{-6} T.
Wang (2005)	Jilin University, China. UV, TEM, SERS	MW = 80 000 10% PAN in DMF	$Ag(NO_3)$ *in situ* reduction to Ag nanoparticles, 10 nm CN:Ag = 1:1. SERS **PAN graphitisation structure at room temperature.**
Wang (2007)	Uni. Hangzhou, PR China.	6% PAN-Co-AA (10% AA), DMF 83 200 $g.mol^{-1}$	Polymer dispersed with MWCNT and redox enzyme. MWCNT increases enzyme activity.
Ye	Drexel University,	MW= 150000	Carbon nanotubes reinforce by

(2004)	Philadelphia, USA. SEM, TEM, Tensile	PAN SWNT, MWNT	hindering crazing, reducing stress concentration, and dissipating energy by pullout.

In an article (Gu & Ren 2005), the history of the electrospinning of PAN as carbon precursors is reviewed in depth. Typical commercial PAN carbon fibres are shown in Figure 2.6.

It is shown with the electrospinning of PAN in DMF that the fibre diameter, (d), is influenced by the viscosity, $\{d = \eta^{0,5}\}$. Increasing field strength at first gives smaller diameter fibres but then, as the field strength increases the diameter of the electrospun fibres also increases (Baumgarten 1971),

Carbon nanofibers with diameters in the range from 100 nm to a few microns from electrospun polyacrylonitrile were produced (Gu et al. 2005). Wang et al. (2002, 2003) produced carbon nanofibers from electrospun PAN fibers and studied the structure and conductivity. A method is reported to use the carbonized electrospun PAN nanofibers as substrates for the formation of well aligned multi-wall carbon nanotubes (Hou et al. 2005). Nanofibres were produced from PAN-based electrospun fibers and studied the electrochemical properties of the web as an electrode for a supercapacitor (Kim et al. 2005). They also investigated the effect of the salt additive, iron acetyl acetonate as an additive to aid the carbonization, on the electrospinning process.

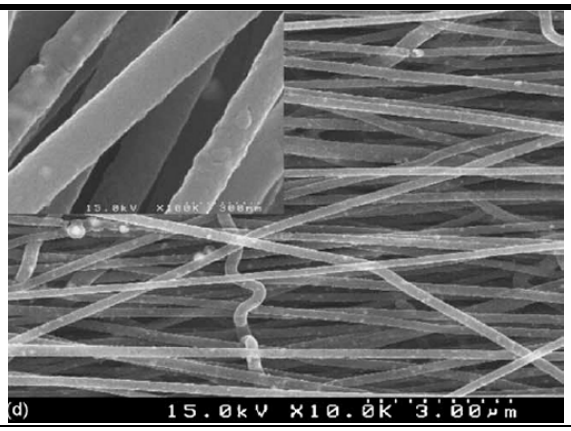

Electrospun carbonized PAN (Park et al. 2005). 10 000 X, fibre diameter about 150 nm

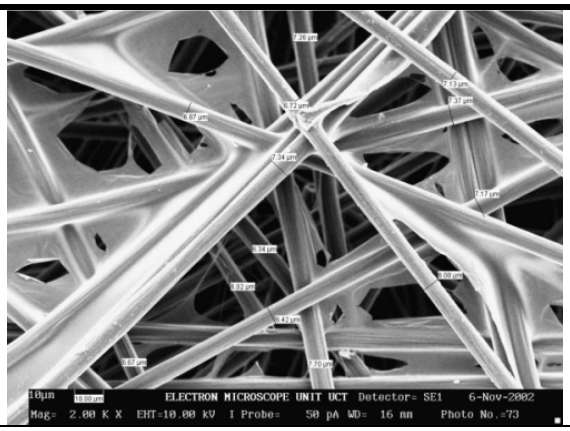

Commercial activated carbon fabric 2000 X, fibre diameter about 7000 nm

Figure 2.6 SEM micrographs of electrospun and commercial carbon fabrics.

2.1.5 Aligned electrospun nanofibres and yarns

Various approaches have been taken to obtain aligned electrospun fibers; spinning onto a rotating drum (Reneker 2000) and a drum with copper wires (Katta 2004), spinning onto the sharp edge of a thin rotating wheel (Zussman 2003), introducing an auxiliary electrode (Deitzel et al. 2001a) using

alternating grounded gold wires (Kameoka 2003), rapidly oscillating a grounded frame within the jet (Fong & Reneker 2001), and using a metal frame as the collector (Dersch et al. 2003). With these approaches, various degrees of alignment are achieved but most suffer from the drawback that only relatively short tows are obtained. Untwisted fibre bundles have been spun by spinning onto the surface of a liquid and collection on a rotating reel (Smit et al. 2005) but the yarns have poor mechanical properties. The SEM of these fibres is given in Figure 2.7.

A recent paper, (Fennessey & Farris 2004) reports on the formation of true twisted yarns from electrospun PAN with a twist angle up to 16,8° using an electronic twister. The maximum orientation factor, as measured by XRD reached a peak maximum at a face take-up speed of 9,8 $m.s^{-1}$. The orientation was reduced at higher face velocity. Continuous yarns of composites of polylactic acid and PAN with single wall carbon nanotubes, (SWNT), have also been prepared (Lyons & Ko 2004).

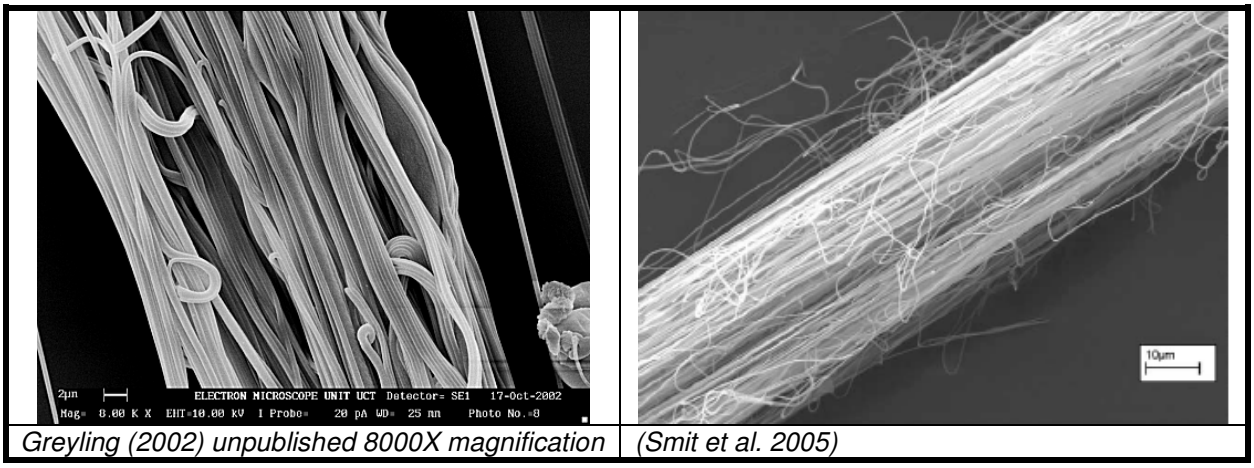

Greyling (2002) unpublished 8000X magnification | *(Smit et al. 2005)*

Figure 2.7 Aligned electrospun PAN fibres prepared at University of Stellenbosch.

2.1.6 The effects of solvents on electrospinning

The effect of the viscosity of the solvent has been studied for cellulose acetate (Liu 2002). Solutions with viscosity, η, ranging between 1.2 and 10.2 poise and surface tension, γ, about 26 $dyne.cm^{-1}$ consisting of various mixtures of acetone and DMAc, produce smooth fibers with diameters from 100 nm to $\pm$ 1 µm. The fibres were collected both on paper and on water. The fully regenerated cellulose membranes are similarly hydrophilic to commercially produced cellulose fibrous matrices but absorb nearly ten times as much water.

The effect of dissolved polyvinyl chloride, PVC, and polyurethane, PU, blends in THF / DMF solvent mixtures on electrospinning was also studied (Lee 2002). A higher surface tension requires a larger electric field. The surface tension is related to the interaction between polymer and solvent. Electrical

conductivity of PVC solution is larger than that of PU, and a higher conductivity was required to facilitate spinning.

Fibers with varying cross-sectional shapes, (ribbons or round), from a number of different polymers and solvents indicated that fluid mechanical effects, the electrical charge carried by the jet, and the rate of evaporation of solvent contributed to the formation of the fibers (Koombhongse et al. 2001).

The effect of solvents on PAN polymers in solution and the resultant effect on electrospun fibre morphology are presented in Section 2.2 in the literature review on polyacrylonitrile polymers.

Copolymers of (PMMA-co-PMAA) type polymers and solvents of various dielectric constants, were used to systematically screen intermolecular interactions and ascertain the influence of hydrogen bonding on electrospinning. Deviations from existing rheological empirical relationships arise for polymer solutions with hydrogen bonding association (McKee 2004).

2.1.7 The effect of metal salts and particles on electrospinning

A literature review on the inclusion of metal salts in electrospun fibres is given in Table 2.4.

Table 2.4 Organic inorganic electrospun nanofibres

Inorganic specie	Date	First Author and Institution	Comment
Ag Nanoparticles	2005	Wang, Y.; Jilin Univ. China.	$Ag(NO_3)$ *in situ* reduction 10 nm diameter. CN:Ag = 1:1. SERS shows PAN graphitisation structure at room temperature.
Ag embedded nanoparticles	2005	Melaiyue, A.; Univ. of Akron, Ohio USA.	Encapsulated slow release anti-bacterial.
Ag nanoparticles in porous silica nanofibres	2007	Patel, A.C.; Dept Chem., Drexel Uni. PA, & The Alan MacDiarmid Inst. Jilin Uni., China.	Porous silica nanofibers with catalytic silver nanoparticles. Sol-gel with TEOS and $AgNO_3$. Calcination at 200 to 800 °C.
$BaTiO_3$	2005	Yuh, J.; Univ. of Florida, USA.	$Ba(CH_3COO)_2$ / $Ba(CH_3COO)_2$ in PVP. Calcined at 750 °C.
Cu, Mn bipyridine complexes	2001	Lu, J.; Univ of Houston-Clear Lake, Texas, USA.	Zeolite structure.
Cu^0 in graphite	2001	Ma, J.; Northeastern Univ., Boston, USA.	Catalyst immobilization.

CuO fibres	2003	Guan, H.; Northeast Normal Univ., China.	PVA / copper acetate.
Fe, Co , Ni nanofibres	2007	Wu, H.; Dept. Mat. Sci. & Eng. Tsinghua University, Beijing, PR of China.	Alligned arrays of 25 nm diameter ferromagnetic metal nanofibres. High density recording, magnetic sensors, flexible magnets.
FePt nanoparticles	2005	Song, T.; National Univ. of Singapore, Singapore.	Encapsulation in core-shell PCL for magnetic application.
$LiCoO_2$ fibres	2005	Gu, Y.; Shandong Univ., Jinan, China.	$(Li(CH_3\text{-}COO))/(Co\text{-}(CH_3COO)_2)$ $(C_6H_8O_7,H_2O)$ Calcined at 700 °C.
Nb_2O_5 fibres	2003	Viswanathamurthi, P.; Chonbuk National Univ., Chonju, Korea.	Niobium ethoxide / PVA. Calcined at 973K.
NiO fibres	2003	Guan, H.; Northeast Normal Univ China.	PVA / nickel acetate composite Calcined at 550 and 700 °C.
Pd imbedded nanoparticles	2004	Demir, M.; Sabanci Univ., Orhanli, Turkey.	Polyacrylonitrile / $PdCl_2$ with hydrazine at room temp.
Sc trifilate homogeneous catalysts	2007	Stasiak, M., Philipps-Universität, Marburg, Germany.	Immobilized enhanced homogeneous catalyst activity, optoelectronic & pharmaceutical.
SiO_2 fibres	2003	Madhugiri, S.; Univ. of Texas at Dallas, USA.	PEO / TEOS or TMOS Mesoporous.
SiO_2 imbedded	2002	Shao, C.; Northeast Normal Univ., PR China.	PVA / silica.
SnO_2 rutile fibres	2005	Wang, Y.; Univ. of Pennsylvania, PA, USA.	PEO MW= 900 000) / dimethyldineodecanoate tin, sintered at 400, 600 and 800 °C
Ta_2O_5 fibres	2005	Dharmaraj, N.; Gov. Arts College, India.	Tantalum pentoxide/poly(vinyl acetate) Calcined at 1173 °C.
TiO_2 anatase fibres	2003	Li, D.; Univ. of Washington, Seattle, USA.	PVP, *M*w =1 300 000 / titanium tetraisopropoxide, porous. Calcined at 500 °C.
TiO_2 fibres	2004	Ding, B.; Chonbuk National	Titanium isopropoxide (TiP) /

		Univ., S. Korea.	poly(vinyl acetate), pure TiO_2. Calcined 600 to 1000 °C.
TiO_2 surface	2004	Choi, S.; Sejong Univ., Koonja-dong, Seoul,	Titania doped silica
V_2O_5 fibres	2003	Viswanathamurthi, P; Kongunadu Arts and Science College, India.	$(VO(OC_3H_7)_3)$ / PVA. Calcined at 700 °C.
Y_2O_3-ZrO_2 , and Gd_2O3-doped CeO_2	2004	Azad, A.; Univ. of Toledo, OH, USA.	$ZrOCl_2$, $Y(NO_3)_3$, $Gd(NO_3)_3$ $(NH_4)_2Ce(NO_3)_6$ in PVP. Calcined at > 1000 °C.
ZnO fibres	2004	Viswanathamurthi, P.; Chonbuk National University, Chonju, Korea.	PVA / zinc acetate Photoluminescence Calcined at 600 °C.
ZrO_2 fibres	2004	Guan, H; Northeast Normal Univ., China.	PVA / zirconium oxychloride.

Nowadays preparation of metal nanoparticles dispersed in polymer nanofibers has drawn great attention because this kind of nanocomposite combines the unique properties of metal nanoparticles (e.g., the high ratio of surface atoms to inner sphere atoms and quantum size effect etc.) with the outstanding characteristics of polymer nanofibers (e.g., the high specific surface area and high interpenetrating capacity available to other materials etc.) Therefore, the metal / polymer nanocomposites are expected to provide potential applications as catalysts, photonic and electronic sensors, filters, and artificial tissue.

Surface-enhanced Raman scattering (SERS) was used to characterize electrospun atactic PAN containing silver ions (Wang et al. 2005). Homogeneously dispersed Ag nanoparticles, average diameter 10 nm were observed by TEM analysis. It is believed that there is coordination between silver ions and cyano nitrogen of PAN, which donates its lone-pair electron from occupied 2p orbitals to the empty s-orbitals of silver ions to form a δ-bond. The donation of electron density from occupied d-orbitals of silver ions into the empty π^*-2p anti-bonding orbitals of cyano nitrogen leads to the formation of π-bonds. Since silver ions are coordinated with cyano groups, silver nanoparticles are prevented from aggregation in the process of reduction in N_2H_5OH aqueous solution. SERS spectra give information on the crystalline perfection of graphite-based materials. Graphite shows a single band at 1582 cm^{-1} (G peak). Less ordered carbon materials show an additional strong band at about 1360 cm^{-1} (D peak). The result indicates that the structure of PAN has been changed after PAN is

doped with Ag nanoparticles. The spectrum is identical to the reported Raman spectra of PAN-based carbon fiber. The Ag nanoparticles give high electrical conductivity and antimicrobial activity.

The influence of added ionic salt on the fibre uniformity has been studied (Lee 2005). When 0,01 mol% salts were added the measured current was twice as high. Fibers without beads were obtained. The results suggest that there is an optimum electric current value for obtaining uniform nanofibres when salts are added.

2.1.8 Nanoscaled morphologies, surface structure and modification of fibres

Block copolymer poly(styrene-b-dimethylsiloxane) fibers with sub micrometer diameters in the range 150 to 400 nm were produced by electrospinning from solution in THF and DMF. Contact angle measurements indicate that the nonwoven fibrous mats are superhydrophobic, with a contact angle of 163° and contact angle hysteresis of 15°. The superhydrophobicity is attributed to the combined effects of surface enrichment in siloxane as revealed by X-ray photoelectron spectroscopy and surface roughness of the electrospun mat itself. Additionally, the fibers are shown by TEM to exhibit **microphase-separated internal structures**. Calorimetric studies confirm the strong individual segregation of the polystyrene and poly(dimethylsiloxane) blocks. (Ma 2005a).

Polycaprolactam electrospun fibres were also coated by chemical vapor deposition, (iCVD), with a fluorocarbon based copolymer. Hydrophobicity was demonstrated to increase with a reduction in the fibre diameter. The contact angle recorded was 175° (Ma 2005b).

The TUFT process (tubes by fiber template) was developed for production of polymer, metal, and hybrid nanotubes and mesotubes, where thin template polymer fibers produced by electrospinning are coated with desired wall materials using various deposition techniques (Bognitzki 2000). Specific bulk morphologies and surface topologies with ternary solutions using polylactide and PVP as polymer model components were obtained (Bognitzki 2001).

At Univ. of Marburg, polylactide, PLA, fibres with a diameter of 1 to 3 mm were first produced and then coated with poly(p-xylene), (PPX), by vapor phase pyrolysis to form pinhole-free PPX tube walls. The PPX/PLA core-shell fibers were annealed above 250 °C leaving the PPX tubes in a layered assembly connected by a PPX film, as a tubular network. PPX tubes with an aluminium, (Al), inner surface were obtained by coating PLA fibers with Al by PVD and subsequent coating with PPX via CVD.

The hybrid PPX/Al tubes were obtained by thermal degradation of the PLA template fibers; EDAX and TEM data show an Al layer on the inside of the PPX tube. Similarly, PPX tubes with gold inner walls were obtained with inner diameter of 0.5-1.5 nm. Co-continuous phase morphologies resulted

from phase separation processes taking place during fiber formation. Next the specific surface topologies were generated by selective removal of one of the components.

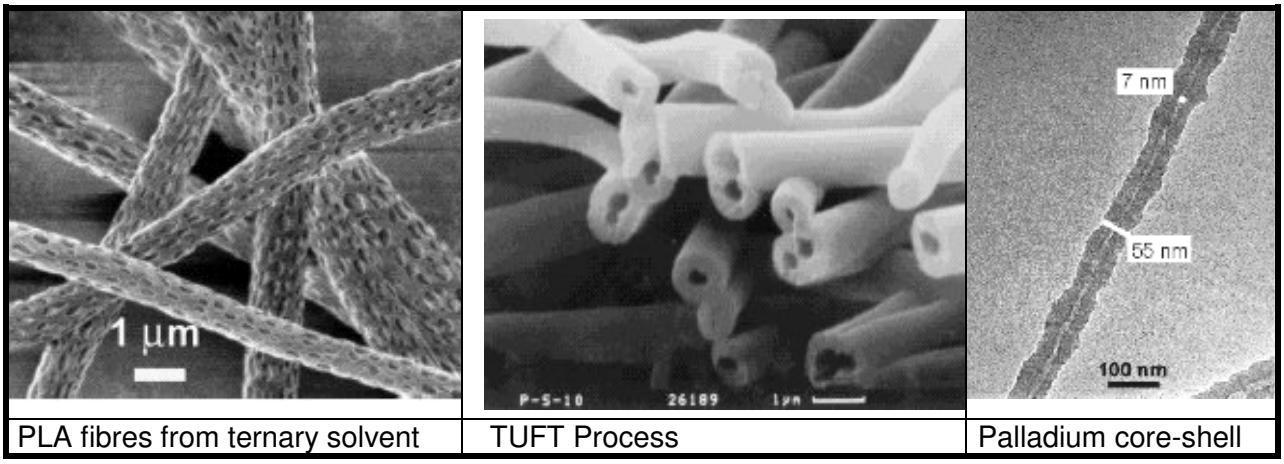

PLA fibres from ternary solvent	TUFT Process	Palladium core-shell

Figure 2.8 Micrographs of surface morphology of fibres spun at the Uni. Marburg.

2.2 FIBRE STRUCTURE

The unique structure and characteristics of PAN fibres are reviewed in detail in Section 2.3.

2.2.1 Introduction to fibre structure

The Textile Institute, UK, defines fibers as units of matter characterized by flexibility, fineness, and high ratio of length to width (Hearle 2002). Nanofibers, down to 10^{-7} dtex (10^{-14} kg.m^{-1}) can be made by electrospinning, in which polymer melts or solutions are extruded in a strong electric field (Reneker & Chun 1996).

Books and reviews concerned with various aspects of fiber science and technology also include information on fiber structure (Lewin & Pearce 1985; Kawai 1985).

The desirable features of the polymer molecule required to form a normally processed fibers are:

- Regularity of structure to form a crystal lattice (tacticity and no bulky side groups).
- Stiffness of the chains and the interaction between them should be high enough to give stability to the crystal, but not too rigid as to cause difficulty in formation or excessive rigidity in the fiber.
- The chains are linear; some fibers may be cross-linked to improve the properties.
- The degree of polymerization (molecular weight) and its distribution; longer chains, ultra-high molecular weight (UHMW), form higher strength fibres. The elimination of short chains is advantageous.
- Impurities should be removed prior to spinning.

2.2.2 Additives for commercial micron sized fibres

- Pigments and antistatic agents are often introduced; titanium dioxide particles are added as a delusterant, carbon black or colored pigments may also often be added. Such components are mixed homogeneously.
- In the production of polymeric fibers, at various stages in processing, surface finishes are added to change the frictional properties of the fibers, to control static electricity; or to influence other properties such as wettability.

2.2.3 Degree of crystallinity of fibres

The discussion of the degree of crystallinity is based on a tacit assumption that the fiber can be regarded as a two-phase mixture of a crystalline component and an amorphous component; however, the reality may be a more complicated distribution of intermediate degrees of order.

If the fine structure is assumed to be a mixture of crystalline and amorphous material, the degree of crystallinity can be determined in various ways. Many physical and chemical measurements can be used to define the degree of order (degree of crystallinity). These include the refractive index, which is proportional to the density; moisture take-up, which occurs within amorphous regions but usually not within crystalline regions, although absorption will occur on crystal surfaces; other absorption techniques; and latent heat of melting, although here the fraction would equal the ratio of fiber latent heat to crystal latent heat (L/L_c), because of the assumption that the amorphous material does not contribute.

Other techniques exist in which the responses X_c and X_a from the crystalline and amorphous materials can be separated, so that the relevant crystalline fraction becomes equivalent to $X_c / (X_c + X_a)$. Such techniques include XRD, electron diffraction, FTIR and NMR spectroscopy. But a problem is that the two responses may overlap, so the separation of X_c and X_a is uncertain.

The use of infrared and Raman spectroscopy in relation to the measurement of PAN orientation and crystal packing is discussed in Section 2.3.3. The application of thermal analytical techniques and the resulting determination of the thermal transitions related to the crystallinity of PAN fibres is discussed in Section 2.3.4. The application of XRD to measure crystallinity and molecular orientation, particularly in PAN fibres is discussed further in Section 2.3.5. Other major analytical techniques used to obtain information on fibers are nuclear magnetic resonance, (NMR) and electron spin resonance, (ESR), spectroscopy, also discussed in Chapter 2.3.

The most important use of refractive index is the determination of birefringence as a measure of orientation. The difference between the refractive index n_1 for light polarized parallel to the fiber axis

and n_2 for light polarized perpendicular to the axis is directly related to the orientation of groups contributing to the dipole moment.

The Herman's orientation function *f*, defined below in terms of n_1 and n_2, is related to the average angle of inclination of molecular segments ($f = (n_1 - n_2 / n'_1 - n'_2) = 1 - 3 \sin^2 \Phi/2$) where n'_1 and n'_2 refer to a perfectly oriented fiber. The orientation determined in this way relates to the whole fiber, whereas the crystal orientation is given by X-ray diffraction. The average amorphous orientation can be calculated from the other two values.

2.2.4 Models of fibre crystal structure

Originally, the first widely used model of textile fiber fine structure was the *fringed micelle* model, illustrated in Figure 2.8 (A). which brings together the indications of the both crystalline and amorphous regions by postulating that a given molecule fringed in and out of the crystalline micelles. In fibers, as distinct from unoriented polymer forms, the orientation was assumed to be preferentially parallel to the fiber axis. This model is plausible since it might be expected to occur if crystallization started at many places within the fiber and it gives reasonable explanations of many fiber properties. When chain folding in polymer crystals was discovered, a modified fringed micelle structure was suggested. Models of this sort, proposed by various scientists, remain the best working models for some types of fiber. All these models are two-phase structures in which crystalline and amorphous regions are clearly differentiated. According to the fringed fibril model, amorphous material as such might not be present, but the structure may be an assembly of fine crystalline fibrils with disorder coming from imperfections in the packing of the fibrils or folded chain crystalline structures. The **existence of additional structural order in PAN**, as that described pictorially in Figure 2.9(D) has been identified in PAN fibres treated with iodine (Kim & Cho, 2003, Murthy et al. 2000).

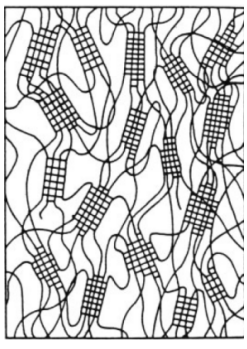

(A) Fringed micelle model

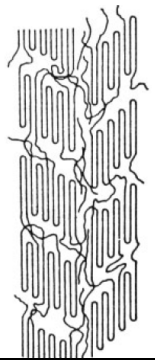

(B) Modified fringed micelle model

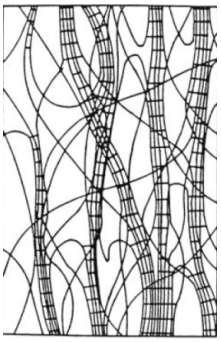

(C) Fringed fibril model

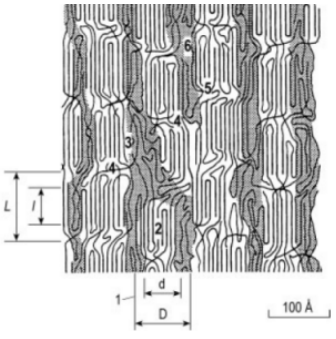

(D) Model of fibre with additives (Murthy et al. 2000)

Figure 2.9 Fibre structure models (Hearle 2002, Murthy, 2000)).

Different polymers fibers have different structures, so different choices of model will give the best representation for particular fibers and the real structures are likely to be much more complicated than the simplified models. Different models specific to PAN fibres are presented and discussed in Section 2.3.

Crystallinity tightens the structure and gives it greater stability. Consequently, increasing degree of order usually yields increased strength, increased stiffness, reduced moisture absorption, improved chemical resistance and less shrinkage under changes of temperature and humidity.

2.2.5 Fiber formation during spinning

Natural fibres are highly specialized structures. In contrast, man-made fibers are formed from a melt or solution of the polymer by high-speed manufacturing. Typical spinning speeds range from 10 to 100 $m.s^{-1}$, so that the solidification, which establishes the structure, occurs in a fraction of a second. Thermodynamically, the structure will be metastable. The degree of localization of order is also an almost inevitable consequence of the manufacturing system, although it may be increased by heat treatment of thermoplastic fibers.

The aspect ratio of the crystallites depends on the circumstances of crystallization, which can be controlled in wet spinning by changing the solvent to non-solvent ratio in the spinning baths, with rapid crystallization from a disordered state tending to give micellar crystals. Crystallite size tends to be increased by heat treatment of thermoplastic fibers. Changes in manufacturing also cause differences. High-speed spinning of polyester fibers, in which all the orientation is induced in the initial spinning operation, gives a structure with larger crystallites than a process of solidification followed by drawing.

Molecular orientation is not easy to control. In manufacturing from solution or melt, the molecular orientation will depend on the natural configuration of the molecule in the disordered state, represented by a radius of gyration, transformed by the elongation during fiber formation. The type of the solvent and the degree of interaction between the polymer molecules and the solvent molecules will affect the molecular orientation.

2.2.6 Structural transitions

In principle, any linear polymer is thermoplastic and will melt, but in practice, a distinction exists between those that melt and those such as PAN that decompose and char before a melting temperature is reached as in the case of polyacrylonitrile.

Below the melting point, a thermodynamic second-order transition, the glass transition(s) occur. They occur in amorphous regions and involve a change in some feature, rotational, translational or

vibrational, of the structure from rigidity to mobility or visa versa. Rigidity, which causes the material to be glassy, can come either from stiff chains (hindered rotation) or from strong interactions between chains. In a simple polymer, on heating, a single transition will occur from a rigid glass to a flexible, rubbery form; however, in PAN fibers, the total change is divided between multiple transitions. These transitions cause a major reduction in fiber stiffness, and cooling through the transition gives a temporary set.

Another form of minor but first-order endothermic transition on heating of some fibers, is between different crystal lattices. This has been identified previously in high speed spinning of UHMW PAN and is discussed in Section 3.4.

2.2.7 Fibre shape

In spinning from solution, coagulation commonly occurs before the solvent has been removed completely from the fiber. The material precipitates in a spongy form containing voids filled with solvent. In further processing, the voids collapse as solvent dries off, and become elongated as the fiber is stretched. The void surfaces seem to disappear to give a solid fiber, but a vestigial effect will remain with the fiber divided into fibrillar zones separated by weaker divisions.

In the faster industrial process, differences between skin and core arise, due to differences in cooling, evaporation, nucleation, and stresses. The patterns of crystallization are consequently different, asymmetric in cross section and if in a flat ribbon-like form the orientation within the cross-section can be random, radial, or circumferential, as indicated in Figure 2.9 (a).

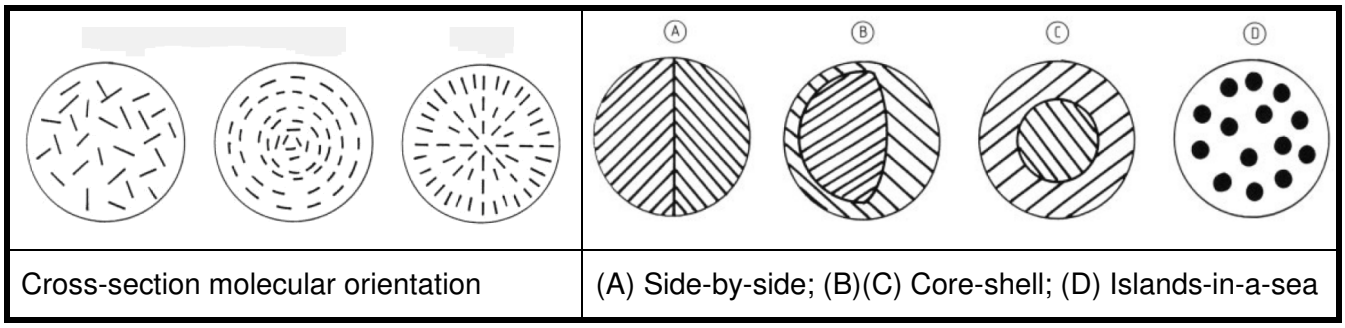

Cross-section molecular orientation	(A) Side-by-side; (B)(C) Core-shell; (D) Islands-in-a-sea

Figure 2.10 Schematic of fibre molecular orientation and shape (Hearle 2002).

Man-made fibers can be produced as a multi-component, usually bicomponent, form. Core-shell fibers are used when some special feature, such as bonding on heating, is required in the surface layer. The islands-in-a-sea fibers, see Figure 2.9 (d), are used to make very fine fibers by removal of the matrix.

The largest scale structural feature of a fiber is its shape. In natural fibers, this is due to genetic control of growth. If a fiber is spun by extrusion through a circular orifice, it will have a circular cross section. In

spinning from solution, the volume reduction modifies the cross-section. Circular forms occur when there is no loss of volume or if the solidification process is controlled so that it occurs uniformly. Solidification occurs on the outside of the fiber; then as solvent is lost from the interior the skin collapses. Dry-spun PAN fibres result in a dog-bone shape (Dralon™) whereas the wet-spun PAN forms a kidney shaped fibre (Ricem™) as seen in Figure 2.11.

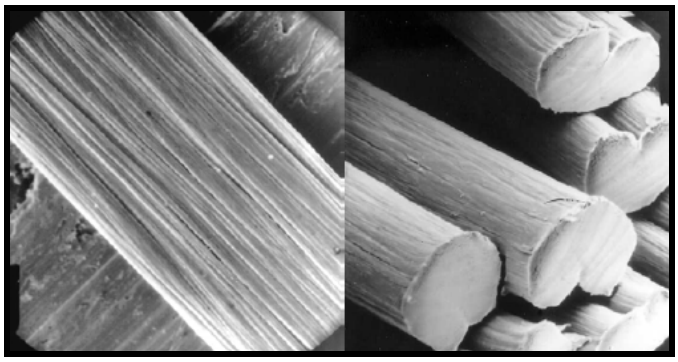

Figure 2.11 Surface and cross-section shape of Ricem™ PAN fibres (Van der Goes 2005).

Most natural fibers have a natural crimp, beneficial in processing and gives bulk, warmth, and softness to the final product. Industrial production gives straight fibers without crimp, which has to be introduced for many applications. In some markets, need for high crimp justifies expense of bicomponent fiber production. Differential shrinkage then gives the fibre curvature.

2.2.8 Fibres produced in nature by invertebrates – Electrospinning for Biomimicry

Silk fibres are generally regarded as being fine but are relatively large with a 20 um diameter. SEM of the silk cocoon are from *Bombyx Mori* moths, are shown in Figure 2.12.

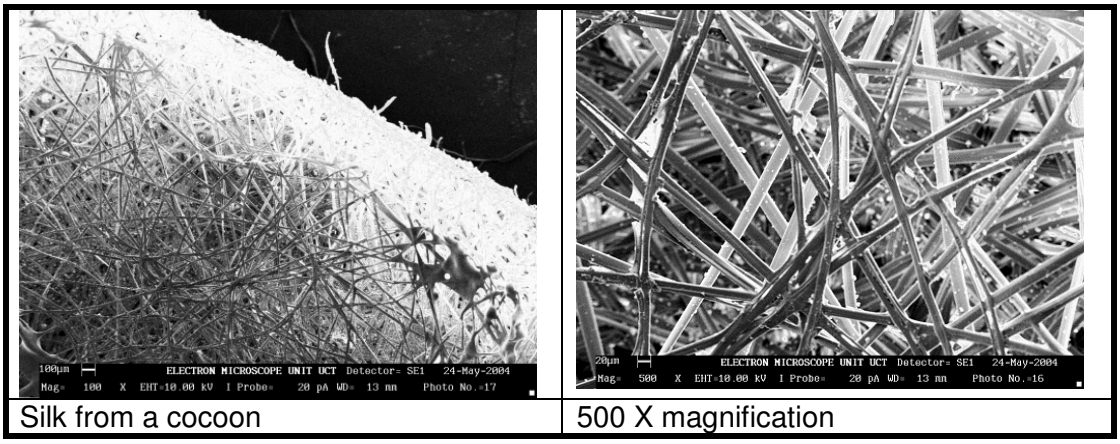

Silk from a cocoon	500 X magnification

Figure 2.12 Micrometer sized fibres produced by silkworm moths (Greyling unpublished).

Spider webs consist of protein silk and contain fibres of 3 different morphologies. The thinnest fibres are about 300 nm as seen in the SEM micrograph in Figure 2.13 below.

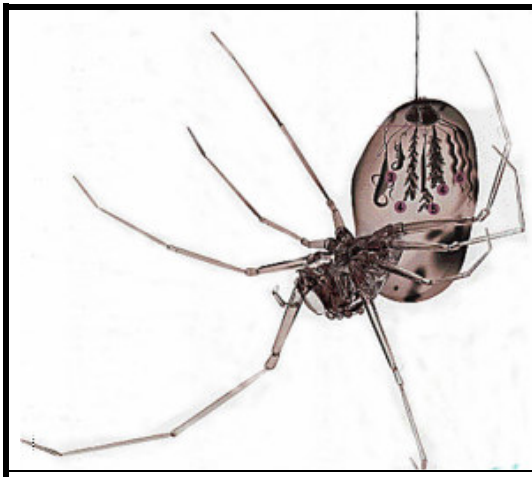

National Geographic spider spinning glands

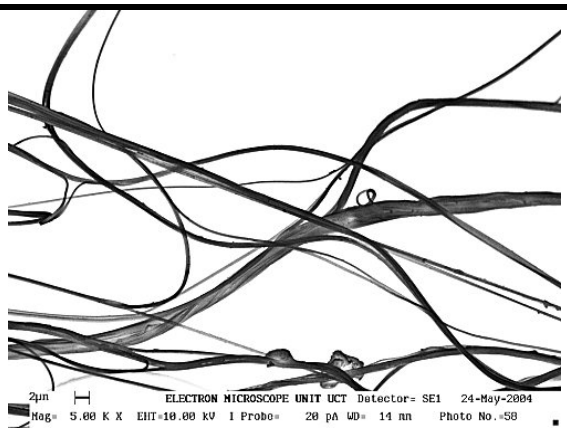

Negative image

Spider web fibres; trimodal size distribution

Figure 2.13 Nanometer fibres produced by spiders (Newman 2003).

2.3 POLYACRYLONITRILE POLYMERS AND FIBRES

2.3.1 Introduction to technical polyacrylonitrile fibres

A major synthetic fiber type has acrylonitrile, {–$CH_2CH(CN)$–}, as its principal repeating unit. The grades of polyacrylonitrile discussed here can all be defined as highly technical fibres. They include the homopolymer PAN fibres and copolymer PAN fibres prepared as carbon fibre precursors. Many grades of acrylic are also used in the apparel industry but these contain 15% or more of the comonomer units, which aid in the processibility and dyeability. These commodity fibres are called acrylic fibres. Some commercial technical grade PAN polymers used for fibre manufacture are presented in Table 2.5. Many patents suggest both the type of comonomer and the form of co-polymerization.

Table 2.5 Typical technical grade PAN fibres

No	SUPPLIER	MOLECULAR WEIGHT	M_w/M_n	COMPOSITION; TRADENAME AND POLYMERISATION SOLVENT
1	Lenzing Plastics. Kelheim plant.	210 000	2,8	AN : MA = 99,5 : 0,5; Dolanit 12™ powder; DMF
2		85 000	2,8	AN : MA = 94,0 : 6,0; Dolan™ powder; DMF
3	BlueStar Grimsby	120 000	?	AN : MA : IA = 93 : 6 :1; Fibre tow; DMF
4	Montefibre, Italy	300 000	2,5	AN VA = >99,8 :<0,2 VA Ricem™ powder; DMAc

All these technical grades are made by free radical polymerization using AIBN as an initiator and an Fe^{2+}/Fe^{3+} redox system and are wet spun. The polyacrylonitrile [25014-41-9] is atactic, as expected for a

polymer synthesized by a free radical polymerisation mechanism. Fibres from type 1, are used in hot gas filtration, type 2 is used for outdoor awning material, type 3 as a carbon fibre precursor and type 4 is used for water and hot gas filtration applications (Huber 2004).

Acrylonitrile monomers are polymerized as a homopolymer of 100% acrylonitrile (see Figure 2.14). The polymer chain is made of a stable hydrocarbon chain with lateral nitrile groups, with strong dipole moments. Neighboring dipoles of the same and or different chains interact by coupling (electrostatic attraction) as shown in Figure 2.14. PAN is an unusual polymer; an atactic sample can crystallize. The crystal of at-PAN has only 2-D order in the chain packing, and significant disorder along the axis, due to heterotactic chain configurations (Van der Goes 2005).

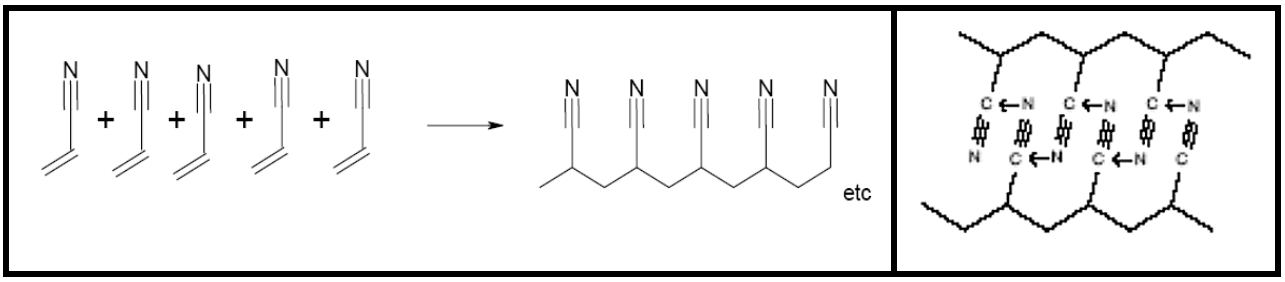

Figure 2.14 Schematic presentation of homo-PAN polymerization and nitrile dipoles

The molecule appears to act as a cylindrical rod with strong, but not very localized, attractive forces coming from the dipole in the –C≡N group. The rods pack regularly side by side. The fine structure is thus assumed to consist of such ordered pseudo-crystalline regions mixed with less ordered regions.

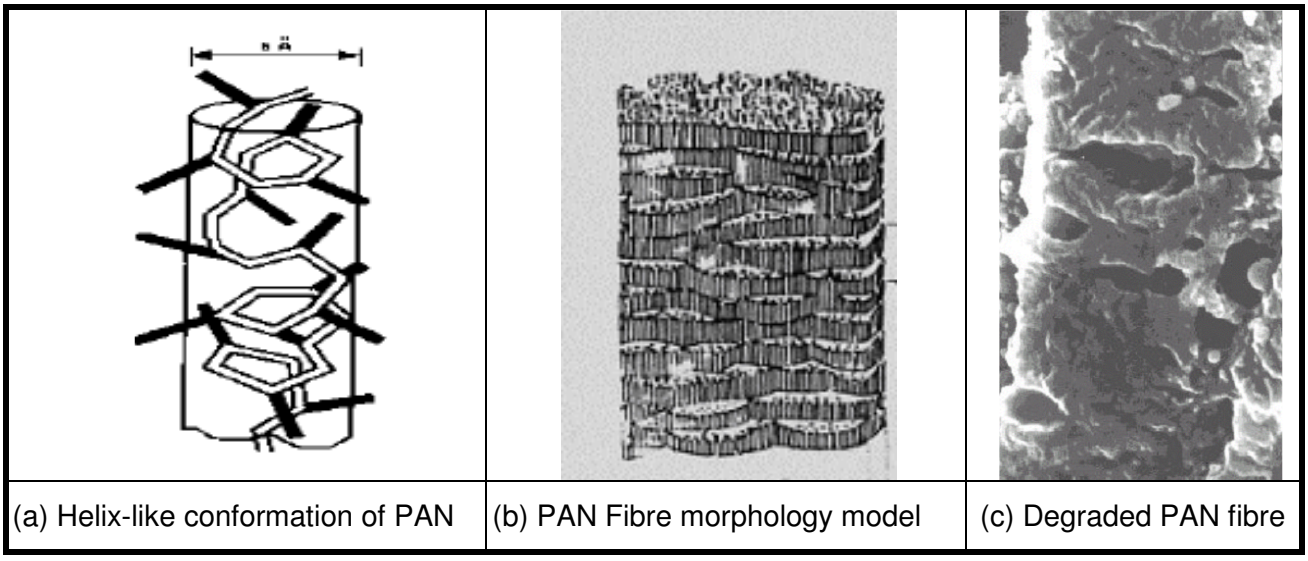

(a) Helix-like conformation of PAN	(b) PAN Fibre morphology model	(c) Degraded PAN fibre

Figure 2.15 PAN molecular packing models and fibre degraded in "amorphous" areas.

The PAN structure has been referred to as "quasi-crystalline". The steric hindrance of bulky co-monomers interrupts these dipole pairings. Figure 2.15 (c) is a SEM micrograph of a degraded commercial PAN fibre from a failed gas filtration plant. It shows that the "less ordered" domains have

been selectively leached. A fibre with a lower proportion of amorphous domains should have higher orientation and crystallinity and improved chemical and thermal resistance

Theoretical ways to improve the crystallinity and chemical and thermal resistance of PAN fibres:

- The possibility of changing the tacticity of the PAN to create increased crystallinity and chemical and thermal resistance was investigated. The urea-clathrate-canal polymerisation technique has produced a PAN with an 82% degree of crystallinity. This small-scale production method using gamma radiation is not viable for up scaling. Studies of this homopolymer PAN structure is of fundamental academic interest (Minagawa et al. 1997, 2001).
- Normally free radical polymerization yields a totally atactic polymer. In Japan, researchers obtained highly syndiotactic PMMA in fluoro-alcohols (Miura 2005).
- Researchers have used the effect of an ultra high molecular weight and a two-stage draw ratio to increase the molecular orientation and crystallinity of PAN fibres (Yamane & Sawai 1997).
- The process of controlled, "living" free radical polymerisation was developed in the 1990's. The advantage of the new polymerisation techniques is the narrow molecular mass distribution, (M_W/M_N), or polydispersity, which should ensure more robust fibres, than fibres produced via conventional free-radical polymerisation. The amorphous domains typically contain chain ends, impurities and very high and very low MW polymer. Since the ATRP controlled "living" polymers, do not contain LMW species and therefore it could be expected that the fibre morphology for such fibres would differ from the conventional model, have a higher percentage crystallinity and higher chemically resistance.

Table 2.6 PAN and comonomer structures

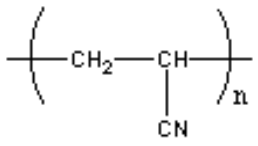	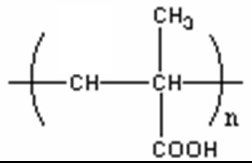	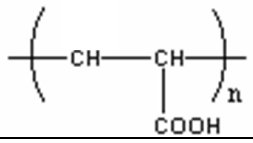
Acrylonitrile = AN	Methacrylic acid = MA	Acrylic acid = AA
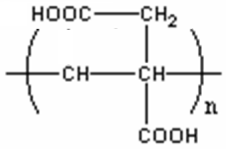	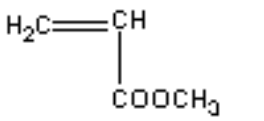	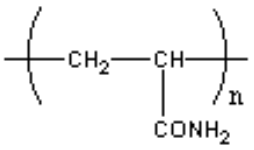
Itaconic acid = IA	Vinyl acetate monomer = VA	Acrylamide

Table 2.6 above gives the chemical structure of the monomers used in commercial PAN.

2.3.2 Crystallinity and molecular orientation of PAN fibres

A high degree of crystallinity and high orientation of the crystalline molecular segments impart high tensile strength and modulus to fibers. The amorphous phase gives rise to toughness and dyeability. A low degree of orientation of the amorphous phase is preferred to minimize shrinkage caused by stress relaxation upon heating the material above its glass transition temperature.

Whether the classical models, discussed in Section 2.2.4 can describe PAN is debatable (Davidson 2000). In the ordered phase, irregularly twisted, yet extended atactic polymer chains are packed hexagonally. Owing to the strong interchain interactions, this hexagonal columnar phase behaves as a solid, and it is often referred to as a (two dimensional, 2D) crystal. However, the nature and even the existence of the amorphous phase is a subject of controversy. As-polymerized and solvent cast materials exhibit an amorphous phase but highly oriented fibers do not. Apparently, the existence of the amorphous phase depends on the processing conditions.

Wet spinning yields a precursor fibre in which the PAN molecules are organized into fibrils, which, are generally orientated parallel to the fibre axis (Edie 1998). As the PAN solution is forced through the spinneret capillaries the shear force tends to orientate the solidifying polymeric structure parallel to the direction of the flow. Various studies have shown that a solvent can decrease the entanglements in polymers during extrusion and enhance orientation. Processing parameters such as coagulation bath temperature, solvent concentration and stretch can influence the fibrillar structure and its orientation within the as spun PAN fibre. TEM shows fibrils joined together in a 3-D network. After spinning the orientation is enhanced by stretching.

The maximum degree of crystallinity within the PAN fibre is 50%. Stretching does not greatly increase the crystallinity or the molecular order. It enhances the axial orientation of the PAN fibrils

2.3.3. Characterization of PAN by FTIR

Fourier Transform Infrared Spectroscopy, FTIR, can be used to detect the presence of particular chemical groups. Its relevance to fine structure results from the fact that the absorption frequency of a chemical group changes with the environment of the group. The degree of order can be determined by separating the bonds associated with crystalline and amorphous materials. Crystallographic chain folds may give a characteristic shift. The use of polarized infrared radiation can yield data on orientation of absorbing groups in the material. Associated Raman spectroscopy is also used extensively as a way of obtaining similar information. The techniques can also be used as a semi-quantitative measurement of crystallinity and orientation of PAN fibres. In addition FTIR of PAN can show the chemical composition of any co-monomers present in a certain grade of PAN.

PAN has been studied fairly extensively by FTIR for many years by various researchers (Minagawa 1996, 1999), (Dalton et al. 1999). There is some disagreement as to the assignment of the peaks in the FTIR spectra of PAN and the resultant carbon fibres, as shown in Table 2.8.

The position of the peaks and their relative intensities may shift slightly depending on the FTIR technique used, the macroscopic structure (i.e. powder, film or fibre) and the type of co-monomer present in the PAN sample.

FTIR PAS has been used to monitor orientation in bulk drawn polymers (Schmidt 2000).

FTIR was used **(**Minagawa et al 1996, 1999) to determine the degree of molecular orientation in highly isotactic urea clathrate polymerized PAN. Results are shown in Figure 2.16. They showed that the ratio of the A_{1230}/A_{1260} was indirectly related to the degree of interaction between adjacent nitrile groups and thus the isotacticity.

There have been 23 potential degradation products identified for PAN after thermal, UV, acid or alkali degradation (Kirby 1968). The type of products formed during thermal degradation are highly dependant on the rate of heating and the atmosphere i.e. air or nitrogen or CO_2, as well as the commoners in the PAN molecules and other additives.

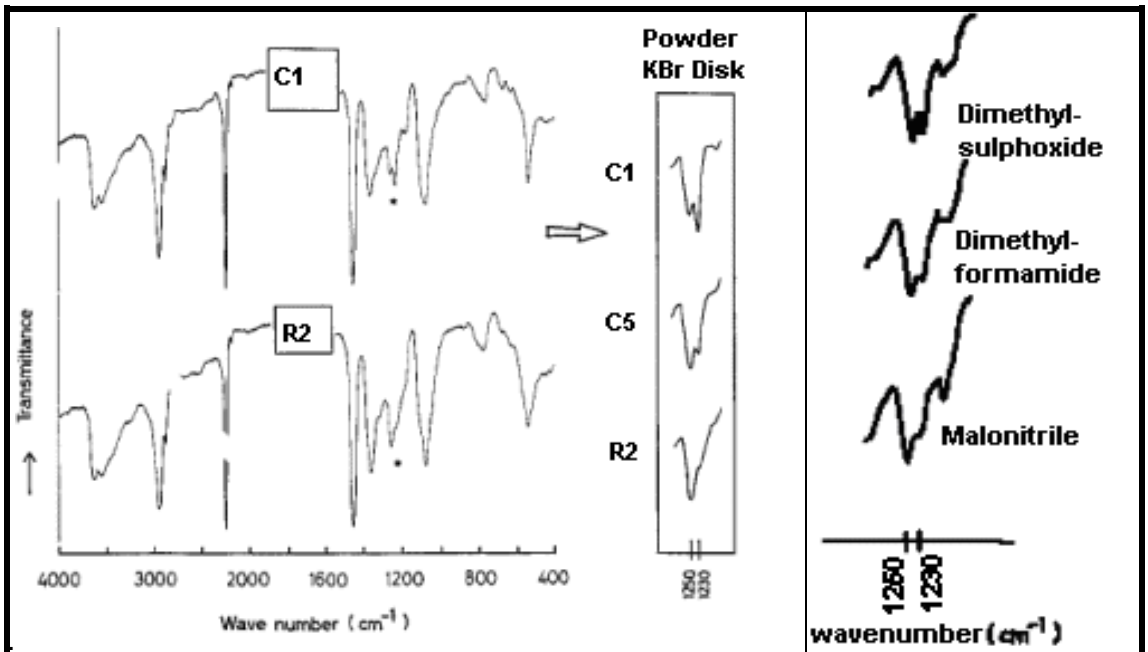

C1 = 72% isotactic, C5 = 48% isotactic, R2 = 28% isotactic	Solvent cast films

Figure 2.16 Orientation by FTIR ratio of peak height at 1230 and 1250 cm^{-1}.

The IR characteristic absorption bands (indicated by asterisks) appearing in the region of 1300 to 1200 cm^{-1} reflect the difference of the stereoregularity of PAN. When the isotacticity was increased, the 1230 cm^{-1} band was enhanced, and the value of the relative intensity between the 1230 and

1250 cm^{-1} bands increased. This ratio can be regarded as a measure of the stereoregularity of PAN but also an indication of the molecular orientation of PAN in atactic samples (Minagawa et al 1998).

Even in the case of solvent-cast PAN film, however, the relative intensity of these bands was strongly dependent on the kind of dipolar aprotic solvents used in the film preparation in Figure 2.17. That is, the intensity ratio was high when good solvents such as DMSO and DMF were used, whereas the intensity ratio was low when a solvent such as malonitrile was used.

The FTIR results are directly defined by the dissolution power of the solvents. Generally, good solvents ensure an expanded chain dimension whereas poor solvents give a contracted dimension of the polymer chain. If the molecular dimension defined by the dissolution power of the solvents is directly retained in the solvent-cast film, the difference of molecular dimension in the solution will be reflected in the IR results of PAN through the difference of molecular conformation in the film.

As an indication of orientation of PAN fibres, dichroic ratios, D, have been calculated for the nitrile absorption (Dalton 1999) and, in the case of the copolymer precursor, the CO absorption, using $D = [(A_{\parallel} - A_{\perp})/(A_{\parallel} + A_{\perp})]$, where $A_{\parallel}$ is the absorption with the electric vector of polarized IR radiation parallel to the fibre axis and $A_{\perp}$ is the absorption with the electric vector of polarized IR radiation perpendicular to the fibre axis. Values of D range in principle from -1 for perfect orientation of the transition moment perpendicular to the fibre axis to +1 for parallel orientation of the transition moment.

Various models of orientation may be applied to polymers in order to obtain orientation parameters and for PAN it has been shown that, if the Kratky orientation model is applicable, the transition moment for the nitrile group is at an angle of 70° to the chain axis (Bashir 2003) Others have argued on empirical evidence that an angle of 73° is more realistic. This value was used in calculations of orientation factors for uniaxially drawn PAN films from dichroism.

FTIR microscopy was carried out on single fibres, mounted under slight tension with double-sided sticky tape, using a liquid nitrogen cooled Hg-Cd-Te detector (Dalton 1999). A gold-wire grid polarizer was used for orientation studies. Spectra were acquired with the polarizer set both parallel and perpendicular for the same region of fibre and are presented in Figure 2.17.

A shear cast PAN membrane shows linear dichroism (Shilton 1997), in the 2241, 1728 and 1450 cm^{-1} peaks. The nitrile groups will be approximately perpendicular to the main polymer backbone when the polymer is elongated. The nitrile would be expected to have preferred orientation perpendicular to the shear direction.

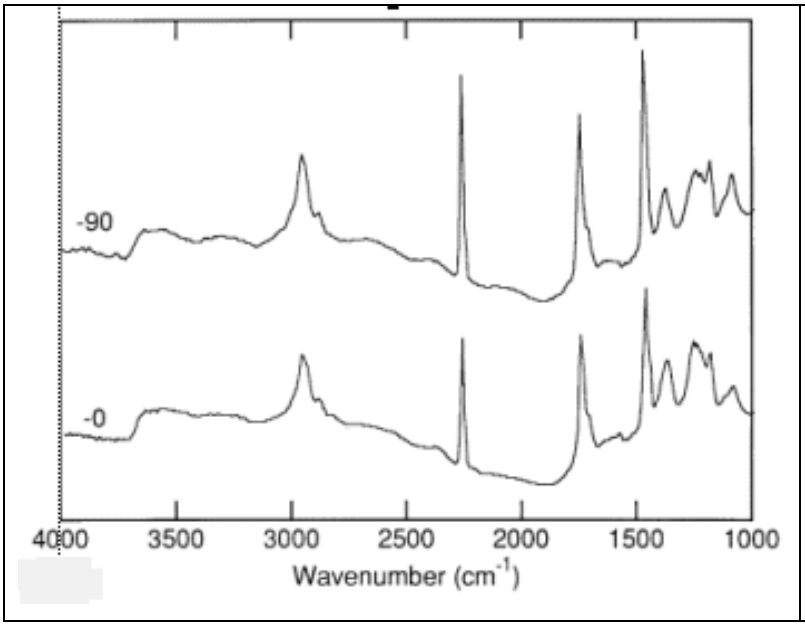

Polarized FTIR spectra of SAF with electric vector parallel (-0) and perpendicular (-90) to the fibre axis

Figure 2.17 FTIR dichroism of PAN fibres (Dalton et al. 1999).

The molecular orientation of aligned electrospun PAN nanofibers was examined by IR dichroism FTIR and XRD. The FTIR results are given in Table 2.7 (Fennessey & Farris 2004).

Table 2.7 FTIR dichroic ratio of aligned electrospun PAN (Fennessey & Farris 2004)

Take-up Speed in $m.s^{-1}$	Dichroic ratio
0	1
9,8	0,75
11,0	0,91
12,3	0,88

The dichroism of the nitrile-stretching vibration was measured for 15 wt% solutions electrospun at 16 kV over a distance of 15 cm onto a collection wheel rotating between 0 and 12.3 $m.s^{-1}$ by FTIR. The nitrile group is oriented approximately perpendicular to the draw direction of the fiber, therefore the absorbance for perpendicular polarization is greater than that for parallel polarization; the nitrile-stretching vibration showed a strong perpendicular dichroism. Similar results were found for fibers electrospun from approximately 15 wt% solutions at 10 and 13 kV under the same conditions (Fennessey & Farris 2004).

2.3.3.1 Peak assignment of the peaks from 1550 to 1660 cm^{-1}

The presence of the absorption at *circa* 1630 cm^{-1} is shown in Figure 4.6 The assignment of the peaks in the region 1550 to 1660 cm^{-1} in the FTIR spectrum of PAN is contested as discussed in Section 2.3.3 and some suggestions of the identification are summarized here.

Table 2.8 FTIR peak assignment of PAN fibres by other researchers

Shilton, S (1997); Courtaulds, PAN; MW = 107 500; AN:MA 85:15, Reflection FTIR

3629 cm^{-1} broad	H_2O
3546 cm^{-1} broad	H_2O
2937 cm^{-1} broad	Aliphatic ν C-H
2870 cm^{-1} very sharp	Aliphatic ν C-H
2241 cm^{-1} very sharp	C≡N
1728 cm^{-1} very sharp	C=O methacrylate
1664 cm^{-1} medium	C=C
1450 cm^{-1} very sharp	Aliphatic ν C-H
1172 cm^{-1} medium	C=O methacrylate

Deng (2003): Daqing China, PAN copolymer composition; AN:VA = 90:10

3632 cm^{-1}	OH stretching vibration
2946 and 2874 cm^{-1}	C–H asymmetric and symmetric in CH, CH_2, and CH_3 groups
2246 cm^{-1}	C≡N stretching vibration
1739 cm^{-1}	C=O stretching vibration
1457 cm^{-1}	CH_3 and δ CH_2 bending vibration
1363 cm^{-1}	CH_3 symmetric in CCH_3 bending vibration
1172 cm-1	C–N stretching vibration
538 cm^{-1}	C=O a twisting vibration

Tang (1996); Zibo Electronic, AN:MA:IA = 93:6:1 dried Cu:CN = 1:2 gradient PAN films

2339.5 and 2191.0 cm^{-1}	complex between the - C≡N and the copper ion
3446,6 and 3357,9 cm^{-1}	stretching of carboxy hydroxyl

Bajaj (1998) India, AN:MA = 89,2:10,8

2920 cm^{-1}	CH_2 stretch
2240 cm^{-1}	C≡N stretch
1728 cm^{-1} shoulders at 1620 &1562 shoulder at 1730	C=O stretch COOH, $CONH_2$ and COO^-) maybe COO^-M^+ $CONH_2$ stretch, C=O stretch
1560 cm^{-1}	stretch of carboxyl in the salt form
1458 cm^{-1}	CH_2 bend
1353 cm^{-1}	CH_2 rocking
1120 cm^{-1}	stretching of π electron cloud

Silverstein (2004); Israel, cast film on KBr (1998): AN:VA = 45:1 ito comonomer units

2925 cm^{-1}	CH stretching
2856 cm^{-1}	CH_3 stretching
1250 cm^{-1}	CH twisting
2242 cm^{-1}	C≡N stretching
1740 cm^{-1}	C=O stretching
1453 cm^{-1}	CH_2 bending
1384 cm^{-1}	CH in plane deformation
659 and 1669 cm^{-1}	residual DMF

Silverstein has argued that on a PAN-VA copolymer (AN:VA = 45:1) the intense absorption bands at 1150, 1255, 1391, and 1630 cm^{-1} after heating to 289 °C reflect C=N and C=C conjugation in a heteroaromatic structure. The absence of a band at 1669 cm^{-1} in his data indicates that there is no residual DMF only after heating to 325 °C.

Bajaj showed that in PAN, on heating some new bands appear, 3260 cm^{-1} at 288 °C and 1600 cm^{-1} at 268 °C, 1400 cm^{-1} and 1060 cm^{-1} at 287 °C, 1275 cm^{-1} at 277 °C. He deduced that the nitrile oligomerization in the homopolymer takes place after 275 °C and at 200 to 265°C in the PAN/Cu complex. In the PAN/Al complex, the absorbance ratio at 1601 cm^{-1} due to C=C—C=C and —C=C—C=N— increases steadily but at an even higher temperature. A new band appears at 1597 cm^{-1} around 220°C, whose intensity increases upon further heating and reaches its maximum at about 265°C, after which it falls around 300 °C. Bands at 3250 cm^{-1} and at 2320 cm^{-1} appear around 271 °C as shoulders. At 340 °C the intensity of both these bands increased.

In the PAN-MA copolymer, upon heating the absorption band at 2243 cm^{-1}, starts diminishing at 200 °C, and the maximum change in absorbance of the band takes place around 295 °C. However, the band at 2926 cm^{-1} starts diminishing at 235 °C, which levels off around 300°C. A new band around 1600 cm^{-1} has been observed. At 215 °C, this band starts appearing, and its intensity increases with an increase in the temperature. It reaches its maximum at around 270 °C The band at 1453 cm^{-1} also disappeared at 340 °C. At 244 °C the band due to C=O at 1726 cm^{-1} has disappeared. Appearances of some new bands have also been noted. A new band at 3250 cm^{-1} appears at 244 °C, and as the temperature increases, the intensity of this band also increases. A new weak band due to C≡N at 2180 cm^{-1} has also been observed at 340 °C.

In the PAN-IA copolymer, the nitrile band at 2241 cm^{-1} starts diminishing at 180 °C up to 290 °C. The band at 2926 cm^{-1} also starts diminishing around 180 °C. A band at 586 cm^{-1} appears around 180 °C, which indicates the formation of anhydride formation from itaconic acid. The prominent absorbance band observed in the 1696 to 1720 cm^{-1} region in PAN-IA and PAN-MA at 180 °C is due to the carbonyl of the COOH group overlapped with free ketones in the form of hydronaphthyridine is absent in PAN-AA, but on subsequent heating a strong band appears around 271 °C (56.5% area in PA). On the contrary, the band in the same region disappears at 270 °C in PAN-MA.

From the peak area of absorbance bands in the 1570 to 1595cm^{-1} region, due to the development of >C=C<, C=C—C=N and (C=C) + (NH) mixed mode at 271 °C, one may conclude that the dehydrogenation and cyclization reactions occur almost simultaneously in PAN-IA at a much lower temperature compared to PAN-MA and PAN-AA.

The deconvoluted peaks in the 1800 to 1550 cm^{-1} region are shown in Figure 2.18. The peak area for the 1660–1745 cm^{-1} region due to the C=O and the 1571 to 1600 cm^{-1} region due to the C=C were considered for comparison.

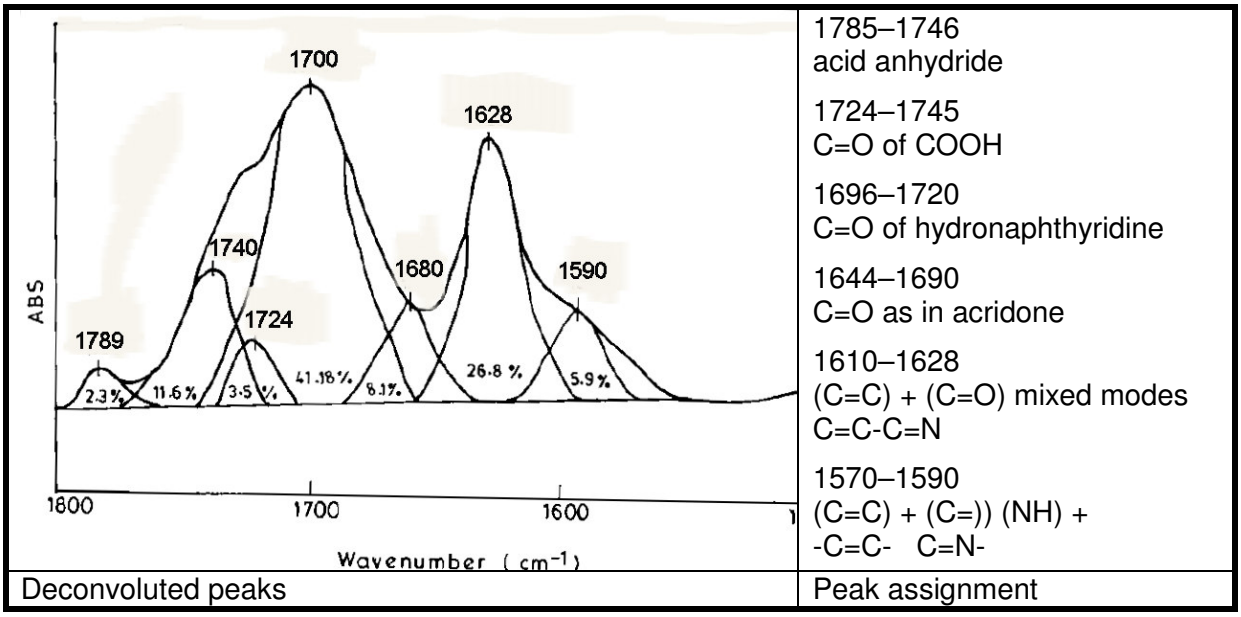

Figure 2.18 FTIR peak deconvolution from 1800 to 1500 cm^{-1} for PAN (Bajaj et al. 1999).

Bajaj et al. in 1998 reported on PAN fibers treated with aqueous solutions of Na_2SO_4, K_2SO_4, Co_2SO_4 and $NiSO_4$. The major absorptions in the spectra are at 2920, 2240, 1728 (with shoulders at 1620 and 1562 cm^{-1}), 1458, and 1353 cm^{-1} are due to the stretching of CH_2, C=N, C=O, bending deformation of CH_2, and rocking of CH_2, respectively. Ebdon (cited in Bajaj et al. 1999) reported that acrylonitrile units may undergo hydrolysis during polymerization by the aqueous free radical slurry method and the species so formed, i.e., acrylamide and AA, may also be polymerized with AN units. These units show IR absorption due to C=O stretching, i.e., 1730 cm^{-1}. Thus, a shoulder which appeared in the band at 1728 cm^{-1} may be attributed to the stretching vibrations due to the $CONH_2$ group.

The band at 1560 cm^{-1} with intensity varying from weak to medium, is assigned to the stretching of carboxyl group in salt form. A change in the intensity of the band at 1120 cm^{-1} (which is attributed to the stretching of the π-electron cloud as reported by Muller and Impekoven. This could be due to the distortion of the π e^--cloud by metal ions. Furthermore, this change is more pronounced in fibers treated with sulphates of transition metal ions, probably because of the smaller size and more positive change density of these ions. Transition metal ions may attract π electrons from COOH, $CONH_2$ and CN groups to establish some linkages with these groups. IR studies of treated samples suggest that

treatment of PAN fibers containing an AA co-monomer with the sulphates of alkali metals affects their chemical structure to a greater extent compared to the ones treated with transition metal sulphates.

2.3.3.2 Peak assignment for PAN with metal salt additives

Deng noticed a peak shift on PAN-VA (AN:VA = 90:10) with chromate salts for FTIR spectra obtained on pure and alkali modified PAN. The peak at 1551 cm^{-1} in the spectrum of the modified PAN is assigned to the bending vibration of the imine groups (NH_2 or NH) on the surface of the fibres. After the adsorption of Cr(III) species at pH 5, the peak at 1551 cm^{-1} was shifted to 1536 cm^{-1} indicating that the Cr(III) species attached to the amine groups and certain chemical bonds were formed, which caused the decrease in the absorption wavelength.

Kim identified the bands in PAN-MA copolymer (AN:MA = 91.5:8,5) spectra as follows; strong bands at 1450 (C–H bending), 1720 (C=O stretching), 2250 (C≡N stretching), and 2945 cm^{-1} (C–H stretching). After addition of $FeCl_3$, new strong peaks appear at 1650, 1491, 1426, and 1363 cm^{-1} while the bands from C≡N and C=O groups of PAN remain at the same position. They recognized that these new peaks are due to DMF molecules, remaining even after a thorough vacuum-drying. The C=O peak at 1650 cm^{-1} of DMF was shifted to a lower wavenumber of 1640 cm^{-1} due to the direct interaction between DMF and Fe^{3+}. This indicated that there is little direct interaction between Fe^{3+} and C≡N groups of PAN molecules, as suggested by XPS.

Silverstein reported on the FTIR data of PAN heat treated with $CuNO_3$. The high-intensity NO_3 band at 1380 cm^{-1} for the virgin PAN/NO_3 completely overwhelms the other peaks. Other absorptions for NO_3 include 830 cm^{-1} attributed to out-of-plane bending, 1045 cm^{-1}, attributed to symmetric stretching, and 1380 cm^{-1} attributed to asymmetric stretching. The relative intensity of the NO_3 absorption band at 1380 cm^{-1} decreases significantly after heating to 215 °C in air. The band at 1380 cm^{-1} almost completely disappears after heating to 325 °C.

The effect of treatment of PAN fibres with aqueous solutions of alkali metal sulphates on the chemical structure was investigated through FTIR (Bajaj et al. 1999). The changes in the chemical structure of the fibers have been noticed as a change in the intensity of characteristic infrared absorption bands. Broadening of the absorption band at 1700 cm^{-1} due to COO^- stretch was also noticed in the case of fibers treated with salts of alkali metals, probably because of formation of a COO^-M^+ structure.

FTIR with KBr discs, was used to characterize a PAN modified with sodium hydroxide, PANF, for adsorption of copper ions at an adsorbed content of 29.32 $mg.g^{-1}$ (Deng 2003). Since the C≡N bonds at the wavenumber 2246 cm^{-1} were not changed, it was deduced that the nitrile groups in the alkali

modified PAN were therefore not involved in the adsorption of copper ions. This is contradictory to the results found in this research and others reported (Bajaj et al. 1999).

The FTIR spectra for the PAN-VA/$CuNO_3$ films (as-cast) the normalized intensity of C≡N stretching at 2243 cm^{-1} is relatively constant, independent of the $CuNO_3$ content. This indicates that the nitrile groups in PAN-VA/$CuNO_3$ have'nt reacted in processing (Bajaj et al. 1998).

Copper–nitrile complex formation is indicated by the appearance of a band at 2300 cm^{-1} in the spectra for 4/1 and 2/1, the higher ratios of NO_3. The dominant NO_3 band in the $CuNO_3$ spectrum (1380 cm^{-1}) splits into two (1298 and 1489 cm^{-1}) in the PAN-VA/$CuNO_3$ spectra. The normalized intensities of these bands increase with the Cu salt content. The NO_3 splitting is related to a change in the NO_3 vibration caused by complex formation. (Silverstein et al. 2004).

FTIR analyses were carried out on copper gradient films on PAN precursor fibres with a Cu:CN ratio of 1:2 (Tang 1998). The formation of a complex between the copper ion and the nitrile was identified as shoulders at 2339.5 and 2191.0 cm^{-1} on the nitrile absorption at 2242 cm^{-1}. FTIR has been used on textile grade acrylic fibres for forensic studies to differentiate between different fibre suppliers (Causin 2005). A method was reported (Tungol 1993), also making use of the ratio between the FTIR signals at 2240 and 1730 cm^{-1} to determine the crystallinity of PAN fibres and an example is shown in Figure 2.19.

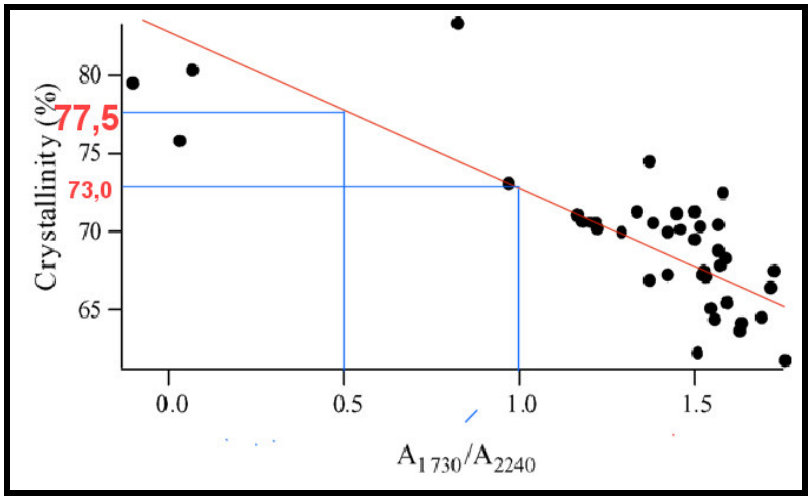

Figure 2.19 Relationship between the [A_{1730}/A_{2240}] and crystallinity of PAN (Causin 2005).

One of the aims was to investigate possible correlation between FTIR absorbance peaks and crystallinity. In the XRD the crystallinity was calculated by the ratio of the area of the crystalline peaks over the total area, after identification of the halo due to the amorphous regions.

No appreciable trend was found for [A_{1730} / A_{1370}] as a function of crystallinity. A rough correlation was identified between the degree of crystallinity and [A_{1730} / A_{2240}] as shown in Figure 2.19. The co-

monomer acts as a hindrance to the structural ordering of the polymer, so if its content, which is proportional to [A_{1730} / A_{2240}], is large, the chains will compose a less ordered framework.

Table 2.9 FTIR peak identification and integration for PAN research (Causin 2005)

Chemical Group	Wavenumber	Integration points
nitrile (-C≡N) from AN monomer	2240 cm^{-1}	2264 to 2220 cm^{-1}
C-H from AN monomer and co-monomer	1370 cm^{-1}	1390 to 1340 cm^{-1}
carbonyl (C=O) from co-monomers and additives	1730 cm^{-1}	1760 to 1700 cm^{-1}

2.3.4 Characterization of PAN by thermal analysis

2.3.4.1 Introduction

The thermal transitions and structure of PAN fibers have been characterized by several thermal analysis techniques including differential scanning calorimetry, DSC, thermal gravimetric analysis, TGA, and dynamic mechanical analysis, DMA.

2.3.4.2 Melting endotherm of PAN by DSC

DSC shows the presence of multiple endotherms indicating the existence of different structures, with the more stable forms, such as larger crystals, melting at the higher temperatures. Generally, any endotherm or exotherm is an indication of some structural change. PAN and its co-monomers at low co-monomer content degrade well below the Tm, because they undergo certain exothermic reactions leading to the formation of ladder structures.

Hinrichsen reported the melting of PAN polymers only at very rapid heating rates (i.e. 100 °C.min^{-1}). Frushour developed a new DSC method to melt and investigate the structure of PAN homopolymer and its fiber-forming copolymers. In this technique, the polymer is mixed with water and sealed in a gold coated sealed capsule that is heated in the DSC cell. Water acts as a plasticizing agent but causes hydrolysis of some of the CN groups. Melting is found to also be influenced by the molecular weight.

2.3.4.3 PAN glass transition temperature measurement

DMA measurements show, in general, two main transitions close to 100 and 150 °C, named by Minami as the α_{II} and α_{I} relaxations, respectively. The attribution of these transitions has not yet been entirely resolved (Rizzo et al. 1996b). Some authors claim the existence of two glass transition temperatures (Masson 1995).

A thermal transition, ascribed to the Tg, has also been shown by XRD measurements conducted at different temperatures. In particular, measurements at different temperatures of the XRD d-spacing of the main reflection of PAN (100) show that the thermal coefficient of lateral expansion of the

pseudohexagonal unit cell changes around 85 °C corresponding to the second order glass transition temperature.

2.3.4.4 PAN crystal-crystal transitions

It has been shown that gel films of UHMW PAN of 230 000 $g.mol^{-1}$ at-PAN are ultradrawable to a total draw ratio, (DRt), of <110-160 by a two-stage draw technique (Sawai 1998). The DRt is the product of draw ratios in the two stages. Such highly drawn samples show an extreme morphology, indicated by a high chain orientation function (fc) (0.996) and a high tensile modulus (28 GPa).

A first order thermal endothermic transition was clearly found at 142 to 150 °C on DSC heating scans only in ultradrawn samples of draw ratio >60 as shown in Figure 2.20. The observed reversible DSC transitions are like crystal / crystal transitions from orthorhombic to hexagonal chain packing at around 150 °C, as revealed by XRD equatorial reflections around $2\theta = 17°$ (Cu Kα radiation).

The relaxation and / or thermal transitions in this polymer have been extensively studied by several other techniques; DMA, dielectric measurements, FTIR, birefringence, and XRD. These studies report the existence of relaxations around 100 and 150 °C, which correspond to the molecular motion in (para)crystalline regions and that in non-crystalline regions (glass transition), respectively. However, no report has been published on any first-order thermal transition in cast or normally drawn at-PAN, studied by DSC.

Uniaxial drawing of iso-PAN, (isotactic triad fraction of 68%) and the resultant structure and tensile properties of drawn products were studied (Sawai 1999). The results were compared to those of at-PAN. Dried gel films prepared from 2 to 10 wt % solutions in DMF were initially drawn by solid-state co-extrusion (first-stage draw) to an extrusion draw ratio of 16, followed by a further tensile draw at 100 to 200 °C (second-stage draw). The results are shown in Figure 2.20.

The ductility of iso-PAN increased rapidly above 100 °C, due to the onset of molecular motion in the crystalline regions, as found by XRD at elevated temperatures. In contrast, the ductility of at-PAN increased above the first order crystal/crystal transition at around 150 °C.

Thus, the temperature for optimum second-stage draw of iso-PAN, 130 to 140 °C, was lower than that (160 to 180 °C) of at-PAN, reflecting their crystal softening temperatures. However, upon increasing the tensile stress on oriented fibers, the helical sequences progressively transform into a planar zigzag conformation, which shows a higher modulus.

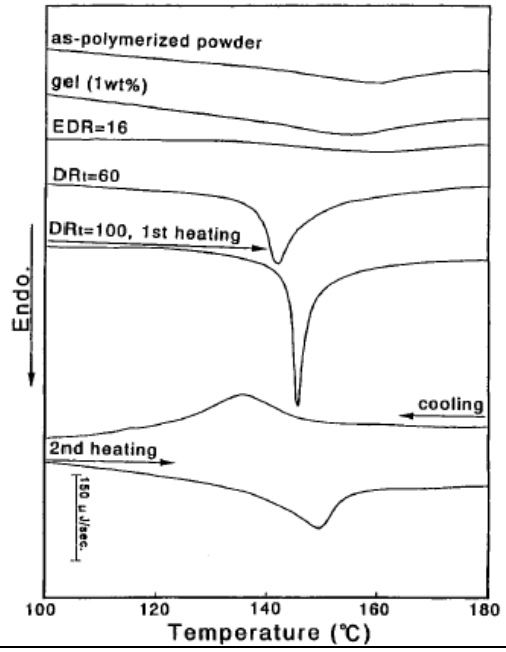

DSC thermograms for an as polymerized powder, gel film, extrudate with an EDR of 16 and ultra-drawn films with DR_t values of 60 and 100. Heating and cooling rates were 10°C/min.

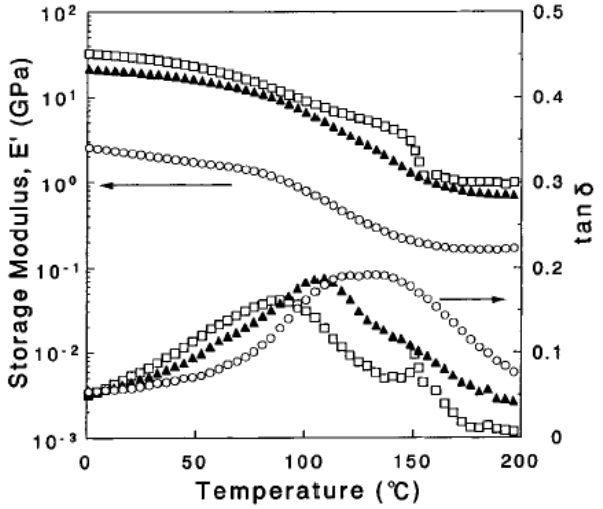

Dynamic storage modulus (E') and loss tangent (tan δ) vs temperature for at-PAN samples in the draw direction at 110 Hz. (O) original gel form, (▲) EDR 16, (□) DR_t of 100.

Figure 2.20 Thermal analysis results showing the PAN crystal-crystal transition (Sawai 1998).

2.3.4.5 PAN cyclisation transitions by DSC and TGA

During the heat treatment of PAN, the exothermic cyclization process starts in the amorphous phase; and, consequently, heat is liberated, causing the slow collapse of the ordered phase (i.e., the crystals), leading to the migration of AN units into the disordered (amorphous) phase. These AN units instantaneously undergo the formation of the ladder structure due to the exothermic cyclization reactions. If the PAN is heated at higher heating rates (80 ℃.min^{-1} or above), the temperature of the polymer very quickly reaches the Tm before the exothermic degradation reactions could approach the ordered phase from the disordered amorphous phase; thus melting of the polymer can be observed.

In a nitrogen atmosphere the DSC exotherm shows a very sharp peak, whereas, in an air atmosphere the DSC exotherm is broad, and starts at a much lower temperature compared to what is observed in nitrogen atmosphere (Grassie 1972). The initiation temperature of PAN homopolymer is higher than that for the copolymers. For instance, the initiation temperature of PAN in air is 244 ℃, whereas, the onset of the exothermic reaction is in the range of 172 to 218 ℃ for AN-VA copolymers (Bahrami et al. 2003).

IR absorptions at 1850 and 1780 cm^{-1} suggest the formation of intramolecular anhydride formation (Bahrami et al. 2003). Molecular propagation needs formation of an imide structure formed by isomerism. These chemical reactions are shown in Figure 2.21.

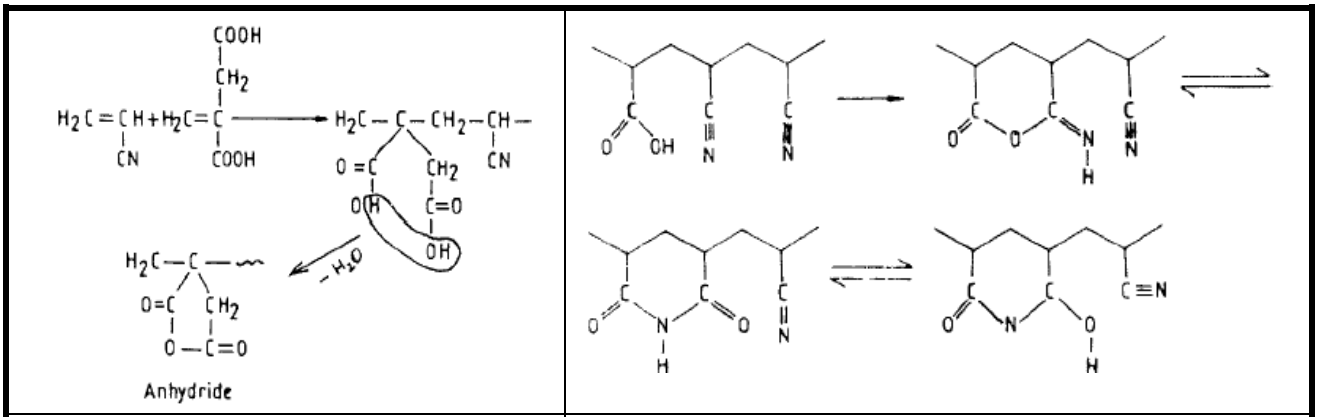

Anhydride formation from itaconic acid | Cyclisation of PAN copolymer, in N_2

Figure 2.21 PAN copolymer cyclisation chemical reactions (Bahrami et al. 2003).

As the vinyl acid content increases the ΔH value reduces. The ΔH value of PAN in air was 7025 $J.g^{-1}$, whereas, for P(AN-AA) with 5.51 mol% of acid it was 3798 $J.g^{-1}$. As the content of AA comonomer is increased to 17.51 mol% the value of ΔH decreases further to 1636 $J.g^{-1}$. The same trend was observed with MAA and IA as well. DSC-FTIR studies depict various chemical changes taking place during heat treatment of these copolymers.

The effect of stretching on the thermal behavior of acrylic fibers was investigated by DSC, TGA, and FTIR (Sen et al. 2003). In an air atmosphere, the peak temperature of the dynamic DSC thermogram was significantly lowered from 289 to 273 °C when the gel fibers were drawn to a draw ratio of 11.2. However, the initiation temperature was unchanged at 202 °C. The shoulder in the region of 310 to 380 °C was gradually converted to a sharp peak during the drawing process. However, the dynamic DSC in nitrogen atmosphere did not change in all cases. In air atmosphere the total heat liberated, of ΔH for gel fiber was 851 $J.g^{-1}$.

However, upon drawing to 11.2, ΔH increased to 1580 $J.g^{-1}$ showing an increase in the total chemical changes. An intimate relationship of chemical changes during the heating process was observed with FTIR of heated samples at various temperatures. The initiation of a DSC exotherm in air begins with nitrile cyclization, and subsequently dehydrogenation was initiated between 220 and 260 °C.

Increasing the temperature in the presence of oxygen, nitrile groups react slowly exothermally by cyclisation (Figure 2.22). This exothermal carbonization reaction yields a cross-linked polymer lattice, less flexible resulting in a fragile fibre, becoming dark yellow, orange, red, brown and eventually black and looses about 50% of its weight.

Generally at 120 to 130 °C the fibre looses the humidity and the finishing oil, between 130 and 230 °C gas is not released but the darkening process is started; at 260 and 400 °C, the maximum volatilization of gas

is achieved. The cyclisation of adjacent -C≡N with the formation of aromatic structures or partially hydrogenised rings starts between 250 and 300 °C, a second peak occurs between 350 and 400 °C.

At 1000°C, about 50% of the weight of the fibre is lost. With long heating (30 hours) at 200 °C a gas is formed that consists of 90% of NH_3, H_2, HCN (although in very low concentrations) and a HCN dimer, the remaining 10% are heavier products such as the monomer. The exothermic reaction of cyclisation is a relatively slow reaction, starts at 250 °C and has its maximum speed at 330 °C (Figure 2.22).

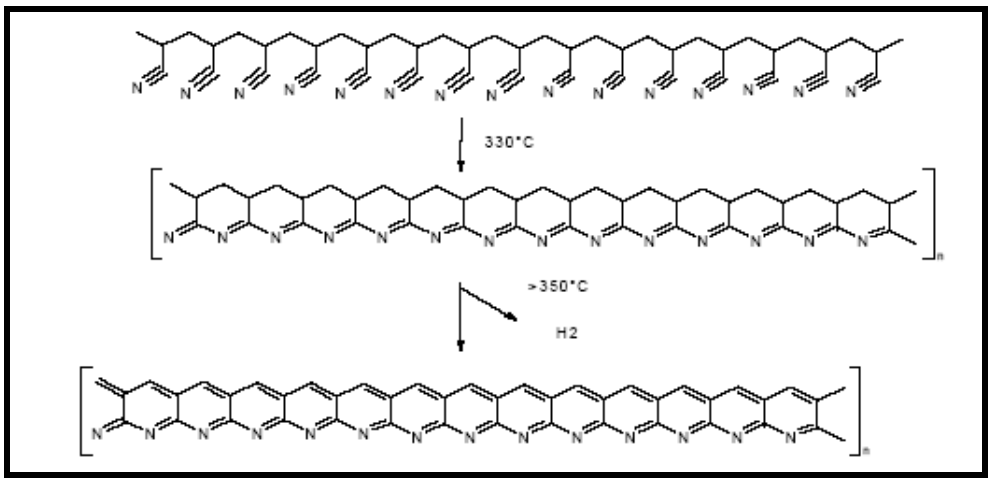

Figure 2.22 Intermediary stages for the cyclization and carbonization of homo PAN.

Thermal decomposition of polyacrylic acid, polyacrylamide, polyacrylonitrile, polymethylacrylate and polystyrene have been studied by thermogravimetry (Girdhar 1988). The order of thermal stabilities of these polymers is in accordance with the relative order of the electron-withdrawing power of the side groups on the hydrocarbon backbone of the repeat unit, i.e. the thermal stabilities of these polymers follow the order: CN > COOH > COOR > Ar > $CONH_2$.

2.3.4.6 Thermal conversion of PAN to carbon fibres

Infrared and NMR have been used to follow the thermal degradation of polyacrylonitrile. Infrared band assignments are made for the degraded material based on comparison with solid state ^{13}C NMR studies and elemental analysis (Fochler, 1985). Solid state ^{13}C NMR studies show that in addition to the previously proposed degradation by cyclization, degradation by unsaturation on the polymer backbone also takes place. When PAN was heat-treated to 250 °C under N_2 it lost weight and the infrared absorption at 2240 cm^{-1} disappeared, but there was little change in the atomic ratios of carbon, hydrogen, and nitrogen (Okamoto 1983). Indicating that fragmentation is accompanied by rapid polymerization of cyano groups. Tri-substituted C-C double bonds are formed in the six-membered rings. A new FTIR absorption band appears at 810 cm^{-1}, assigned to the C-H out-of-plane bending vibration in such a double bond.

A PAN fibre, Dralon-T® and a carbon fibre precursor copolymer were studied after heat-treatment in air at various temperatures up to 300 °C (Dalton 1999). XRD was undertaken on single fibres, fibre bundles and films, utilizing both conventional and synchrotron sources. With a conventional source, the normal XRD pattern was observed for both polymers, i.e. two main equatorial reflections, a diffuse equatorial reflection and a diffuse off equatorial reflection. With a synchrotron source, seven equatorial XRD reflections are detected in the homopolymer PAN fibre. Also, a sharp, meridional reflection is observed in the copolymer as received and in the homopolymer after stretching at 100 °C.

Unpolarized and polarized FTIR spectra were obtained from single fibres and films by FTIR microscopy. A measure of the extent of reaction (EOR) following heat-treatment was derived from the intensity of the nitrile absorption, (I_{CN}) and the intensity of absorption at 1600 cm^{-1} (EOR= I_{CN}[-1600/(I_{CN}1600)]). Two complementary measures of orientation were used to follow changes on heat-treatment: the peak width at half-height of an azimuthal plot of the most intense XRD reflection and the nitrile dichroic ratio from FTIR microscopy. For fibres held under tension during heat-treatment, the degree of orientation by either measure did not decrease until the EOR exceeded 0.5. Solid-state ^{13}C NMR, together with IR results, indicated that at least three chemical processes occurred on heat-treatment: nitrile cyclisation, conjugated C=C formation and oxidation.

Conditions for manufacturing a new generation of precursor PAN fibres containing nanosilica have been developed (Mikolajczyk 2005). The fibres show an increased porosity and a tenacity that is suitable for the carbonisation process. The control of parameters of the fibre-spinning process makes it possible to obtain precursor PAN fibres containing nanosilica with either an increased tenacity of 25 $cN.tex^{-1}$ and considerably lower porosity, or with an increased porosity, beneficial distribution of pores and a tenacity of 16 $cN.tex^{-1}$ that is at the limit of processing into carbon fibres.

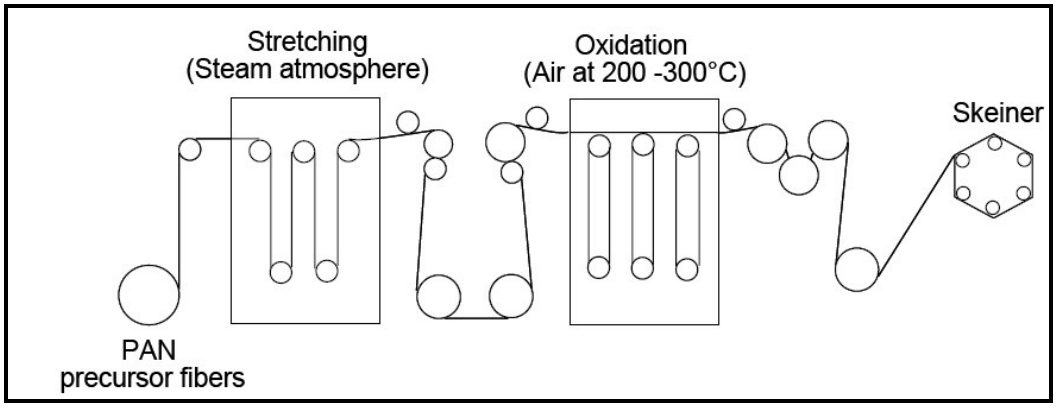

Figure 2.23 Commercial PAN oxidation oven (Lam, 2004)**.**

The addition of nanosilica into spinning solutions changes their coagulation capabilities, and decreases the deformability of the fibre-forming polymer during the plasticising drawing stage. A typical PAN oxidation processing oven is shown in Figure 2.23.

2.3.5 Characterization of PAN by XRD

2.3.5.1 Introduction to XRD theory related to polymer crystallinity and orientation analyses

The graphic in Figure 2.24 is used to explain the use of wide angle X-ray Diffractometry, (WAXD or XRD) in determining polymer crystallinity and orientation (Hearle 2002). *A* perfectly crystalline, perfectly oriented fiber would give a XRD pattern of the form shown in Figure 2.24 A (a). The symmetry of crystals oriented parallel to a single axial direction, but with random orientation around this axis, leads to the reflections from particular lattice spacings appearing on lines with the separate orders at increasing distance from the meridian.

Real textile fibers give patterns of the form indicated in Figure 2.24 B (a). The first-order reflections are easily seen, but higher orders are usually very faint. The sharp spots are diffused, and more general scattering occurs in the form of a halo from disordered material. In Figure 2.24 (b) and (c) is illustrated how quantitative parameters can be determined roughly, but much more detailed analysis is needed to obtain precise measures, including the size, shape, and perfection of the crystals and statistical features of the amorphous material.

The relation between various features of the XRD pattern and structure is as follows:

1. Location of spots: size and shape of unit cell; arrangement of atoms in crystal lattice
2. Radial broadening of spots: increasing with reduced size and perfection of crystals
3. Circumferential spread into arcs: decreasing orientation of crystals
4. Ratio of sharp spots to diffuse scattering: degree of crystallinity

In textile fibres the polymer chains are always orientated parallel to the fibre axis so that the tensile forces lie along the covalent bonds of the polymer chains (Hearle 2002).

d spacing is calculated using the Bragg equation: $\sin\theta = n\lambda / 2d$ (1)

L is calculated using the Scherrer equation: $L = 0{,}89\,\lambda / (B\cos\theta)$ (2)

Where:

B is the full width (as a function of the scattering angle 2θ in radians) at half maximum of the (110) reflection. The coherence length is often called the crystal size, because small crystal size is a major contribution to peak broadening. *L* is a measure of packing perfection. The coherence length depends on the co-monomer composition and on thermal annealing which is accomplished during the commercial

fiber production by passing the fibers over heated rolls or annealing cast films. *L* also indicates the degree of fiber orientation.

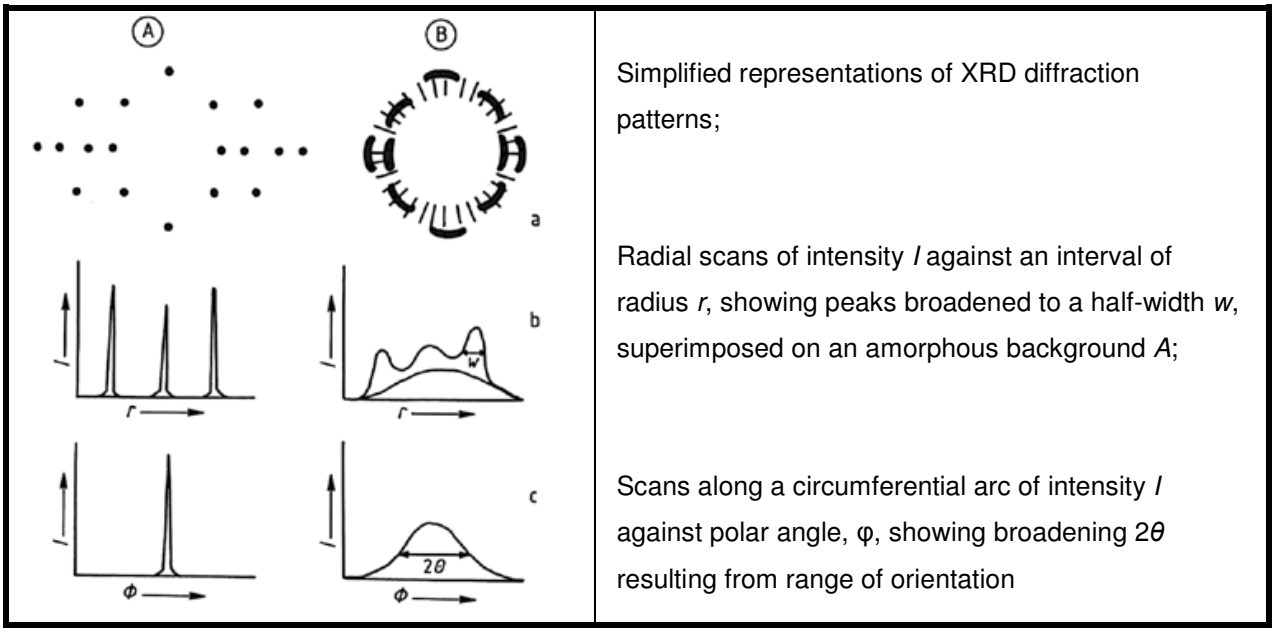

Simplified representations of XRD diffraction patterns;

Radial scans of intensity *I* against an interval of radius *r*, showing peaks broadened to a half-width *w*, superimposed on an amorphous background *A*;

Scans along a circumferential arc of intensity *I* against polar angle, φ, showing broadening 2*θ* resulting from range of orientation

Figure 2.24 Graphic explanation XRD spectra of fibres (Hearle 2002).

Two important morphological features can be determined from the sharpness of the reflections. First, scanning the peak along the equatorial (Figure 2.24 (b)), the width of the peak measures the coherence length. The coherence length depends strongly on the co-monomer composition and more weakly on thermal annealing (which was accomplished during fiber production by passing the fibers over heated rolls) and/or the degree of fiber orientation.

Through analysis of the shape and intensity of the primary (10) reflection, the molecular orientation and coherence length can be determined By convention the 4 Miller indices (*hkil*) are used for identification of planes in hexagonal crystals (Hearle 2002).

$i = -(h + k)$ and is therefore normally omitted.

- For 2D structures such as PAN , index $i = 0$.
- Therefore planes are identified using only indices h and k

The molecular orientation can be calculated from the distribution of intensity as a function of the azimuthal angle i.e. at a fixed distance from the center of the pattern.

Second, azimuthal scans of the intensity of the (10) reflection (Figure 2.24 c) are used to measure the degree of molecular orientation in the fiber, through the application of Equation (2). A linear relationship between the orientational order parameter from XRD and the birefringence has been observed. Extrapolation of the line on a graph of the orientation order parameter and the birefringence to the unit order parameter, the maximum birefringence, (Δn_{max}) of PAN copolymers has been estimated to

be = 0:007, which is weak in comparison to poly(ethylene terephthalate), for example. A relatively small value is to be expected, because the highly polarizable CN groups are oriented nearly perpendicular to the backbone direction, so that the horizontal and vertical orientation of the side groups and the backbone nearly compensate one another.

Digital collection of data and computational analysis increase the useful information which can be generated. The use of intense synchrotron sources of X-rays enables information to be obtained in much shorter times and allows dynamic studies of structure development in a thread spinning line to be performed.

If the XRD patterns of PET and an acrylic fibre are compared: the PET has both the equatorial and off-equatorial which are indicative of 3-dimensional order while PAN has only the 2 equatorial positions. The primary reflection (10) has a *d*-spacing of approximately 5.3 Å, and the weaker (11) reflection is at approximately 3.05 Å. Although, there are slight variations in the lattice parameter as a function of co-monomer ratio and drawing condition, the ratio of the *d*-spacing of the two peaks remains $\sqrt{3}$: 1 within experimental accuracy, indicating hexagonal packing.

The diameter of the chain is: $(2 \times \sqrt{3})d_{(10)}$ = 6,1 Å. The lack of a meridional reflection indicates the lack of regularity along the chain, as expected from the 2D nature of the “crystalline” phase. Results show that oriented copolymer PAN fibers do not exhibit a significant amount of amorphous phase. Values of the coherence length range from 40 Å for poorly oriented material containing 25% comonomer, to 145 Å for a more highly oriented fiber containing only 15% co-monomer. Post-drawing gives an increase in the coherence length calculated from the XRD.

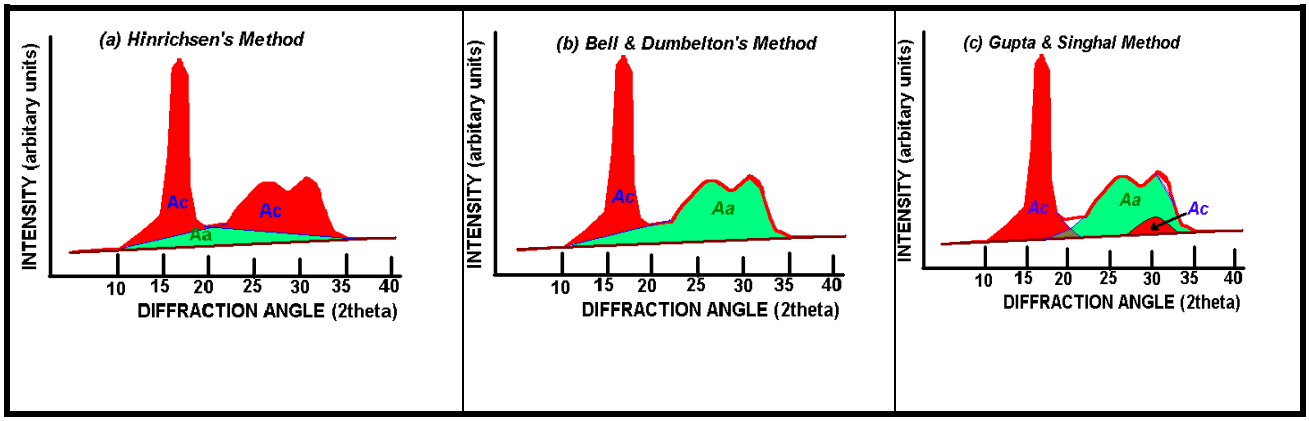

Figure 2.25 XRD data interpretation of crystalline / amorphous contributions (Masson 1995).

XRD of PAN interpretation is also a matter of contention and 3 theories are given in Figure 2.25.

2.3.5.2 XRD characterisation of PAN by other researchers

Several papers discuss packing and chain conformation in the paracrystalline phase of PAN. It is well established that PAN, although substantially atactic, with a distribution of triads and pentads following Bernoullian statistics, is able to crystallize. Configurationally disordered chains generate highly disordered crystals. XRD measurements for a highly oriented PAN fiber suggest the presence, in the pseudo-hexagonal form of PAN, of sequences with an average periodicity close to 2.4 Å (Rizzo 1996a). This is in qualitative agreement with the mean periodicity anticipated by the knowledge of lateral spacing of the pseudo-hexagonal cell and of the experimental density value.

The Fourier transforms of these minimum energy extended model chains have been calculated and compared to the experimental XRD data. This indicated that the paracrystalline pseudohexagonal phase of PAN is formed by elongated atactic chain stretches. The backbone dihedral angles of these atactic stretches in the minimum energy conformation assume values close to 180°, corresponding to r diads, but may present also large deviations from 180°, corresponding to *m* diads. Where deviations occur, the length of the projection along the chain axis of the vector connecting the centers of consecutive monomeric units is shorter than 2.5 Å and close to 2.3 Å, giving a mean chain periodicity in a good agreement with the experimental value.

As far as the mean chain periodicity and conformation of PAN molecules in the pseudo-hexagonal phase are concerned, some indications come from density data. In fact, the measured densities of conventional PAN samples are in the range 1.17 to 1.22 $g.cm^{-3}$. It is reported by Lindenmeyer and Hosemann that small variations in density are observed when crystallization occurs under a variety of conditions. From the knowledge of the lateral packing of chains, the distance between the axes of first neighboring chains can be calculated as being equal to 6.0 Å. One can calculate that the distance along the c direction per monomeric unit must be 2.31 Å.

Liu and Ruland, to reconcile the results of the XRD studies with the tacticity and density measurements, suggested that, while short isotactic sequences could be accommodated as well in the planar zigzag conformation, long isotactic sequences would reduce the intramolecular energy by kink formation. These kinks would shorten the chains while their trans planar portions were kept parallel (but not co-axial) on both sides of the defect. The presence of about 1 kink per 10 monomeric units would increase the density to the experimental value.

A detailed XRD study (Minagawa et al. 2001) was carried out for a series of stereoregular PANs having different isotacticities (25% to 83%). The degree of crystallinity did not depend on the extent of their isotacticity, in contrast to what has been reported previously. The main peak shifted from 17.1 to 16.8°, and the half value width of the main peak decreased (1.70 to 0.97°) with an increase in stereoregularity.

Drastic XRD changes were observed when PAN was dissolved in a good solvent and recovered. It is concluded that the crystallinity of the PAN powder does not depend on the extent of stereoregularity, although its inherent value, depending on the XRD evaluation procedures, ranges from 40% to 70%.

In Figure 2.26 the amorphous halo is coloured blue. All remaining areas are due to crystalline diffraction peaks. In Figure 2.26 the tacticity–crystallinity relationship in iso-PAN fibres is shown. It is seen that the crystallinity is independent of the degree of isotacticity. For other fibres such as isotactic polypropylene there is a direct relationship between the tacticity and the crystallinity, where for a 100% isotactic polypropylene fibre a crystallinity of > 75% has been identified.

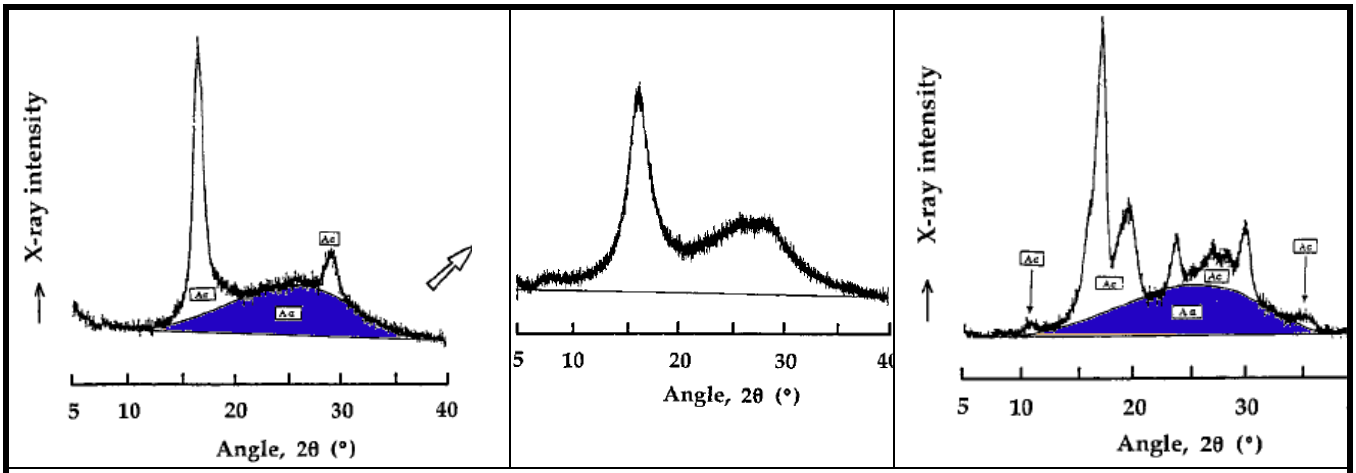

Definition of the crystallinity and comparison of XRD between powder and crystalline. Left iso-PAN (C-1 powder). Middle; recovered PAN(C-1/powder) from DMSO solution. Right Iso-PAN (C-1/crystallites) . The degrees of crystallinity of these samples were about 42, 40 and 55% respectively.

Figure 2.26 XRD of crystallinity for isotactic PAN powder and film (Minagawa et al. 2001).

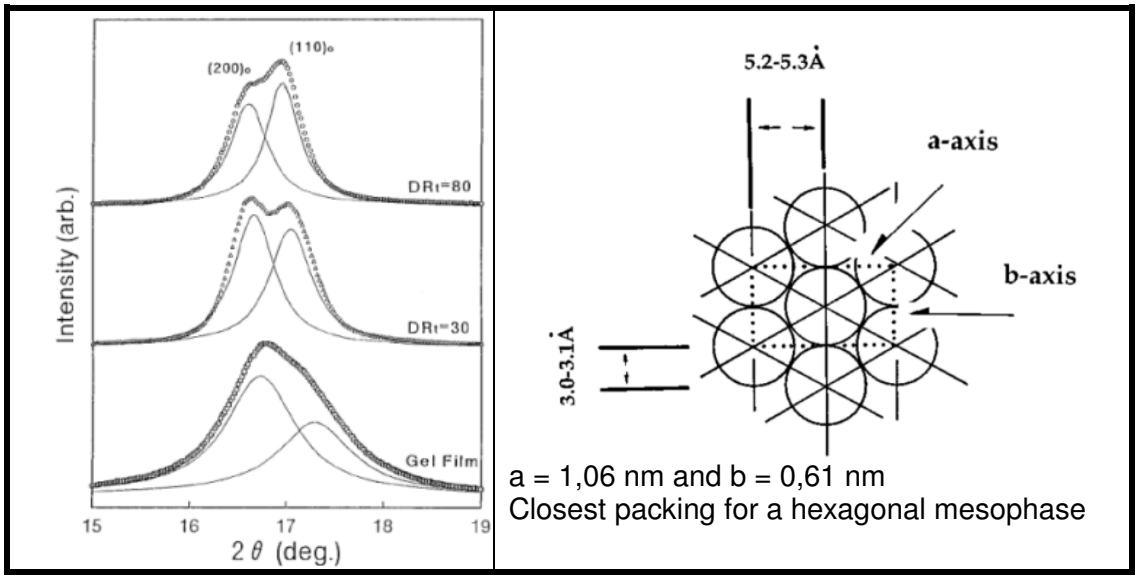

Figure 2.27 Equatorial peak deconvolution in *iso*-PAN fibres (Yamane et al. 1997) **and Geometrical considerations for molecular packing of rodlike PAN chains** (Minagawa et al. 2001).

2.3.6 Characterization of PAN by NMR and ESR

An analytical technique used to a small extent to obtain information on fibres is nuclear magnetic resonance spectroscopy, NMR. Statton in 1975 pioneered the use of wide-line NMR, which relates to mobility of molecular segments within a fiber structure (Hearle, 2002).

Chemical shift anisotropy, (CSA) has been used to determine the molecular orientation in deformed PTFE and in biaxially drawn films of poly(ethylene terephthalate) (Koenig 1999). The cp-MAS experiment has been used on various polymer fibres i.e. PET, nylon and polypropylene to determine the degree of molecular orientation.

The use of solid state NMR has increased in many fields of research. Compared to high-resolution liquid NMR, there are certain complications including strong dipole-dipole couplings and chemical shift anisotropy. However, solid state NMR has several advantages. The dipolar coupling which is averaged out in liquids due to molecular motion is active in the solid state and can be used to deduce distances within one molecule or between adjacent molecules.

In recent years, there have been major improvements in solid state NMR analytical techniques. The effects of line broadening have been diminished by a combination of multiple pulse sequences (also used as filter techniques) and fast magic angle spinning, MAS. New MAS rotors are capable of spinning speeds of up to 35 kHz improving resolution even in strongly coupled systems like ^{1}H. Certain multiple-quantum NMR techniques were developed to reduce the strong quadru-polar broadening.

Electron paramagnetic resonance spectroscopy, EPR, also called electron spin, resonance spectroscopy, ESR, is one the few methods that can characterize structural features in the range between 0.5 and 5 nm in systems that lack long-range order (Jeschke 2002). Approaches based on EPR provide good structural contrast even in complex materials, as the sites of interest can be selectively labeled or addressed by suitably functionalized spin probes using well-established techniques.

ESR is a spectroscopic technique which detects species that have unpaired electrons, generally meaning that it must be a free radical if it is an organic molecule, or that it has transition metal ions if it is an inorganic complex. Since most stable molecules have a closed-shell configuration without a suitable unpaired spin, the technique is less widely used than NMR.

The basic physical concepts of the technique are analogous to those of NMR, but instead of the spins of the atom's nuclei, electron spins are excited. Because of the difference in mass between nuclei and electrons, weaker magnetic fields and higher frequencies are used, compared to NMR. For electrons in a magnetic field of 0.3 Tesla, spin resonance occurs at around 10 GHz.

A review article (Jeschke 2001) assesses the EPR experiments available for distance measurements on nanoscales in terms of the accessible distance range, precision, and sensitivity. Recommendations are derived for the proper choice of experiment for a given problem. Both simple and sophisticated methods for data analysis are described and their limitations are evaluated. Applications to the study of polymer chain conformation and the structure of ionically functionalized diblock copolymers are highlighted.

A combination of EPR and orientation-selective pulse ENDOR methods provides enough constraints to characterize the structure of the metal centre in the copper(II) complex of poly(4-vinylpyridine). The structure derives from a propeller structure of the tetrapyridino copper(II) complex in pyridine glass determined by the same methods.

It features more disorder with respect to the angle between the pyridine ring and complex plane but only moderate tetrahedral distortion. The enhanced resolution of high-field EPR allows one to detect another metal centre at higher copper loading of the polymer that probably involves only three pyridyl side group ligands.

2.3.7 The effect of the solvent on PAN structure

The solvent casting effect on the infrared characteristic absorption bands of stereoregular isotactic PAN film was studied in comparison with those of an atactic sample (Minagawa et al. 1997), and is also discussed in Section 2.3.3. A linear relationship between the intensity ratio of the FTIR bands and the dissolution power of nine different kinds of dipolar organic solvents was found. The IR characteristic bands of stereoregular PAN were dependent on not only configuration but also conformation through the difference of the molecular cohesion state in the solvent-cast film. The effect of configuration and conformation on the IR results was quantitatively studied as a function of the film preparation conditions.

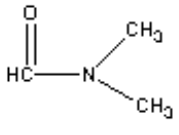	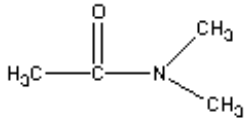	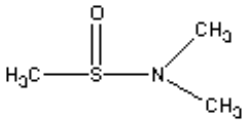
Dimethylformamide, DMF	Dimethylacetamide, DMAC	Dimethyl sulphoxide, DMSO
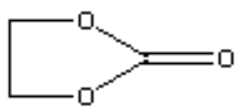	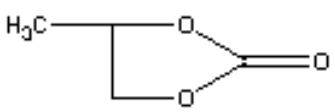	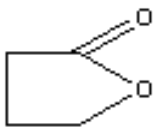
Ethylene carbonate, EC	Propylene carbonate, PC	Butyrolactone, BL

Figure 2.28 Chemical structures of some typical PAN solvents.

The physical and mechanical properties of the fiber are affected by several parameters; one parameter is coagulation conditions: bath temperature, bath composition, and drawing (Bahrami et al. 2003). The coagulation process of PAN wet-spinning was modeled and simulated based on the numerical analysis of the coagulation of a viscous polymer solution by diffusional interchange with a bath (Cheon 1996).

Acrylonitrile–carboxylic acid copolymers were converted into fibers using the dry-jet wet spinning technique and the properties of the fibers were investigated. The effect of the final drawing ratios (6.5 and 8.5) on such physical and mechanical properties were also investigated. The high intensity of the (110) diffraction is known to be associated with the preferential positioning of the nitrile group. As the coagulation bath temperature increased, two equatorial reflections became broad and more diffused, indicating a reduction in crystallinity and crystal size. Arcs in the equatorial direction also broadened as the coagulation temperature was increased; indicative of a reduction in the crystallite orientation.

The crystallisation behaviour on cooling of concentrated solutions of PAN in two organic solvents, butyrolactone and ethylene carbonate, was investigated (Bashir 2003). XRD showed that the peaks from the solvent-containing gel films were different from those in the dry PAN powder. Polarised-IR spectroscopy on uniaxially drawn gel films indicated not only preferential orientation of the nitriles perpendicular to the draw direction but also orientation of the residual solvent in such a way as to suggest pairing of the g-butyrolactone or ethylene carbonate molecules with the nitriles on the chains. The diffractograms of the gels may be due to the formation of polymer-solvent complexes during crystallisation of PAN from solvents with carbonyl groups. DSC showed gel-melting endotherms on heating and crystallisation exotherms on cooling.

An approach is proposed to understanding the nature of chromaticity of PAN solutions thermally treated at 140 ℃ in dimethylformamide (DMF) (and films), which is based on the idea of complexes forming between molecules of the basic solvent and the polymer functional groups modified by the solvent (Platonova & Klimenko 1993). Manifestation of these structures is registered in electronic spectra as absorption bands within the visible wave band. .

An H_2O / dimethyl sulfoxide (DMSO) mixture was used as the coagulation bath of the wet-spun process for PAN fibers (Hou et al. 2005). Diffusion behaviors of coagulate and solvent of the proto-fibers was studied. It was found that diffusion coefficients of H_2O and DMSO in the proto-fibers prepared by AN homopolymers, are higher in solution polymerization than in suspension polymerization.

2.3.8 Influence of metal ions on structure and properties of acrylic fibres

The introduction to PAN of certain inorganic salts i.e. $AgNO_3$, $Cr(OCOCH_2)_2$, $K_2Cr_2O_7$, $Pb(OCOCH_2)_2$ into the fibres make them suitable as antimicrobial fibres for air sterilization, thermostable bag filter fibres,

catalysts for carbon production and as radiation protection fibres respectively (Bajaj et al. 1998). Conductive fibres have been produced through surface modification with nitrogen, copper of sulphur containing compounds. The effect of the inorganic salts on the thermo-oxidative stabilization has also been reported. It has been shown that NaCl, $CuCl_2$ and $AlCl_3$ increase the total gas evolution during oxidation. Carbon fibre precursors are modified with transition metal salts to improve structural perfection and properties of the resultant carbon fibres.

The acrylic fibers containing 10.8 wt% of acrylic acid as a comonomer were treated with 5% aqueous solution of sulphates of alkali metals (Na^+ and K^+) and transition metals (Co^{3+} and Ni^{3+}) at 90°C for 5 minutes (Bajaj et al 1998). The effect of this treatment on the chemical structure, thermal behavior and mechanical properties of this fiber was investigated through FTIR, X-ray, DSC, and TGA techniques. The changes in the chemical structure of the fibers have been noticed as a change in the intensity of characteristic infrared absorption bands. Broadening of the absorption band at 1700 cm^{-1} due to COO^- stretch was also noticed, as in Figure 2.28, in the case of fibers treated with salts of alkali metals, probably because of formation of a $COO^{-}M^+$ structure.

XRD studies of the fibers treated with metal salts showed a decrease in the crystallinity of the treated fibers. DSC curves of metalated fibers showed the onset of exothermic cyclization at a higher temperature. The initial modulus of the samples increased after this treatment. The fibers treated with sulphates of alkali metals showed an approximately twofold increase in elongation at break compared to the untreated ones. A further investigation on the effect of metal salt complexes on PAN fibres structure was published in 1999 by the same research group in India and the reaction scheme is shown in Figure 2.29 (Bajaj 1999).

The effect of the addition of metal salts in poly(acrylonitrile– acrylic acid) copolymer, PAN-AA, on the thermal and rheological behavior was reported. Incorporation of $CuSO_4$, $FeSO_4$, $ZnSO_4$, and $Al_2(SO_4)_3$ (1 to 5 wt%) salt in the polymer solution affects its solubility in DMF. The complexes of PAN-AA with $ZnSO_4$, took a longer time to dissolve in DMF, whereas the complexes with $Fe(SO_4)$ and $Al_2(SO_4)_3$ were almost insoluble in DMF, perhaps due to intermolecular ionic crosslinking. Addition of these metal salts to the PAN solution also affects its Brookfield viscosity. FTIR spectra show the participation of both COOH and CN groups in the complex formation, which is responsible for the enhanced Brookfield viscosity. Thermal behavior of the polymer–metal salt complex showed that these salts also affect the exothermic reaction. The initiation of the cyclization reaction takes place at a lower temperature compared to neat PAN-AA copolymer. However, the heat liberated per unit time in an N_2 atmosphere in case of neat polymer is 6.3 $J.g^{-1}.min^{-1}$, which reduces to 5.5 $J.g^{-1}.min^{-1}$ in the case of the PAN-AA/Al complex, confirming the role of $Al_2(SO_4)_3$ in retarding the rate of cyclization reaction.

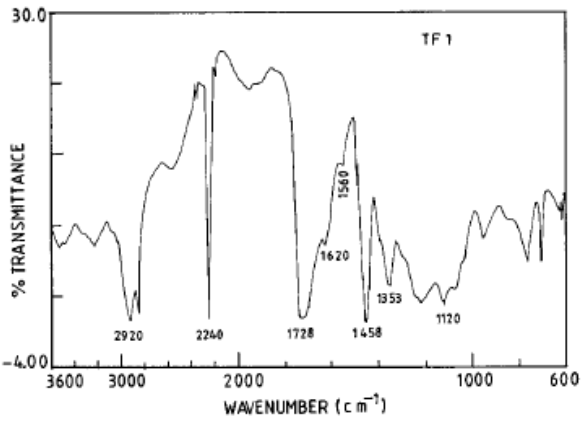

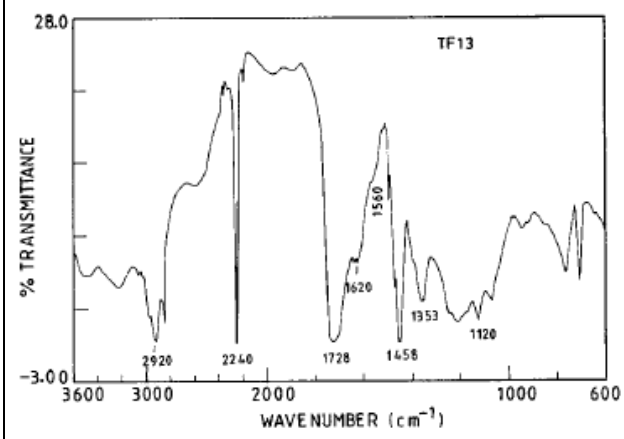

Relative Intensities of various IR absorption bands In treated and untreated PAN fibers

Fiber	I_{1720}/I_{2240}	I_{1620}/I_{2240}	I_{1590}/I_{2240}
TF1	0.90	0.56	0.21
TF11	0.82	0.56	0.51
TF12	0.75	0.50	0.43
TF13	0.94	0.57	0.22
TF14	0.96	0.54	0.28

TF1 is a copolymer PAN AN:AA = 89,2:10,8

TF11 and TF12 are treated with alkali metal salts Na and K.

TF13 and TF14 are treated with transition metal salts, Ni and Cu.

Figure 2.29 Effects of metal salts on PAN FTIR spectra (Bajaj et al. 1998).

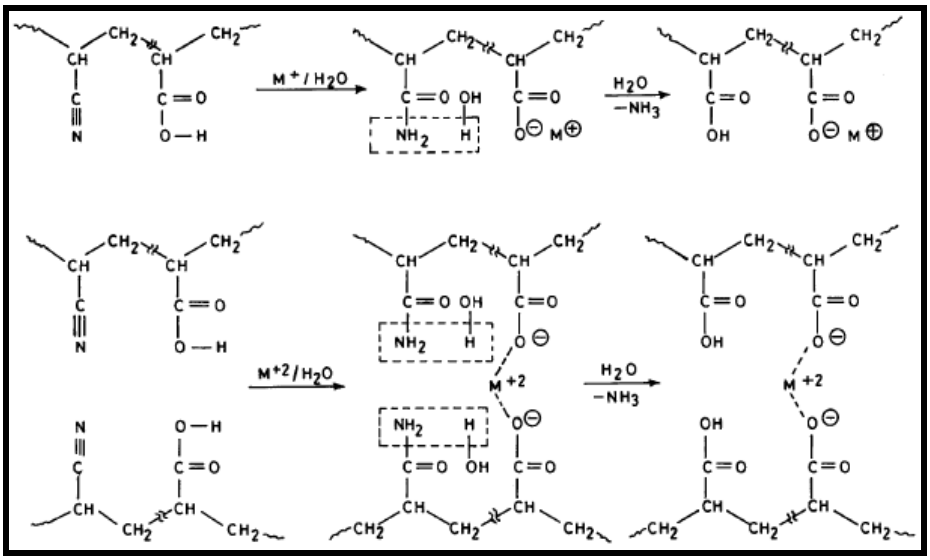

Figure 2.30 Reaction scheme PAN treatment with aqueous metal ions (Bajaj et al. 1999).

The pyrolysis of polymers containing metal nitrates may provide a relatively simple, rapid, and advantageous method of producing high-temperature superconductors (Silverstein et al. 2004). The advantage lies in the ability to use conventional polymer processing or micro-lithographic patterning before pyrolysis. Complex formation with the polar acrylonitrile groups was expected to enhance atomic-

level mixing and hinder nitrate recrystallization. PAN-VA containing $CuNO_3$, exhibited complex formation and an exothermic decomposition that began at about 170 °C. For a PAN-VA/$CuNO_3$ ratio of 2:1, there was no nitrile cyclization, and the thermo-oxidative degradation temperature was reduced by approximately 200 °C.

Adsorption of PAN and its copolymers with PAN-AA, at a copper surface and kinetics of copper dissolving in the presence of carboxyl-containing polymers and hydrogen peroxide have been investigated. The adsorption of polymers at the surface of the copper powder passes through a maximum when the content of acrylonitrile in copolymers rises (Kislenko & Verlinskaya 2003). The rate at which copper dissolves increases with increased polymer concentration in solution, reaches a constant value, and does not depend on the hydrogen peroxide concentration.

Silica coated with PAN and heated at 200 °C for 8 hours to stabilize the PAN by forming a fused ring structure, was used as support for copper catalysts (Liu & Hongxiao 2001).

A method to improve the durability of electrically conductive polyacrylonitrile (PAN) fibers treated with the Cu_xS method was developed (Cui et al. 1999). The durability of the electrically conductive fiber increased. This is attributed to the swelling and etching effects of the activator as well as the formation of uniform, thick, and compact conductive layers with copper sulfide treatment.

The ionic and electronic conductivities of pure PAN films and of PAN films which contained salts of copper have been investigated (Galer & Hudson 1994). The conductivities in both types of film (10^{-8} $S.cm^{-1}$ and 10^{-3} $S.cm^{-1}$, respectively) were predominantly due to ionic species. PAN films which possessed pendant amino moieties were treated with reducing copper-and sulphur-containing solutions to obtain films with surface electronic conductivities as high as 10^{-3} $S.cm^{-1}$.

2.3.9 PAN with metal salts for use as solid electrolytes

Combinations of the components of the PAN-based electrolytes have been studied by Raman, FTIR, fluorescence, XPS, and NMR spectroscopy (Wang 1999). It was found that the mixed-phase polymer electrolytes are not simple mixtures of electrolytic salt, plasticizer and polymer. There are strong interactions between each two of the components of the electrolytes and strong competition between plasticizer and PAN to associate with Li^+ ions though different systems.

Impedance studies on polyacrylonitrile–CuX_2–DMSO (X=Cl, Br, CF_3SO_3) solid polymer electrolyte were conducted, (Lewandowski 2000). Foils were prepared by solution casting. The conductivity increased with an increase of the salt content up to 8 wt%; at higher concentrations (>8 wt%) the conductivity is more or less stable, and reaches, for $Cu(CF_3SO_3)_2$ and $CuCl_2$, the level of 10^{-3} Ω^{-1} cm^{-1} at room

temperature. The foils based on the $CuBr_2$ show even higher conductivity, close to 10^{-2} Ω^{-1} cm^{-1} at room temperature, comparable to liquid solutions.

The use of a plasticizer for solid polymer electrolytes, in the form of a cascade nitrile compound ($[CH_2N(CH_2CH_2CN)_2]_2$, made by addition of acrylonitrile to alkyldiamine (1,2-diaminoethane), has been studied (Tsutsumi & Kitagawa 2001). Interaction between the compound and Li^+ ions in the complex was confirmed by FTIR. The nitrile group peak shifted to the high-energy side. The shift indicated that the nitrile groups interacted with the Li^+ in the electrolytes. Conductivity enhancement was observed in the PAN-based electrolytes containing the nitrile compound.

2.3.10 PAN modified for absorption studies and applications

Polyacrylonitrile fiber was hydrolyzed in a solution of sodium hydroxide and the hydrolyzed PAN fiber was used as an adsorbent to remove copper ions from aqueous solution (Deng et al. 2003). FTIR spectroscopy revealed that the modified PAN contained conjugated imine (–C=N–) sequences. Batch adsorption results indicated that the fibre was very effective in adsorbing copper. FTIR analysis indicated that copper adsorption caused a decrease of the light adsorption intensity of the imine (–C=N–) groups at 1573 and 1406 cm^{-1} wavenumbers. Complexation of Pt in sorption of $PtCl_6$ complex by fibrous PAN-based sorbent modified with thiosemicarbazide was studied (Simanova 1998).

2.3.11 Coating of PAN films and fibres

PAN fibres coated with titania were produced and UV-Vis spectroscopy showed this provided excellent UV protection. The fibers with anatase coatings showed a high photocatalytic property and better repetition on photodegradation (Liuxue 2006).

Deposition of Fe and Ni onto the nitrile-terminated self-assembled monolayer, CN-SAM resulted in the production of metal–nitrogen bonds (Wagner et al. 2003). In contrast, Cu exhibited little or no reactivity and failed to activate C≡N bond cleavage.

Thermal evaporation of iron and nickel on a CN-SAM lead to the production of new Fe–N and Ni–N bonds, respectively, while the nitrile group remained intact during the vapor deposition of either Cu or Au atoms. The metal reactivity trend is governed by the strength of new bonds (e.g. metal–nitrogen bonds) that can form during metallization.

2.3.12 Copper complex and nanoparticle chemistry

Copper forms compounds in the oxidation states of +1 (cuprous) and +2 (cupric). The relatively small change in electrochemical potential between the cuprous and cupric ions in solution gives the

usefulness of copper compounds in chemical reactions. Copper compounds are used as catalysts in reactions, especially oxidation (cupric chloride) and heterogeneous reactions.

The description and applications of copper compounds used in this study are (Richardson 2002);

- Cupric Acetate (Copper Acetate), $Cu(C_2H_3O_2)_2 \cdot H_2O$, blue to green crystals which are soluble in water; used to make organic reaction catalyst; textile dyeing; and as a fungicide.

- Cupric Chloride (Copper (II) chloride), $CuCl_2$, yellowish to brown, deliquescent powder soluble in water, alcohol, DMF, DMAc and ammonium chloride is used as in dyeing and printing textile fabrics and in the refining of copper, gold, and silver. Dilute solutions of copper(II) chloride are blue. As the chloride concentration increases, the color of the solution shifts toward green, intensifying as the concentration of the distorted tetrahedral $[CuCl_4]^{2-}$ ion increases. Copper(II) compounds have been isolated that contain either the $[CuCl_4]^{2-}$ anion or the $[CuCl_3]^{-}$ anion, e.g., $CsCuCl_4$ and $KCuCl_3$, respectively, and also in ammonia .

- Cuprous Chloride (Copper Chloride) CuCl or Cu_2Cl_2, green, tetrahedral crystals which are insoluble in water and are used as a heat and light stabilizer for nylon and as a catalyst for chemical synthesis. The diamine complex is favored. Insoluble copper (I) chloride, CuCl can be solubilized by chloride-containing solutions, with the formation of the $[CuCl_2]^{-}$ ion.

- Cupric Oxide (Copper Oxide) CuO, black, monoclinic crystals which are insoluble in water are used in making fibers and ceramics, in organic and gas analyses, catalyst, fungicide, antiseptic; red pigment for glass, ceramics; antifouling agent applications.

- Copper(II) nitrate tri-hydrate, $Cu(NO_3)_2 \cdot 3H_2O$, is a blue, deliquescent salt. It is soluble in water and ethanol. Conversion to copper (II) oxide is complete at 180 °C.

- Copper sulfate is the common name for the blue crystalline cupric sulfate. It is soluble in water but insoluble in alcohol. It usually crystallizes as a penta-hydrate compound containing five molecules of water ($CuSO_4 \cdot 5H_2O$). Cupric sulfate is utilized chiefly for agricultural purposes, as a pesticide, germicide, feed additive, and soil additive.

- Copper(II) acetate monohydrate, neutral verdigris, $Cu(CH_3COO)_2 \cdot H_2O$, decomposes at 240°C; it forms dark green, monoclinic crystals; its solubility in water at 25 °C is 6.8 g.100 g^{-1} solution. Copper(II) acetate monohydrate is used in textile dyeing and as a pigment.

Nanometer-sized metals, semiconductors, and oxides are of great interest because they can have physical and chemical properties that are neither characteristic of the atoms nor of the bulk

counterparts (Fan 2004). The large ratio of surface area to volume can contribute to some of the unique properties of nanoparticles.

For a number of applications the surface characteristics of inorganic particles must be compatibilized by coating them with organic polymers. For example, it is possible to alter the solubility, magnitude, and sign of the surface charge or the bonding properties of cores by covering them with appropriate macromolecules. In some cases, the conductivity of particles can be enhanced by the choice of the polymer coatings. The coordination sphere of copper (II) ions in bulk oxides is usually distorted due to the Jahn-Teller effect. The effect of the electronic configuration of Cu (II) on the electronic and photonic characteristics of mixed oxides has made CuO a fundamental compound of several high-temperature superconductors.

Among various 3d transition metals and their derivatives, cupric oxide (CuO, tenorite) is a unique monoxide compound (in monoclinic phase, different from normal rock-salt type structure) for both fundamental investigations and practical applications.

CuO has been used as heterogeneous catalysts in many important chemical processes, such as the degradation of nitrous oxide, selective catalytic reduction of nitric oxide with ammonia, and oxidations of carbon monoxide, hydrocarbon, and phenol in supercritical water. Cupric oxide (CuO) has been extensively studied (Jiang et al. 2002) because of its close connection to high-Tc superconductors. The valence of Cu and its fluctuation are believed to play important roles in determining the superconductivity of various types of cupric compounds. Cupric oxide has also been known as a p-type semiconductor that exhibits a narrowband gap (1.2 eV) and a number of other interesting properties. For example, monoclinic CuO solid belongs to a particular class of materials known as Mott insulators, whose electronic structures cannot be simply described using conventional band theory. Recent studies by several groups indicate that CuO could exist in as many as three different magnetic phases. It was a 3D collinear anti-ferromagnetic at temperatures below 213 K. When the temperature was raised, it first became an intermediate non-collinear incommensurate magnetic phase up to 230 K and then acted like a 1D quantum anti-ferromagnetic material.

2.4 CRITICAL SUMMARY OF REVIEWED LITERATURE

This literature review is expansive to include critical analysis on proposed fibre molecular structure models and different fibre spinning processes, various grades of uniquely performing polyacrylonitrile polymers and polymer salt complexes, as well as, the use of solid state analytical techniques to measure molecular orientation and fibre crystallinity, using some less conventional experimental methodology and data handling techniques.

PAN performs in many respects uniquely in comparison to most other fibre forming polymers. Some of these unusual properties include; the fact that it is a thermoplastic which degrades before it melts, the PAN polymer is claimed by many researchers to have a double glass transition temperature due to molecular vibrations in the more ordered and less ordered quasi-crystalline phase domains and the polymorphic nature of PAN. Debate still remains regarding whether PAN fibres have orthorhombic or hexagonal packing and planar zig-zag or helical conformations or combinations thereof. The interpretation of XRD data on PAN remains also contentious with numerous different models proposed for the interpretation of the data for quasi-crystalline PAN.

The assignment of the FTIR adsorption peaks is cause for debate amongst researchers with major disagreements particularly when salts are added to the PAN.

Whilst in October 2009, as shown in Figure 2.2, according to the *Science Direct* Website, there were in excess of 2000 publications on the topic of electrospinning, more than 500 of these concern the electrospinning of PAN and of these about 100 which also contain the keyword "orientation", the following gaps are noted in the electrospinning related research reported in Chapter 2;

- Most electrospinning publications are short two page documents looking at one type of polymer grade and the resultant fibres are analysed by only one analytical technique.
- The PAN grade is often not described in terms of co-monomer content and molecular weight or molecular weight distribution which all in theory will affect the orientation and crystallinity of the fibres.
- The analysis of the electrospun PAN fibres is conducted predominantly after heat treatment through the stabilization and carbonization processes on carbon fibres.
- The publications on electrospun PAN fibres, generally do not contain salt additives. Two articles include studies of the inclusion of silver nitrate salt at a single loading concentration in electrospun PAN (Wang *et al*. 2005 and Chen *et al*. 2008), to investigate it's effect on the carbonization process and the formation of silver nanoparticles and one reference includes a study of the effect of lithium chloride addition at 2 concentrations in electrospun PAN (Qin 2004) on only the fibre diameter during spinning. There are numerous reported studies on the inclusion of carbon nanotubes and other nanoparticles on electrospun carbon nanofibres, where mostly only the effect of the additives of the electrical conductivity of the electrospun mat is studied.

- The keyword “orientation” in these publications refers mostly to the macro-scale alignment of the fibres using different take-up devices in the electrospinning process .and not to the internal molecular orientation of the polymeric fibres.

  There are no publications in which the molecular orientation of electrospun fibres is studied in depth. One article (Dersh et al., 2003) does compare the structure of melt spun nylon with commercial melt spun nylon and claims the degree of orientation to be comparable based on XRD data.

The analytical techniques used to measure fibre crystallinity and molecular orientation are limited and the analysis relies on small yet persistent changes in the recorded data. Some unique methods to measure crystallinity and orientation specifically only applicable in PAN fibres have been developed (Causin, 2005 and Minagawa *et al*. 2002). Whilst the method of Minagawa was applied to measure the degree of crystallinity in PAN cast films in relation to various degrees of tacticity, the same argument applies to measure crystalinity in fibres produced under different conditions whereby in effect the draw ratio is altered due the changed spinning conditions and this alters the amount of interaction between the anti-parallel nitrile groups inter- and intramolecularly.

Fibre structure models are generally contentious for semi-crystalline PP and PES fibres and even more so in the case of quasi-crystalline PAN. A third phase domain was previously postulated for electrospun PAN fibres spun from DMF with a polycarbonate plasticizer (Vaismann *et al*., 2007) and in melt spun nylon fibres with salts (Murthy et al. 2000)

The effect of salt additives in micron-sized PAN fibres and films with different grades of PAN copolymers have been studied in depth by researchers in India (Bahrami *et al*., 2003, 2005 and Bajaj *et al*., 1998) mostly using DSC and FTIR studies and not XRD but no references were found for copper based additives or for a range of salt additives at different concentrations in electrospun fibres.

2.5 REFERENCES

Arca, M., 2003. Coordination chemistry of nitrile and amino pendant arm derivatives of [9]anen$_2$s and [9]anens$_2$ with PdII and CuII. *European Journal of Inorganic Chemistry*, p.1232-33.

Agend, F., Naderi, N. & Fareghi-Alamdari, R., 2007. Fabrication and Electrical Characterization of Electrospun Polyacrylonitrile-Derived Carbon Nanofibers. *Journal of Applied Polymer Science*, 106, p.255-59.

Ali, A., 2003. Carbon nanotube reinforced carbon nano composite fibrils by electro-spinning, Thesis Drexel University, http://hdl.handle.net/1860/17

Azad, A., 2005. Processing and characterization of electrospun Y_2O_3-stabilized ZrO_2 (YSZ) and Gd_2O3-doped CeO_2 (GDC) nanofibers. *Materials Science and Engineering B,* 123, p.252-58.

Bahrami, S., Bajaj, P. & Sen, K., 2003. Effect of Coagulation Conditions on Properties of Poly(acrylonitrile– carboxylic acid) Fibers. *Journal of Applied Polymer Science,* 89, p.182-37.

Bahrami, S., Bajaj, P. & Sen, K., 2005, Thermal Behavior of Acrylonitrile Carboxylic Acid Copolymers. *Journal of Applied Polymer Science,* 88, p.685-98.

Bai, R. & Chen, J., 2003. Behaviors and mechanisms of copper adsorption on hydrolyzed polyacrylonitrile fibers. *Journal of Colloid and Interface Science*, 260, p.265-72.

Bajaj, D. K., Paliwal, A. K. & Gupta, 1998. Influence of Metal Ions on Structure and Properties of Acrylic Fibers. *Journal of Applied Polymer Science***,** 67, p.1647-59.

Bartkowiak, A., Jezierska, J. & Spychaj, T. 1998. An EPR study of polysaccharide copper(II) complexes in composite dextran/epichlorohydrin gels**.** *Polymer Bulletin,* 41 (2), p.199-206.

Bashir, Z., 1993. The formation of polymer-solvent complexes of polyacrylonitrile from organic solvents containing carbonyl groups. *Acta Polymerica,* 44 (5), p.211-18.

Baumgarten, P., 1971. Electrostatic spinning of acrylic microfibers. *Journal of Colloid Interface Science,* 36, p.71.

Bognitzki, 2001. Preparation of fibers with nanoscaled morphologies: electrospinning of polymer blends. *Polymer Engineering Science,* 41 (6), p.982-89.

Bognitzki, M., Hou, H., Ishaque, M., Frese, T., Hellwig, M., Schwarte, C., Schaper, A., Wendorff, J.H. & Greiner, A., 2000. Polymer, metal, and hybrid nano- and mesotubes by coating degradable polymer template fibers (TUFT process). *Advanced Materials,* 12 (9), p.637-40.

Boland, E.D., Bowlin, G.L., Simpson, D.G. & Wnek, G.E., 2001. Electrospinning of tissue engineering scaffolds. *Polymer Mater. Science Eng*, 85, p.51-52.

Bredas, J. & Salaneck, W., 1986. Electronic-structure evolution upon thermal treatment of polyacrylonitrile: A theoretical investigation. *Journal of Chemical Physics,* 85 (4), p.2219-26.

Causin, V., 2005. A quantitative differentiation method for acrylic fibers by infrared spectroscopy. *Forensic Science International*, 151, p.125-31.

Chang, X., 2002. Efficiency and application of poly(acryldinitrophenylamidrazone-dinitroacrylphenylhydrazin chelating fiber for pre-concentrating and separating trace Au(III), Ru(III), In(III), Bi(III), Zr(IV), V(V), Ga(III) and Ti(IV) from solution samples. *Talanta,* 57, p.253-61.

Chang, Y. & Zeng, H., 2004. Controlled Synthesis and Self-Assembly of Single-Crystalline CuO Nanorods and Nanoribbons. *Crystal Growth and Design,* 4 (2), p.397-402.

Chen, R., Zhao, S & Han, G & Dong, J. (2008). Fabrication of the silver/polypyrrole/polyacrylonitrile composite nanofibrous mats. *Materials Letters*, 62. p.4031–4034.

Cheon, S., 1996. Modeling and Simulation of the Coagulation Process of Poly(acrylonitrile) Wet-Spinning. *Indian Engineeriing Chemical. Research*, 35, p.4796-800.

Choi, B.K., 2005. Ionic conductivity enhancement in Na_2SO_4–PAN polymer composites. *Materials Science and Engineering B*, 119, p.177-81.

Choi, S.S., 2004. Titania-Doped Silica Fibers Prepared by Electrospinning and Sol-Gel Process. *Journal of Sol-Gel Science and Technology,* 30 (3), p.215-21.

Chronakis, I., 2005. Novel nanocomposites and nanoceramics based on polymer nanofibers using electrospinning process – A review. *Journal of Materials Processing. Technology,* 167, p.283-93.

Cui, S., Zhao, Z., Wei, W., 1999. Investigation on the Effect of Activators and Polysulfide on Durability of Electrically Conductive PAN Fibers. *Journal of Applied Polymer Science*, 72, p.1039-045

Dai, H., 2002. A novel method for preparing ultra-fine alumina-borate oxide fibres via an electrospinning technique. *Nanotechnology***,** 13, p.674-77.

Dalton, S., 1999. Thermal Stabilization of polyacrylonitrile fibres**.** *Polymer*, 40, p.5531-543.

Davidson, J., 2001. Investigation of molecular orientation in melt-spun high acrylonitrile fibers. *Polymer*, 41, p.3357-364.

Deitzel, J. M., Kleinmeyer, J., Harris, D. & Beck Tan, N. C., 2001a. The effect of processing variables on the morphology of electrospun nanofibers and textiles. *Polymer*, 42 (1), p.261-72.

Deitzel, J. M., Kleinmeyer, J. D., Hirvonen, J. K. & Beck Tan, N. C., 2001b. Controlled deposition of electrospun poly(ethylene oxide) fibers. *Polymer*, 42 (19), p.8163-170.

Dersch, R., Liu, T., Schaper, A. Greiner, A., Wendorff, J., 2003. Electrospun nanofibers: Internal structure and intrinsic orientation. *Journal of Polymer Science Part A: Polymer Chemistry*, 41, p. 545-553

Demir, M.M., 2004. Palladium Nanoparticles by Electrospinning from Poly(acrylonitrile-co-acrylic acid)-$PdCl_2$ Solutions: Relations between Preparation Conditions, Particle Size, and Catalytic Activity. *Macromolecules*, 37 (5), p.1787-792.

Deng, S,; Bai, R., Chen J. P. 2003. Behaviors and mechanisms of copper adsorption on hydrolyzed polyacrylonitrile fibers. *Journal of Colloid and Interface Science*, 260 (2), p. 265-272

Ding, B., 2004. Titanium dioxide nanofibers prepared by using electrospinning method. *Fibers and Polymers.* 5 (2), p.105-09.

Ding, B., Kim, H.Y., Lee, S.C. & Shao, C.L., 2004. Preparation and characterization of a nanoscale poly(vinyl alcohol) fiber aggregate produced by an electrospinning method. *Journal of Polymer Science Part B: Polymer Physics.* 40, p.1261-268.

Drew, C., Wang, X., Senecal, K., Schreuder-Gibson, H., He, J., Tripathy, S. & Samuelson, L., 2001. Electrospun nanofibers of electronic and photonic polymer systems. *Society of Plastics Engineering*. 58 (2), p.1477-481.

Drew, C., 2003. Metal Oxide-Coated Polymer Nanofibers. *Nano Letters.* 3 (2), p.123-25.

Dzenis, Y., 2004. Spinning Continuous Fibers for Nanotechnology**.** *Science*. 304 (25), p.1918-920.

Edie, D., 1998. The Effect of processing on the structure and properties of carbon fibers. *Carbon*, 46 (4), p.345-62.

Erickson, M., 2003. Solid polymer/salt electrolytes based on linear poly((N-2-cyanoethyl)ethylenimine). *Electrochimica Acta,* 48, p.2059-063.

Fan, H., Yang, L., Hua, W., Wu, X., Wu, Z. & Xie, S., 2004. Controlled synthesis of monodispersed CuO nanocrystals. *Nanotechnology*, 15, p.37-42.

Fennessey, S. & Farris, R., 2004. Fabrication of aligned and molecularly oriented electrospun polyacrylonitrile nanofibers and the mechanical behavior of their twisted yarns. *Polymer,* 45, p.4217-225.

Fochler, H., Mooney, J., Ball, L., Boyer, R., & Grasselli, J., 1985. Infrared and NMR spectroscopic studies of the thermal degradation of polyacrylonitrile. *Spectrochimica Acta Part A: Molecular Spectroscopy,* 41, (1-2), p. 271-278

Fong, H. & Reneker, D., Elastomeric nanofibers of styrene-butadiene-styrene triblock copolymer. *J Polymer Science B: Polymer Physics,* 37, p.3488-493.

Fong, H. & Reneker, D, 2001. *Electrospinning and the formation of nanofibres*. Amsterdam. Carl Hanser Verlag.

Frenot, A., 2003. Polymer nanofibers assembled by electrospinning. *Current Opinion in Colloid & Interface Science,* 8, p.64-75.

Galer J.M. & Hudson M.J., 1994. Electrically Conducting Poly(Acrylonitrile) Films. *Solid State Ionics*, 69 (1), p.21-27.

Ge, J., 2004. Assembly of Well-Aligned Multiwalled Carbon Nanotubes in Confined Polyacrylonitrile Environments: Electrospun Composite Nanofiber Sheets. *Journal of the American Chemical. Society*, 126, p.15754-5761.

Geskin, V., 1996. Acrylonitrile on Cu(100): A density functional theoretical study of adsorption and electrochemical grafting. *Journal of Chemical Physics.*, 105 (8), p.3278-289.

Gibson, P., Schreuder-Gibson, H. & Rivin, D., 2001. Transport properties of porous membranes based on electrospun nanofibers. *Colloids and Surfaces*, A, p.187-88 & 469-81.

Greiner, A. & Wendorff, J.H., 2007. Electrospinning: A Fascinating Method for the Preparation of Ultrathin Fibers. *Aangewandte Chemie,* 46, p.5670-703.

Gu, Y., Chen, D. & Jiao, X., 2005. Synthesis and Electrochemical Properties of Nanostructured $LiCoO_2$ Fibers as Cathode Materials for Lithium-Ion Batteries. *Journal of Physical Chemistry. B.*, 109 p.17901-7906.

Gu, S.Y., Ren, J. & Vancso, G., 2005. Process optimization and empirical modeling for electrospun polyacrylonitrile (PAN) nanofiber precursor of carbon nanofibres. *European Polymer Journal*, 41 (11), p.2559-568.

Guan, H., 2004. Fabrication of ZrO_2 nanofibers by electrospinning. *Gaodeng Xuexiao Huaxue Xuebao,* 25 (8), p.1413-415.

Guan, H., 2003. Preparation and characterization of NiO nanofibres via an electrospinning technique. *Inorganic Chemistry Communications*, 6, p.1302-303.

Guan, H., Shao, X., Chen, B., Gong, J. & Yang, X., 2003. A novel method for making CuO superfine fibres via an electrospinning technique. *Inorganic Chemistry Communications*, 6 (11), p.1409-411.

Gupta, A., Paliwal, D. & Bajaj, P., Melting Behavior of Acrylonitrile Polymers. *Journal of Applied Polymer Science*, 70, p.2703-709.

Hajra, M., Mehta, K. & Chase, G., 2003. Effects of Humidity, Temperature and Nanofibres on drop coalescence in glass fibre media. *Separation and Purification Technology,* 30, (1), p79-88

Hearle, J., 2002. *Fibers, 2. Structure; Ullmann's Encyclopedia of Industrial Chemistry*. Wiley Verlag

Hou, H., 2005. Electrospun PAN Nanofibers Containing a High Concentration of Well-Aligned Multiwall Carbon Nanotubes. *Chemical Materials,* 17, p.967-73.

Hou, C., Qu, R.J., Liang, Y., & Wang, C.G., 2005. Kinetics of Diffusion in Polyacrylonitrile Fiber Formation. *Journal of Applied Polymer Science*, 96, p.1529-533.

Huang, Z.M., Zhang, Y.Z., Kotaki, M. & Ramakrishna, S., 2003. A review on polymer nanofibers by electrospinning and their applications in nanocomposites. *Composites Science and Technology*, 63, p.2223-253.

Huber, Bernd; Kelheim Faserwerk; Germany; (2004), personal communication.

Isobe, Y., Yamada, K., Nakano, T. & Okamoto, Y., 1999. Stereospecific Free Radical Polymerization of Methacrylates Using Fluoroalcohols as Solvents. *Macromolecules,* 32, p.5979-981.

Jeschke, G., 2002. Determination of the Nanostructure of Polymer Materials by Electron Paramagnetic Resonance Spectroscopy. *Macromolecules. Rapid Communications*, 23, p.227-46.

Jeschke, G., 2000. Structure Characterization of the Copper(II) Complex of Poly(4-vinylpyridine) by a Combination of EPR, ENDOR and Molecular Modelling Techniques. *Journal of Physical Chemistry,* 104 (B), p.8382-390.

Jin, H.J., 2002. Electrospinning *Bombyx Mori* Silk with Poly(ethylene oxide). *Biomacromolecules,* p.1233-1239.

Jiang, X., Herricks, T. & Xia, Y., 2002. CuO Nanowires Can Be Synthesized by Heating Copper Substrates in Air. *Nano Letters*, 2 (12), p.1333-1338.

Kalayci, V., 2005. Charge consequences in electrospun polyacylonitrile (PAN) nanofibres. *Polymer*, 46, p.7191-200.

Kameoka, J., 2003. A scanning tip electrospinning source for deposition of oriented nanofibres. *Nanotechnology*, 14, p.1124-129.

Katta, P., 2004. Continuous Electrospinning of Aligned Polymer Nanofibers onto a Wire Drum Collector. *Nano Letters*, 4 (11), p.2215-218.

Kakudo, M., Kasai; X-ray Diffraction by Polymers; Kodansha Ltd; Tokyo; 1972: 231-320;

Katii, K., 2003. Conductivity model and photoacoustic FT-IR surface depth profiling of heterogeneous polymers. *Polymer;* 44, p.3319-325.

Kawai (ed.): *High-speed Fiber Spinning*, Wiley-Interscience, New York 1985.

Kenawy, E.R., 2002. Release of Tetracycline hydrochloride from electrospun poly(ethylene-co-vinylacetate), poly(lactic acid), and a blend. *Journal of Controlled Release*, 81, p.57-64.

Kim, H.S. & Cho, H.H. 2003. Crystalline structure of polyacrylonitrile-iodine complex. Journal of Applied Polymer Science, 53, 11, p. 1403-13**.**

Kim, C., 2005. Electrochemical characterization of electrospun activated carbon nanofibres as an electrode in supercapacitors. *Journal of Power Sources*, 142, p.382-88.

Kirby, J., Brandrup, J. & Peebles, L., 1968. On the chromophore of polyacrylonitrile II: The Presence of Ketonic Groups in Polyacrylonitrile. *Macromolecules*, 1 (1), p.53-58.

Kislenko, V. & Verlinskaya, R., 2003. Kinetics of copper dissolving in the water solution of polyacrylic acid or its copolymers with acrylonitrile and hydrogen peroxide. *Journal of Colloid and Interface Science,* 265 (1), p.129-33.

Ko, F., Gogotsi, Y., Ali, A., Nagruib, N., Ye, H., Yang, G., Li, C. & Willis, P. 2003. Electrospinning of continuous nanotube-filled nanofibre yarns, Advanced Materials, 15, 14, p. 1161-65.

Koenig, J. (ed), 1999. *Spectroscopy of Polymers.* 2nd Edition, New York, Elsevier,

Koombhongse, S., Liu, W. & Reneker, D., 2001. Flat polymer ribbons and other shapes by electrospinning. *Journal of Polymer Science, Part B: Polymer Physics*., p.2598-606.

Laffin, C., Mc Nally, G.M., Sanderson, R.D., Greyling, C.J., 2005. The Manufacture of Aligned Poly(Acrylonitrile) Fibres By Electrospinning. *Proceedings of ANTEC*, Boston, p.1825-829.

Lam, H., 2004. Electrospinning of single wall carbon nanotube reinforced aligned fibrils and yarns, Drexel University thesis, http://hdl.handle.net/1860/368

Larrondo, L. & Manley R., 1981. Electrostatic fiber spinning from polymer melts, I. Experimental observations on fiber formation and properties. *Journal of Polymer Science Polymer Physics Edition.*,19, p.909-20.

Lee, C.K., 2005. The influence of added ionic salt on nanofiber uniformity for electrospinning of electrolyte polymer. *Synthetic Metals*, 154, p.209-12.

Lee, H., 2005. One-step preparation of ultrafine poly(acrylonitrile) fibers containing silver nanoparticles. *Materials Letters*, 59, p.2977-980.

Lee, K., 2002. Influence of a mixing solvent with tetrahydrofuran and N,N-dimethylformamide on electrospun poly(vinyl chloride) nonwoven mats. *Journal of Polymer Science Part B: Polymer Physics*, 40, p.2259-268.

Lewandowski, A., 2000. Impedance studies on polyacrylonitrile–CuX_2–DMSO (X=Cl, Br, CF_3SO_3) solid polymer electrolyte, *Solid State Ionics*, 128, p.1-4 &145-50.

Lewin, M, (1985) Pearce, E (ed.): *Fiber Chemistry,* Marcel Dekker, New York 1985;

Li, D., 2003. Fabrication of Titania Nanofibers by Electrospinning. *Nano Letters*, 3 (4), p.555-60.

Li, D. & Xia, Y.E., Electrospinning of Nanofibres: Reinventing the wheel. *Advanced Materials,* 16 (14), p.1151-170.

Li, W.J., Laurencin, C., Caterson, C., Tuan, R. & Ko, F., 2002. Electrospun nanofibrous structure: A novel scaffold for tissue engineering. *Journal of Biomedical Materials Research*, 60, p.613-21.

Liu, H., & Hsieh, Y.L., 2002. Ultrafine fibrous cellulose membranes from electrospinning of cellulose acetate. *Polymer Physics*, 40, p.2119-129.

Liuxue, Z., Peng, L. & Zhixing, S., 2005. Photocatalysis anatase thin film coated PAN fibers prepared at low temperature. *Materials Chemistry and Physics.* 96 (1), p.110-15.

Lyons, J. & Ko, F., 2004. Nanofibres. *Encyclopaedia of Nanoscience & Nanotechnology*, 6, p.727-38.

Ma, J., 2001. Characteristics of Copper Particles Supported on Various Types of Graphite Nanofibers. *Journal of Physical Chemistry B.*, 105 (48), p.11994-2002.

Ma, M., et al., 2005. Superhydrophobic Fabrics Produced by Electrospinning and Chemical Vapor Deposition. *Macromolecules*, 38 p.9742-748.

Ma, M., Hill, R., Lowery, J., Fridrikh, S. & Rutledge, G.C., 2005. Electrospun Poly(Styrene-block-dimethylsiloxane) Block Copolymer Fibers Exhibiting Superhydrophobicity. *Langmuir*, 21 (12), p.5549-554

Mack, J.J., Viculis, L.M., A. Ali, Luoh, Yang, R., G., Hahn, H.T., Ko, F.K., & Kaner, R.B., 2005. Graphite Nanoplatelet Reinforcement of Electrospun Polyarylonitrile Nanofibers, Advanced Materials, No.1, p.77-80.

Madhugir , S., 2003. Electrospun mesoporous molecular sieve fibers. *Microporous & Mesoporous Materials*, 63, p.75-84.

Martindale, D., 2000. Scar No More: Biodegradable scaffolds give skin cells a better road map for self-repair. *Scientific American*, p.34-36.

Masson, J.C (ed), 1995. *Acrylic Fibre Technology and Applications*; NY, Marcel Dekker, 197-219;

Matthews, J., 2002. Electrospinning of Collagen Nanofibers. *Biomacromolecules,* 3 (2), p.232-38.

McClelland, J.F., Bajic, et al., 1996. Introduction of Photoacoustic Spectroscopy with Step Scan and Constant Velocity Scan FTIR Spectrometers, MTEC Photoacoustics, p. 7.

McKee, M., 2004. Influence of self-complementary hydrogen bonding on solution rheology / electrospinning relationships. *Polymer*, 45, p.8705-715.

Melaiye, A., 2005. Silver(I)-Imidazole Cyclophane gem-Diol Complexes Encapsulated by Electrospun Tecophilic Nanofibers: Formation of Nanosilver Particles and Antimicrobial Activity. *Journal of the American Chemical Society,* 127, p.2285-291.

Mikolajczyk, T., 2005. Effect of Fibre-spinning Conditions on The Properties of Nanosilica-containing PreCursor PAN Fibres. *Fibres and Textiles in Eastern Europe*, 13 (51), p.31-34.

Minagawa, M., Yoshida, W., Kurita, S., Takada, S. & Yoshii, F., 1997. Solvent Casting Effect on the Infrared Characteristic Absorption Bands (1230/1250 cm^{-1}) of Stereoregular Isotactic Poly(acrylonitrile) Film. *Macromolecules*, 30, p.1782-786.

Minagawa, M., Taira, T., Yabuta, Y., Nozaki, K. & Yoshii, F., 2001. An Anomalous Tacticity-Crystallinity Relationship: A WAXD Study of Stereoregular Isotactic (83-25%) Poly(Acrylonitrile) Powder Prepared by Urea Clathrate Polymerization. *Macromolecules*, 34, p.3679-683.

Minagawa, M., Taira, T., Yabuta, Y., Nozaki, K. & Yoshii, F., 2002. Conformational Effect and FT-IR Diffuse Reflection Spectroscopy of Stereoregular Isotactic Poly(acrylonitrile) Prepared by Urea Clathrate Polymerisation. *Macromolecules*, 33 (12), p.1653-656.

Mironov, A., Demir, M., Ignatev, Y. & Sitnikova, N., 2002. Nanofibers based on associating polyacrylonitrile-acrylamide copolymers produced by electrospinning; *Chemistry & Computational Simulation. Butlerov Communications*, 2 (6), p.260-65.

Miura, Y., Satoh, T., Narumi, A. & Okamoto, Y. 2005. Atom Transfer Radical Poltmerisation of Methyl Methacrylates In Fluoroalcohols: Simultaneous Control of Molecular Weight and Tacticity. *Macromolecules*, 38, p.1041-043.

Morozov, V., Morozova, T. & Kallenbach N., 1998. Atomic force microscopy of structures produced by electrospraying polymer solutions. International Journal of Mass Spectrometry, 178, p.143–59.

Murthy, N.S., Reimschussel, A.C., & Kramer, V.J, 1990. Changes in void content and free-volume during heat setting and their influence on dye diffusion and mechanical properties. *Journal of Applied Polymer Science*. . 40, p. 249 – 265.

Newman, C., 2003. Dreamweaver; National Geographic. Jan. 2003.

Okamoto, M., 1983. Assignment of a Characteristic Infrared Absorption Band at 810 cm^{-1} in Heat-treated Polyacrylonitrile. *Bulletin of the Chemical Society of Japan*, 56 (9), p.2802-2804.

Oral, Y., Mensur, E., Aslan, M. & Basaran, E., The preparation of CuO thin films and the study of their microstructures and optical properties. *Materials Chemistry & Physics,* 83 (1), p.140-44.

Pannier, M., et al., 2000. Dead-Time Free Measurement of Dipole-Dipole Interactions between Electron Spins. *Journal of Magnetic Research*, 142, p.331-40.

Park, S.H., Jo, S.M., Kim, D.Y., Lee, W.S. & Kim, B.C. 2005. Effects of iron catalyst on the formation of crystalline domain during carbonization of electrospun acrylic nanofiber. *Synthetic Metals*, 150 (3), p.265-70.

Patel, A.C., Li, S., Wang, C., Zhang, W. & Wei, Y., 2007. Electrospinning of Porous Silica Nanofibers Containing Silver Nanoparticles for Catalytic Applications. *Chemical Materials,* 19, p.1231-238.

Perepelkin, K., 2003. Chemistry and Technology of Chemical Fibre: Oxidised (cyclised) polyacrylonitrile fibres. *Fibre Chemistry*, 35 (6), 114-116.

Pethrick, R., 2003. *Characterisation of Molecular Organisation in Polymeric Materials;* Techniques for Polymer Organisation and Morphology Characterisation. New York; John Wiley & Sons

Pfragner, J. & Schurz, J., 1980. Dependence of Viscosity on Concentration and Temperature of Solutions of Polyacrylonitrile in Dimethylformamide. *Monatash Chemistry*, 111, p.1053-060.

Platonova, N. & Klimenko, I., 1993. Peculiarities of The Interaction of Polyacrylonitrile With Basic Solvents During Heat Treatment. *Russian Journal of Applied Chemistry,* 66 (3.2), p.546-51.

Qin, X., 2004. The effect of LiCl on electrospinning of PAN polymer solution: theoretical analysis and experimental verification. *Polymer*; 45, p.6409-413.

Ra, E., 2005. Anisotropic electrical conductivity of MWCNT/PAN nanofiber paper. *Chemical Physics Letters*, 413, p.188-93.

Reneker, D., & Chun, I., 1996. Nanometer diameter fibres of polymer produced by electrospinning. *Nanotechnology*. 7, p216-23.

Reneker, D., Yarin, A.L., Fong, H. & Koombhonge S., 2000. Bending instability of electrically charged liquid jets of polymer solutions in electrospinning. *Journal of Applied Physics*. 87, p.4531-547.

Richardson, H.W., 2002. Copper and Copper compounds. *Ullmann's Encyclopaedia of Industrial Chemistry*. Copyright © 2002 by Wiley-VCH Verlag GmbH & Co., DOI: 10.1002/14356007.a07_567

Rizzo, P., Auriemma, F., Guerra, G., Petraccone, V. & Corradini, P., 1996. Conformational Disorder in the Pseudohexagonal Form of Atactic Polyacrylonitrile. *Macromolecules,* 29 (27), 8852-861.

Rizzo, P., Guerra, G. & Auriemma, E., 1996. Thermal Transitions of Polyacrylonitrile Fibers. *Macromolecules.* 29 (5), p.1830-832.

Saunier, J., 2000. Electrochemical and spectroscopic studies of polymethacrylonitrile based electrolytes. *Electrochimica Acta*. 45 (8-9), p.1255-263.

Sawai, D., & Kanamoto, T., 1998. Differential Scanning Colorimetry Evidence for the Existence of a First-Order Thermal Transition in Ultraorientated at-PAN. *Macromolecules*. 31, p 2010-012.

Sawai, D., 1997. Development of Ductility and Tensile Properties upon Two-stage Draw of Ultrahigh Molecular Weight Poly(acrylonitrile). *Macromolecules*. 30, p.4170-178.

Sawai, D., 1999. Uniaxial Drawing of Isotactic Poly(acrylonitrile): Development of Oriented Structure and Tensile Properties. *Macromolecules*. 32, p.5622-630.

Schreuder-Gibson, H., 2000. Characteristics of electrospun fibers containing carbon nanotubes. *Proceedings of the Electrochemical Society.* 10, p.210-21.

Sen, K., Bajaj, P. & Sreekumar, T., 2003. Thermal Behavior of Drawn Acrylic Fibers. *Journal of Polymer Science Part B: Polymer Physics*. 41, p.2949-958.

Shilton, S., et al., 1997. Molecular Orientation and performance of synthetic polymeric membranes for gas separation. *Polymer*. 38 (9), p.2215-220.

Shin, Y. M., Hohman, M. M., Brenner, M. P. & Rutledge, G. C., 2001. Electrospinning: A whipping fluid jet generates submicron polymer fibers. *Applied Physics Letters*. 78 (8), p.1149-151.

Shono, T., 1984. New Systems for the Storage of Electricity using Nitrile and Iodine as the Anodic Active Substances. *Journal of the Chemical Society Chemical Communications.* 18, p.1204-205.

Silverstein, M., Najary, Y., Grader, G. & Shter, G., 2004. Complex Formation and Degradation in Poly(Acrylonitrile co-Vinyl Acetate) Containing Copper Nitrate. *Journal of Polymer Science: Part B: Polymer Physics*. 42, p.1023-032.

Simanova, S., 1998. Complexation of Platinum in Sorption of Platinum(IV) Hexachloride Complex by Fibrous Polyacrylonitrile-based Sorbent Modified with Thiosemicarbazide. *Russian Journal of Applied Chemistry*. 71 (2), p.228-34.

Smit, E., Buttner, U. & Sanderson, R., 2005. Continuous yarns from electrospun fibers. *Polymer*; 46, p.2419-423.

Song, T., Zhang, Y., Zhou, T. Lim, C., Ramakrishna, S. & Liu, B., Encapsulation of self-assembled FePt magnetic nanoparticles in PCL nanofibers by coaxial electrospinning. *Chemical Physics Letters*. 415, p.317-22.

Stasiak, M., Studer, A., Greiner, A. & Wendorff, J.H., 2007. Polymer Fibers as Carriers for Homogeneous Catalysts. *Chemical European Journal*, 13, p.6150-156.

Subbiah, T., Bhat, G., Tock, R.W., Parameswaran, S. & Ramkumar, S., 2005. Electrospinning of Nanofibers. *Journal of Applied Polymer Science*. 96, p.557-69.

Sutasinpromprae, J., Jitjaicham, S., Nithitanakul, M., Meechaisue, C. & Supaphol, P., 2006. Preparation and characterization of ultrafine electrospun polyacrylonitrile fibers and their subsequent pyrolysis to carbon fibers. *Polymer International*,.55, p.825-33.

Swai, H., Cingo N., Greyling C; 2004. New Ways of Delivering Anti-Tuberculosis Drugs (Atd). Poster Presentation. *Nanomed Conference*. Berlin.

Tang, J., 1998. Relationship between Structures of Polyacrylonitrile (PAN) - Copper Gradient Composite Film and Electrochemical-Reaction Conditions. *Journal of Applied Polymer Science*, 69, p.1159-165.

Taylor, G (1969); *Proceedings of the Royal Society.* London, A313; (1969); 453;

Tsutsumi, H., 2000. Conductivity enhancement of polyacrylonitrile-based electrolytes by addition of cascade nitrile compounds. *Journal of Power Sources.* 90 (1), p.33-38.

Tungol, M., 2003. Forensic analysis of acrylic copolymer fibers by infrared microscopy. *Applied Spectroscopy.* 47, p.1655-658.

Usami, T., Ohtani, I. & Tsuge, S., 1990. Structural Study of Polyacrylonitrile Fibers during Oxidative Thermal Degradation by Pyrolysis-Gas Chromatography, Solid-state ^{l3}C NMR, and Fourier Transform Infrared Spectroscopy. *Macromolecules.* 23, p.2460-465.

Vaisman, L., Wachtel, E., Wagner, D & Marom, G. (2007). Polymer-nanoinclusion interactions in carbon nanotube based polyacrylonitrile extruded and electrospun fibers**.** *Polymer,* 48 (2007) p.6843-54.

Van der Goes, Dr Wim; Montefibre, Italy; (2005); personal communication

Viswanathamurthi, P., 2004. The photoluminescence properties of zinc oxide nanofibres prepared by electrospinning. *Nanotechnology*. 15, p.320-23.

Viswanathamurthi, P., Bhattarai, N., Kim, H. & Lee, D., 2003. Vanadium pentoxide nanofibers by electrospinning. *Scripta Materialia*. 49, p.577-81.

Viswanathamurthi, P., Bhattarai, N., Kim, H., Lee, D.R., Kim, S. & Morris, M.A., 2003. Preparation and morphology of niobium oxide fibres by electrospinning. *Chemical Physics Letters*. 374, p.79-84.

Wagner A., Wolfe, G. & Fairbrother, H., 2003. Reactivity of vapor-deposited metal atoms with nitrogen-containing polymers and organic surfaces studied by XPS. *Applied Surface Science*. 219, p.317-28.

Wang, X. & Lee, S.H., 2001. Electrospun nanofibrous membranes for optical sensing. *Polymer Material Science & Engineering*. 85, p.617-618.

Wang, Q., 1999. Preparation of novel polymer materials through intermacromolecular complexation. *Materials Science and Engineering* C. 10 (1-2), p.1235-240.

Wang, Y., Serrano, S., Santiago-Avile´, J., 2003. Raman characterization of carbon nanofibers prepared using electrospinning. *Synthetic Metals*. 138, p.423-27.

Wang, Y., Aponte, M., Leon, N., Ramos, I., Furlan, R., Evoy, S. & Santiago-Avile, J., 2004. Synthesis and characterization of tin oxide microfibres electrospun from a simple precursor solution. *Semiconductor Science & Technology*. 19, p.1057-060.

Wang, Y., Aponte, M., Leon, N., Ramos, I., Furlan, R., Evoy, S. & Santiago-Avil´e, J., 2005. Preparation of silver nanoparticles dispersed in polyacrylonitrile nanofiber film spun by electrospinning. *Materials Letters*. 59, p.3046-049.

Wang, Z.G., Ke, B.B., Xu, Z.K., 2007. Covalent Immobilization of Redox Enzyme on Electrospun Nonwoven Poly(Acrylonitrile-co-Acrylic Acid) Nanofiber Mesh Filled With Carbon Nanotubes: A Comprehensive Study. *Biotechnology & Bioengineering*,. 97 (4), p.708-20.

Wang, Z., 1999. Spectroscopic investigation of interactions among components and ion transport mechanism in PAN electrolytes. *Solid State Ionics*. 121 (1-4), p.141-56.

Ward, I.M (ed), 1982. *Developments in Orientated Polymers* – 1. Applied Science Publishers.. 1-46.

Wu, H., Zhang, R., Liu, X., Lin, D. & Pan, W., 2007. Electrospinning of Fe, Co, and Ni Nanofibers: Synthesis, Assembly, and Magnetic Properties. *Chemical Materials.* 19, p.3506-511.

Yamane, A. & Sawai, D., 1997. Development of Ductility and Tensile Properties upon Two-stage Draw of Ultrahigh Molecular Weight Poly(acrylonitrile). *Macromolecules*. 30, p.4170-178.

Yarin, A. L., Koombhongse, S. & Reneker, D. H., 2001. Bending instability in electrospinning of nanofibres. *Journal of Applied Physics.* 89 (5), p.3018-026.

Ye, H., et al., 2004. Reinforcement and rupture behavior of carbon nanotubes polymer. *Physics Letters.* 85 (10), p.1775-777.

Yu, J., et al., 2001. A New Metal-Organic Polymer with Large Grid Acentric Structure Created by Unbalanced Inclusion Species and Its Electrospun Nanofibers. *Inorganic Chemistry*. 40, p.4516-517.

Yuh, J., 2005. Barium titanate ($BaTiO_3$) nanofibers via electrospinning. *Materials Letters*. 59, p.3645-647.

Zhang, Y., Dong, H., Norris, I., MacDiarmid, A. & Jones, W., 2001. High surface area chemosensor material by electrospinning of fluorescent conjugated polymer. *Polymer Material Science & Engineering.* 85, p.622-23.

Zhu, J. & Chen, H., 2004. Needle-shaped nanocrystalline CuO prepared by liquid hydrolysis of $Cu(OAc)_2$. *Materials Science & Engineering A*. 384, p.172-76.

Ziegler, D., Sung, C., Dolukhanyan, T. & Schreuder-Gibson, H. L., 2000. Microcharacterization of composite membranes of electrospun nanofibers and microparticles. *Institute of Physics Conference,* 165. p.171-72.

Zussman, E., Chen, X., Ding, W., Calabri, L., Dikin, D., Quintana, J. & Ruoff, R., 2005. Mechanical and structural characterization of electrospun PAN-derived carbon nanofibres. *Carbon*. 43, p.2175-185.

CHAPTER 3: EXPERIMENTAL AND RESULTS

THE EFFECT OF VARIABLES ON ELECTROSPINNING OF PAN

3.1 INTRODUCTION

In this chapter, the effect of changes in the electrospinning parameters on the resultant mat and fibre morphology are reported and discussed.

3.2 ELECTROSPINNING PROCESS EXPERIMENTAL SET-UP

Spinning apparatus

A *Gamma HV ES30*^{TM} positive DC power supply was used. A copper wire electrode was inserted into the nose of the pipette to about 5 mm from the end. All spinning was conducted inside a fume-hood but without the extraction fan operating. The grounded flat foil electrode was always mounted at 45° and grounded in 4 positions with crocodile clips. All were spun from a 45° angle to prevent droplets on the spun mat and to minimize wastage from dripping.

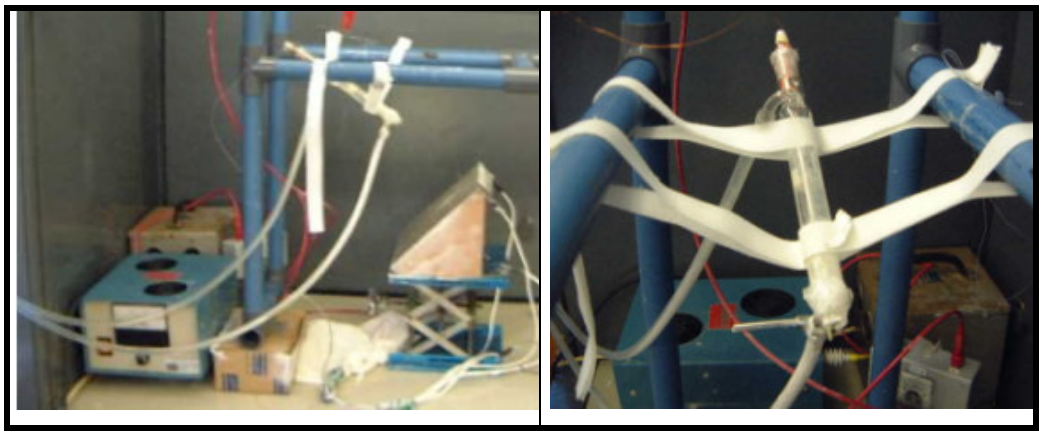

Figure 3.1 Photographs of the electrospinning set-up with temperature control.

Figure 3.2 Photograph of electrospinning set-up with multi pipettes and rotating electrode and using an IR lamp for heating to drive off the solvent.

The rotating grounded electrode shown in Figure 3.2 was designed and built by Chris Laffin during a visit from Queen's University, Belfast, Ireland. The driving motor was a variable speed *Bosch*® drill. It was operated with Teflon™ yarns or thin copper wires. The multi-spinneret was designed and built by Ullrich Buttner of the Uni. of Stellenbosch. The rotating electrode was always run in a clockwise direction such that the fibres were pulled first over the top of the rotating mandrel.

Electrospinning procedure

Each solution was spun from a new long-nosed, glass Pasteur pipette. The temperature of the solution was allowed to equilibrate at the desired temperature where temperature control was employed.

Temperature was controlled due to the ambient laboratory temperature fluctuations between 10°C in winter and 30°C in summer. Temperature control was only possible on the single pipette setup, shown in Figure 3.1. The IR heating lamp was used with the multiple spinnerets.

All samples were dried at room temperature in a vacuum oven for 12 hours, prior to any analysis to remove any residual solvent. A new EpindorffTH pipette yellow plastic tip was used for each sample

Polymers

The grades of PAN polymer used in this research are listed in Table 3.1 below. All are used commercially to make PAN fibres. Samples numbered 1 and 4 are considered hompolymers and samples numbered 2 and 3 are copolymer PAN. The polymerisation techniques are presented in Section 2.3.1.

Polymer powder or fibres were dissolved in various solvents at 50°C and stirred for 24 hours. The grades of PAN used are described in Table 3.1. Sample 4 required 80°C to dissolve.

After dissolution the solutions were stored at room temperature in sealed containers, on a magnetic stirrer till electrospun to prevent the formation of a gel network.

Table 3.1 PAN grades used in this research

No	Supplier	Molecular Weight in g.mol^{-1}	M_w/M_n	Composition, tradename and olymerization solvent
1	Lenzing Plastics Kelheim	210 000	2,8	AN : MA = 99,5 : 0,5; Dolanit 12™ powder; DMF
2		85 000	2,8	AN : MA = 94,0 : 6,0; Dolan™ powder; DMF
3	Acordis UK	120 000	2,7	AN : MA : IA = 93 : 6 :1; fibre tow; DMF
4	Montefibre	300 000 ??	2,5	AN : VA = 99,8 : 0,2%; Ricem™ powder; DMAc

All solvents were obtained from *Aldrich,* are Analytical Grade and were used as received. The chemical formulae of the highly polar solvents for PAN are listed in Figure 2.21. The samples prepared by electrospinning for analyses are described in Table 3.2 below. The variables include

the different grades of PAN at various concentrations (4% to 12% w/w), different voltages (10 to 30 kV), and variable spinning distances (10 cm to 35 cm). The solvent and the spinning temperature is also noted for each sample produced.

Samples prepared

The electrospinning variables that were investigated included and are recorded in Table 3.2 for each sample prepared include:

- different PAN grades (85k, 120k copolymers and 210k, 300k homopolymer PAN)
- various concentrations of PAN (4% to 12% w/w)
- different voltages (10 to 30 kV)
- variable spinning distances (10 cm to 35 cm).

The solvent and spinning temperature used were also noted for each sample produced

Table 3.2 Description of electrospun samples

CODE	MW (k)	Conc. %	Distance in cm	Voltage in kV	Comments
8% 210k at different voltages (20 cm fixed distance). No temperature control in DMF					
001	210	8	20	**25**	
002	210	8	20	**20**	
003	210	8	20	**15**	
004	210	8	20	**30**	3-D spinning
006	210	8	20	**20**	Repeat 002
8% 85k at different voltages (20 cm fixed distance). No temperature control in DMF					
009	85	8	20	**20**	
010	85	8	20	**25**	
011	85	8	20	**15**	
012	85	8	20	**30**	
013	85	8	20	**30**	Long spin
6% 210k at different voltages (20 cm fixed distance). No temperature control in DMF					
014	210	6	20	**20**	
015	210	6	20	**15**	
016	210	6	20	**25**	
017	210	6	20	**30**	3-D spinning
018	210	6	20	**10**	droplets
6% 210k at different distances (20 & 10 kV). No temperature control in DMF					
019	210	6	15	**20**	3-D spinning
020	210	6	15	**10**	
021	210	6	17.5	**10**	
022	210	6	25	**20**	
023	210	6	30	**20**	
024	210	6	35	**20**	
6% 85k at different distances (20 & 10 kV) – No temperature control in DMF					
025	85	6	20	**20**	
026	85	6	20	**25**	

027	85	6	20	**30**	
028	85	6	20	**15**	
029	85	6	20	**20**	Repeat 025,
030	85	10	Vary	**Vary**	
031	85	9	Vary	**Vary**	
6% 210k at different distances (20 & 10 kV). No temperature control in DMF repeat 001					
A001	210	6	20	**20**	± 9 cm circular
A002	210	6	15	**20**	± 11 cm circular
A003	210	6	17.5	**20**	
A004	210	6	22.5	**20**	
A005	210	6	25	**20**	
A006	210	6	20	**20**	
4% 210k at different voltages (20 cm fixed distance). No temperature control in DMF					
B001	210	4	20	**25**	
B002	210	4	20	**30**	
B003	210	4	20	**20**	
B004	210	4	20	**15**	
B005	210	4	20	**10**	
4% 210k at different distances (20kV). No temperature control in DMF					
B006	210	4	15	**20**	blotches
B007	210	4	17.5	**20**	
B008	210	4	22.5	**20**	
B009	210	4	25	**20**	
B010	210	4	30	**20**	
4% 85k at different voltages (20 cm fixed distance). No temperature control in DMF					
C002	85	4	20	**20**	
C003	85	4	20	**25**	
C004	85	4	20	**30**	
4% 85k at different distances (20 & 30 kV). No temperature control in DMF					
C013	85	4	12.5	**20**	
C008	85	4	15	**20**	
C001	85	4	15	**20**	
C010	85	4	17.5	**20**	
C011	85	4	22.5	**20**	
C012	85	4	25	**20**	
C007	85	4	35	**20**	
C009	85	4	15	**30***	
10% 120k at different voltages (20 cm fixed distance). In DMF, 20°C, for 2 hrs					
D005	120	10	20	**15**	
D001	120	10	20	**20**	
D007	120	10	20	**20**	
D004	120	10	20	**25**	
D002	120	10	20	**30**	
D006	120	10	25	**30**	
D003	120	10	30	**30**	
10% 120k at different voltages (20 cm fixed distance). In DMF, 25 °C, plastic tip for 2 hrs					
E005	120	10	20	**15**	
E001	120	10	20	**20**	
E004	120	10	20	**25**	
E002	120	10	20	**30**	
E006	120	10	25	**30**	

E003	120	10	30	**30**	
10% 120k at different voltages (20 cm fixed distance). 30 °C, plastic tip, for 2 hrs					
F005	120	10	20	**15**	
F001	120	10	20	**20**	
F007	120	10	20	**20**	
F004	120	10	20	**25**	
F002	120	10	20	**30**	
F006	120	10	25	**30**	
F003	120	10	30	**30**	
10% 120k at different voltages and concentration In DMSO, 70°C, plastic tip					
G001	120	10	20	**20**	IR Lamp
G002	120	6	25	**20**	IR Lamp
G003	120	10	30	**30**	IR Lamp
G004	120	8	30	**20**	IR Lamp
10% 85k at different voltages (20 cm fixed distance). In DMF, 30 °C, plastic tip					
H005	85	10	20	**15**	
H001	85	10	20	**20**	
H002	85	10	20	**30**	
H004	85	10	20	**25**	
H003	85	10	30	**30**	
10% 85k at different voltages and distances 30 °C, plastic tip					
H008	85	10	15	**15**	
H007	85	10	15	**25**	
H006	85	10	25	**30**	
8% 210k at different voltages (20 cm & 25 cm) fixed distance. 30 °C, plastic tip					
I001	210	8	20	**20**	
I002	210	8	20	**30**	
I005	210	8	20	**15**	
I006	210	8	25	**30**	
10% 85k onto spun-bonded polyester at 30 °C, plastic tip					
J001	85	10	20	**20**	
J002	85	10	20	**20**	
J005	85	10	20	**20**	
J003	85	10	20	**15**	
J004	85	10	20	**15**	
10% 85k onto spun-bonded polyester at 30 °C, plastic tip					
K001	85	10	20	**20**	
K002	85	10	20	**20**	
K003	85	10	20	**20**	
PAN / PANi blends in DMF (will not spin in DMSO)					
L001	85	10	20	**20**	On foil, 30 °C
L002	85	10	20	**20**	On ATI PAN fabric
L003	85	10	20	**20**	On foil 50 °C
PAN in DMAc at 50°C					
M001	120	10	20	**20**	
M002	85	10	20	**20**	

10% 85k with Chemisorb at 20 cm fixed distance. 30 °C, plastic tip for mercury absorption					
N001	85	10	20	**30**	0,25g DMAc
N002	85	10	20	**20**	DMF
N003	85	10	20	**20**	
N004	85	10	20	**20**	
N005	85	10	20	**20**	S, Hg
N006	85	10	20	**20**	
N007	85	10	20	**20**	S, Hg
PAN Chemisorb blends in DMF for mercury removal					
P001	85	10	20	**20**	
P002	85	10	20	**20**	
P003	85	10	20	**20**	
P004	85	10	20	**20**	
P005	85	10	20	**20**	
P006	85	10	20	**20**	
P007	85	10	20	**20**	
P008	85	10	20	**20**	
P009	85	10	20	**20**	
P010	85	10	20	**20**	
PAN / PANi blends in DMF for voltammetry measurements					
Q001	85	10	20	**20**	03a499 0,25 g PANi
Q002	85	10	20	**20**	03a500 0,5 g PANi
Q003	85	10	20	**20**	03a501 0,75g PANi
Effect of the take-up speed, in DMF					
S001	210	4	20	**20**	14 $m.s^{-1}$
S002	210	4	20	**20**	21 $m.s^{-1}$.
S003	210	4	20	**20**	14 $m.s^{-1}$
S004	210	4	20	**20**	21 $m.s^{-1}$.
S005	210	4	20	**20**	14 $m.s^{-1}$
S006	210	4	20	**20**	21 $m.s^{-1}$.
6 % 120k with CuO nanoparticles onto flat foil electrode at 20 cm, 20 kV and 30 °C					
	MW	**wt%**	**Type**	**wt %**	
S001	120	6	control	0	
S002	120	6	CuO	9	
S003	120	6	CuO	15	
S004	120	6	CuO	13.5	30 min sonication
S007	120	6	CuO	9	ConFloc surfactant
S008	120	6	CuO	9	non-ionic surfactant
S009	120	6	CuO	9	Anionic surfactant
Rotating take-up in DMAc from 5 clustered spinneret's onto 5 cm wide foil at 21 °C					
V001	120	12	20	**20**	7 $m.s^{-1}$
V004	120	12	20	**20**	10 $m.s^{-1}$.
V002	120	12	20	**20**	14 $m.s^{-1}$.
V003	120	12	20	**20**	21 $m.s^{-1}$
V005	120	12	20	**20**	28 $m.s^{-1}$.

Rotating Take-up in DMAc from 5 clustered spinneret's onto 5 cm wide foil at 20 °C					
W001	120	10	20	**20**	7 $m.s^{-1}$
W002	120	10	20	**20**	10 $m.s^{-1}$.
W003	120	10	20	**20**	14 $m.s^{-1}$.
W004	120	10	20	**20**	21 $m.s^{-1}$
W005	120	10	20	**20**	28 $m.s^{-1}$.

6% 500k in DMAc, different voltages (20 cm), 20 cm distance. 30 °C, plastic tip onto foil					
X003	500	6	20	**10**	
X005	500	6	20	**15**	
X001	500	6	20	**20**	
X004	500	6	20	**25**	
X002	500	6	20	**30**	
6% 500k in DMAc at different distances (20 & 30 kV). 30 °C, plastic tip onto foil					
X006	500	6	10	**20**	
X007	500	6	15	**20**	
X008	500	6	25	**20**	
X009	500	6	30	**20**	
X010	500	6	30	**30**	
8% 85k in DMAc rotating electrode at various face speed and distances at 23 °C, 5 spinnerets					
Z001	85	8	9	**20**	14 $m.s^{-1}$.
Z002	85	8	14	**20**	14 $m.s^{-1}$.
Z003	85	8	14	**20**	7 $m.s^{-1}$.
Z004	85	8	14	**20**	14 $m.s^{-1}$.
Z005	85	8	14	**20**	21 $m.s^{-1}$.
Z006	85	8	14	**20**	28 $m.s^{-1}$.
Z007	85	8	14	**20**	32 $m.s^{-1}$.
Z008	85	8	14	**20**	38 $m.s^{-1}$.
Z009	85	8	14	**20**	43 $m.s^{-1}$
8% 210k in DMAc rotating electrode at different face speed and distances at 26 °C, 5 spinnerets					
Z011	210	8	14	**20**	14 $m.s^{-1}$. On foil strip
Z012	210	8	14	**20**	21 $m.s^{-1}$. On folil strip
Z013	210	8	14	**20**	28 $m.s^{-1}$. On foil strip
Z014	210	8	14	**20**	32 $m.s^{-1}$. On foil strip
Z015	210	8	14	**20**	38 $m.s^{-1}$. On foil strip
Z016	210	8	14	**20**	43 $m.s^{-1}$ On foil strip
6% 210k in DMAc rotating electrode at different face velocity and distances at 27 °C, 5 spinnerets					
Z017	210	6	14	**20**	14 $m.s^{-1}$. On yarns
Z018	210	6	14	**20**	21 $m.s^{-1}$. On yarns
Z019	210	6	14	**20**	28 $m.s^{-1}$.On yarns
Z020	210	6	14	**20**	32 $m.s^{-1}$. On yarns
Z021	210	6	14	**20**	38 $m.s^{-1}$. On yarns
Z022	210	6	14	**20**	38 $m.s^{-1}$. On foil strip
Repeat of A series with temperature control and a plastic tip					
A1	210	6	20	**20**	30°C, DMF
A2	210	6	15	**20**	50°C, DMF
A3	210	6	17,5	**20**	50°C, DMF
A7	210	6	20	**30**	50°C, DMF

3.3 CHARACTERISATION OF NON-WOVEN MAT MORPHOLOGY

3.3.1 Measurement of fibre diameter

The scanning electron microscopy, (SEM), analyses were performed by Miranda Waldron at the University of Cape Town Microscopy Unit on a *LEO 244S* SEM after carbon sputter coating was applied. A typical micrograph of an electrospun PAN sample at a high magnification (20 000X) is shown in Figure 3.3 below. The magnification was chosen such that 10 to 20 fibres were included in the image. Dependant on the spinning conditions and thus the fibre diameter, this was done at between 20000 to 40000 times magnification on the electrospun PAN samples.

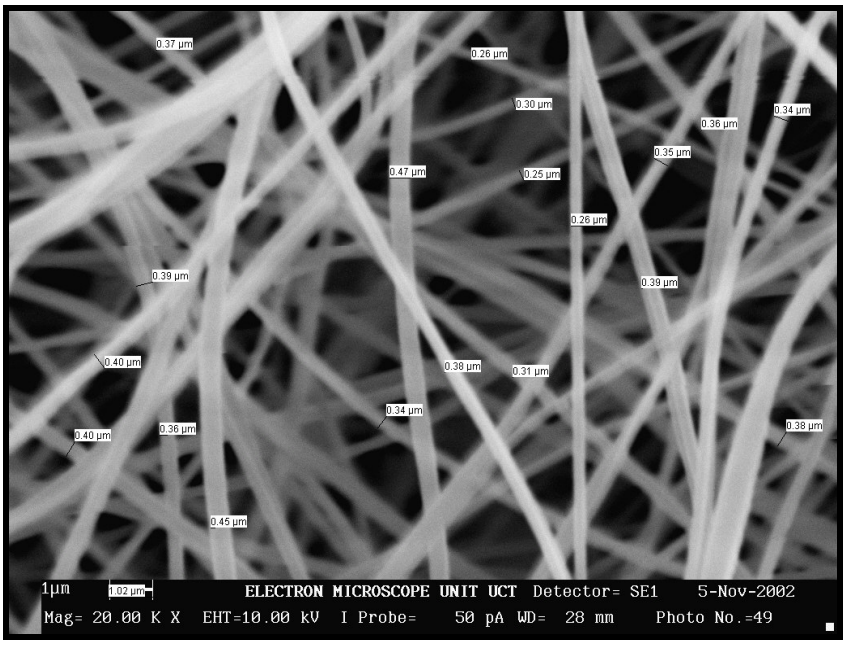

Figure 3.3 SEM at 20 000 X; ES PAN mat using Mirage™ Software for fibre diameter.

Each such image was then processed using SEM *Analysis™ Software*. A minimum of 12 measurements was taken and the highest and lowest values discarded prior to calculating the average. The diameter of beads on fibres where present, were ignored as well as merged fibres. Typical data is shown in Table 3.3 below which shows 18 individual fibre diameter measurements, as well as, the maximum, minimum and average for a PAN fibres electrospun at 30 kV and a distance of 25 cm.

Table 3.3 Example of measurement of the electrospun fibre diameter in nanometers
For sample H006; PAN electrospun at 30 kV and a distance of 25 cm.

382	335		403	Average diameter in nm	356
454	340		373	Spinning voltage in kV	30
382	346		388	Spinning distance (cm)	25
264	309		253	Max	471
393	398		298	Min	253
471.70	362.4		256.63		

3.3.2 Characterization of electrospun mat roughness

An indication of the roughness of a non-woven electrospun mat can be obtained from a horizontal intensity scan across the SEM micrograph. The measurements of the intensity using a grey scale can be imported into another software programme, i.e. *Origin*® for further processing.

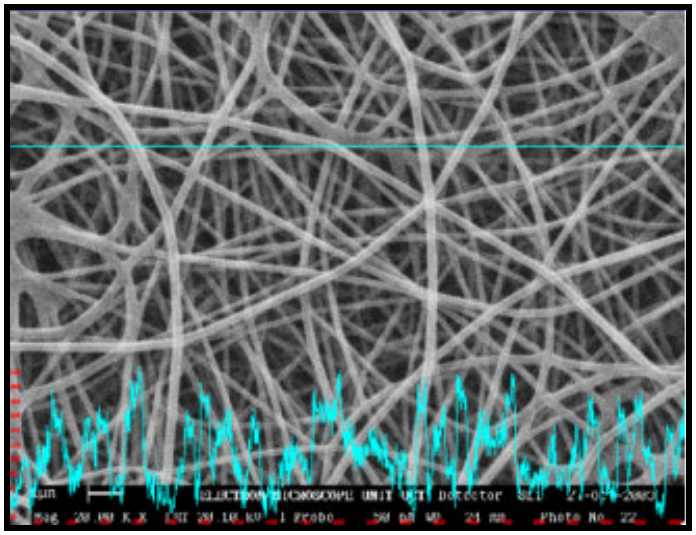

Figure 3.4 SEM at 20 000 X magnification of ES PAN using Mirage® software for roughness.

The graphic at the right in Figure 3.5 shows the data after mathematical manipulation using FFT smoothing. This provides an additional means of characterizing the thickness of the fibres. The value of the grey scale on the abscissa could, in theory, be calibrated with a depth distance thereby giving information on the size of the gaps between the fibres. Care must be taken to always ensure the beam voltage, thus intensity and the degree of contrast and brightness of the images are kept constant if the results are to be used for the purpose of comparison of pore opening size distribution and mat uniformity. The author has not previously noted techniques to characterize the mat roughness of electrospun non-wovens.

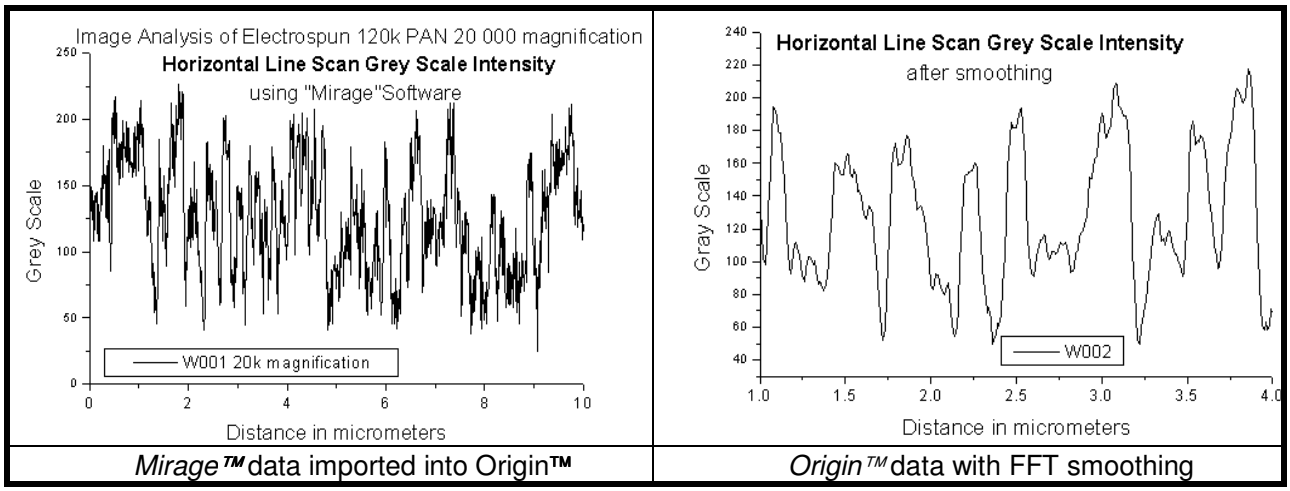

Mirage™ data imported into Origin™ | *Origin™* data with FFT smoothing

Figure 3.5 *Mirage® software* for electrospun PAN mat roughness evaluation.

3.3.3 Characterization of electrospun mat porosity

An area light intensity scan, which indicates the porosity of the non-woven mat material can also be obtained using the SEM Mirage Software. The porosity is related to the air and water permeability (Aydilek 2002). The determination of the threshold limit is highly subjective but if kept constant for a series of similar samples, with the same constant image contrast and brightness, the values can be used for comparative purposes. The result has been termed the "Coverage Factor". The author has not previously noted techniques to characterize the mat porosity of electrospun non-wovens.

Figure 3.8 shows the application of image analysis manipulation of SEM micrographs using Mirage™ software. The two samples of electrospun PAN fibres shown were prepared from the same PAN polymer but with different take up speeds on the grounded rotating electrode.

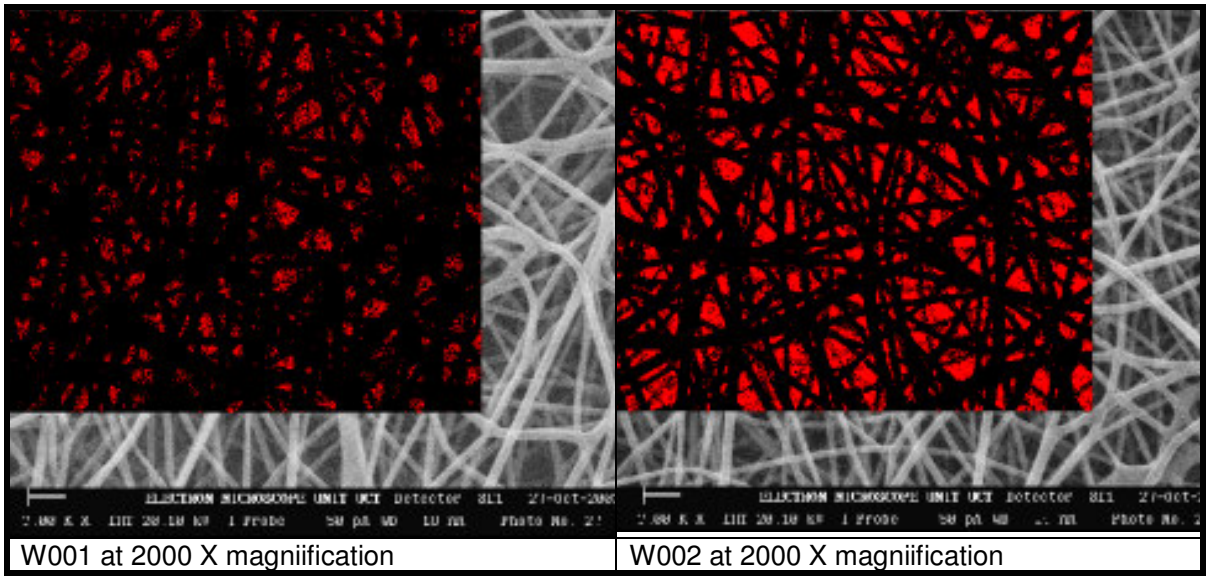

W001 at 2000 X magniification	W002 at 2000 X magniification

Figure 3.6 ***Mirage®* software image to determine electrospun mat porosity.**

The Mirage software was used to calculate the area of the "red" spaces relative to the "black" fibres and the results are resented in Table 3.4.

Table 3.4 **Results of the "Coverage Factor" to determine mat porosity**

Sample ID	Description	Phase 0 (red)	Coverage Factor
		mm²	% Area of Pores
W001	7 $m.s^{-1}$	502.90	7.05
W002	14 $m.s^{-1}$	1412.24	19.79

3.4 THE EFFECT OF SPINNING VOLTAGE ON FIBRE DIAMETER

The micrographs in Figure 3.7 show that the voltage slightly affected the fibre diameter on the 10% 210k PAN spun from DMF spun at a distance of 20 cm. It also illustrates that the lower polymer molecular weight and resultant lower viscosity has a far greater influence on the diameter than the

spinning voltage. In general, the higher the voltage the lower the fibre diameter but only if extreme care is taken to ensure that the conditions are stable and repeatable, including humidity, temperature and the size of the spinneret orifice. These fibres were spun at Drexel University by C Greyling in a controlled environment.

Voltage	500X Magnification	2000X Magnification	15 000X Magnification
Homopolymer PAN (<0,5% MA) 10% w/w, 210k			
10 kV	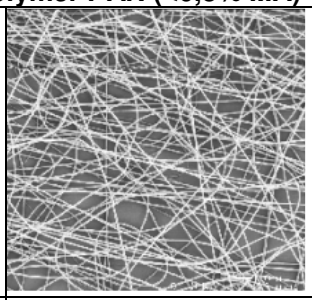	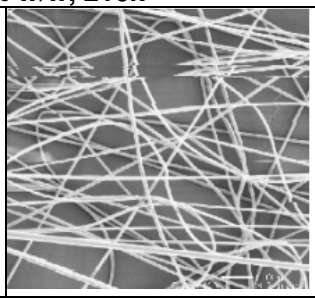	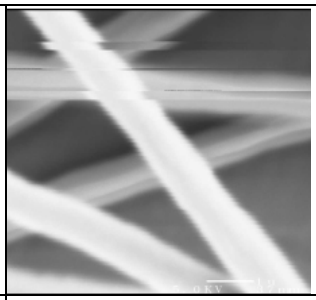
			1000 nm diameter
15 kV	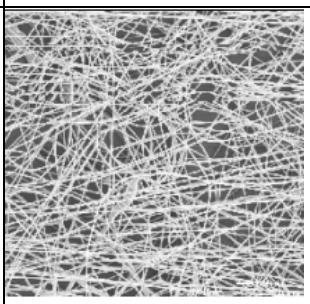	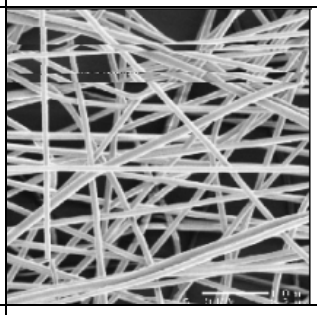	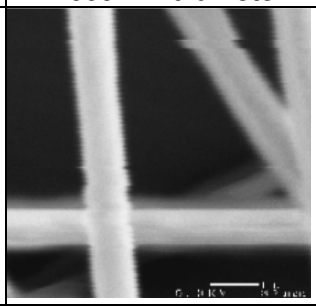
			800 nm diameter
20 kV	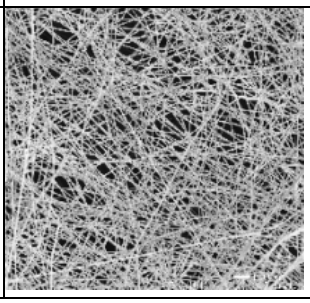	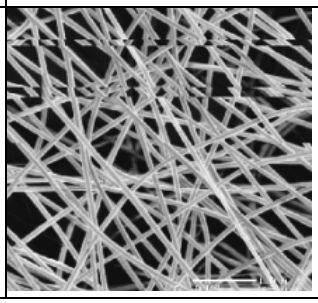	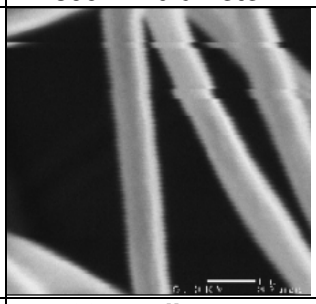
			700 nm diameter
Copolymer PAN (6% MA) 10% w/w, 85k			
25 kV	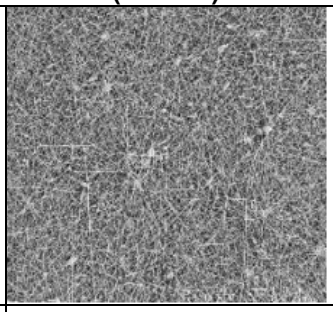	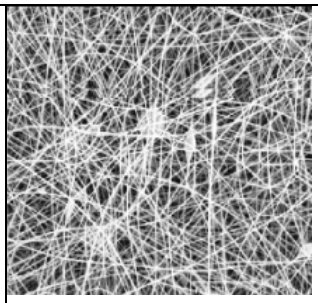	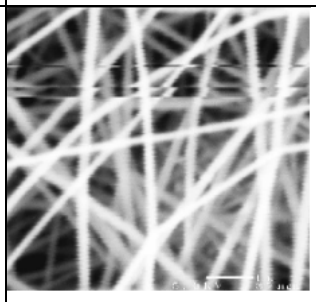
			100 nm diameter

Figure 3.7 SEM results to show the effect of voltage on fibre diameter.

The graph in Figure 3.8 shows the effect of the voltage on fibre diameter measured from uncapped glass pipettes at room temperature and humidity, which fluctuated slightly. It can be noted that there a moderate correlation here (1000 to 700 nm) between the voltage and the fibre diameter. In

addition there is a broader fibre diameter distribution reported in general in literature by other researchers with PEO (Deitzel et al. 2001), PU (Demir et al. 2002) and PVA (Ding 2004).

Under more controlled conditions a linear relationship between the voltage and the fibre diameter was established. The results in Figures 3.8 and 3.9 are both obtained using the same 10% 120k PAN copolymer in DMAc solution. In the case of Figure 3.9, the temperature was controlled at 30°C and a Epindorff yellow plastic pipette tip was used, These plastic tips have more constant hole size than the glass Pasteur pipettes.

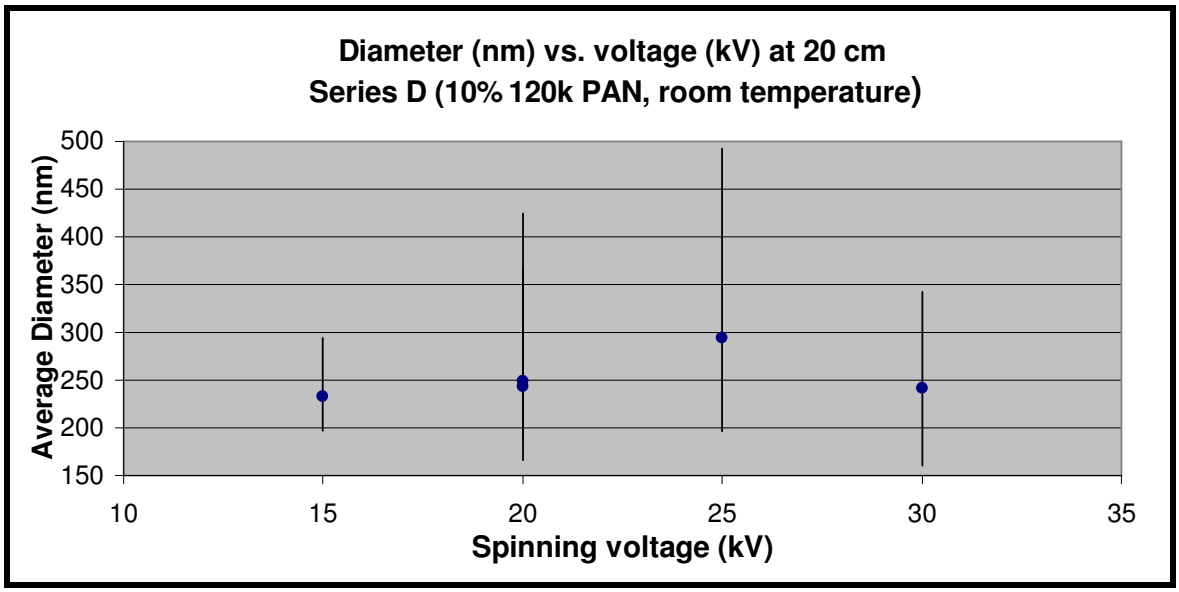

Figure 3.8 The effect of voltage on fibre diameter at <u>variable</u> room temperature.

The mass flow rate for Series F in Figure 3.9 was also determined by weighing the foil ground electrode before spinning and after spinning. The results for the diameter and mass flow rate are tabulated in Table 3.5 The sample was dried in a vacuum oven prior to the mass measurement to remove any residual solvent

A linear relationship is shown between the mass flow rate and the voltage and thus between the mass flow rate and the fibre diameter. These results show that with careful control over the spinning conditions the fibre diameter is controlled by the spinning voltage.

Table 3.5 Description of series F ES PAN samples

CODE	MW (k)	%	cm	kV	kV/cm	Diameter in nm	Mass transfer in g.2 hrs^{-1}	Mass$_{After}$-mass$_{Befo}$
F005	120	10	20	**15**	0,75	307	0,1242	2,5432 – 2,4719
F007	120	10	20	**20**	1,00	288	0,0389	2,2221 – 2,1832
F004	120	10	20	**25**	1,25	274	0,0156	2,1620 – 2,1464
F002	120	10	20	**30**	1,50	267	0,0058	2,1918 – 2,1860

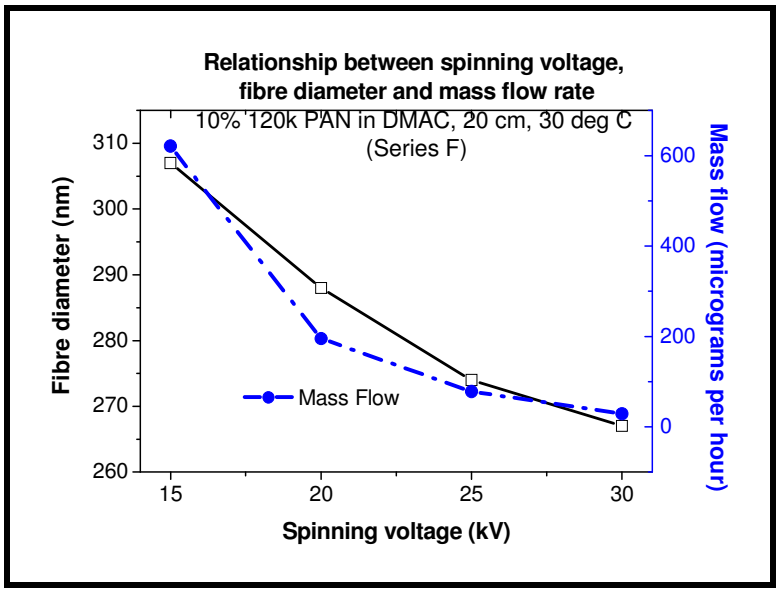

Figure 3.9 The effect of voltage on PAN fibre diameter spun at 30 °C with a plastic tip.

The SEM micrographs of the samples of series F (see Table 3.2) are shown in Figure 3.10.

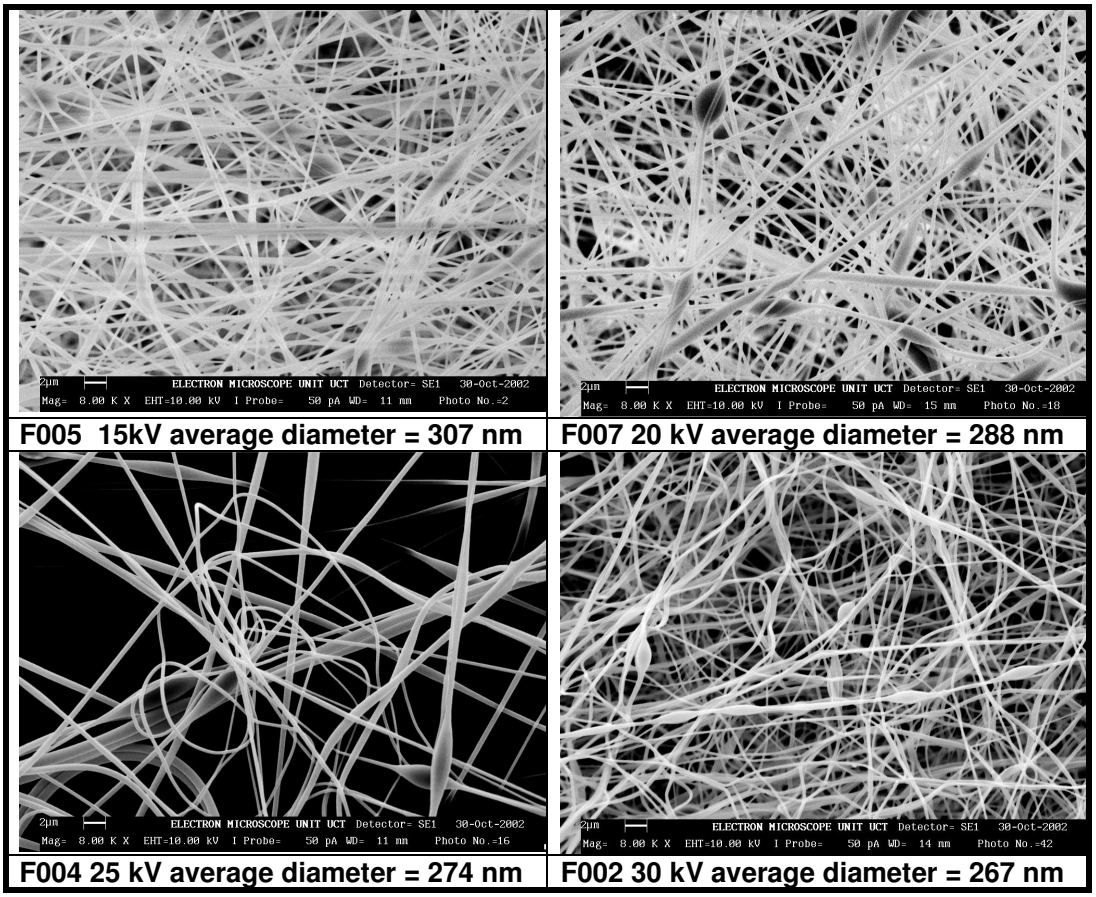

Figure 3.10 SEM micrographs 8000 X magnification of F series (120k PAN copolymer).

3.5 THE EFFECT OF SPINNING DISTANCE ON FIBRE DIAMETER

There is not a linear relationship between the spinning distance (field strength) and the fibre voltage as shown in Figures 3.11 and 3.12. In general there is an increase in the fibre diameter at the medium spinning distance in these series and seen in many additional examples, not reported here.

The significantly narrower fibre size distribution for the conditions depicted in the series in Figure 3.12 could be due to the fact that the DMAc is a better solvent than DMF or due to spinning at a higher voltage of 30 kV.

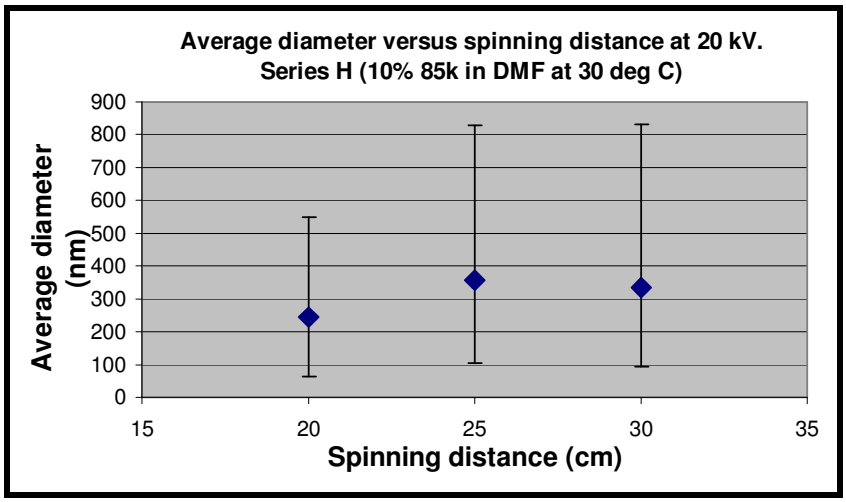

Figure 3.11 Effect of spinning distance on fibre diameter (10% 85k in DMF).

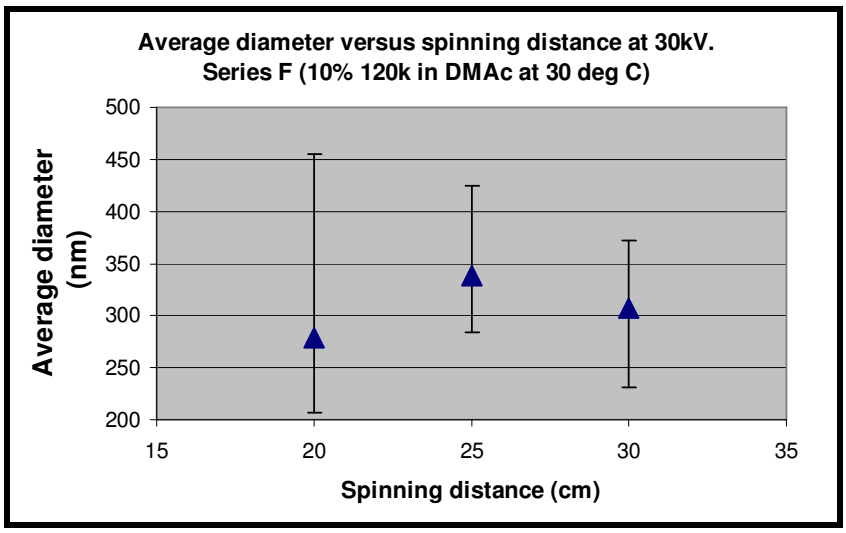

Figure 3.12 Effect of spinning distance on fibre diameter (10% 120k in DMAc).

3.6 THE EFFECT OF VISCOSITY ON ELECTROSPINNING

The results of the rheology measurements for different grades and concentration of PAN in different solvents, measured at 25 °C are shown in Figure 3.13. Measured on a *Paar Physica Modular*

Compact Rheometer (MCR 300). The four samples with initial viscosity values (η) >1 Pa.s would not spin at 25°C. The 6% 500k and the 12% 120k PAN did spin at 30°C. The viscosity shear measurements were conducted by Y. Koen in the laboratories of Plascon Research based at the University of Stellenbosch.

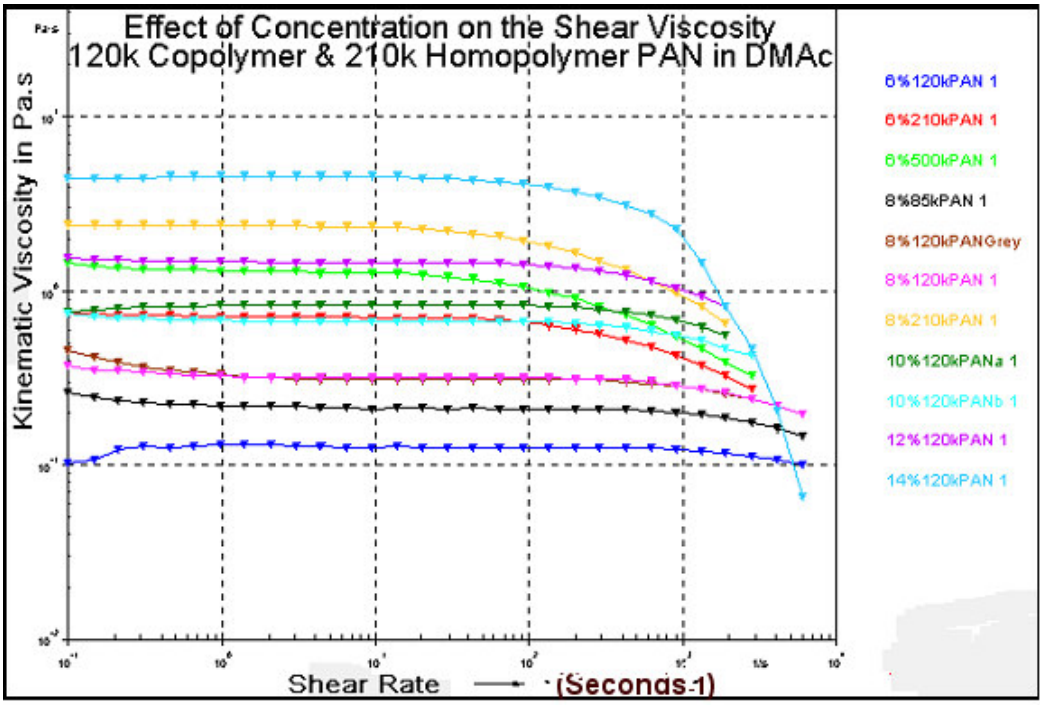

Figure 3.13 Effect of molecular weight and concentration on shear viscosity of PAN.

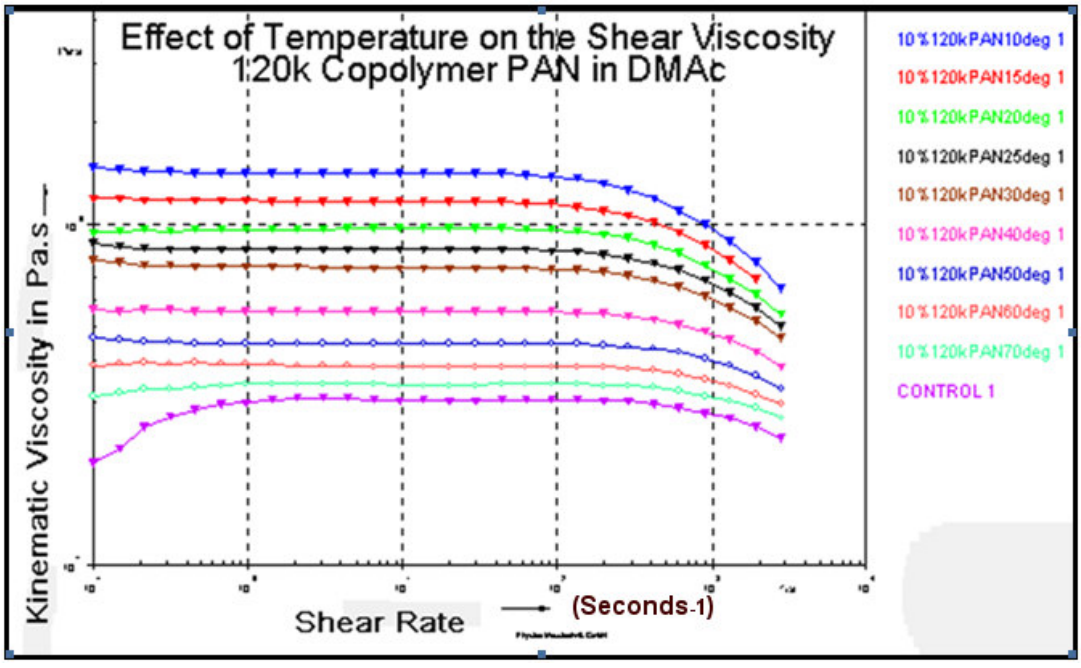

Figure 3.14 Effect of temperature on the shear viscosity of 10% 120k PAN.

The viscosity of the spinning dope is influenced by the temperature, the type of solvent, the solubility parameter of the polymer in the solvent, the concentration, the grade of polymer (copolymers configuration), additives, the molecular weight and the molecular weight distribution.

In Figure 3.14 the rheology results for the 10% 120k PAN copolymer are shown. The sample would not spin below 20 °C, i.e. for samples with an initial viscosity >1 Pa.s. It would thus appear that a viscosity of less than 1 Pa.s is required for electrospinning of PAN under the given conditions.

In Figure 3.14 it can also be seen that there is a relative large step change in the viscosity between the temperatures of 30 and 40 °C. It was noted that samples spun in the laboratory in the middle of summer when ambient temperature was above 30 °C in the laboratory, that the solution drip rate from the pipette was markedly higher. The minimum viscosity for electrospinning under the conditions used here, i.e. gravity pressure (no syringe pump) and a pipette at a 45° angle appears to be about 0,1 Pa.s, below which the surface tension of the solution is too low for the formation of a steady droplet at the tip of the pipette, which is required to form the Taylor cone for the electrospinning process.

Table 3.6 Physical constants of PAN solvents (CRC Handbook, 2008)

Solvent	MW	Density ($g.cm^{-3}$)	Tb (°C)	Tm (°C)	Viscosity (10^{-3} $N.m.s^{-2}$)	Surface tension ($dynes.cm^{-1}$)
DMF	72	0.949	153	-58	0,8	37
DMSO	78	1.102	189	19	2,0	43
Ethylene carbonate	89	1.334	238	36		
Propylene carbonate	102	1.201	242	-49	2,8	41
Butyrolactone	89	1.129	206	-44	1,7	
DMAc	87	0.937	163	-20	0.92	34

A study of the effect of solvents and the spinning temperature was conducted when it was found that DMSO is a solid at room temperature (Tm = 19 °C) in winter. When using DMSO, it was necessary to increase the temperature of the pipette to 70 °C to initiate electrospinning. However the fibres on the grounded electrode were still in the gel state, containing large amounts of solvent. PAN could be spun from DMSO into a uniform mat if the air surrounding the electrified jet was also heated to 70 °C to increase the rate of solvent evaporation. Problems were experienced with “3-D” spinning as seen in Figure 3.2. Inserting a positively charged screen between the lamp and the spinneret enabled normal electrospinning.

Dilute solution viscosity was performed by C Greyling at Drexel University to attempt to measure the exact molecular weight of the various PAN polymer grades obtained for this project. The dilute solution viscosity results are given in the Figure 3.15 below. The experiment was repeated 3 times. The extrapolated y intercept, intrinsic viscosity, gave some negative values in all the tests. The results were mathematically manipulated (highest and lowest values discarded), to give the values shown in the 4 graphs in Figure 3.16. The measurements are usable if this procedure is used.

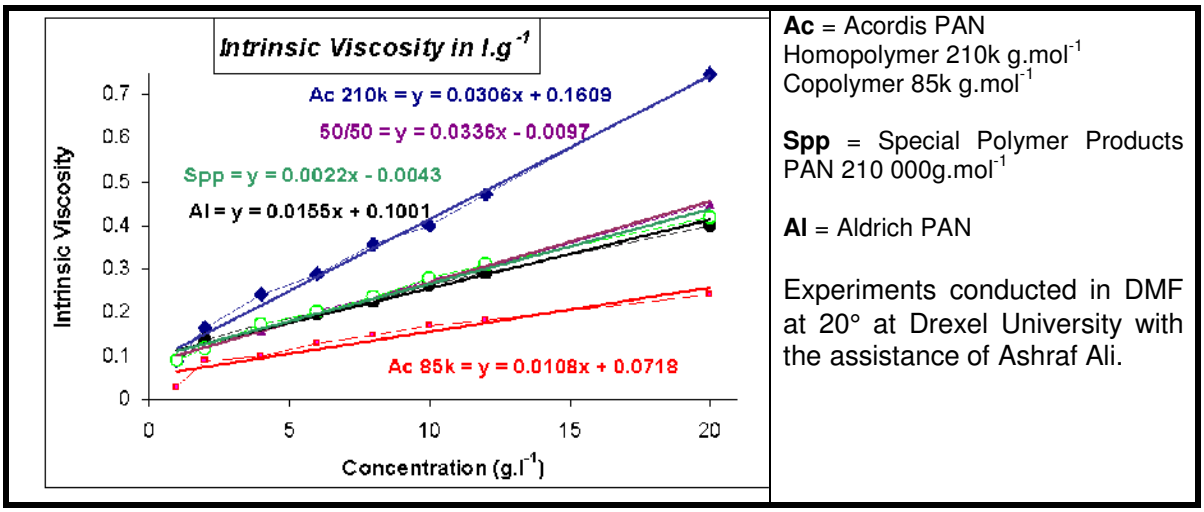

Ac = Acordis PAN Homopolymer 210k g.mol^{-1} Copolymer 85k g.mol^{-1}

Spp = Special Polymer Products PAN 210 000g.mol^{-1}

Al = Aldrich PAN

Experiments conducted in DMF at 20° at Drexel University with the assistance of Ashraf Ali.

Figure 3.15 Dilute solution viscosity results for PAN grades.

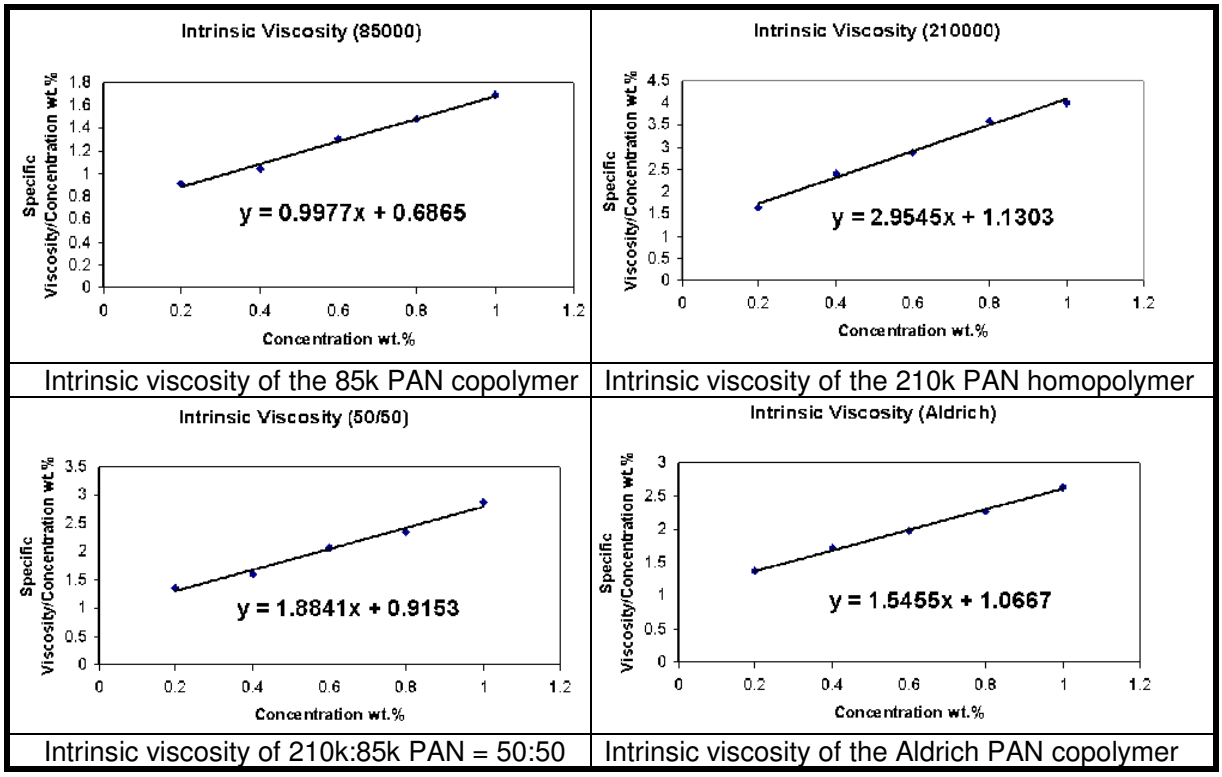

Intrinsic viscosity of the 85k PAN copolymer | Intrinsic viscosity of the 210k PAN homopolymer

Intrinsic viscosity of 210k:85k PAN = 50:50 | Intrinsic viscosity of the Aldrich PAN copolymer

Figure 3.16 Adapted PAN dilute solution viscosity results.

The most likely reason for the unusable data is due to the strong nitrile dipole interactions within PAN even in solution and complexation of the PAN with the DMF solvent. The addition of LiCl is used in the molecular weight determination of PAN by gel permeation chromatography to ensure an extended chain conformation.

The “Berry Number” (Be) for the electrospinning PAN dope solutions is given in Table 3.7 below. Polymer chain conformation in solution plays an important role in the structure of electrospun nanoscale fibres. Under the same processing conditions, the morphology of electrospun fibres is affected by the degree of chain entanglement and is related to the dimensionless “Berry Number”,

(Be). This number is the product of the intrinsic viscosity and the concentration. Generally fibre diameter increases with increasing Berry number as shown (Ali, 2001). by measuring the fibre diameter of electrospun Poly(L-lactic acid) with different molecular weights. The results for PLA are given in Figures 2.4 and 3.17 and discussed in Section 2.1.2. .For different molecular weights, the experimental correlation between fibre diameter and Berry Number is obtained. There are 4 distinct regions of "Berry Number" corresponding to different fibre diameter range and fibre morphology for a Poly(L-lactic acid) - chloroform system.

Table 3.7 "Berry Number" versus average diameter for electrospun PAN and PLA

Polyacrylonitrile, PAN (Greyling)			**Polylactic acid, PLA** (Ali 2003)	
PAN Description	**"Berry Number"**	**Diameter in μm**	**"Berry Number"**	**Diameter in μm**
6% 85 k	4.1193	0.16	1.0	0.1
4% 210 k	4.5212	0.10	1.8	0.2
8% 85 k	5.4918	0.40	2.3	0.5
6% 50:50 Blend	5.4920	0.32	2.6	0.5
6% 210 k	6.7818	0.70	2.9	1.8
10% 85 k	6.8650	0.50	3.1	2.2
8% 50:50 Blend	7.3224	0.57	3.6	2.8
12% 85 k	8.2380	0.60	4.4	2.6
8% 210 k	9.0424	0.96	4.6	2.7
10% 50:50 Blend	9.1530	0.84		
10% 210 k	11.3030	3.275		

Han discovered, with PAN, that if the Be was lower than 1 that beads would be formed because the viscosity of the solution would not be sufficient to hold together during the electrospinning process (Lyons & Ko 2004). No droplet or bead formation was not observed on PAN electrospun fibres made for this research, even at a Be<1. Bead formation was reported for electrospun PLA at Be<1.

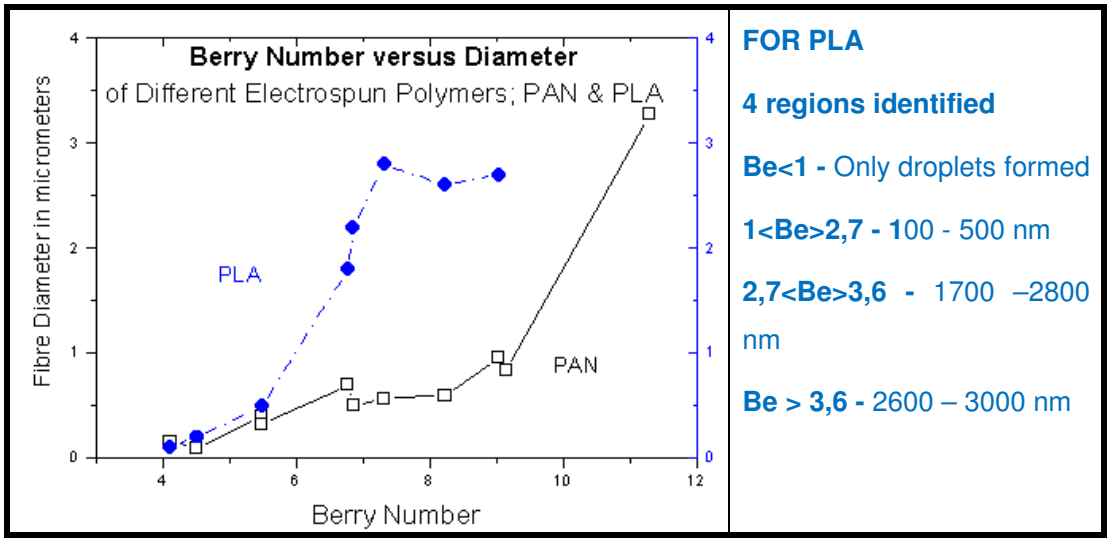

Figure 3.17 "Berry Number" versus diameter for mixed PAN grades and for PLA.

The results for the Be versus diameter in Figure 3.18 were obtained from pure 210k homopolymer, 85k copolymer and a blend of these two PAN grades from Acordis Kelheim Fibres. The 210k polymer graph is extrapolated using Origin Software.

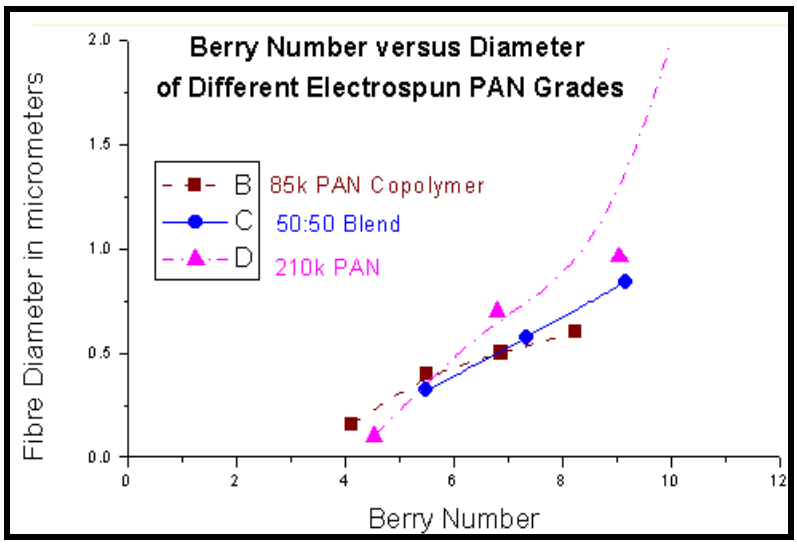

Figure 3.18 "Berry Number" versus diameter for different PAN grades and a blend.

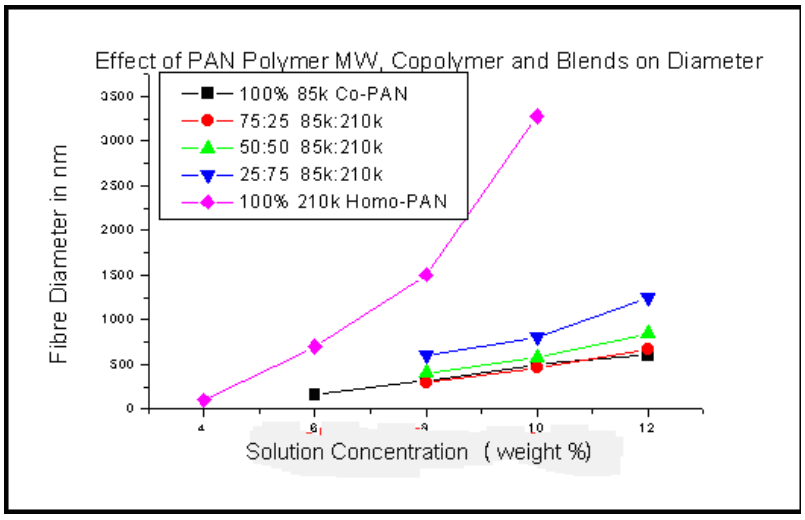

Figure 3.19 Dope concentrations versus diameter for PAN grades and blends.

The Berry Number results illustrated in Figures 3.18 and 3.19 show that the relationship between the Berry Number and the electrospun fibre diameter is comparable up to Be<5 but unique at higher Be for not only each type of polymer (PAN versus PLA) but also for the different PAN grades, as expected due to the different interaction with the solvent due to the change in solubility with an increase in molecular weight and different solvent interaction with the comonomer moieties in the molecule. The results show that the rate of increase in fibre diameter is higher for the higher Berry Number value and also thus a high intrinsic viscosity. A deduction from this finding is that in order to spin very small nanofibres it is necessary to use either a relatively low molecular weight polymer or a low concentration. The molecular must be sufficiently long to form enough entanglements to allow for fibre formation.

The results of the author are shown in Figure 3.18 and 3.19. It is noted that a change in the solution concentration has a greater effect on the rate of change in fiber diameter at higher molecular weight. These samples were produced by the author in a textile laboratory at Drexel University, PA, USA, under controlled conditions of constant temperature and humidity. The average fibre diameter for the 85k copolymer PAN, the 210k homopolymer PAN and their blends are given in Table 3.8.

Table 3.8 Average fibre diameter in µm of electrospun (85k / 210k PAN blends)

Solution Concentration	100% 85k	75/25	50/50	25/75	100% 210
4% w/w	Viscosity too low to spin				0,100
6% w/w	0,160	0,300	0,400	0,600	0,700
8% w/w	0,320	0,460	0,570	0,800	1,050
10% w/w	0,500	0,670	0,840	1,250	3,275
12% w/w	0,600				Too viscous

3.7 EFFECTS OF CHANGES IN THE EXPERIMENTAL SETUP

3.7.1 Spinning onto a rotating manifold grounded electrode

Theory suggests (Reneker et al. 2000) that aligned electrospun fibres could be produced by developing a suitable means of fibre collection which both gathers and stretches the fibres before reaching the grounded electrode. To achieve this, a device was designed which would rotate at high speed incorporating collecting threads situated above the grounded electrode. The device consisted of a standard variable high speed motor (*Bosch PSB 650 RE*), which was connected to a steel bar via a section of plastised PVC tubing, The plastised PVC tubing eliminated the effect of vibration during rotation and insulated the motor from the electric current present in the central steel bar which acted as the collecting electrode. Current was passed to the steel bar via a carbon brush riding on a copper sleeve located on the end of the steel bar.

The results in Figures 3.20 and 3.21 were obtained using the equipment described by Laffin (2005), who worked on his diploma research report with the author's guidance, show that:

- There is a linear relationship between the fibre diameter and the speed of rotation of the take-up device. The higher the take-up speed, the lower the fibre diameter
- The higher the concentration, the higher the fibre diameter for the same take-up speed. The fibres produced from 4% (w/w) solution had a greater reduction in diameter with increasing collector speed in comparison to fibres produced from 6% (w/w) solution.

(This research was conducted in conjunction with C. Laffin, Queens University, Belfast, Ireland. When he worked with the author at the University of Stellenbosch as an exchange student).

The graphs in Figures 3.20 and 3.21 show the average diameter in nm and the linear average diameter. At least 10 fibres were measured and averaged for each data point.

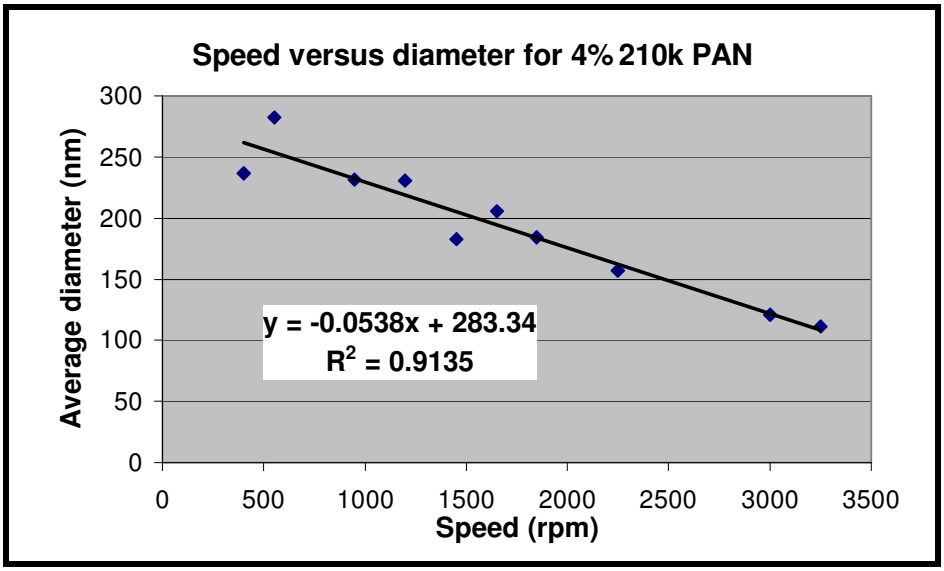

Figure 3.20 Change in fibre diameter with take-up speed for 4% 210k PAN.

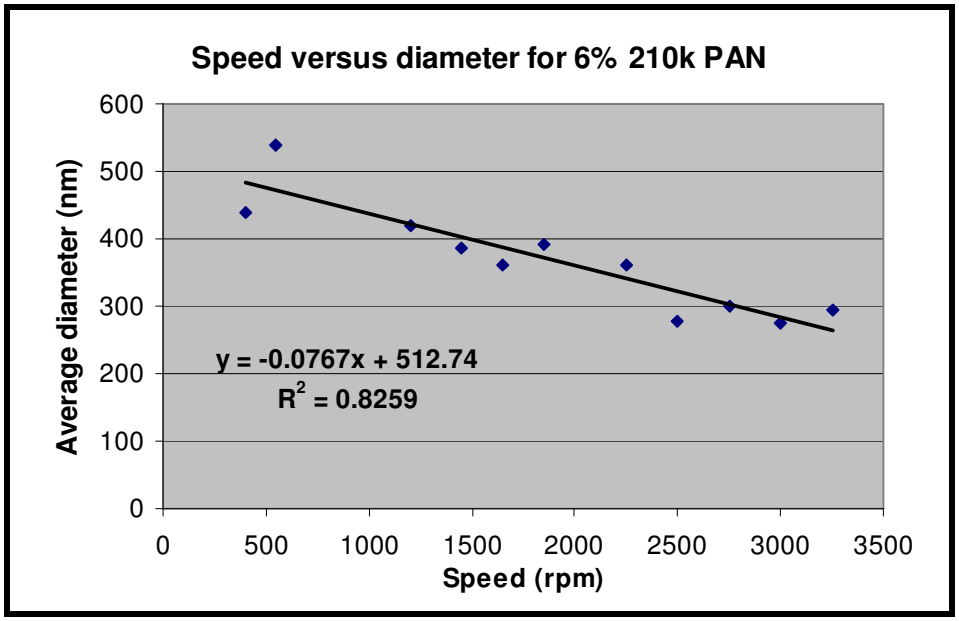

Figure 3.21 Change in fibre diameter with take-up speed for 6% 210k PAN.

Figures 3.22 and 3.23 show SEM micrographs of fibres produced using rotational speeds of 2250 and 1200 rpm respectively. The4 % solution PAN fibres have an average diameter of 120 nm whilst the higher viscosity 6% PAN at the lower rotational speed has a significantly higher average diameter of 430 nm.

The distance from the Teflon® threads onto which the fibres were spun and the center of the rotating electrode was 4.5cm. Thus the face velocity at 500 rpm was 2,36 $m.s^{-1}$ and at 3200 rpm it was 10,8 $m.s^{-1}$.

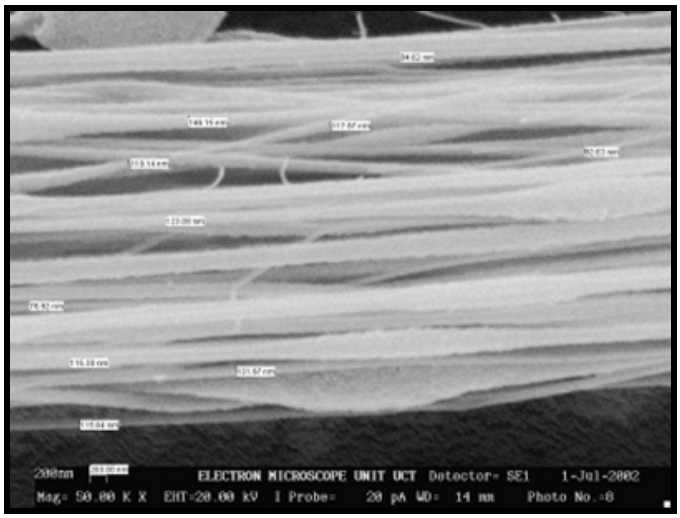

Figure 3.22 Straight fibers produced from a 4% 210k PAN solution at 3250 rpm.

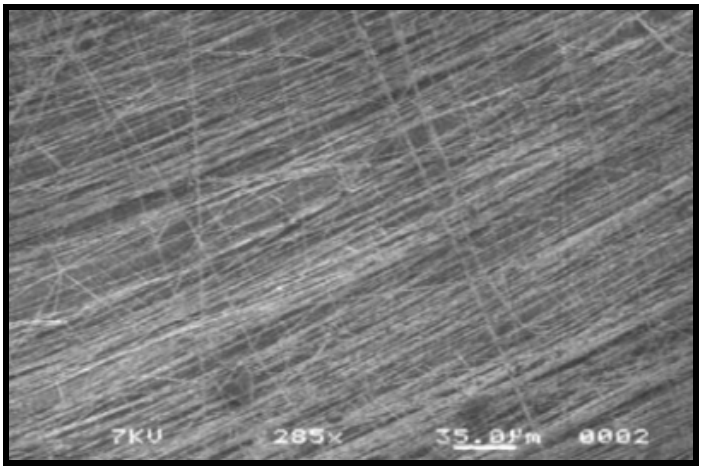

Figure 3.23 Parallel fibers produced from 6% 210k PAN solution at 1200 rpm.

3.8.2 The effect of the type of flat grounded electrode

An investigation was conducted to assess the effect of the type of grounded electrode and the SEM images of samples spun onto a wire grid are shown in Figure 3.24.

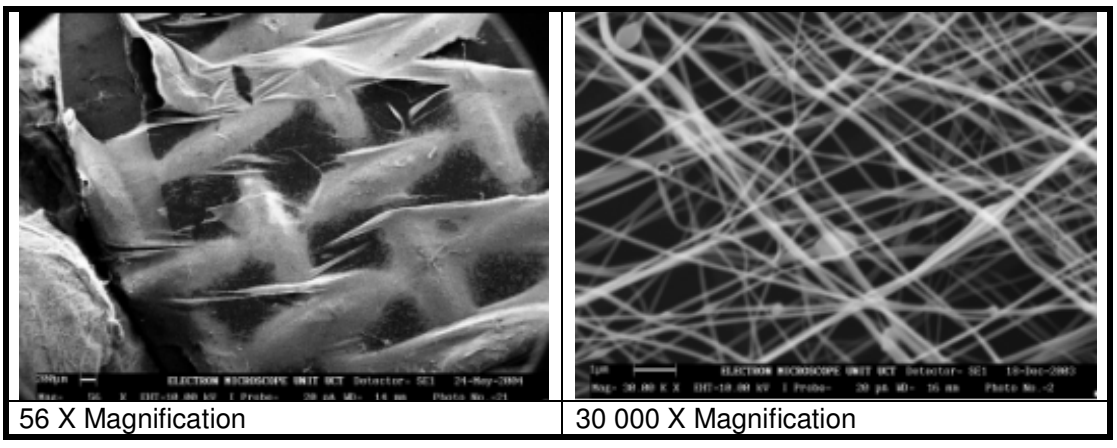

56 X Magnification	30 000 X Magnification

Figure 3.24 SEM Images of fibres on a wire grid grounded electrode.

The image at the higher magnification in Figure 3.24 shows a degree of alignment of the elelctrospun fibres in the gaps of the wire grid.

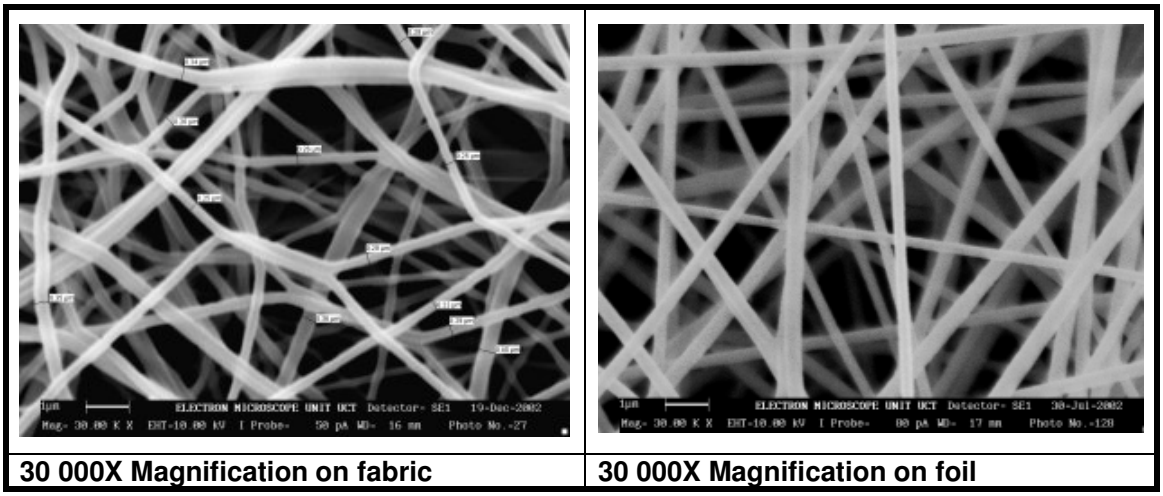

30 000X Magnification on fabric	30 000X Magnification on foil

Figure 3.25 SEM images of fibres on a non-woven fabric and foil electrodes.

Figure 3.25 shows the effect of spinning either directly onto a grounded flat aluminium foil electrode or onto a spun-bonded polyester fabric mounted over the electrode. The fibres spun onto the fabric are more ribbon-like and more curved than those on the hard metal electrode. It is more difficult to dispose of surface charge on the fabric which can explain the change to larger fibre surface area.

3.8 CONCLUSIONS ON THE EFFECTS OF SPINNING VARIABLES

- Novel image analysis methods to characterize elecrospun mat roughness and mat porosity have been developed.
- Under controlled conditions there is a linear relationship between the voltage and the fibre diameter.
- There is not a linear relationship between the spinning distance (field strength) and the fibre voltage. There is generally an increase in the fibre diameter at the medium spinning distance in these series of PAN evaluated for this thesis.
- It appears that a viscosity of less than 1 Pa.s is required for electrospinning of PAN under the given conditions of 20 cm and 20 kV in DMSO at 30 °C under gravity feed.
- The relationship between the Berry Number and the electrospun fibre diameter for the PAN grades used is comparable with PLA only up to Be<5 but unique at higher Be for not only each type of polymer (PAN versus PLA) but also for the different PAN grades.
- A change in the solution concentration has a greater effect on the rate of change in electrospun fiber diameter for higher molecular weight polymer PAN.

- The higher the take-up speed, the lower the fibre diameter. There is a linear relationship within the domain of the face velocities used in these experiments.
- The higher the concentration, the higher the fibre diameter for the same take-up speed. The fibres produced from 4% (w/w) solution had a greater reduction in diameter with increasing collector speed in comparison to fibres produced from 6% (w/w) solution.
- The mat morphology is dependant on the shape and conductivity of the grounded electrode.

3.9 REFERENCES

Ali, A., 2003. Carbon nanotube reinforced carbon nano composite fibrils by electro-spinning, Thesis Drexel University, http://hdl.handle.net/1860/17.

Aydilek, A., 2002. Digital image analysis to determine pore opening size distribution of nonwoven geotextiles. *Journal of Computation in Civil Engineering.* p.280-90.

Deitzel, J.M., Kleinmeyer, J., Harris, D. & Beck Tan, N., 2001. The effect of processing variables on the morphology of electrospun nanofibers and textiles. *Polymer*, 42 (1), p.261-72.

Demir, M.M., Yilgor, I., Yilgor, E. & Erman, B., 2002. Electrospinning of polyurethane fibers. *Polymer*, 43 (11), p.3303-309.

Ding, B., Kim, H.Y., Lee, S.C. & Shao, C.L., 2004. Preparation and characterization of a nanoscale poly(vinyl alcohol) fiber aggregate produced by an electrospinning method. *Journal of Polymer Science Part B: Polymer Physics,* 40, p.1261-268.

Laffin, C., Mc Nally G.M., Sanderson, R.D. & **Greyling, C.J.,** 2005. The manufacture of aligned poly(acrylonitrile) fibres by electrospinning. *Procedings of ANTEC 2005*, Boston, p.1825-829.

Lide, D.R ed., 2008. *CRC Handbook of Chemistry and Physics, 88th Edition (Internet Version 2008),* CRC Press, Taylor and Francis, Boca Raton, FL

Lyons, J. & Ko, F., 2004. Nanofibres. *Encyclopaedia of Nanoscience & Nanotechnology*, 6, p.727-38.

Reneker, D.H. , Yarin, A.L., Fong, H. & Koombhongse, S., 2000. Bending instability of electrically charged liquid jets of polymer solutions in electrospinning. *Journal of Applied Physics*, 87, p.4531-547.

CHAPTER 4 – EXPERIMENTAL AND RESULTS

THE EFFECT OF ADDITIVES ON ELECTROSPUN PAN FIBRES

4.1 INTRODUCTION

The effect of copper salts and copper nanoparticle additives on the crystallinity, molecular orientation structure and thermal properties of electrospun PAN nanofibres, experimental conditions and results are discussed here in Chapter 4. The analytical techniques employed include FTIR, DSC, TGA, SEM, TEM, NMR, ESR and XRD.

The structure of the electrospun polymers are compared with wet spun commercial PAN polymers made from the same polymer grades and with annealed cast films, (with and without additives), and the "as-polymerized" powder. Whilst the electrospun fibres are also wet spun, in this document the term "wet spun" refers to fibres spun by conventional commercial spinning lines.

Then in addition the effect of the inclusion of oligomers and conductive polyaniline blends in PAN on the resultant electrospun fibres is reported in Sections 5.2 and 5.3 respectively.

4.2 EXPERIMENTAL

All PAN electrospinning solution samples containing metal salts or nanoparticles were prepared using an 8% solution of the 120k PAN copolymer in DMAc or the 6% 210k PAN homopolymer also in analytical grade DMAc supplied by *Aldrich,* unless otherwise stated. The PAN polymer grades are described in detail in Section 3.1.

The polymer was first added to the DMAc solvent and the solution was left to stir at 50 °C overnight. The polymer solution was then cooled and divided into 20 ml aliquots. The weight of copper additive as indicated in Table 4.1 was added to the polymer solution whilst stirring and left to stir overnight. All the salts used were completely soluble in DMAc.

Films were also cast from the copper containing PAN solutions and annealed overnight in an oven at 90°C and then vacuum dried at room temperature for 24 hours.

The samples described in Table 4.1 were spun during the author's visit at the University of Marburg and the samples described in Table 4.2 were prepared and electrospun at the University of Stellenbosch.. The sample series labeled "*M*Cx" and "*S*Cx" were identical chemically but spun by the author in Marburg and Stellenbosch respectively using identical electrospinning set-ups) to assess the repeatability of the control containing $CuCl_2$ where Cu:CN equals 1:100, 1:75, 1:50, 1:20 and 1:10..

All were spun at 20 kV, at a distance of 20 cm at 30 °C using an Epindorff® yellow plastic tip. The copper acetyl acetonate salt was supplied by Marburg University and used since it had been

identified as a salt, which was easy to electrospin as an additive in other polymers (Graeser 2004). The copper acetate salt was found to only dissolve at a Cu:CN ratio of 1:50 if amine ligands were included. The ligand containing solutions spun included tetraethyl-triamine, (TETA) and ethylene-diamine, (ED) obtained from *Aldrich* and added at a concentration of 0,25% w/w.

Table 4.1 Mass of Copper additive in 20 ml 8% 120k PAN in DMAc solution

Cu:CN Mol Cu	MW	Film	1:100 0,0003	1:75 0,00045	1:50 0,0006	1:20 0,0015	1:10 0,0030	1:2 0,0151	1:1 0,0302	2.1 0,0604
LiCl	42,39		**MA7** 0,0127	**MA8** 0,0178	**MA1** 0,0254 **spun, XRD**	**MA2** 0,0640 **spun XRD**	**MA3** 0,1280 **film 3D web**	**MA4** 0,6401 **wont spin film**	**MA5** 1,2802	**MA6** 2,5604
CuCl NaOH	99,00		**MB7** 0,0299	**MB8** 0,0399	**MB1** 0,0598 **wont spin film**	**MB2** 0,1494	**MB3** 0,2989	**MB4** 1,4949	**MB5** 2,9899	**MB6** 5,9796
$CuCl_2$	134.45	**Film 1:5**	**MC7** 0,0406 **film spun, XRD**	**MC8** 0,0541 **film spun, XRD**	**MC1** 0,0812 **film spun, XRD**	**MC2** 0,2030 **film spun, XRD**	**MC3** 0,4060 **spun, XRD**	**MC4** 2,0302 **wont spin**	**MC5** 4,0604	**MC6** 8,1208
Cu(Ac) NaOH	122,57		**MD7** 0,0370 **film**	**MD8** 0,0494	**MD1** 0,0740 **wont spin film**	**MD2** 0,1851	**MD3** 0,3702	**MD4** 1,8508	**MD5** 3,7020	**MD6** 7,4030
$Cu(Ac)_2$	181,59		**ME7** 0,0548	**ME8** 0,0731	**ME1** 0,1097 **wont spin**	**ME2** 0,2742	**ME3** 0,5484	**ME4** 2,7420	**ME5** 5,4840	**ME6** 10.9680
CuO	79,55		**MF7** 0,0240	**MF8** 0,0360	**MF1** 0,0480 **spun,**	**MF2** 0.1202	**ME4** 0,2402	**MF4** 1,2020	**ME6** 2,4024	**MF6** 4,8048
$CuSO_4.$ $5H_2O$	245.55		**MG7** 0,0742	**MG8** 0,0989 **wont spin**	**MG1** 0,1483 **spun XRD**	**MG2** 0,371 **spun XRD**	**MG3** 0,7416 **wont spin**	**MG4** 3,708	**MG5** 7,4156	**MG6** 14,8312
$Cu(NO_3)_2$ $3H_2O$	241,55		**MH7** 0,0742	**MH8** 0,0989 **wont spin**	**MH1** 0,1483 **spun, XRD**	**MH2** 0,371 **spun, XRD**	**MH4** 0,7416 **wont spin**	**MH4** 3,708	**MH6** 7,4160	**MH6** 14,8312

Addition of copper (I) salts , CuCl and Cu(Ac) to PAN was found to form a highly viscous gel. The gel was bright green in the case of CuCl in PAN in DMAc. The gel became a spinnable solution when the pH was adjusted to pH = 9 with concentrated ammonia, NH_3.

Samples with CuO nanoparticles, 40 to 70 nm, also added to the 120k PAN were prepared. Problems were experienced with particle agglomeration. A combination of intensive sonication and the addition of amine ligands gave a more homogeneous distribution of the nanoparticles in the electrospun fibres and is discussed further in Section 4.7.

CuO was also formed in-situ from $CuNO_3$ salts which were calcined in carbonized 120k PAN electrospun fibres. The TEM micrographs of the electrospun carbon fibres with CuO are shown in Section 4.7. CuO was additionally deposited as a 3 to 20 nm thick coating on the surface of the PAN nanofibres at room temperature using a process of laser vapor deposition is also discussed further in Section 4.7.

Table 4.2 8% 120k PAN & 6% 210k PAN with Cu- salts (Univ. of Stellenbosch)

CODE	MW (k)	%	cm	kV	Cu:CN	Comments
8% 120k with $CuCl_2$ in DMAc at 20 cm fixed distance and 20 kV, 30 °C, plastic tip						
SC3	120	8	20	**20**	1:10	
SC2	120	8	20	**20**	1:20	
SC1	120	8	20	**20**	1:50	
SC8	120	8	20	**20**	1:75	
SC7	120	8	20	**20**	1:100	
SCO	120	8	20	**20**	control	
6% 210k with $CuCl_2$ in DMAc at 20 cm fixed distance and 20 kV, 30 °C, plastic tip						
TC3	210	6	20	**20**	1:10	
TC2	210	6	20	**20**	1:20	
TC1	210	6	20	**20**	1:50	
TC8	210	6	20	**20**	1:75	
TC7	210	6	20	**20**	1:100	
TC0	210	6	20	**20**	control	
8% 120k with $CuCl_2$ in DMAc at 20 cm fixed distance and 20 kV, 30 °C, plastic tip						
SI1	120	8	20	**20**		Copper acetyl acetonate
SE1(a)	120	8	20	**20**		Copper acetate + TETA
SE1(b)	120	8	20	**20**		Copper acetate + EDA
SB1	120	8	20	**20**		CuCl + ammonia

The chemical composition and chemistry of the copper salts used in these experiments and general nanoparticle chemistry were discussed in Section 2.4. The sample preparation and experimental procedure relevant to each analytical technique is described in the following sections of Chapter 4.

4.3 STRUCTURE AND ANALYSES OF PAN FIBRES

After the conventional melt, wet or dry spinning of PAN fibres higher levels of orientation can be achieved by post-drawing processes, where after they are subjected to annealing by heating and cooling under tension in a continuous process over rollers. The degree of crystallinity and molecular orientation is critical to the tenacity, chemical and thermal performance of the fibres. Methods to measure crystallinity and molecular orientation of polymers are listed in Table 4.3.

The methods used and reported in this document are highlighted in Table 4.3. In addition the fibres were characterized by **thermal gravimetric analysis**, (TGA), and **electron microscopy.**

Table 4.3 Analytical techniques to measure crystallinity and orientation of fibres

Crystallinity	Molecular Orientation
Infra-red Spectroscopy, (FTIR)	Infra-red Spectroscopy, (FTIR)
Wide Angle X-ray Diffraction, (XRD)	Wide Angle X-ray Diffraction, (XRD)
Small Angle Neutron Scattering, (SANS)	Birefringence
Differential Scanning Colorimetry (DSC)	Solid State cp-MAS Nuclear Magnetic Resonance Spectroscopy, (NMR)
Density	Electron Spin Resonance Spectroscopy, (EPR) or (ESR)
	Polarised Raman or FTIR Spectroscopy

The results of researchers using these techniques specifically on PAN and / or electrospun fibres is discussed briefly in Chapter 2 where the results of the analyses on the electrospun PAN fibres and films with additives for each individual technique are presented and discussed.

4.4 INFRARED SPECTROSCOPY STUDY OF ELECTROSPUN PAN: RESULTS, DISCUSSION AND CONCLUSIONS

4.4.1 Introduction

Fourier Transform Infrared spectroscopy, FTIR, is used in this study on PAN samples with and without additives to determine the following characteristics and properties of the PAN electrospun fibres, PAN wet-spun fibres, as polymerized PAN powders and cast PAN films

1 Identification of the grade of PAN by semi quantitative measurement of the carboxylic acid group of the copolymer in the PAN samples.
2 The degree of molecular orientation, Orientation Factor, (OF).
3 Complexation of the nitrile and or carboxylic groups of PAN and the solvent with lithium and copper metal salt additives.
4 The degree of crystallinity of PAN.
5 The presence of residual solvent in electrospun fibres.

The theory of FTIR data interpretation on PAN samples to determine each of the characteristics listed above and references on similar work conducted by other researchers on PAN samples is discussed in Section 2.3.3.

4.4.2 FTIR PAS equipment and FTIR experimental procedure

Photoacoustic detection, (PAS), is a useful FTIR detector technique for samples, which cannot be analyzed by other FTIR methods, specifically for non-soluble and solid samples. It requires longer sampling time than the other IR techniques, Attenuated Total Reflectance, (ATR}, which can also be used on solid state sampels.

When IR radiation strikes the sample, some energy is absorbed; the sample transfers some of the heat to the ambient gas, which results in a pressure wave. A microphone detects the pressure wave.

Carbon black is used as reference background (McClelland et al. 1993; Katii 2003). All FTIR spectra were recorded on a Perkin Elmer Paragon® 100 Infra-red Spectrophotometer with an MTEC® photo-acoustic, (PAS), detector in a helium atmosphere. Spectra were recorded at a mirror speed of 0,3 $m.s^{-1}$ and a resolution of 8.cm^{-1}. Each spectrum reported in this document is the average of 128 scans.

All spun PAN samples and PAN cast films were dried in a vacuum oven overnight at 50°C to remove residual solvent. Electrospun samples were analyzed directly on the backing aluminium foil, which is "invisible" in the FTIR spectrum without additional sample preparation. The data was processed using *Perkin Elmer Spectrum®* software.

The procedure of data analysis (unless otherwise stated) involved the following steps, which have been found to be ideal for FTIR PAS interpretation previously by the author.

- Automatic baseline correction
- Smoothing with factor 13
- Normalization of the nitrile peak at 2242 cm^{-1}
- ATR correction

Sometimes it is necessary to perform a deconvolution of two or more overlapping peaks especially for spectra recorded on solid state polymeric samples where the FTIR peaks tend to be broader and overlap. The results of the deconvolution process are illustrated in Figure 4.1. The figure on the right shows a spectrum, which has been baseline corrected, smoothed with a factor 13 and normalized. The process is highly subjective. Constant values for the gamma value (2,3) and length value (7,3) were used throughout and consistency in data manipulation is required when comparing samples.

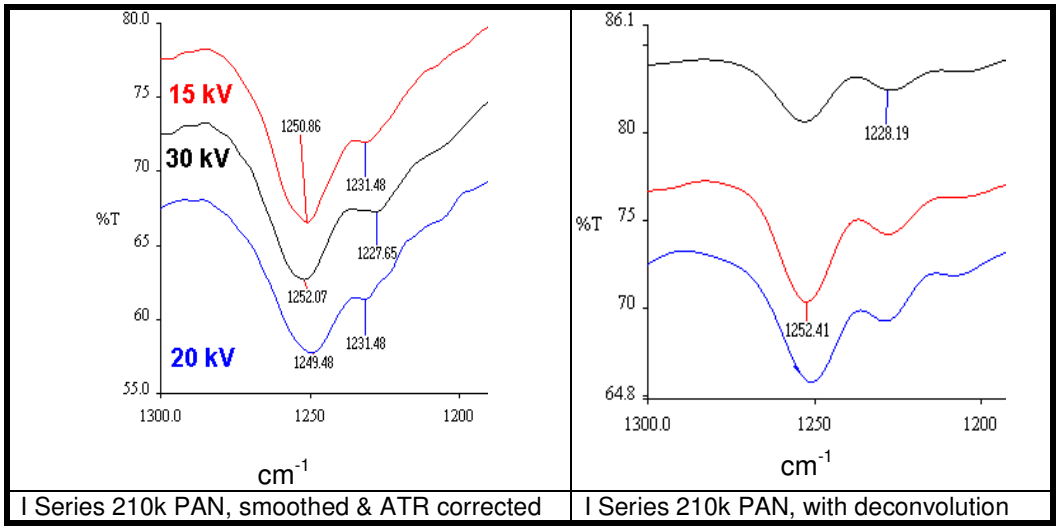

I Series 210k PAN, smoothed & ATR corrected | I Series 210k PAN, with deconvolution

Figure 4.1 Deconvolution of the peaks at 1228 and 1252 cm^{-1} of ES homo-PAN.

4.4.3 FTIR for PAN grade identification

FTIR is most often used as a qualitative analytical technique for polymer identification. In Figure 4.2, this application is demonstrated to differentiate between 100% homopolymer 500k PAN with < 0,2% VA and PAN copolymers containing carboxylic acid groups, used in this research. The main peaks of interest in identification of PAN; the nitrile group stretching vibration absorbs at 2242 cm^{-1} and the copolymer caboxylate groups around 1730 cm^{-1}. All FTIR results are semi-quantitative.

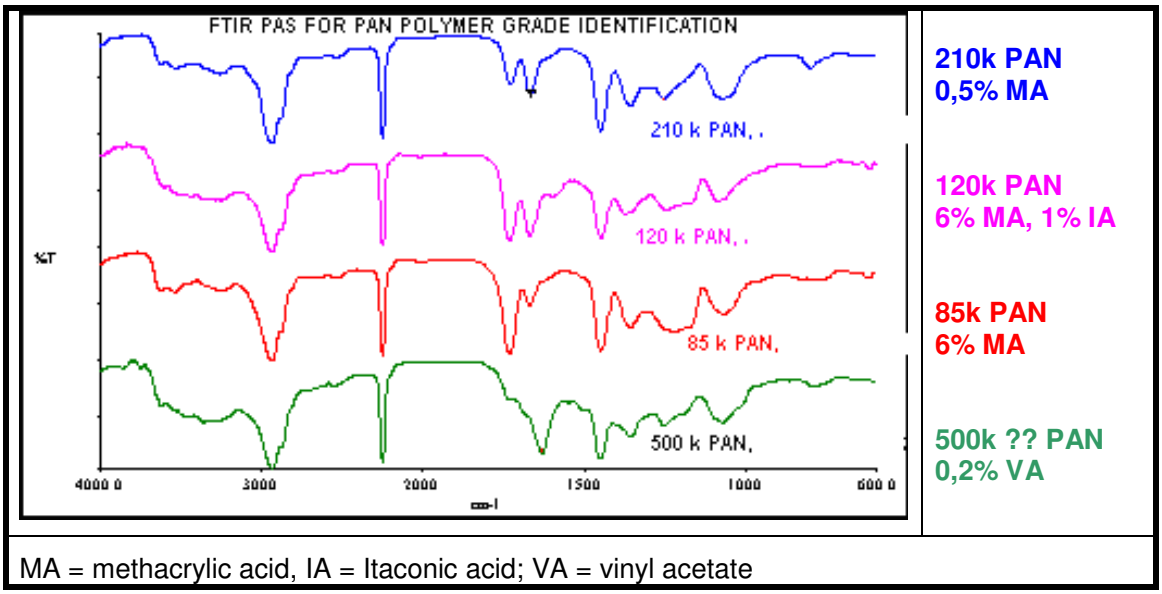

MA = methacrylic acid, IA = Itaconic acid; VA = vinyl acetate

Figure 4.2 FTIR PAS results for PAN grades Identification.

The 500k, 210k and 85k PAN samples were analyzed in the form of powders and the 120k as a wet spun fibre spun from DMAc solvent. The intensity of the peak at 1730 cm^{-1} is seen to increase as the relative percentage of the carboxylic acid monomer (MA and / or IA) present in the copolymer increases from the 500k to the 210k, to the 85k and to the 120k PAN grades. The exact MW of the 500k PAN is not known. GPC analysis is difficult since the highly polar PAN solvents degrade the resins in the GPC columns. MALDI-TOF MS was also attempted but even low MW PAN (MW = 12 000 made by ATRP) would not fly to the detector.

4.4.4 "Orientation Factor" at different field strengths – results and discussion

The use of FTIR to provide a semi-quantitative measurement of the Orientation Factor, (OF), in PAN films and fibres by Minagawa et al. (1998) is discussed in Section 2.3.3. The results for sample Series C (Table 3.1) are shown in Figure 4.3 where the OF is evaluated as a function of the spinning distance, i.e. field strength during the electospinning of 4% 85k copolymer PAN in DMF electrospun at 20k V.

The results shown in Figure 4.3 show an inverse linear relationship between the spinning distance and the ratio of the A_{1230}/A_{1260} for a 4% 85k PAN copolymer electrospun at 20 kV and changes in

the electrode spacing from 10 to 35 cm. Researchers at Yamagata University, Japan, (Minagawa et al. 1997, 2001), showed that the ratio of the A_{1230}/A_{1260} was indirectly related to the degree of interaction between adjacent nitrile groups and thus the isotacticity.

However these absorbance peaks are due to the interaction between adjacent polar nitrile groups and are thus also proportional to the degree of molecular orientation, termed the Orientation Factor, OF. The further the distance used for electrospinning, i.e the lower the electric driving force, the lower the degree of molecular orientation i.e the nitrile groups are less aligned with lower interaction via dipole bonding in the resultant electrospun fibres.

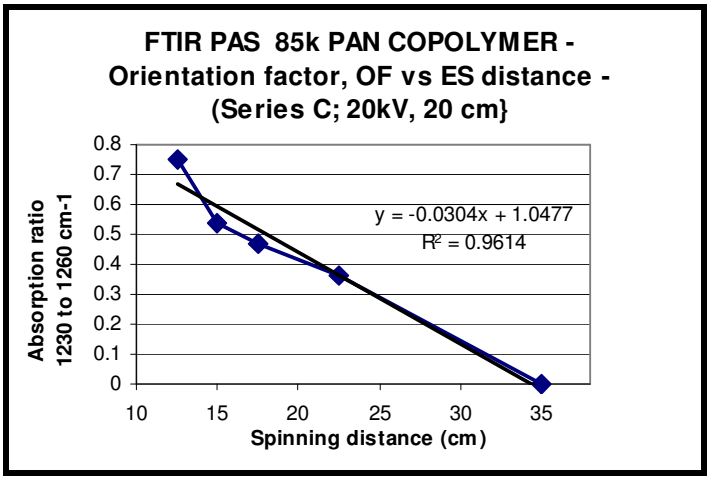

Figure 4.3 OF by FTIR of 4% 85k PAN after ES at 20 kV at different field strengths.

Highly isotactic PAN, 72% isotacticity, shows the A_{1230}/A_{1260} values between 1,2 and 1,4 and atatactic PAN shows values between 0,4 and 0,6. Thus samples electrospun from this 4% 85k PAN in DMAc are only comparable with the degree of orientation of atactic, commercially wet spun fibres if the field strength is $\geq 0{,}75$ kV.cm^{-1}, i.e. the electrospinning distance is ≤ 20 cm.

4.4.5 "Orientation Factor" of ES PAN with LiCl salts – results and discussion

Figure 4.4 shows the effect of various concentrations of LiCl salt (Li:CN = 1: 50 and 1:20) in 8% 120k PAN in DMAc on the OF of the nanofibres after being electrospun at 20cm and 20 kV and of a commercial wet spun fibre on the shape of the FTIR peaks from 1300 and 1200 cm^{-1} .

The addition of LiCl salts to a PAN solution is known to yield a solution with PAN molecules in the extended chain conformation as a result of the lithium ions disrupting the intramolecular antiparallel nitrile bonds in the PAN solution (Masson 1995).

For the control samples without LiCl addition, the Orientation Factor of the wet spun fibre is 0,90 compared with the electrospun control with an OF of 0,40, which indicates a much higher degree of molecular orientation in the wet spinning process. The fibre containing the higher salt concentration with Li:CN at 1:20 showed a significantly higher OF of 0,67, in comparison with the ES 1:50 sample which had a OF of 0,41 similar to the control electrospun sample. As expected

the cast film has a low OF of 0,28 even though annealed at 90 °C, which would have optimized the chance for nitrile interaction but no orientation.

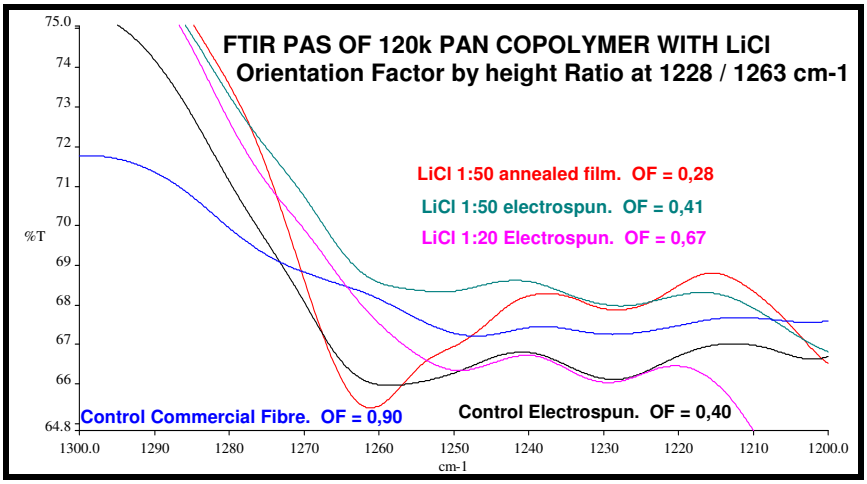

Figure 4.4 OF by FTIR of 120k PAN with LiCl, ES and annealed.

4.4.6 FTIR to determine PAN / $CuCl_2$ complexation – results and discussion

Figures 4.5 and 4.6 below for the 120k PAN copolymer shows the FTIR peaks which have been previously identified by other researchers (Bajaj et al. 1998, Tang 1996) as being involved in the interaction between PAN and Cu ions i.e. complex formation between -C≡N groups and Cu (II), as shoulders on the nitrile peak at 2242 cm^{-1} and a carboxyl Cu salt at 1600 to 1630 cm^{-1} as discussed in Section 2.3.3.

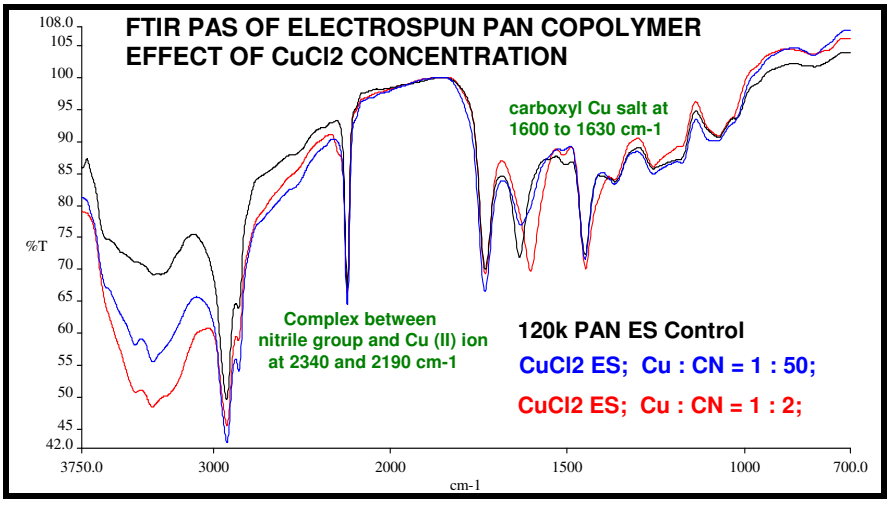

Figure 4.5 FTIR PAN copper complex at high $CuCl_2$ concentration (Cu:CN = 1:2).

Some researchers (Deng 2003) have argued that the Cu does not complex with the -C≡N of PAN. It is seen in the spectra in Figure 4.5 that at high Cu:CN = 1:2 there are clear shoulders on the 2242 cm^{-1} - C≡N peak at 2340 and 2190 cm^{-1}. As noted previously the shoulders may appear at higher [Cu^{2+}] (Tang et al. 1996, Bajaj et al, 1998) as due to the Cu-CN complex.

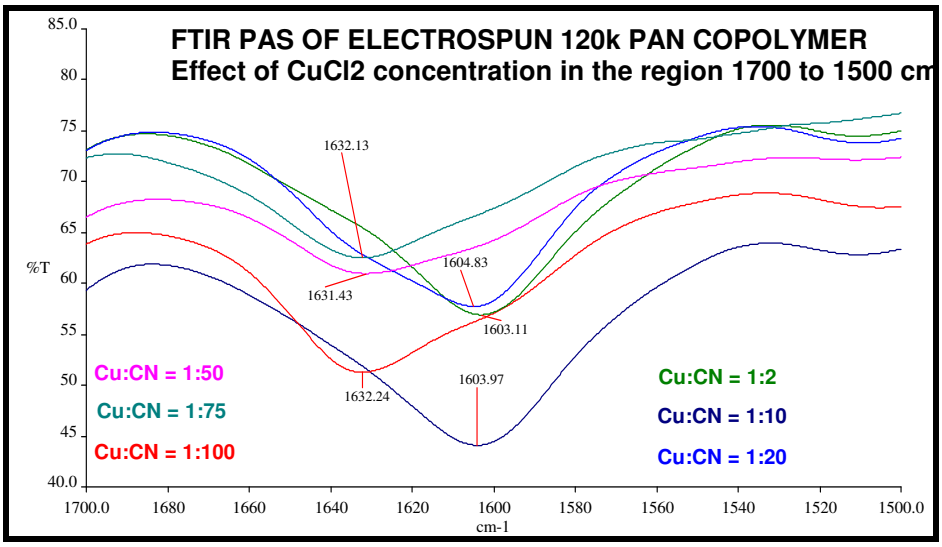

Figure 4.6 FTIR of ES PAN showing Cu complexation of the carboxylic group.

The position and intensity of the carboxylic absorption changes with the concentration of the $CuCl_2$ salt added to the spinning dope as listed in Table 4.4. For low copper concentrations, ≤ Cu:CN of 1:50 the peak position is around 1632 cm^{-1} but it shifts to lower wavelengths at ± 1604 cm^{-1} for high copper salt concentration indicating complex formation as suggested in literature (Silverstein 2004).

Table 4.4 FTIR peak data for various $CuCl_2$ conc. in ES 120k PAN (1700 to 1500 cm^{-1})

Cu:CN	1:100	1:75	1:50	1:20	1:10	1:2
Height	14,9	10,5	8,5	15,3	18,9	19,3
Position(cm^{-1})	1632,2	1632,1	1631,4	1603,1	1604,0	1604,8

The position of the carboxylic absorption peak in the FTIR spectrum of the electrospun PAN fibres shifted from ± 1632 cm^{-1} to ±1604 cm^{-1} when the ratio of Cu:CN ≥ 1:20.

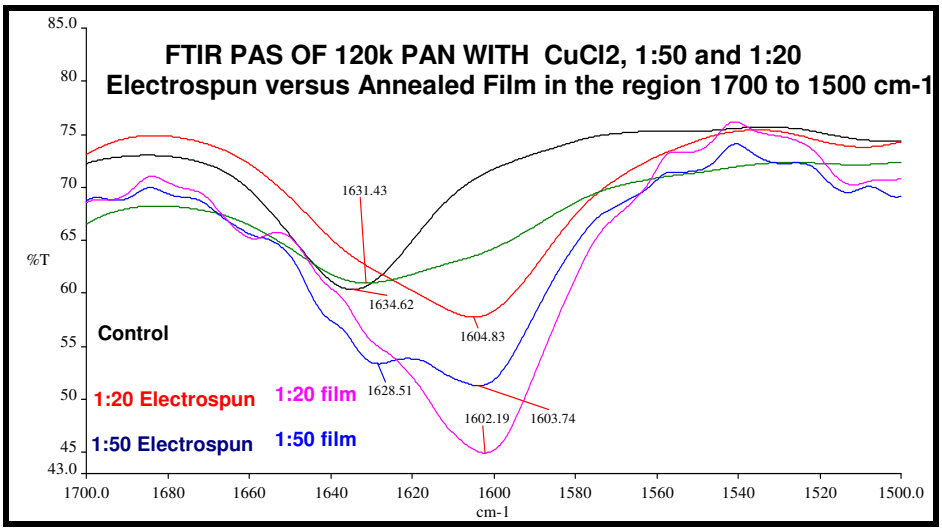

Figure 4.7 FTIR of ES and film PAN showing Cu complexation of the carboxylic group.

The effect of annealing of cast PAN films with copper salts on the carboxyl – metal ion interaction process was investigated and the results were compared with electrospun PAN fibres from the same solutions as shown in Figure 4.7.

Films were cast and annealed from the ES dope solutions for the $CuCl_2$ with both Cu:CN equal to 1:50 and 1:20 samples. The results for the peak height and peak position for the FTIR results showing the copper complexation on the carboxylic group presented in Table 4.5.

Table 4.5 FTIR peak data for various $CuCl_2$ concentrations in ES and film 120k PAN

Cu:CN	Control	1:50 spun	1:50 film		1:20 spun	1:20 film
Height 1685 cm^{-1} to 1565 cm^{-1}	13,4	8,5	15,6	15,2	15,3	24,6
Position (cm^{-1})	1634,6	1631,4	1628,0	1602,2	1603,1	1603,8

In the annealed film the peak at 1630 cm^{-1} splits and shifts to lower wavelength at a Cu:CN concentration ≥ 1:50 with 2 peaks at ± 1632 cm^{-1} to ± 1604 cm^{-1}. In the electrospun fibre the peak shifts only at a higher $CuCl_2$ concentration ≥ 1:20. The interaction between the carboxyl group and the metal ion appears to be time dependant or related to the degree of shear on the polymer chains, where the mechanical energy leads to orientation and exclusion of the formation of the metal ion-PAN complex to higher Cu^{2+} concentrations.

It would be interesting to assess the change in the complex formation during normal wet-spinning where the fibre spends a longer time period in the gel or semi-gel state in comparison with the electrospinning fibre and a large percentage of residual solvent is evaporated.

4.4.7 Identification of residual solvent in ES PAN - results and discussion

The presence of the absorption at *circa* 1630 cm^{-1} is shown in Figure 4.6 The assignment of the peaks in the region 1550 to 1660 cm^{-1} is contested as discussed in section 2.3.3.

Silverstein and Bajaj have shown the peaks which appear in this region as being due to the products formed during heat treatment below 300 °C and identified as being due to C=N and C=C conjugation in a heteroaromatic structure. Silverstein also to totally removed residual solvent from cast film PAN samples by drying at 60 °C for a few days. He could thus show that the peak at 1660 cm^{-1} was due to the DMF solvent. Bajaj removed the solvent by heating to > 320 °C, which also caused partial cyclisation of the PAN. Kim in 2005 assigned a peak in the PAN FTIR spectrum at 1650 cm^{-1} as being due to the presence of residual DMF solvent. However Deng in 2004 claimed the peak at 1573 cm^{-1} as being due to imine groups on a PAN fibre surface.

Electrospun samples of 120k PAN copolymer spun from both DMF and DMAc solvent were prepared by electrospinning at 20 cm, 20 kV and 30 °C. The spun samples were then both dissolved again in DMAc solvent and cast into films. The results of the FTIR PAS on the electrospun fibres spun in both solvents and the cast films are given in Figure 4.8.

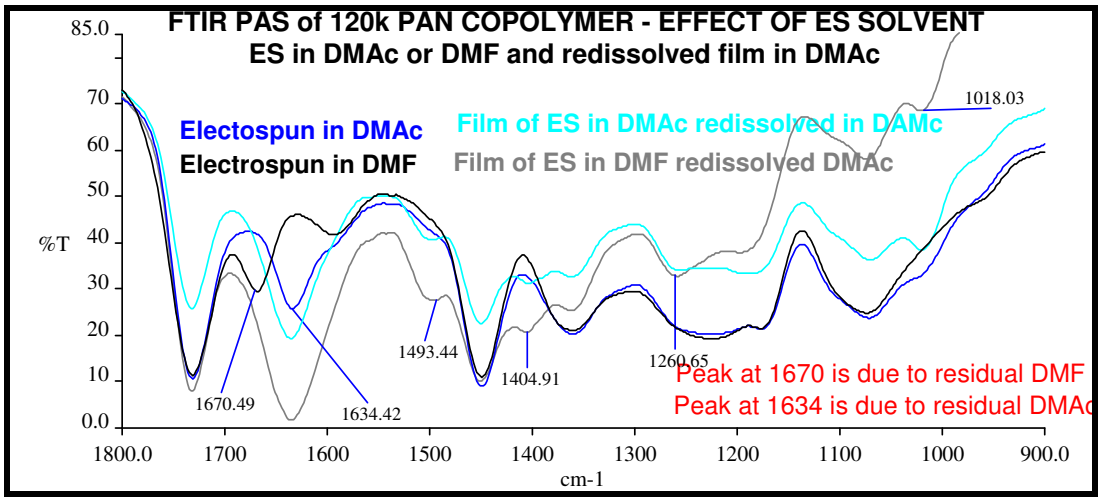

Figure 4.8 FTIR of ES 120k PAN and redissolved films.

The results show that the peak at 1670 cm^{-1} in the samples electrospun in DMF disappears when the sample is redissolved in DMAc, where a new peak at 1634 cm^{-1} appears. Thus it is proven that the peak in the FTIR spectrum in the region 1600 to 1670 cm^{-1} is due to the presence of residual solvent in the electrospun samples even after the samples were dried at 50°C overnight in a vacuum oven.

4.4.8 Crystallinity of copolymer PAN fibres with lithium and copper salts

A method to measure the degree of crystallinity of PAN fibres was reported (Causin 2005) and has been applied to electrospun and commercial wet spun samples and the annealed films with various copper salts. The crystallinity is inversely proportional to the A_{1730}/A_{2240} absorbance or the height ratio H_{1730}/H_{2240}.

The effect of lithium chloride salts on the crystallinity of ES and cast film 120k copolymer PAN was evaluated and the results of the height ratio H_{1730}/H_{2240}. are presented in Table 4.6.

Table 4.6 FTIR peak data for various LiCl concentrations in ES and film 120k PAN

Li:CN (LiCl) Baseline	Height at 1730 cm^{-1} 1825 - 1680	Height at 2242 cm^{-1} 2325 - 2205	H_{1730}/H_{2240}
Comm. Fibre	31,5	44,2	0,71
Spun control	45,2	66,3	0,67
Spun 1:50	38,9	59,9	0,65
Spun 1:20	35.2	52.2	0.67
Film 1:50	26.8	39.2	0.68
Film 1:20	23.5	37.2	0.63

The addition of lithium chloride in the concentration range used in this research does not appear to change the degree of crystallinity of either the electrospun fibres or the annealed films significantly but does indicate a slight increase in the crystallinity for the electrospun fibre for the control and the Li:CN = 1:50.

The crystallinity of the electrospun fibre control without additives is lower than that of the commercial wet spun PAN copolymer fibre from the same grade as shown by the values given in Table 4.6 where the ratio H_{1730}/H_{2240} for the commercial fibre is 0,71.

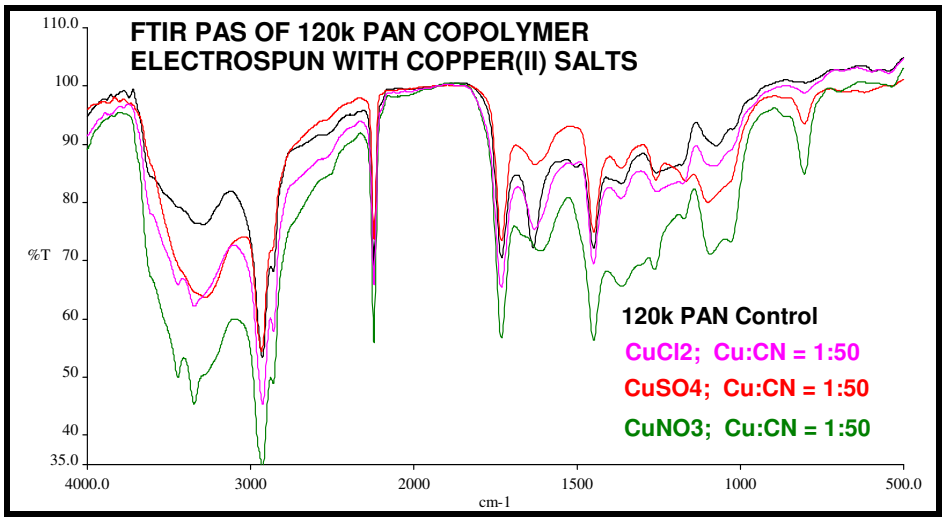

Figure 4.9 FTIR of ES fibres with $CuCl_2$, $CuSO_4$ and $Cu(NO_3)_2$ (Cu:CN = 1:50).

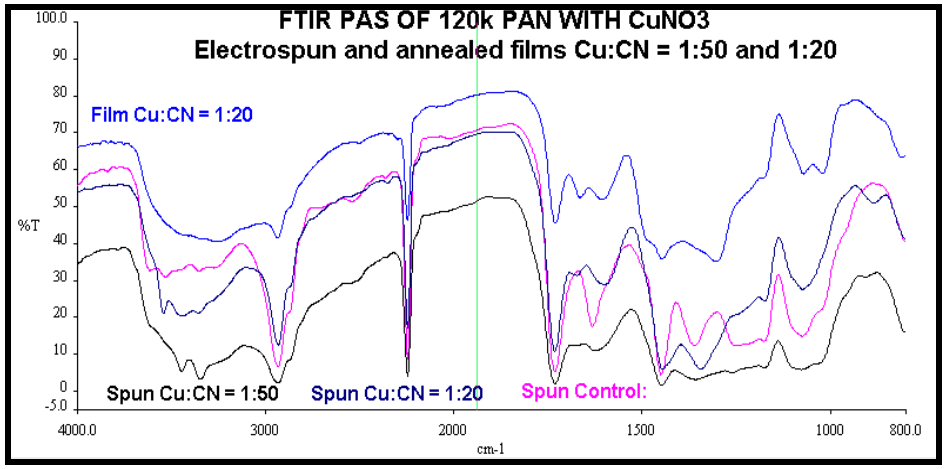

Figure 4.10 FTIR of ES fibres and annealed film with $Cu(NO_3)_2$.

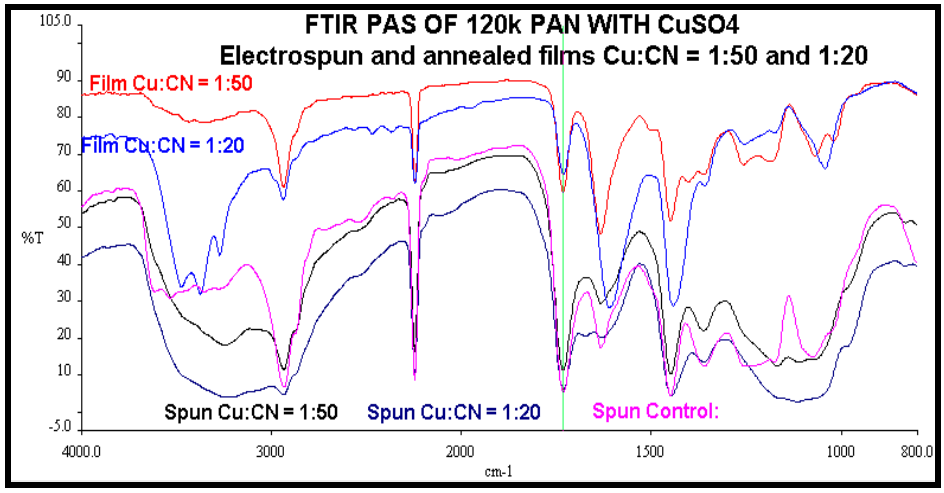

Figure 4.11 FTIR of ES fibres and annealed film with $CuSO_4$.

Copper (II) salts as $CuCl_2$, $CuNO_3$ and $CuSO_4$, with 120k PAN were spun and also cast as films and the FTIR spectra of samples with Cu:CN = 1:50 and 1:20 are compared in Figures 4.9, 4.10 and 4.11. The effect of copper (II) chloride salts on the crystallinity of ES and cast film 120k copolymer PAN was evaluated and the results of the height ratio H_{1730}/H_{2240}. are presented in Table 4.7. All samples were spun and cast from DMAc solvent.

Table 4.7 FTIR peak data for various $CuCl_2$ concentrations in ES and film 120k PAN

Cu:CN ($CuCl_2$) Baseline (cm^{-1})	Height at 1730 cm^{-1} 1825 - 1680	Height at 2242 cm^{-1} 2325 - 2205	H_{1730}/H_{2240}
Spun control	19,0	28,2	0,67
Spun 1:50	24.8	29,9	0,83
Spun 1:20	23,1	28,6	0,81
Film 1:50	25,84	47,1	0,55
Film 1:20	31,3	45,0	0,69

The addition of $CuCl_2$ salts to the dope decreases the degree of crystallinity of the electrospun 120k copolymer, indicated by the increase in the H_{1730}/H_{2240} from 0,67 to 0,81 of the control and the ES Cu:CN = 1:20 sample, respectively. When cast and annealed then the addition of a $CuCl_2$ at 1:50 gives the highest degree of crystallinity shown by the H_{1730}/H_{2240} of 0,55.

Table 4.8 FTIR data for various Cu-salts (Cu:CN = 1:50) in ES and film 120k PAN

Cu:CN Baseline	Height at 1730 cm^{-1} 1825 - 1680	Height at 2242 cm^{-1} 2325 - 2205	H_{1730}/H_{2240}
Spun control	24,3	36,3	0,67
$CuCl_2$ 1:50	28,2	33,9	0,83
CuCl 1:50	29,3	36,6	0,80
$CuSO_4$ 1:50	33,3	36,3	0,91
$(CuNO_3)_2$ 1:50	22,1	34,3	0,65

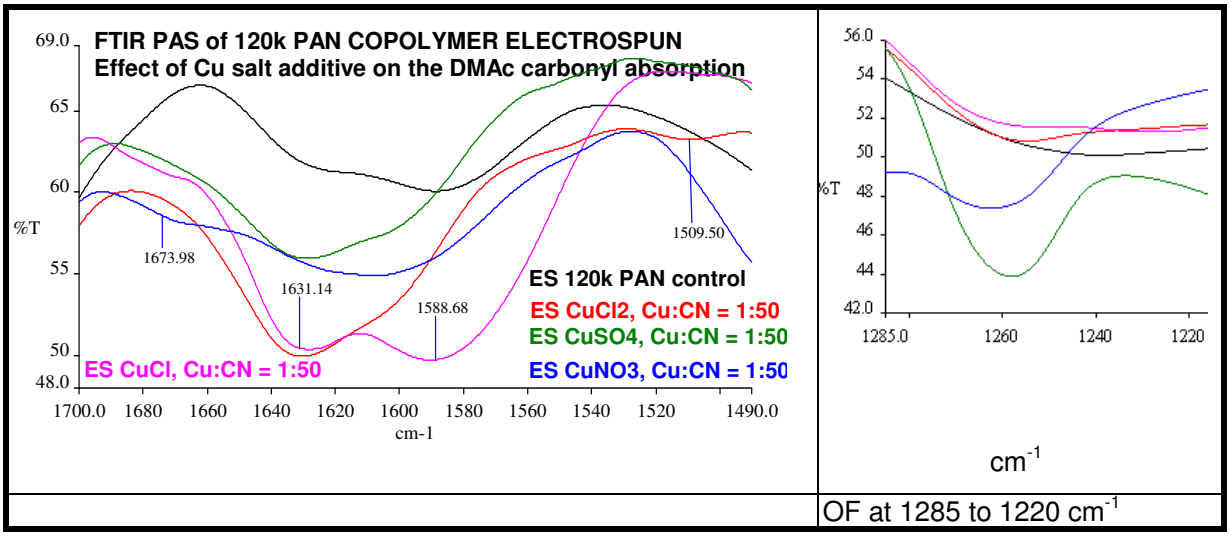

Figure 4.12 FTIR of ES 120k PAN fibres with Cu salts.

The ratio of H_{1730}/H_{2240} in Table 4.8 which is an indicator of the crystallinity shows that copper (II) chloride and copper sulphate additives in PAN at a concentration where Cu:CN = 1:50 all reduce

the crystallinity of the electrospun fibres in comparison with the electrospun PAN control. The $Cu(NO_3)_2$ salt appears to slightly enhance the crystallinity as the ration of ratio of H_{1730}/H_{2240} slightly decreases to 0,65 relative to the control of 0,67. The orientation on the $CuNO_3$ containing ES sample also increases as shown in the figure on the right in Figure 4.12 by the increase in the band at 1260 cm^{-1} relative to the FTIR absorption band at 1230 cm^{-1} in a similar way to LiCl addition to PAN as explained by the discussion on the "Orientation Factor" in Section 4.4.5.

This peak shift to lower wavelength for the ES sample with Cu:CN = 1:20, relative to ES with Cu:CN = 1:50 is seen for $CuNO_3$ and $CuSO_4$ in Figures 4.10 and 4.11 respectively and to even lower wavelength when the Cu:CN = 1:20 is cast as a film. It can be seen in Figure 4.10 for the samples with $CuNO_3$ that the high-intensity of the NO_3 band at 1380 cm^{-1} for the sample electrospun with Cu:CN = 1:50 completely overwhelms the other peaks, the intensities of which are orders of magnitude smaller. This peak shifts to lower wavelength for the ES sample with Cu:CN = 1:20 and to even lower wavelength when the Cu:CN = 1:20 is cast as a film. The other absorptions for NO_3 include 830 cm^{-1} attributed to out-of-plane bending, 1045 cm^{-1} attributed to symmetric stretching, and the 1380 cm^{-1} attributed to asymmetric stretching (Silverstein 2004).

It was noted previously in the results given in Figure 4.6 that the concentration of $CuCl_2$ salt added to electrospun 120k PAN causes the peak at 1634 cm^{-1} in the control sample to shift to 1630 cm^{-1} when the concentration of the additive $CuCl_2$ salt is increased to Cu:CN > 1:50.

This phenomenon of the carbonyl FTIR peak shifting position when salts are included in PAN solutions has been previously noted and discussed in depth in Section 3.2.2. It is due to complexation of the metal salt with the carbonyl group of the polar solvent. This shift has been previously noted for PAN with Ag(I) (Sergides et al. 1986), Fe (III) (Silverstein 2004), Cr(II) (Deng & Bai 2004), Cu(II) (Deng 2003) and various sulphates (Bajaj et al. 1998).

As discussed in Section 2.3.3 the absorptions in the region 1600 to 1580 cm^{-1} in the FTIR spectra of PAN are composite absorptions which have been deconvoluted and the individual contributors identified by Bajaj. The onset of thermal oxidation and dehydrogenation is also first noted in this region of the PAN FTIR spectra and the possibility that these bands include signs of cyclisation products is discussed further in Section 4.4.11.

4.4.9 Crystallinity of homopolymer PAN ES with Cu additives

The effect of $CuCl_2$ salts at various concentration was evaluated in the electrospun 210k homopolymer PAN (<0,5% MA) polymer and compared with the "as-polymerized" PAN powder in terms of the effect of the salt on the crystallinity of the fibre and the spectra are shown in Figure 4.13. The expanded spectra for the 210k homopolymer PAN with $CuCl_2$ salts where Cu:CN equals 1:100, 1:75, 1:50 and 1:20 from 1860 to 1550 cm^{-1} is shown in Figure 4.14.

The ratio of the peak height at 1730 to the peak height at 2240 cm^{-1} was calculated and the results are presented in Table 4.9. The 210k homopolymer was electrospun from DMF solvent.

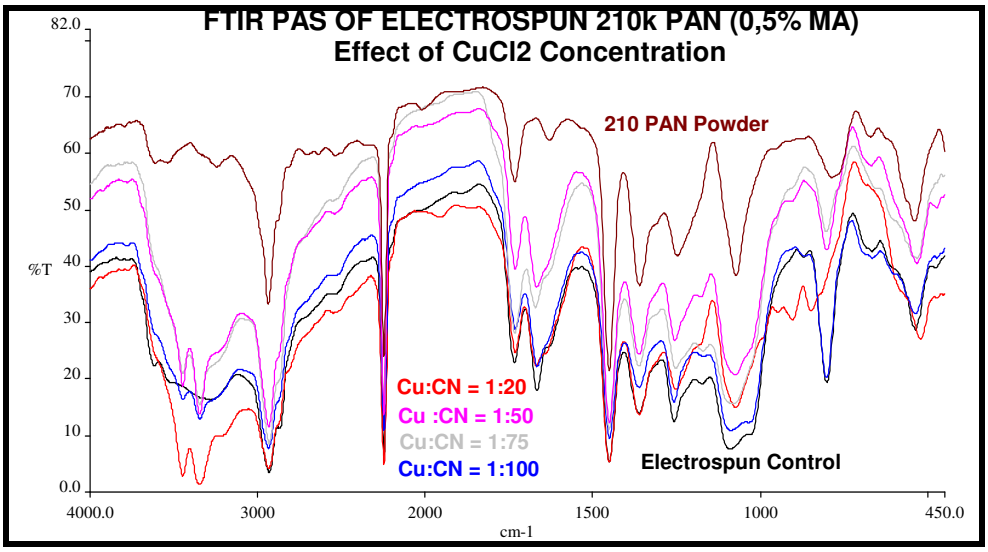

Figure 4.13 FTIR of 210k PAN ES fibres with $CuCl_2$ (4000 to 450 cm^{-1}).

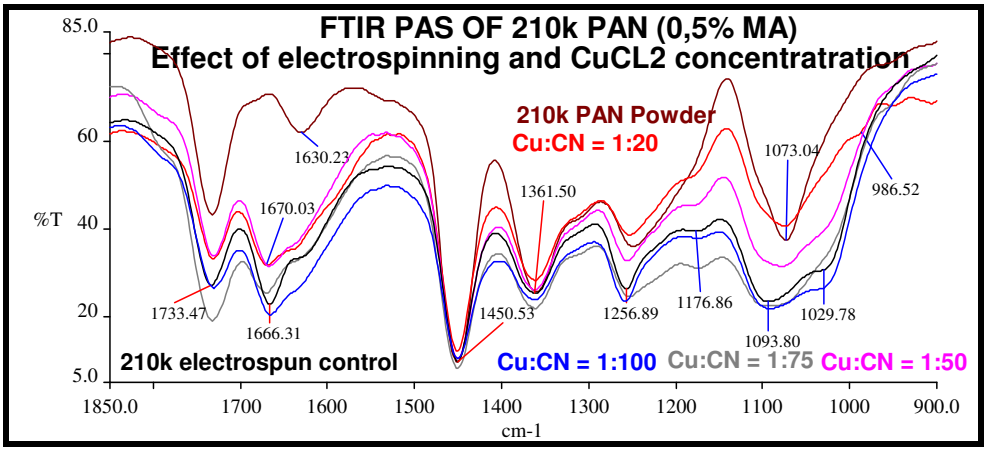

Figure 4.14 FTIR of 210k PAN ES fibres with $CuCl_2$ (1850 to 900 cm^{-1}).

The peak at 1665 cm^{-1} is only present in the electrospun samples. The peak at 1630 cm^{-1} is more pronounced in the 210k PAN powder and appears only as a slight shoulder on the 1665 cm^{-1} peak in the electrospun samples. The height ratio is inversely proportional to the degree of crystallinity. The $CuCl_2$ is shown to increase the degree of crystallinity in the homopolymer PAN whereas the addition of $CuCl_2$ in the 120k PAN copolymer disrupted the crystallinity of the electrospun fibres.

Table 4.9 FTIR peak data for various $CuCl_2$ concentrations in ES and film 120k PAN

Cu:CN $CuCl_2$ in 210k	Height at 1730 cm^{-1}	Height at 2242 cm^{-1}	H_{1730}/H_{2240}
Baseline	**1825 - 1680**	**2325 - 2205**	
210k Powder	12,9	37,8	0,34
Spun control	11,1	35,7	0,31
Spun 1:100	8,9	35,2	0,25
Spun 1:75	18,3	44,4	0,41
Spun 1:50	10,2	42,5	0,24
Spun 1:20	8,8	34,2	0,25

The addition of Cu salts to the homopolymer 210k PAN shifts the absorption of carbonyl group of the residual DMF to a higher wavelength from 1666cm^{-1} to 1670 cm^{-1}. This same phenomenon is noted on commercial wet spun 210k PAN homopolymer with Fe_2O_3 as shown in Figure 4.15. The wet spun 210k homopolymer and the wet spun 210k PAN sample containing Fe_2O_3 were both obtained in fibre form from Kelheim Faserwerk, Germany.

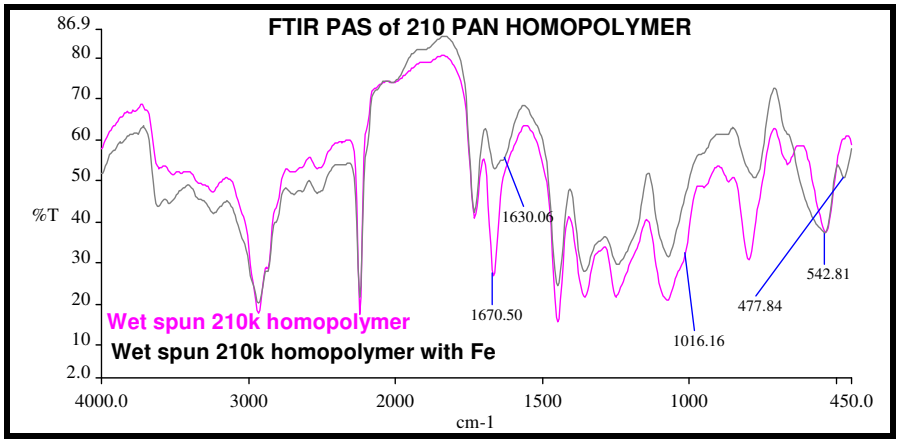

Figure 4.15 FTIR of commercial wet spun 210k PAN with iron oxide.

4.4.10 FTIR of homo PAN ES fibres and PAN "as-polymerized" powders

The effect of electrospinning on the FTIR absorption peaks in the region 1800 to 900 cm^{-1} for the 500k and the 210k PAN homopolymers relative to the "as-polymerized" powders are shown in Figure 4.16.

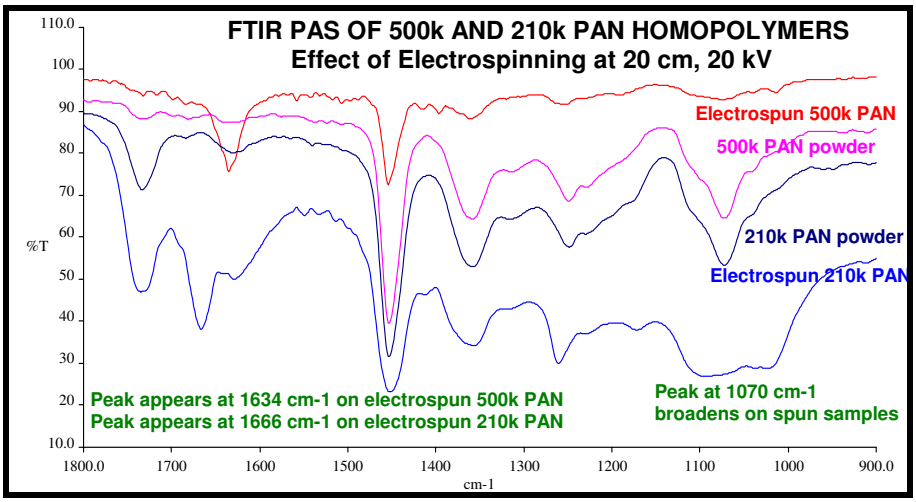

Figure 4.16 FTIR of 500k and 210k PAN ES and the powders.

For both grades of homopolymer PAN the peak at 1070 cm^{-1} broadens FTIR spectra of the electrospun fibres. In the electrospun 500k PAN, a peak appears at 1634 cm^{-1} and in the electrospun 210k PAN, a peak appears at 1666 cm^{-1}.

4.4.11 FTIR of electrospun and wet spun PAN fibres

The effect of electrospinning on the FTIR absorption peaks in the region 1900 to 900 cm^{-1} for the 120k PAN copolymer relative to the commercial wet spun fibre from the same grade are shown in Figure 4.17.

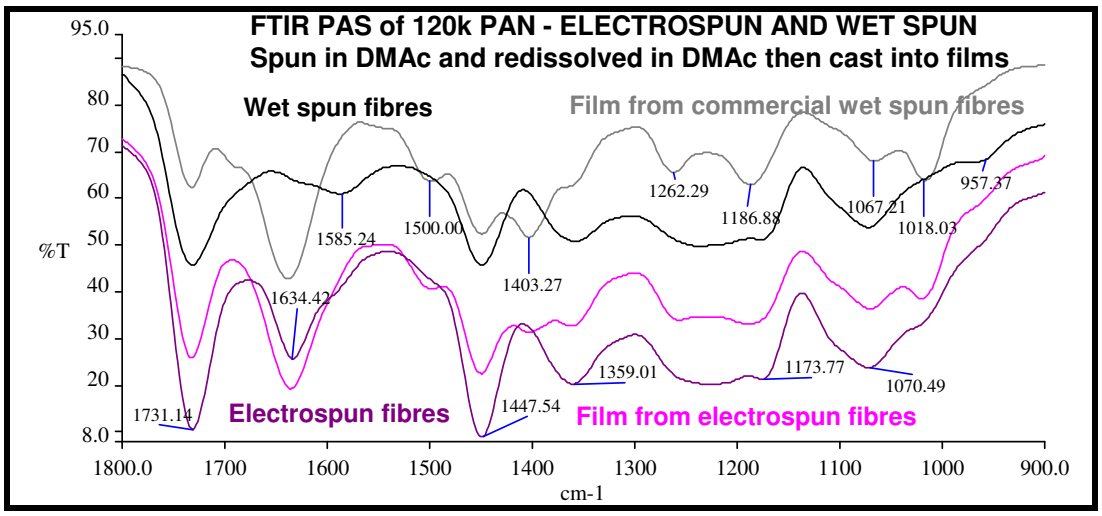

Figure 4.17 FTIR of wet spun and ES 120k PAN fibres.

The commercial wet spun fibre contains a smaller amount of remnant DMAc solvent than the electropun fibre even after both samples were dried at 50 °C in a vacuum oven for 12 hours. The position of the DMAc peak in the wet spun fibre at 1585 cm^{-1} is at a lower wavelength than the electrospun fibre at 1634 cm^{-1}. For the copolymer electrospun PAN the peak at 1070 cm^{-1} broadens slightly with a new peak at 1018 cm^{-1} in the electrospun fibre relative to the wet spun fibre. In the electrospun 120k PAN, a peak appears at 1634 cm^{-1} whereas in the wet spun fibre a peak appears at 1590 cm^{-1}.

There are indications of the formation of oxidation and cyclised species on the electrospun sample even after being redissolved and cast as a film. Peaks in the region of 1731, 1260 and around 1070 cm^{-1}, are known to be an increase in absorption after heat treatment are more pronounced in the redissolved electrospun fibres than in the redissolved wet spun fibre as seen in Figure 2.17. Peaks were also more intense in the region 3200 to 3600 cm^{-1} on the redissolved electrospun sample (not shown here).

The degree of oxidation on the electrospun fibre may be higher than on the wet spun fibre due to;

- The higher concentration of oxygen in air around the electrospinning fibres than the amount of oxygen in the DMAc coagulation bath in wet spinning.
- The degree of shear is higher on the electrospun fibre than the wet spun fibre as the PAN dope exits the spinneret.

- The electrospun fibre has a thinner diameter and therefore a higher aspect ratio and thus a higher surface area, which increases the likelihood of oxidation in a given environment.
- Oxidation may be catalyzed by the energy of the high surface charge on the ES fibre.

4.4.12 Conclusions from the FTIR study of electrospun PAN

- The degree of orientation of homopolymer 85k PAN as determined by FTIR on electrospun PAN may be comparable to the orientation factor, OF, of wet spun PAN if the electrospinning field strength is $\geq$ 0,75 kV.cm^{-1} . Cu complexation on the CN group in the FTIR spectra at 2242 cm^{-1} is seen for fibres electrospun from solutions where Cu:CN $\geq$ 1:2.
- Addition of LiCl salts at a concentration of Li:CN of $\leq$ 1:50 provides higher molecular orientation than the electrospun PAN control based on the FTIR, OF, results. The orientation of electrospun PAN fibre even with LiCl addition is still much lower than the orientation of commercial PAN fibres made via the wet spinning process.
- Cu complexation on the carboxylic acid group in the FTIR spectra at 1630 cm^{-1}; for electrospun samples the 1630 cm^{-1} peak shifts from 1632 cm^{-1} for Cu:CN $\leq$ 1:50 to 1600 cm^{-1} for Cu:CN $\geq$ 1:20. This has been shown to be due to residual solvent which complexes the Cu-salt and is "frozen-in" the electrospun fibre morphology.
- In the case of the annealed films; the shift from $\pm$ 1630 to $\pm$ 1600 cm^{-1} occurs at Cu:CN $\leq$ 1:20. Therefore the complexation is assumed to be time dependant during gelation. For complexation in the rapid electrospinning process, higher concentration is needed.
- Addition of $CuCl_2$ salt to the spinning dope of the 120k PAN copolymer leads to a 74% reduction in the crystallinity relative to the control, whereas in the 210k homopolymer the salts yield an increase in the crystallinity by 29% as determined by the inverse relationship between the ratio of the heights of the peaks in FTIR at 1730 and 2240 cm^{-1} and the FTIR calculated degree of crystallinity.
- The crystallinity of the homopolymer electrospun PAN is significantly higher than the crystallinity of the electrospun 120k PAN copolymer.
- For all grades of PAN the peak at 1070 cm^{-1} broadens in the FTIR spectra of the electrospun fibres. In the electrospun 500k PAN, a peak appears at 1634 cm^{-1} and in the electrospun 210k PAN, a peak appears at 1666 cm^{-1}. In the electrospun 120k PAN, a peak appears at 1631 cm^{-1} whereas in the wet spun fibre a peak appears at 1585 cm^{-1}. The peak broadening on the electrospun fibres indicates a less dense molecular packing with more room for stretching vibrations on the nitrile groups.

- There is residual solvent in the electrospun samples even after the samples are dried in a vacuum oven at 50°C for 12 hours.
- The degree of oxidation and or cyclisation on electrospun PAN fibres is higher than that on wet spun PAN fibres. The presence of the salts may have catalysed the cyclisation of the nitrile groups causing the typical decrease in the absorption wavelength.

4.5 THERMAL ANALYSIS STUDY OF ELECTROSPUN PAN: RESULTS, DISCUSSION AND CONCLUSIONS

4.5.1 Introduction

The theory related to thermal analysis and thermal transitions of PAN as studied by other researchers is discussed in Section 2.3.4.

DSC is used in this study to investigate;

- the effect of wet spinning versus electrospinning on the cyclization exotherm
- the change in the Tg and other low temperature crystal-crystal transitions
- thermal transitions on co- and homo-polymer PAN containing Cu salts

TGA is used to study the effect of copper salts on the thermal degradation of copolymer and homopolymer electrospun PAN samples containing copper salts.

4.5.2 DSC and TGA equipment and experimental procedure

All DSC thermograms were recorded on a TA Instruments TA Q100 in N_2 and unless otherwise stated, at a heating rate of 10 ºC.min^{-1}. All TGA thermograms were recorded on a TA Instruments, Q500 in air at 10 ºC.min^{-1}. All data was analyzed using *Universal Analysis Software*. Samples were spun according to the method given in Section 3.1. PAN grades are described in Table 3.1. The results given Section 4.5 are described in Tables 4.1 and 4.2.

4.5.3 DSC of wet spun versus electrospun PAN copolymer

The repeatability of the DSC analysis was checked on three different samples of the 8% 120k PAN control in DMAc without additives, spun at 20 kV, 20 cm and 30 °C. The thermograms are compared to a commercial wet spun PAN of the same copolymer PAN in Figure 4.18.

The wet spun sample, (black line), shows a slightly higher exotherm temperature, a higher enthalpy, (ΔH_f), 440,5 J.g^{-1} versus 394,5 J.g^{-1} and a broader temperature range at half peak height (21,7°C versus 20,2°C) than the electrospun samples (red line). The T_{onset} of the exotherm for the wet spun sample is also lower at 267,5 °C. These results indicate a closer packing in the electrospun copolymer PAN sample.

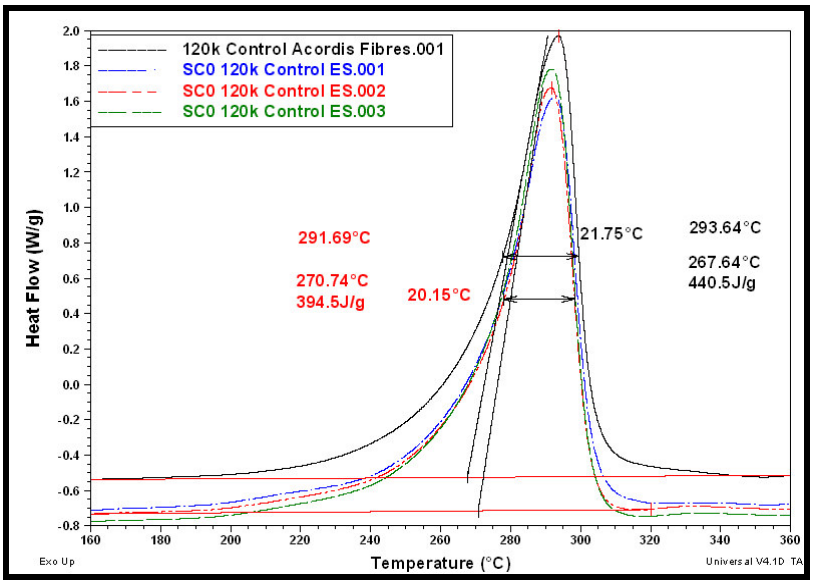

Figure 4.18 Effect of spinning type on the DSC exotherm of PAN fibres.

Copolymer PAN undergoes cyclization faster than a homopolymer PAN through initiation by intramolecular anhydride formation on the carboxylic acid co-monomer groups. The onset goes to lower temperatures as the itaconic acid content increases. In other words, the wet spun fibre can be regarded as similar to a high acid content copolymer as during annealing in the gel state, a low energy conformation is assumed.

In electrospinning the dope is frozen quickly into a solid conformation with tight packing. This rapid tight packing retards the rate for the intramolecular rearrangement of the itaconic acid into the anhydride form.

The propagation step then in the wet spun fibre is slower as shown by the broader exotherm as once the anhydride is formed; an imide structure is formed by isomerism. The propagation step of the carbonization reaction requires this isomerism rearrangement for cyclization.

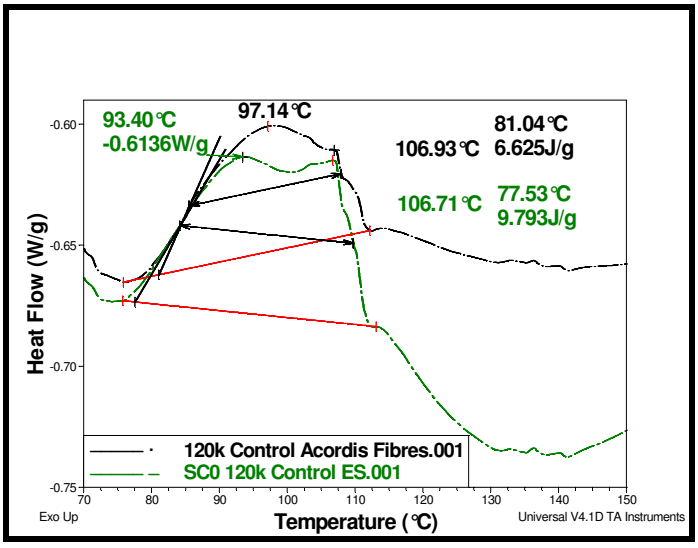

Figure 4.19 Effect of spinning type on the Tg of PAN copolymer fibres (70 to 150 °C).

The differences in the Tg values are shown in Figure 4.19 (70 °C to 150 °C) and expanded in Figure 4.20 (106 °C to 113 °C). The shape of the endothermic peak in both fibres is indicative of a polymer sample, which has internal stress (Sanderson 2007). When the internal energy or "frozen-in stress" in a processed polymer is released on heating in the DSC, molecules revert from the deformed state into the relaxed state giving rise to endotherms. This involves energy release due to segmental translation and flow of all the molecular chains.

The large exothermic peak appears to have two convoluted peaks; on the wet spun fibre having maxima at 97 and 107 °C and on the electrospun control at 93 and 107 °C. These are most likely ascribed to rotational and vibrational segmental motions, normally referred to as the α transitions. Some authors claim the existence of a double Tg in PAN. The three repeats on the electrospun control show good repeatability with the DSC procedure employed.

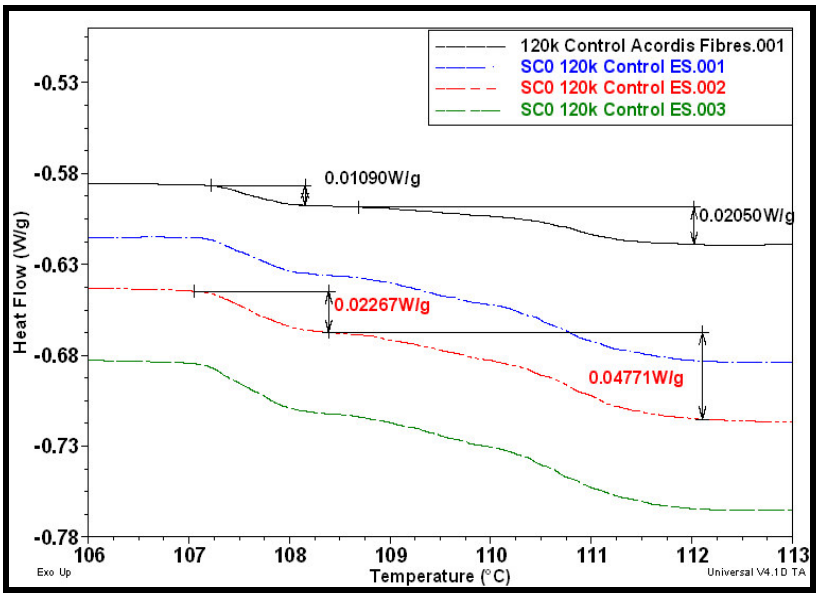

Figure 4.20 Effect of spinning type on the Tg of PAN copolymer fibres (105 to 113 °C).

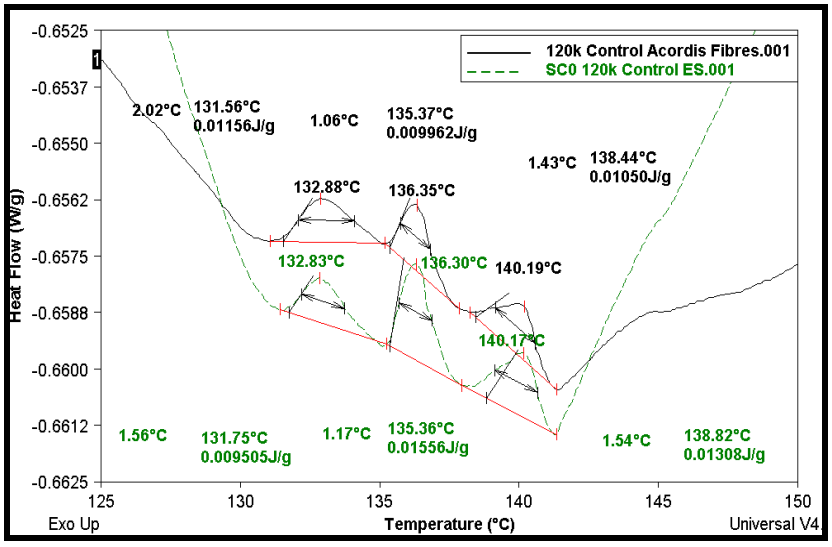

Figure 4.21 Low temperature crystal / crystal transitions in PAN copolymer fibres.

The transition in the fibres between 106 and 113 °C takes place in two steps. For both steps the enthalpy change is twice as large in the electrospun fibre in comparison with the wet spun fibre. This is most likely due to the fact that the gelation and solvent diffusion rate is much higher in the case of electrospinning, resulting in higher frozen-in stress. In the wet spinning process the fibre is drawn through a series of baths with mixed solvent and non-solvent, where the ratio of the non-solvent becomes progressively higher along the production line, till pure water non-solvent is used in the heated drawing baths. In the case of wet spinning, the time to reach the dry gel state i.e. almost total residual solvent removal, is longer and in addition the drawing baths are heated. Both these factors contribute to allowing for some molecular relaxation / annealing.

The presence of repeatable exothermic peaks was noted in the region of the DSC thermograms from 125 °C to 150 °C and are shown for the wet-spun and ES 120k PAN fibres in Figure 4.21. Small endothermic humps are present at 132, 136 and 140 °C in both the wet spun and control electrospun 120k PAN fibres. A first order thermal transition was clearly identified previously only at 142 to 150 °C on DSC heating scans only in ultradrawn PAN fibre samples of draw ratio >60. The observed reversible DSC transitions were ascribed to crystal / crystal transitions from orthorhombic to hexagonal chain packing at around 150 °C, as revealed by XRD using a different grade of PAN in ultradrawn fibre form (Sawai 1999).

4.5.4 DSC to show the effect of $CuCl_2$ salts on homopolymer ES PAN

The effect of the addition of $CuCl_2$ salts to the homopolymer ES 210 k PAN on the transitions by DSC was evaluated and the thermogram from 200 to 350 °C is shown in Figure 4.22.

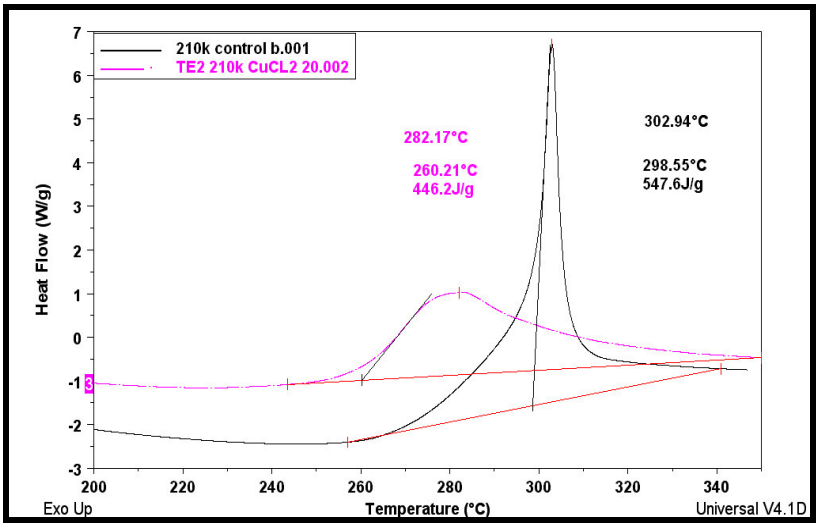

Figure 4.22 DSC for cyclization exotherm of ES homo PAN with $CuCl_2$.

Figure 4.22 shows the thermograms of the 210k homopolymer PAN and the homopolymer with $CuCl_2$ added, such that Cu:CN = 1:20. Data was recorded at a heating rate of 10 ºC.min^{-1}. The

results show that the $CuCl_2$ causes a depression in the cyclisation exotherm from 547,6 to 446,2 $J.g^{-1}$. The onset of the cyclisation exotherm was reduced from 303,9 to 282,2 ºC.

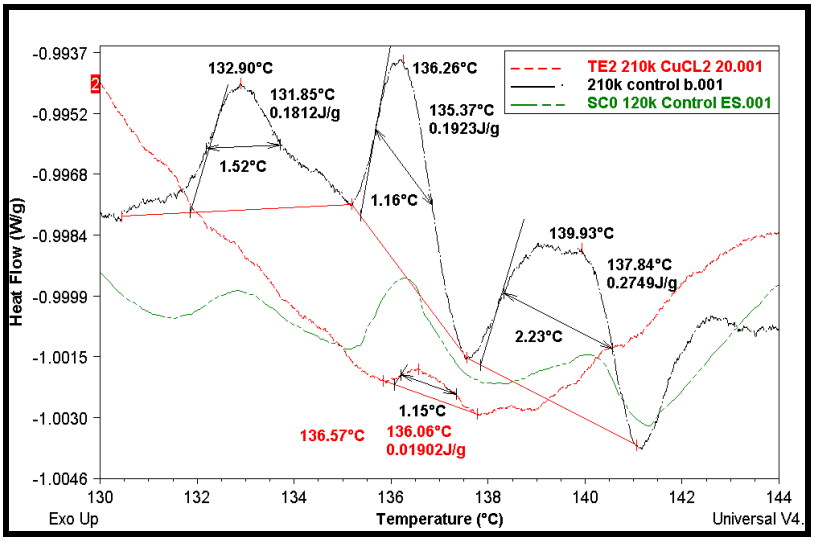

Figure 4.23 DSC crystal transition of ES homo PAN with $CuCl_2$.

The presence of repeatable exothermic peaks was noted in the region of the DSC thermograms from 130°C to 144 °C and are shown for the ES 210k PAN fibres with $CuCl_2$ in Figure 4.23. Table 4.10 shows that the data related to the three exothermic peaks in the DSC thermograms for the 120k PAN copolymer and the 210k PAN homopolymer, centered at 133, 136 and 140 °C.

Table 4.10 DSC data of PAN fibres crystal transitions (130 to 150°C)

	Peak I @ ± 133 cm^{-1}			Peak II @ ± 136 cm^{-1}			Peak III @ ± 140 cm^{-1}		
	T (°C)	$J.g^{-1}$	Width	T (°C)	$J.g^{-1}$	Width	T (°C)	$J.g^{-1}$	Width
Wet spun 120k PAN	132,8	0,0115	2,02	136,4	0,0099	1,06	140,2	0,0105	1,43
Electrospun 120k PAN	132,8	0,0095	1,56	136,3	0,0155	1,17	140,2	0,0130	1,54
Electrospun 210k PAN	132,9	0,1812	1,52	136,3	0,1923	1,16	139,9	0,2749	2,23
Electrospun 210k PAN with $CuCl_2$	-	-	-	136,6	0,0190	1,15	-	-	-

Whilst the enthalpy change is relatively tiny in comparison to the change at the Tg and the cyclization exotherm it has been shown that the appearance of these exothermic peaks above the Tg are repeatable. For the 120k PAN wet spun copolymer the enthalpy change at the exotherm is 395 $J.g^{-1}$, the enthalphy change at the glass transition temperature is 6,625 $J.g^{-1}$ and at the crystal / crystal transition <0,1 $J.g^{-1}$.

The enthalpy change for the peaks on the 210k homopolymer control electrospun PAN fibres is generally 10 fold higher than the enthalpy of the peaks of the 120k PAN electrospun copolymer control. The addition of $CuCl_2$ (Cu:CN = 1:20) removes the peaks at 133 and 140 °C and greatly

reduces the enthalpy of the peak at 136 °C indicating fewer ordered structures (crystals) in the samples containing the $CuCl_2$ salt.

The cyclisation exotherm data for the electrospun 120k PAN and 210k PAN controls and samples containing $CuCl_2$ at a concentration of Cu:CN of 1:20 is shown in Table 4.11.

Table 4.11 The effect of $CuCl_2$ on Tm of ES homopolymer and copolymer PAN fibres.

Sample (Cu:CN)	Cyclisation onset in °C	Peak in °C	Enthalpy in $J.g^{-1}$
210k PAN Control	298	304	548
210k PAN 1:20	260	282	446
120k PAN Control	268	292	403
120k PAN 1:20	259	277	336

The enthalpy change at the cyclization exotherm is higher for the 210k PAN homopolymer as expected than for the 120k PAN copolymer where the bulky carboxylic acid co-monomers disrupt the packing density in the more ordered "crystalline" domains of the electrospun fibres and serve to catalyse the cyclization reaction through the formation of imine groups shown in Figure 4.20.

This lowering in the cyclization exotherm may be attributed to the incorporation of the comonomers in the polymer chain that might bring down the average crystal size and may also generate the defects in the crystals / ordered phase, thereby decreasing the cyclization temperature. This exotherm is broader, starts at a lower temperature, and has a lower peak temperature, compared with those for the 210k PAN homopolymer. This is because of the increase in the variation of crystal size and generation of defects in the crystals due to the incorporation of the comonomer.

4.5.5 DSC to show the effect of $CuCl_2$ concentration on copolymer ES PAN

The effect of $CuCl_2$ salt concentration on the cyclization exotherm of electrospun 120k PAN was evaluated and the thermograms are shown in Figure 4.24. The $CuCl_2$ concentrations prepared were Cu:CN equals 1:100, 1:75; 1:50; 1:20 and 1:10. The dope would not electrospin at 20kV, 20 cm if Cu:CN > 1:10.

The onset of the cyclisation exotherm temperature and the enthalpy for the $CuCl_2$ containing 120k PAN are listed in Table 4.12.

The addition of small amounts of $CuCl_2$ disrupts the crystallinity of the electrospun PAN fibres and lowers the melting peak endotherm from 292 °C for the unfilled control sample to 279 °C for the electrospun fibre containing Cu:CN at a ratio of 1:10. The peak width also broadens indicting a change in the molecular packing in the more ordered "crystalline" domains. The effect of the salts on the glass transition temperature of the fibres is shown in Figure 4.24. It is shown in Figure 4.25 that the cyclisation enthalpy decreases as the conductivity of the spinning dope increases. However a 100% increase in the conductivity results in a 2% decrease in the peak enthalpy,

indicating that the change in enthalpy is not dependant on the spinning conductivity but due to copper complexed inside the PAN fibres.

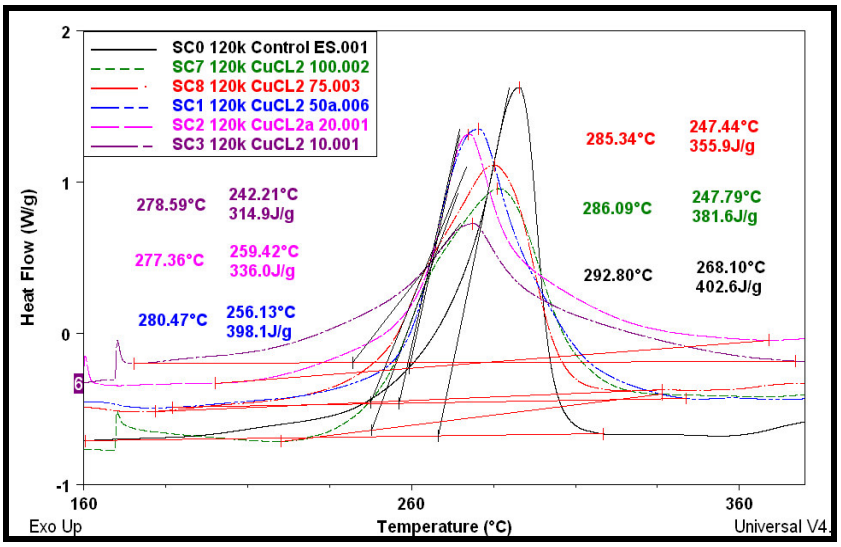

Figure 4.24 DSC for cyclisation exotherm of ES copolymer PAN with various [$CuCl_2$].

Table 4.12 Thermal data for the cyclization exotherm for ES 120k PAN with $CuCl_2$

Sample (Cu:CN)	$CuCl_2$ concentration $mol.dm^{-3}$	Conductivity $mS.cm^{-1}$	Onset (°C)	Peak (°C)	Enthalpy $(J.g^{-1})$
Control	0	0.0555	268	292	403
1:100	0.015	0.987	248	286	381
1:75	0.0225	0.5000	247	285	356
1:50	0.0300	1.0753	256	280	350
1:20	0.0750	1.7241	259	277	336
1:10	0.1500	2.6316	242	279	314
1:5	0.3000	6.2500			

The results in Table 4.12 were plotted on a graph shown in Figure 4.25.

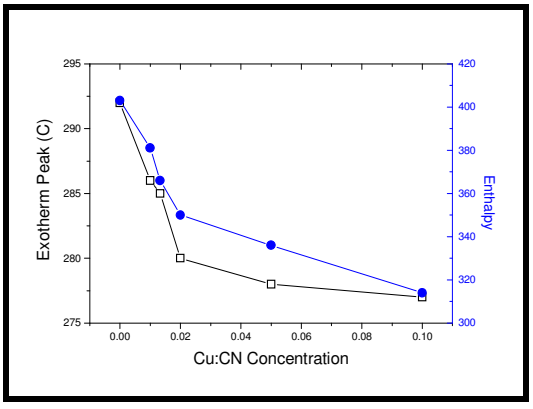

a) Exotherm temperature and enthalpy

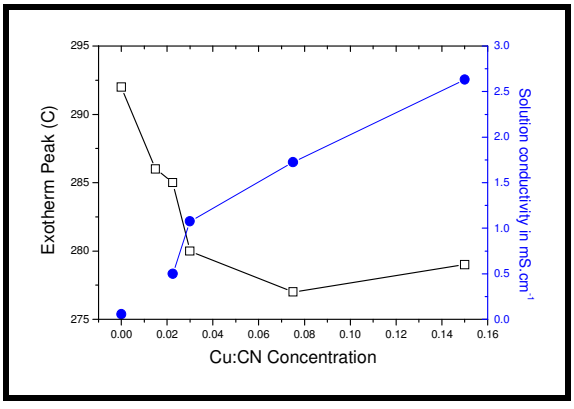

B) Exotherm temperature and conductivity

Figure 4.25 Cyclization exotherm and conductivity for ES 120k PAN with $CuCl_2$.

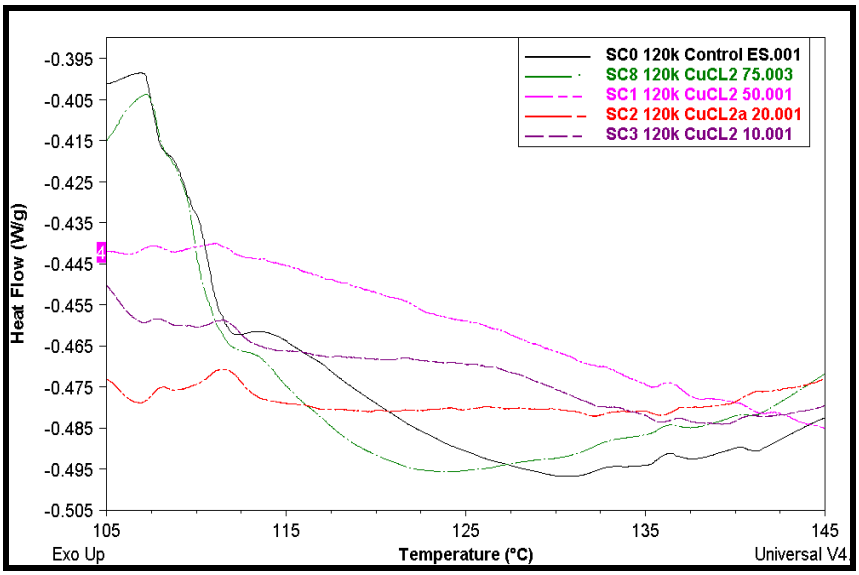

Figure 4.26 DSC for Tg of ES copolymer PAN with various [$CuCl_2$].

The addition of $CuCl_2$ at the low concentration of Cu:CN ratio of 1:75 still gives a prominent glass transition temperature where at a concentration of more than Cu:CN of 1:50 does not give a glass transition exotherm.

4.5.6 DSC to show the effect of Cu salts on copolymer ES PAN

The effect of copper chloride, copper sulphate, copper nitrate and copper acetyl acetonate with ligands on the cyclization endotherm and the glass transition of the 120k PAN copolymer was evaluated and the thermograms are presented in Figure 4.27 and Figure 4.28 respectively.

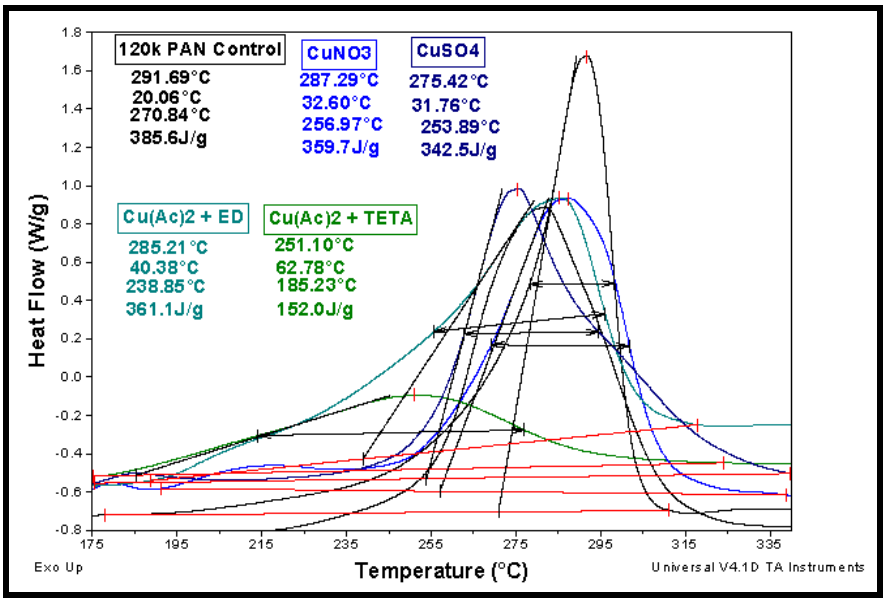

Figure 4.27 DSC for cyclization exotherm of ES 120k PAN with Cu-salts (Cu:CN = 1:50).

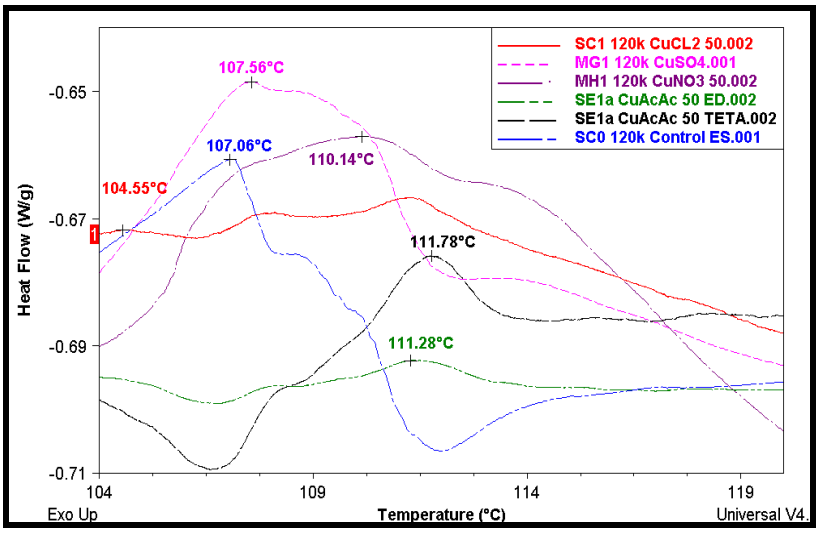

Figure 4.28 DSC for Tg of ES 120k PAN with Cu-salts (Cu:CN = 1:50).

The thermal transitions in the graphics above are tabulated in Table 4.13.

Table 4.13 Enthalpy versus Cu:CN ratio for ES 120k PAN with Cu-salts.

	Onset (°C)	Peak (°C)	Enthalpy ($J.g^{-1}$)	Tg (°C)
Control	268.2	292.8	396	107,1
$CuCl_2$	256.-	280.0	350	104,6
$CuSO_4$	255.7	276.2	374	107,6
$Cu(NO_3)_2$	258.5	287.5	298	110,1
Cu(acetate) + ED	241.0	285.8	397	111,3
Cu(acetate)+TETA	185.4	250.2	138	111,8

The addition of all copper salts with the exception of $CuCl_2$ increases the Tg. The crystal / crystal transitions of the electrospun 120k PAN fibres with various copper salts at a concentration of Cu:CN of 1:50 are shown in Figure 4.27 and 4.28.

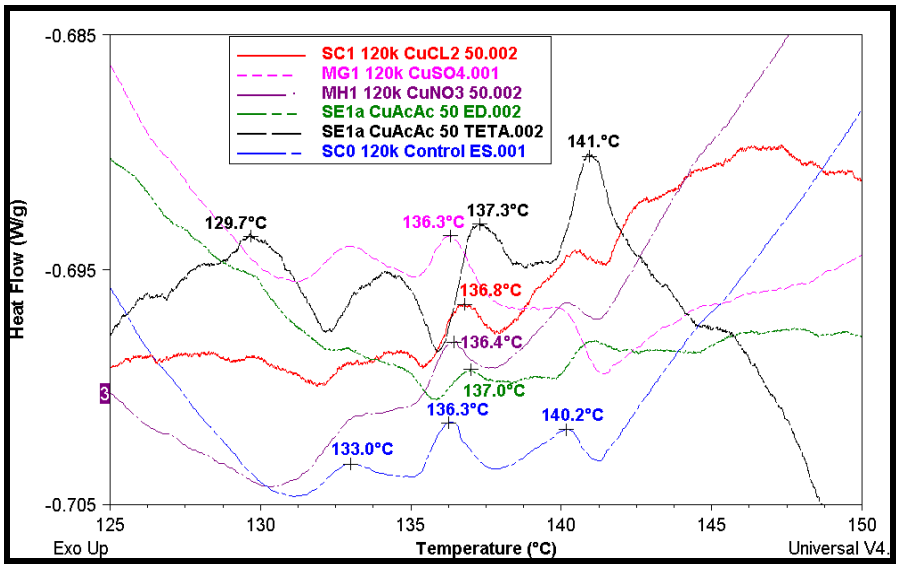

Figure 4.29 DSC from 125 to 150 °C of ES 120k PAN with Cu-salts (Cu:CN = 1:50).

The copper acetyl-acetonate provides increased exotherms indicating a more ordered crystal structure than either the control or the samples with other salt additives.

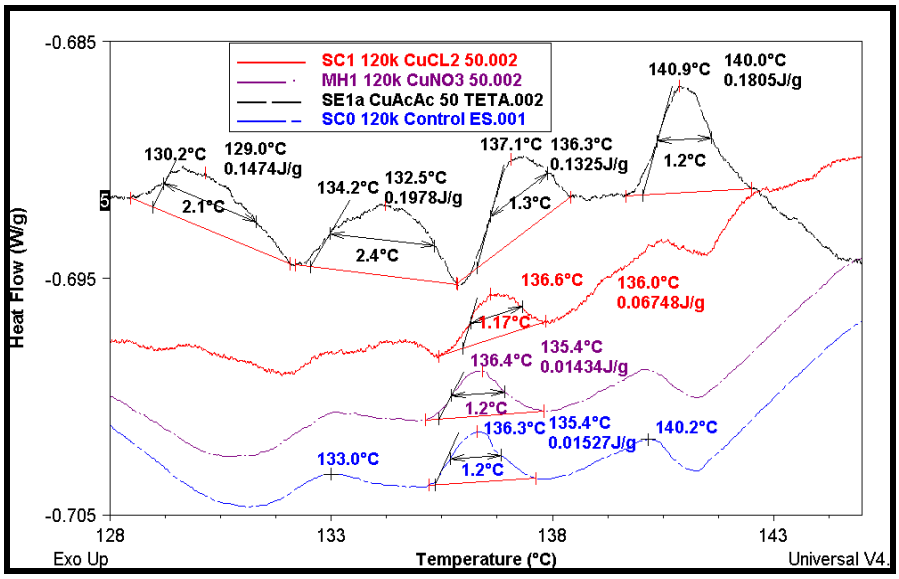

Figure 4.30 DSC 128 to 145 °C of ES 120k PAN with Cu-salts (Cu:CN = 1:50).

4.5.7 TGA of homopolymer and copolymer ES PAN with $CuCl_2$

The effect of $CuCl_2$ in various concentrations on the thermal stability and decomposition temperature of 210k PAN homopolymer and the 120k PAN copolymer were evaluated using TGA and the thermograms are shown in Figure 4.31 and Figure 4.32 respectively. The products involved in the initial degradation of PAN copolymers are HCN and NH_3. On-line TGA/FTIR was used to show that the formation of polymethacrylic anhydride at elevated temperatures (250 to 300 °C) results with the formation of H_2O as the major product along with CO_2 due to a decarboxylation reaction. The fast weight loss in the second zone may be attributed to the evolution of H_2O and CO_2 along with other products of degradation like HCN and NH_3. The weight loss above these temperatures is due to chain scission (Sen et al. 2003).

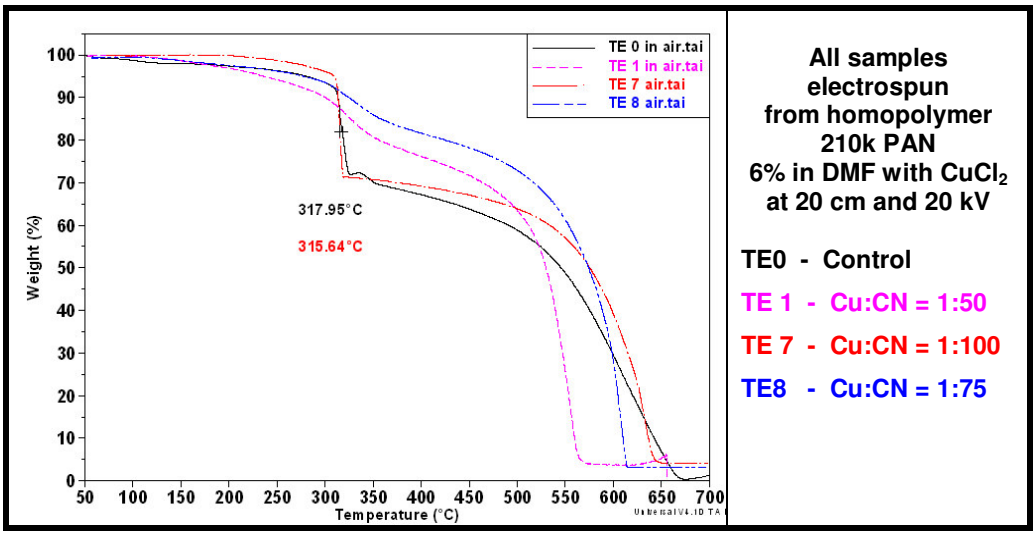

Figure 4.31 TGA of 210k PAN with $CuCl_2$ (Cu:CN = 1:100, 1:75 and 1:50).

The control electrospun 210k PAN and the sample with low Cu:CN = 1:100 show a sharp mass loss at 316 and 318 °C respectively. The sharp mass loss is due to the exothermic ladder formation, which is self-catalytic and eliminates CO_2 in the process. The weight loss for the samples with Cu:CN ratios of 1:75 and 1:50 show gradual weight loss up to about 500 °C. The effect of $CuCl_2$ in various concentrations on the thermal stability and decomposition temperature of 120k PAN copolymer was evaluated using TGA and are shown in Figure 4.32.

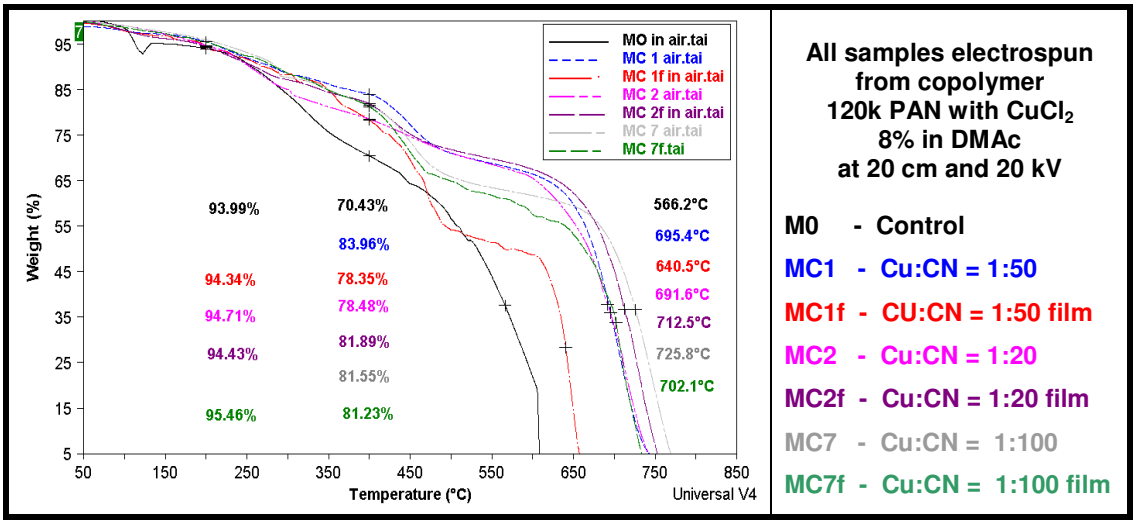

Figure 4.32 TGA of 120k PAN with $CuCl_2$ (Cu:CN = 1:100, 1:75, 1:50 and 1:20).

The TGA curves of 210 k PAN homopolymer in Figure 4.31 PAN and 120k PAN copolymer in Figure 4.32 reveals that the incorporation of carboxylic acid comonomers brings interesting changes. The TGA curves of the PAN homopolymer in air atmosphere does not show any substantial weight loss in the first zone, while in the second zone starting from 300 °C the weight loss is fast and rapid. The final zone shows a steady and slow weight loss up to 600 °C. Above 600°C the weight loss is rapid, as expected for the final decomposition of the carbonized PAN. The 120k PAN copolymer showed a steady region up to 295 °C without much weight loss (about 5%). In the second step, ranging from 265 to 465 °C, the weight loss is fast.

Table 4.14 TGA data of 120k PAN with $CuCl_2$ (Cu:CN = 1:100, 1:75, 1:50 and 1:20)

Code	Description	Weight %		Temperature (°C) @ 50% final weight loss
		@ 200 °C	@400 °C	
MO	Control	94,0	70,5	560,0
MC1	$CuCl_2$ (1:50)	95,5	84,0	695,4
MC1f	$CuCl_2$ (1:50) film	94,3	78,4	640,5
MC2	$CuCl_2$ (1:20)	94,7	78,5	691,6
MC2f	$CuCl_2$ (1:20) film	94,4	81,9	712,5
MC7	$CuCl_2$ (1:100)	94,3	81,5	725,8
MC7f	$CuCl_2$(1:100) film	95,5	81,2	702,1

The weight loss associated with the first step was not substantial, i.e., up to 295 °C, whereas in the second zone ranging from 285 to 409 °C, the weight loss is quite high (about 30%) and

becomes steady. Gradual weight loss in the third zone, i.e., 400 to 600 ℃ is slow for the samples containing $CuCl_2$ salts but essentially non-existent for the control.

4.5.8 TGA of copolymer PAN with other copper salts

The effect of various Cu on the thermal stability and degradation of ES PAN fibres are shown in the three figures below. In Figure 4.33 the thermograms for the salts incorporated in the electrospun 120k PAN include CuO particles, $CuSO_4$, $CuNO_3$ and CuCl. In Figure 4.34, the salts include Cu(ac)/ED, Cu(ac)/TETA and copper acetyl-acetonate with EA and NH_3.

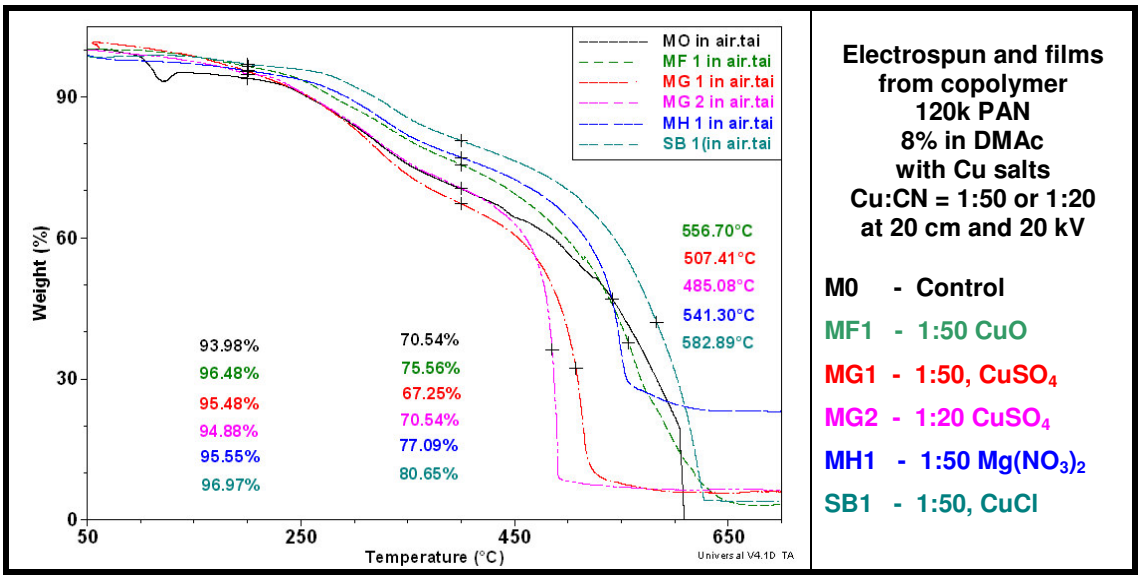

Figure 4.33 TGA of 120k PAN with Cu-salts (Cu:CN = 1:50).

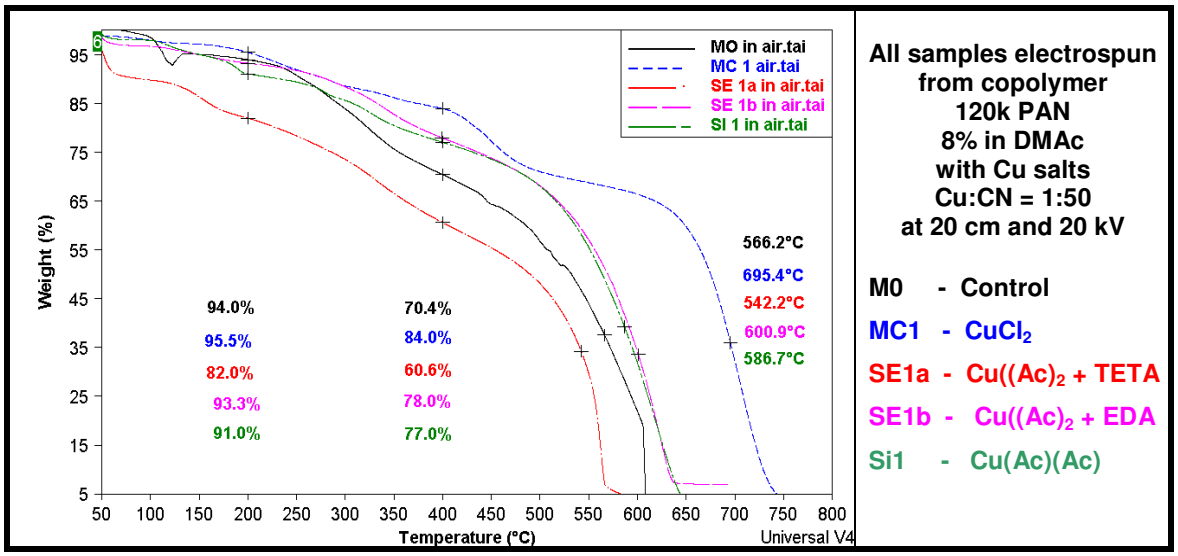

Figure 4.34 TGA of 120k PAN with Cu-salts and dispersants (Cu:CN = 1:50).

In Figure 4.35 the TGA thermogram of PAN with LiCl is shown.

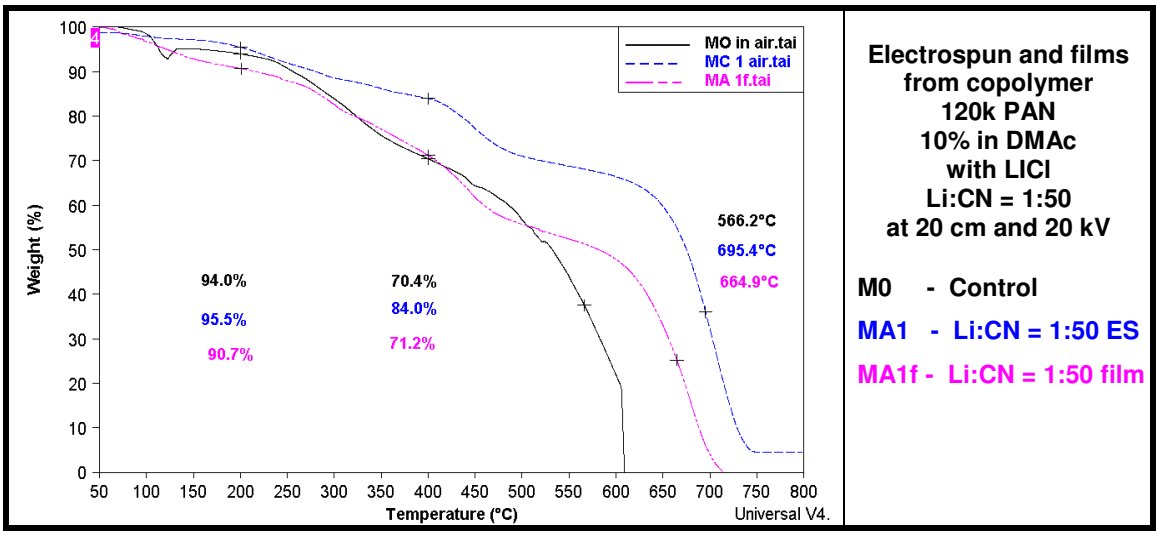

Figure 4.35 TGA of 120k PAN with LiCl (Li:CN = 1:50).

Table 4.15 TGA of 120k PAN with Cu-salts (Cu:CN = 1:50)

Code	Description	Mass Loss Weight % at *x* °C		Temperature (°C) @ 50% final weight loss
		@ 200 °C	@400 °C	
MO	Control	94,0	70,5	560,0
MF1	CuO nanoparticles (1:50)	96,5	75,6	556,7
MG1	$CuSO_4$ (1:50)	96,5	67,3	507,4
MG2	$CuSO_4$ (1:20)	94.4	70,6	485,1
MH1	$Cu(NO_3)_2$ (1:50)	95,6	77,1	541,3
SB1	CuCl	96,0	80,7	582,9
SE1a	$Cu(Ac)_2$ + ED	82,0	60,6	542,2
SE1b	$Cu(Ac)_2$ + TETA	93,0	78,0	600,9
SI1	Cu-acac + EA + NH_3	91,0	77,0	586,7
MA1	LiCl (1:50)	90,7	71,2	664,9

The electrospun PAN containing LiCl where Li:CN = 1:50 shows a marked increase in the thermal decomposition profile.

4.5.9 Conclusions from the thermal analysis results

- Wet spun PAN shows a slightly higher exotherm temperature, a higher enthalpy, and a broader temperature range at half peak height than the electrospun samples. These results indicate a slightly higher degree of order and closer packing in the wet spun PAN fibres relative to the electrospun PAN fibres.
- The electrospun fibre has higher frozen-in stress than the wet spun fibres which go through an annealing stage during the commercial fibre processing.
- Wet spun PAN has a prominent thermal transition at 97,1°C with a single large exotherm. The electrospun PAN has 2 distinct transitions, at 93,4 and 106,7°C. This indicates the presence of different phases within the looser packed the less ordered “amorphous” regions

allowing for molecular vibrations below the real Tg at 136°C. Many researchers call the transition at around 90 to 100°C a second actual Tg, named Tg_{11}. It has been argued that electrospinning has a plasticizing effect on the glass transition.

- The addition of copper chloride salt to electrospun PAN lowers the cyclisation exotherm and the onset temperature for cyclisation and will therefore be a beneficial addition in the carbon fibre production process. This is more pronounced in the homopolymer than the copolymer. In addition it disrupts the low temperature crystal-crystal transitions. The disappearance of these crystal-crystal transition peaks is due to a tighter packing in the homopolymer PAN nanofibres with $CuCl_2$ which disallows the conversion between hexagonal and orthorhombic (and other) polymorphic crystal structures during heating.
- It is shown in Figure 4.25 that the cyclisation enthalpy decreases as the conductivity of the spinning dope increases. However a 100% increase in the conductivity results in a 2% decrease in the peak enthalpy, indicating that the change in enthalpy is not dependant on the spinning conductivity but due to copper complexed inside the PAN fibres.
- All the salts added in this investigation increase the Tg of the resultant electrospun fibres.
- The salts also decrease the onset of the cyclisation temperature and reduce the enthalpy of the cyclisation exotherm. This results in a lower activation energy been required for the carbonization process and high strength resultant carbonized fibres.
- The effect of salts on the mass loss during heating of the electrospun PAN is evaluated. It is reported that the addition of salts to the copolymer increase the weight % remaining on heating at 200 and 400°C.

4.6 MICROSCOPY OF ES FIBRES WITH ADDITIVES AND MODIFICATIONS: RESULTS, DISCUSSION AND CONCLUSIONS

4.6.1 Introduction to microscopical analysis of ES fibres

Microscopy is used to visually assess the fibre diameter, surface structure, degree of fibre alignment and mat morphology of electrospun samples.

In this section SEM results are used to assess the structural integrity and diameter of carbonized PAN electrospun fibres with and without $Cu(NO_3)_2$, the degree of homogeneity of CuO nanoparticles dispersed in electrospun fibres, the structure of a laser deposited CuO coating on electrospun PAN and the effect of various salt additives on fibre diameter and morphology are presented and discussed. The maximum useful and clear resolution magnification on the SEM is a 50 000 times magnification.

TEM results for the carbonized PAN with nanoparticle copper oxide obtained from calcined copper nitrate are presented as a means to assess the dispersion of the inorganic nanoparticles within and on the surface of the nanofibres.

EDAX elemental mapping was also used to assess the dispersion of the copper oxide nanoparticles.

4.6.2 Equipment used and experimental procedure

The equipment used to capture the SEM and TEM images and process the EDAX analyses reported in this section, is based at The University of Cape Town, Microscopy Unit, managed by Miranda Waldron and Mohammed Jaffer. The experimental procedure for the SEM is explained in Section 3.2.1. The experimental procedure for the preparation of the electrospun fibres is presented in Section 3.1. and for the samples with additives in Section 4.1.

4.6.3 SEM of 120k PAN control and carbonized 120k ES PAN control

The SEM micrographs of the 120k PAN electrospun control and the carbonized fibres are shown in Figure 4.36 at 2 000 times, 20 000 times and 50 000 times magnifications.

The carbonized fibres were prepared according to a method suggested in literature (Park et al. 2005), on the same grade PAN copolymer containing AN:MA:IA = 93:6:1 supplied by BlueStar Fibres, Grimsby, UK. For the carbonization process, the electrospun fibres were supported on a backing wire scrim and the edges of the non-woven were folded over the edge wires to immobilize the 2 cm by 2cm PAN mat and minimize shrinkage.

The covered wire was placed in a horizontal quartz tube furnace and heated at a rate of 1 °C per minute up to 260 °C in an air atmosphere. A dwell time of 2 hours was allowed at this temperature and then the sample was heated at a rate of 2 °C per minute up 1000 °C in a nitrogen atmosphere. It was held at 1000 °C for 1 hour and then allowed to cool to back to ambient temperature.

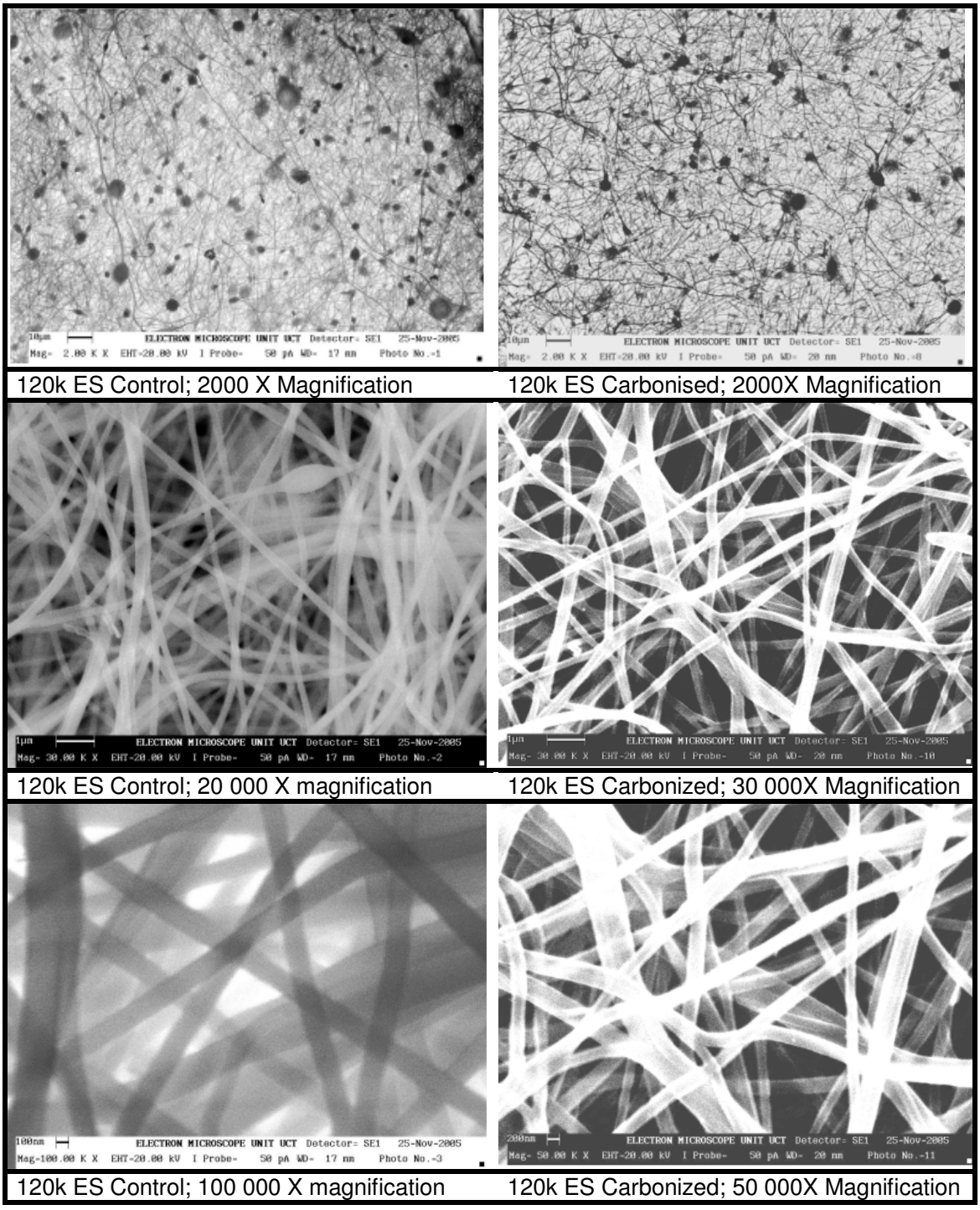

120k ES Control; 2000 X Magnification | 120k ES Carbonised; 2000X Magnification

120k ES Control; 20 000 X magnification | 120k ES Carbonized; 30 000X Magnification

120k ES Control; 100 000 X magnification | 120k ES Carbonized; 50 000X Magnification

Figure 4.36 SEM of ES control and ES carbonized 120k PAN.

A slight decrease in fibre diameter was noted; 150 to 280 nm for the control and 100 to 220 nm for the same electrospun PAN sample after carbonization. It can be seen that the SEM X-rays are able to pass through the fibres due to their low diameter.

The carbonization procedure used by others on grades of PAN homo and copolymers is listed in Table 2.2. The carbonization setup and electronic temperature controller was developed by Ulrich Buttner of the University of Stellenbosch, Electronic Engineering Department.

4.6.4 Microscopy of ES control and carbonized 120k PAN with $Cu(NO_3)_2$

The SEM micrographs of the 120k PAN electrospun control with $Cu(NO_3)_2$ where Cu:CN = 1:50 and the carbonized fibres $Cu(NO_3)_2$ are shown in Figure 4.37 at 5000 times, 30 000 times and 40 000 times magnifications.

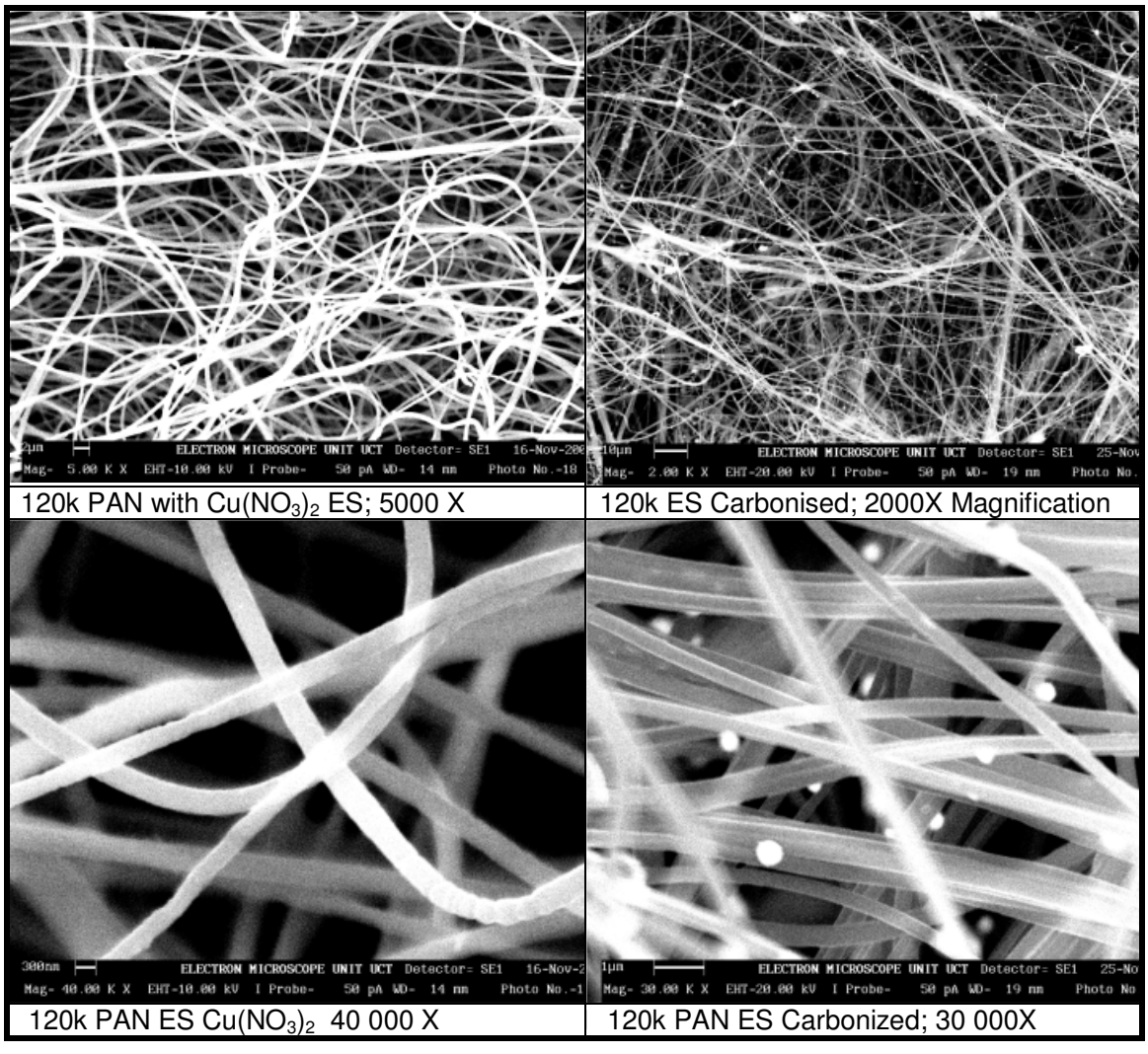

120k PAN with $Cu(NO_3)_2$ ES; 5000 X | 120k ES Carbonised; 2000X Magnification

120k PAN ES $Cu(NO_3)_2$ 40 000 X | 120k PAN ES Carbonized; 30 000X

Figure 4.37 SEM of ES control and carbonized 120k PAN with $Cu(NO_3)_2$.

The presence of inorganic CuO nanoparticles in the carbonized 120k PAN with $Cu(NO_3)_2$ can be clearly seen. This sample was investigated further using EDAX analysis with elemental mapping as shown in Figure 4.38.

The sample was held at a 45 000 times magnification and after an initial quick scan for copper (right), the data for the elemental map was collected over a 12 hour period (middle image).

The bright spots were analyzed by EDAX elemental analysis and found to contain copper and oxygen, confirming the formation of copper oxide nanoparticles.

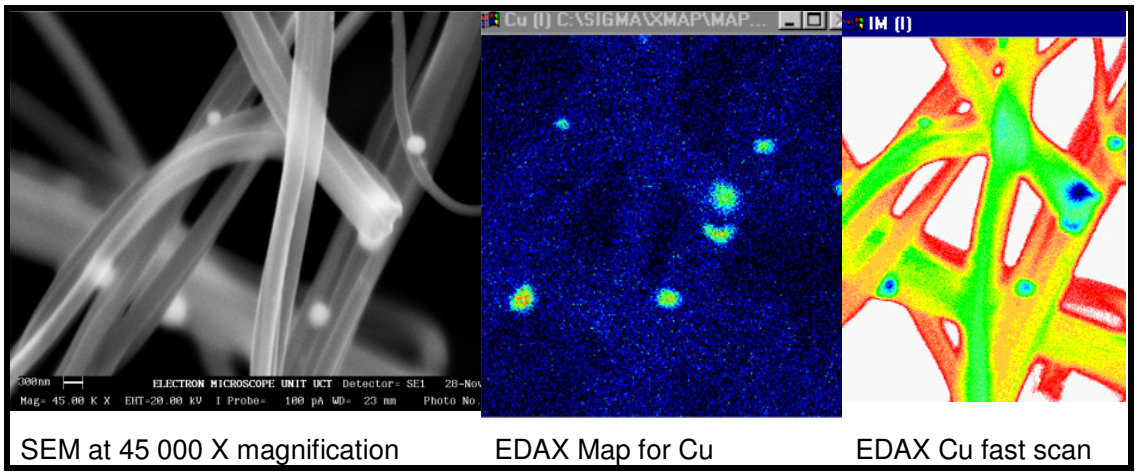

Figure 4.38 EDAX mapping of Cu of ES carbonized 120k PAN with $Cu(NO_3)_2$.

TEM analyses were performed on the same samples in order to assess if the CuO nanoparticles were only present on the surface of the fibres or in the bulk and the micrographs are shown in Figure 4.39.

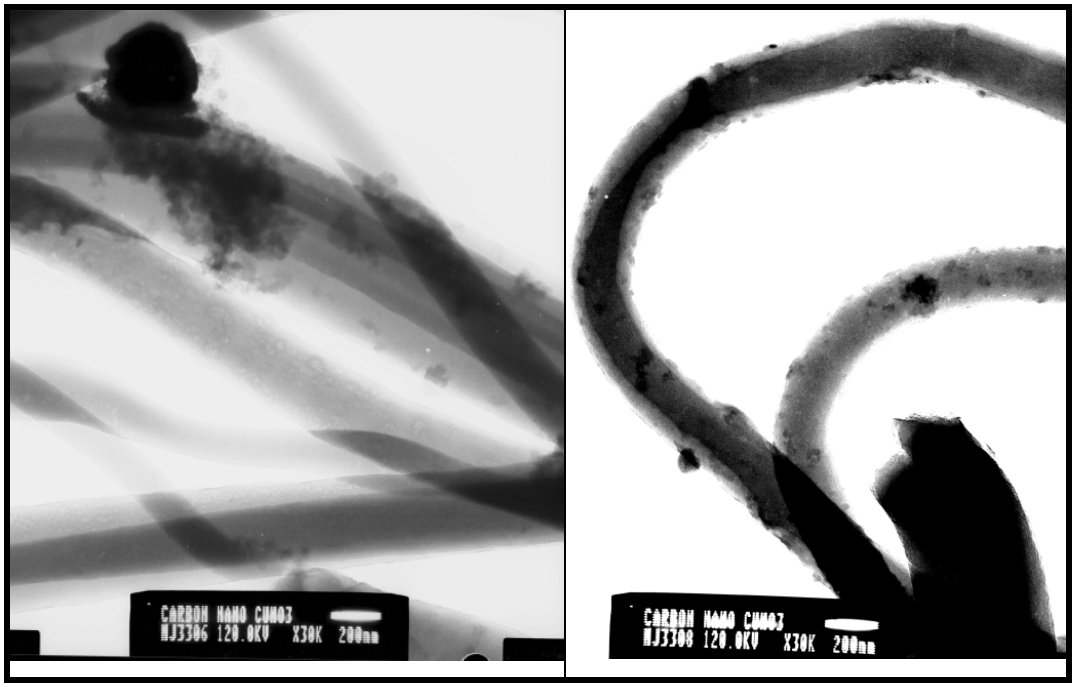

Figure 4.39 TEM of ES carbonized 120k PAN with $Cu(NO_3)_2$ (bar = 200 nm).

The TEM results confirmed that the CuO nanoparticles were both on the surface and imbedded in the bulk of the electrospun PAN fibres and in the size range of 20 to 50 nm with some agglomerates of CuO measuring up to 150 nm.

4.6.5 Laser vapor deposition CuO coating of ES PAN

Pulsed laser vaporization and deposition has been used to apply nanometer thick coatings of metals and metal oxides onto polymer surfaces at ambient temperatures (Willmott & Huber (2000). Photons have many advantages for vaporizing condensed systems, and laser vaporization sources have flexibility not available with other methods. These sources are applied to making thin films in the technique of pulsed laser deposition (PLD). The vaporized material may be further processed through a pulsed secondary gas, lending the source additional degrees of freedom. Pulsed-gas sources used for fundamental studies are promising for film deposition; an alternative to chemical vapor deposition or molecular beam epitaxy.

A pulsed laser vapor deposition equipment has been build by Ulrich Buttner of the University of Stellenbosch and was used to apply a nanometer thick layer of CuO onto the surface of electrospun 120k PAN fibres. The SEM micrographs of the coated mat and fibres is shown in Figure 4.40.

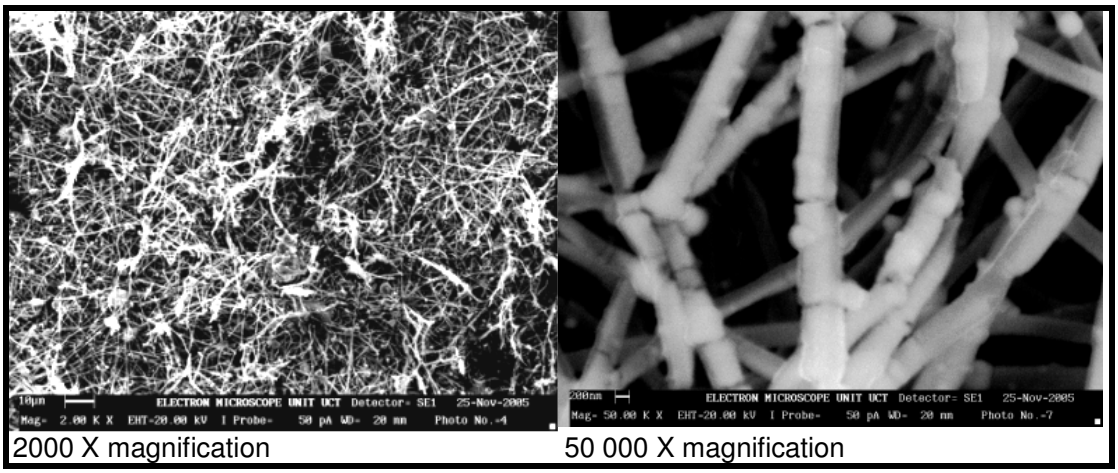

2000 X magnification 50 000 X magnification

Figure 4.40 SEM of PLD CuO on ES 120k PAN.

It can be seen in Figure 4.40 that the CuO coated individual fibres with a layer thickness of about 10 nm and did not bridge the fibres. The coating does however appear to be brittle as seen by the cracks in the surface of the coating.

4.6.6 SEM of ES PAN with Cu and Li salts and CuO nanoparticles

The effect of various Cu, e.g. $CuCl_2$, $Cu(NO_3)_2$ and LiCl and CuO nanoparticles on fibre diameter and uniformity, shape, surface roughness, degree of beading and the morphology of the non-woven mat of ES PAN was assessed. All samples were spun from a 8% 120k PAN in DMAc at 20 cm, 20 kV at 30 °C inside a fume-hood onto a flat grounded electrode covered with Al. The SEM micrographs of the control sample without additives are shown in Figure 4.43.

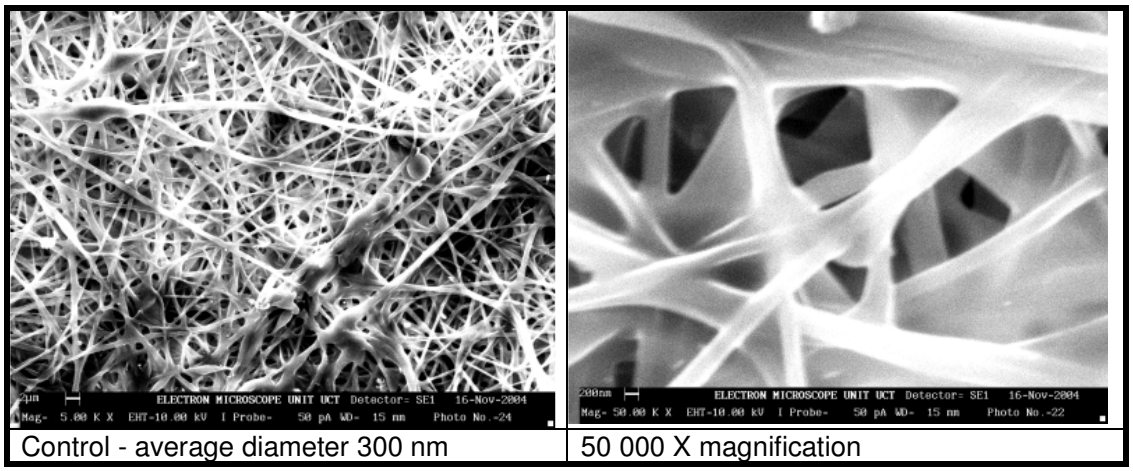

Control - average diameter 300 nm | 50 000 X magnification

Figure 4.41 SEM micrographs of ES 120k PAN control.

The relative humidity in the laboratory was high at 70% RH. The fact that the fibres are seen to merge is due to them still being in the partial gel state when they reached the grounded electrode i.e. they still contained solvent which allowed the formation of some interpenetrating networks. The average diameter of the electrospun control is 300 nm under these conditions.

The micrographs of the fibres spun from a PAN dope containing LiCl salts in the concentrations of Cu:CN = 1:50 and 1:20 are shown in Figure 4.44.

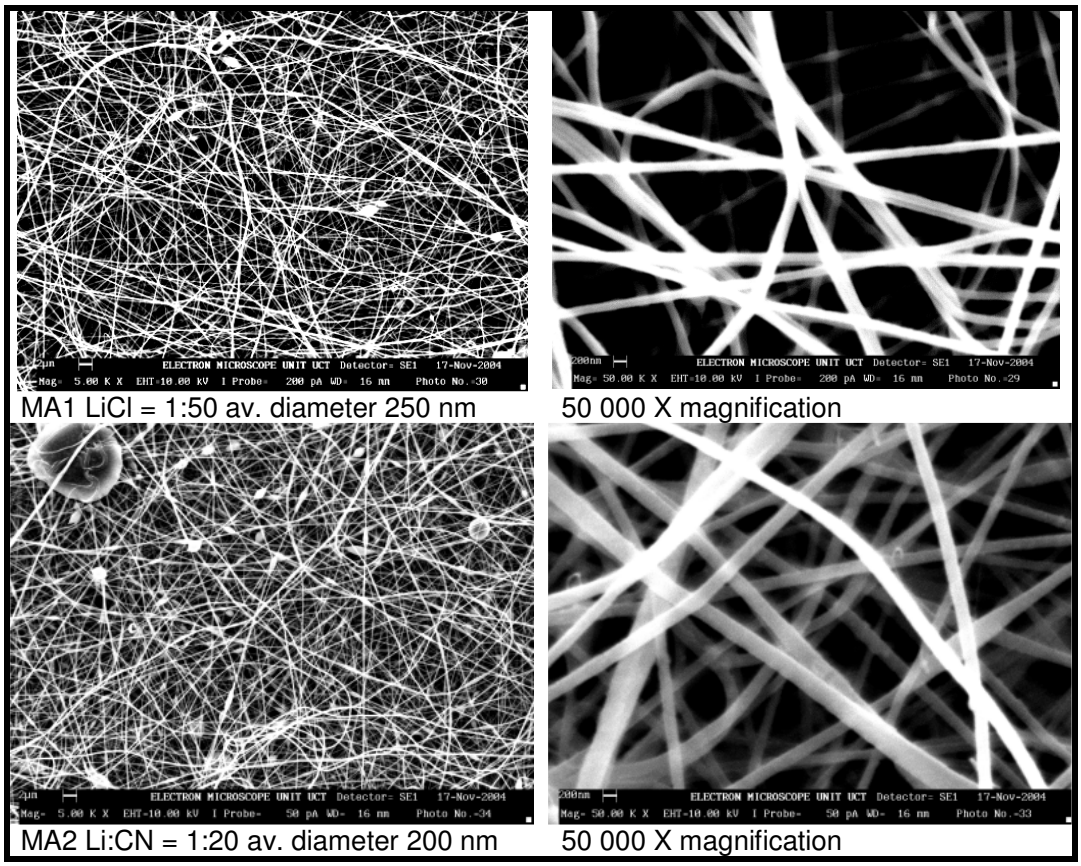

MA1 LiCl = 1:50 av. diameter 250 nm | 50 000 X magnification

MA2 Li:CN = 1:20 av. diameter 200 nm | 50 000 X magnification

Figure 4.42 SEM micrographs of ES 120k PAN with LiCl.

In order to conduct useful GPC analyses of PAN polymers it is known that the addition of LiCl provides a higher extended chain conformation of the molecules in solution, allowing more accurate MW results. This is due to the Li^+ ions interrupting the dipole nitrile inter and intra-molecular coupling on the PAN polymer chains. The fibre diameter for the higher LiCl concentration where Cu:CN = 1:20 is lower at 200 nm than for either the sample with Cu:CN of 1:50 or the control at 250 and 300 nm average fibre diameter respectively.

The FTIR results for the Orientation Factor presented in Section 4.5.6 indicate a far higher degree of molecular orientation and the TGA results in Figure 4.4.1. indicate a more ordered partially cyclized ladder structure of the chain packing within the fibre containing the higher LiCl concentration. The higher molecular alignment with the LiCl salt allows a tighter packing and the aligned polymer chains and thus the decreased average fibre diameter. In addition the LiCl increased the electrical conductivity, thereby increasing the field strength applied during electrospinning.

CuO nanoparticles, 40 to 70 nm diameter, were added to the spinning dope at a Cu:CN ratio of 1:50. CuO is known DeNOx catalyst and it was intended to immobilize the particles in and on the fibres. The solution would not spin into fibres as the pipette orifice became blocked by the agglomerated nanoparticles. The solution phase separated after standing for a few minutes with the nanoparticles sinking.

After 5 minutes of sonication of the dope and then addition of a cationic surfactant and further sonication for 5 minutes, a solution of CuO nanoparticles in PAN was able to be electrospun and was stable after standing for a few hours. The SEM micrograph of the PAN nanofibres containing CuO nanoparticles is shown in Figure 4.43.

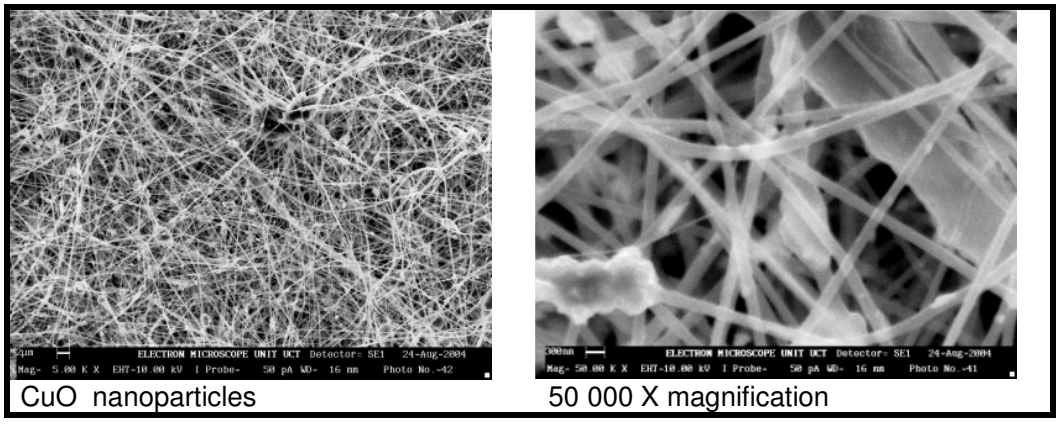

CuO nanoparticles 50 000 X magnification

Figure 4.43 SEM micrographs of ES 120k PAN with CuO nanoparticles.

Whilst there can be seen a fairly homogeneous dispersion of CuO nanoparticles in the 40 to 70 nm range, there are also many agglomerates up to 500 nm diameter. The results of the SEM micrographs of electrospun 120k PAN containing $CuCl_2$ salts such that Cu:CN = 1:100, 1:75, 1:50, 1:20 and 1:10 are shown in Figure 4.44. The fibre diameters and fibres structures in Figure 4.46 are described briefly in Table 4.16.

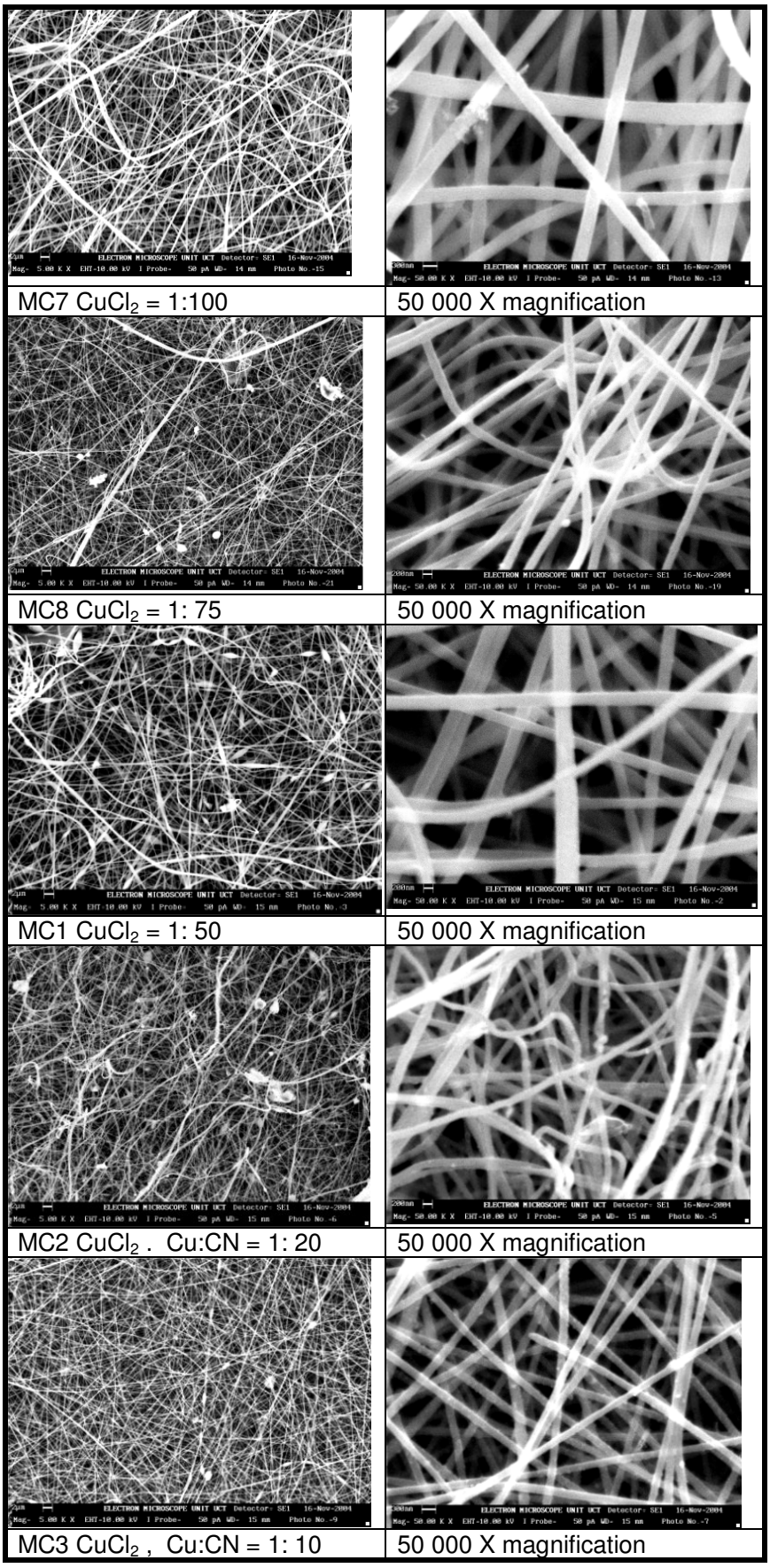

Figure 4.44 SEM micrographs of ES 120k PAN with different $CuCl_2$ concentrations.

Table 4.16 Description of micrographs of ES 120k PAN with $CuCl_2$

Code	Cu:CN	Diameter (nm)	Description
MC7	1:100	300	Even diameter & smooth surface
MC8	1:75	200	Even diameter & slightly roughened surface
MC1	1:50	180	Uneven diameter, curved fibres
MC2	1:20	150	Uneven diameter & rough surface
MC3	1:10	120	Uneven diameter & very rough surface

The fibre diameter decreases with increasing $CuCl_2$ content. This is due to the higher solution conductivity and associated higher electric force at a given voltage, which causes higher instabilities in the jet, additional whipping motion which effectively increase the draw ratio within a given spinning distance.

The effect of copper (I) chloride on the electrospinning of PAN was evaluated and the SEM micrograph and EDAX map of the resultant fibres is shown in Figure 4.45. The solution formed a dark green gel and spinning was only initiated at 30 kV.

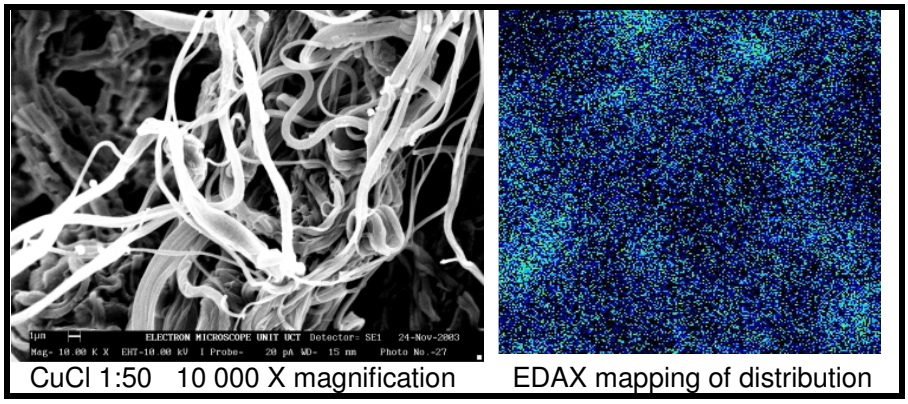

Figure 4.45 SEM micrographs of ES 120k PAN with CuCl.

The fibre diameter range for the electrospun PAN containing CuCl at a Cu:CN ratio of 1:50 is 500 nm to 2 μm. The fibres are ribbon shaped and the diameter is very uneven. The copper was homogeneously dispersed throughout the bulk of the fibres. It has previously been found that copper (1) salts form highly viscous gel with PAN, which was ascribed to the fact that Cu (I) forms co-ordination compounds with six ligands, whereas Cu (II) forms co-ordination compounds with 4 ligands. Thus the chance of intermolecular co-ordination is higher for the copper (I) compounds.

4.6.7 TEM of Electrospun PAN with Copper Salts

High resolution Transmission Electron Microscopy, HRTEM, was conducted at the University of Cape Town, UCT and the University of the Western Cape, UWC, South Africa.

Figure 4.46 shows the TEM micrographs, obtained at UCT, of the homopolymer and the copolymer PAN with Cu:CN = 1:50, (samples SC1 and TE1 respectively). Samples were prepared by Mr Mohammed Jaffer by embedding electrospun fibres in an epoxy resin and slicing 100 nm thick sections using an ultra-microtome, in November 2009.

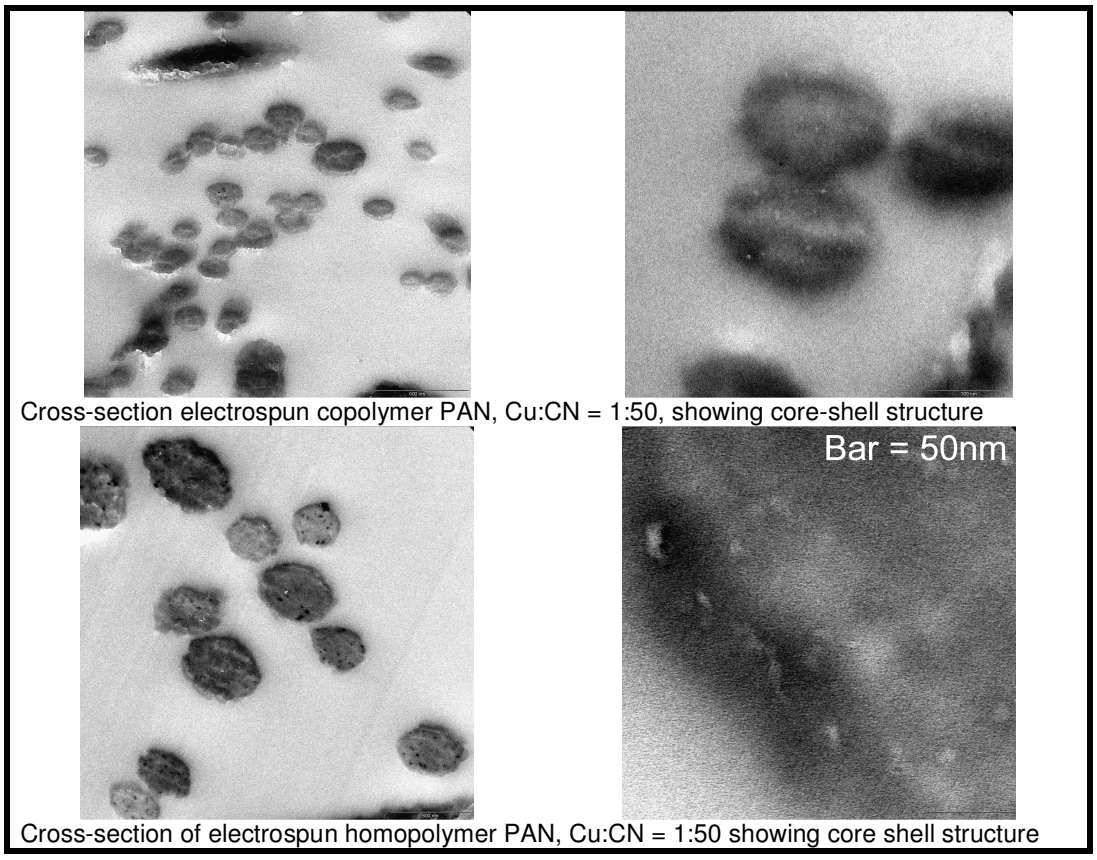

Figure 4.46 TEM of Electrospun Co- and Homo-PAN Fibres.

A core-shell type structure is seen for both the copolymer and the homopolymer where the central region appears to have a lower density and is believed to be due to a solvent enriched core in the electrospun PAN fibres. The TEM displayed fibres are oblong, a result of the slicing process, where round fibres were squashed during sample preparation in a resin matrix, mostly in the direction of cutting, as clearly seen in the upper LHS graphic in Figure 4.46.

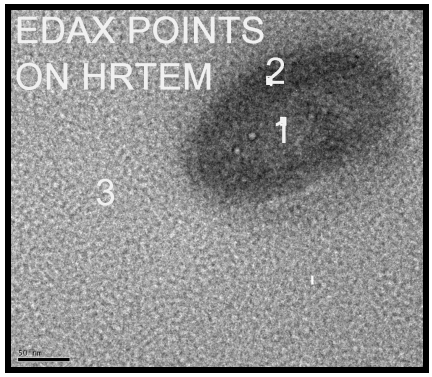

Figure 4.47 EDAX Analysis Points on HRTEM on Co-PAN with $CuCl_2$ (Cu:CN = 1:50).

In an attempt to determine if there is a Cu rich domain, which may be phase-separated, EELS and EDAX analyses were tried. EELS was not possible as the ultra-microtomed sample slices were too thick. EDAX elemental mapping on the HRTEM was not possible as the X-ray beam burnt the sample over a time period required to gather data.

Rapid spot EDAX analyses results recorded at UWC are presented in Figure 4.48 to show the ratio of the carbon, chlorine and copper peaks as measured in the positions shown in Figure 4.47 for the electrospun co-PAN with Cu:CN = 1:50. It was found that the element copper could not be utilized as a firm indicator of the position of the salt in the electrospun fibres as the TEM grid is copper based and this provides a strong copper background X-ray dispersion across the whole TEM sample. However the copper relative to the carbon was slightly (yet consistently) increased in the interior of the electrospun fibre at position 1 (Cu:C = 0.153 versus 0.151). The EDAX analyses show that the chlorine from the $CuCl_2$ salt is distributed homogeneously across the cross-sectioned samples, within the fibres.

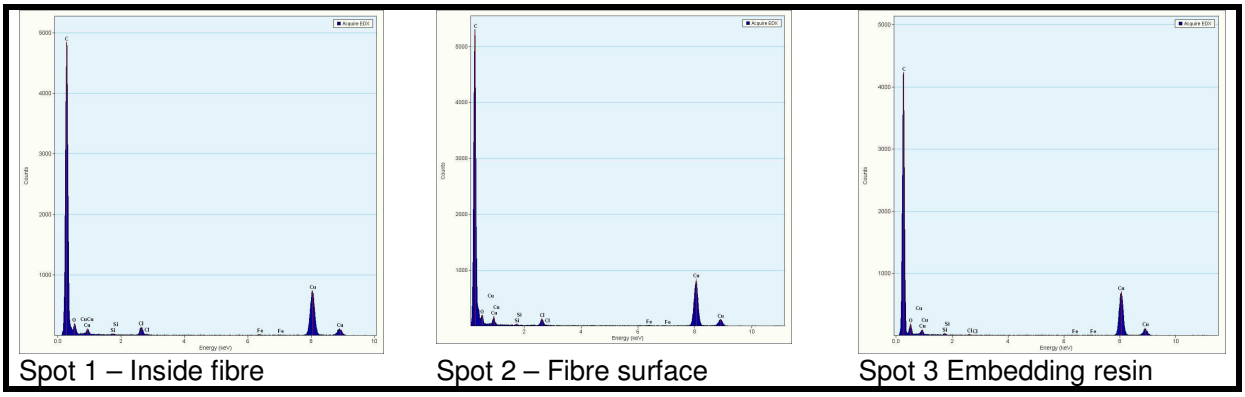

Figure 4.48 EDAX with HRTEM on Co-PAN, with $CuCl_2$ (Cu:CN = 1:50).

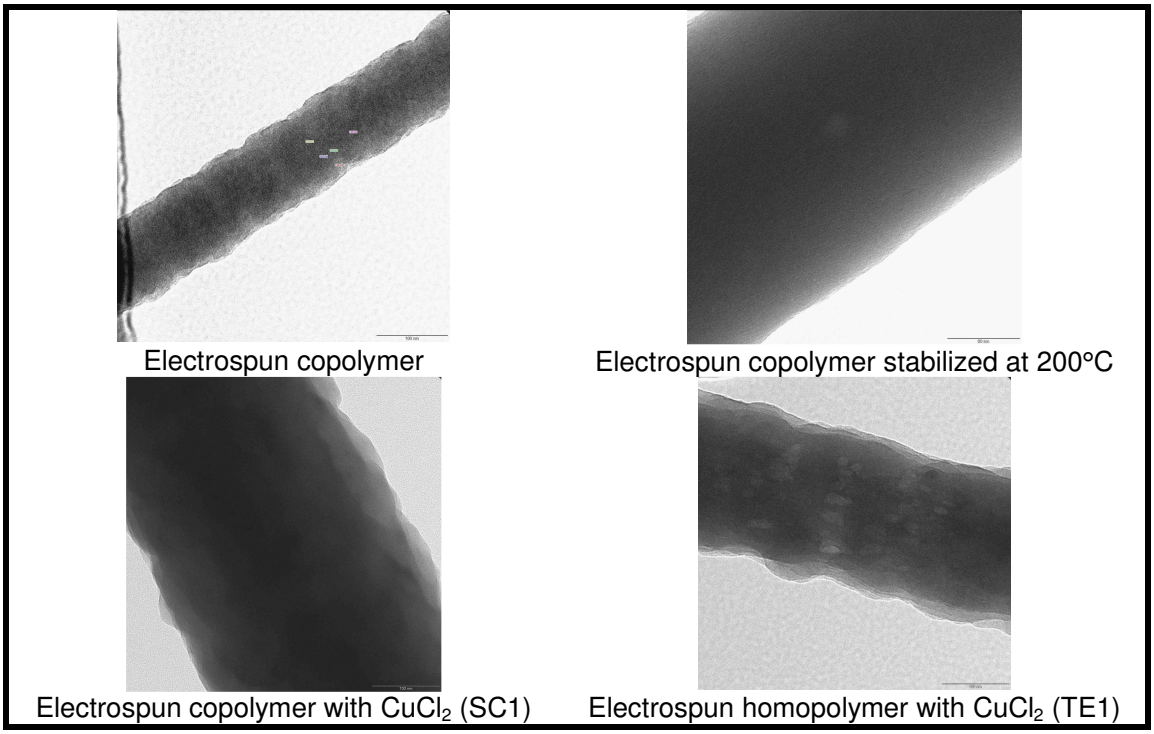

Figure 4.49 HRTEM on Co- and Homo-PAN.

Figure 4.49 at the top LHS shows, the TEM of the co-PAN fibres are shown from a vertical position. This micrograph shows that the structure of the fibre has phase-contrasted dark

portions, indicating the crystallite (higher density) phase domains, distributed within an amorphous phase. The size of these dark domains believed to be the crystallites were measured as 1.6 to 2.4 nm.

The micrograph at the bottom of the LHS in Figure 4.49 shows the onset of a graphitic type structure in the base polymer of the electrospun co-PAN fibre, when $CuCl_2$ is added to the copolymer PAN. The figure at the bottom at the RHS shows that for the electrospun homo-PAN, when $CuCl_2$ is added there is also an onset of a graphitic type structure in the fibre.

4.6.8 Conclusions of the Microscopy Analyses

- The nanofibres could be carbonized and showed a narrower fibre diameter than the diameter of the non-carbonized PAN fibres electrospun under the same conditions.
- Copper nitrate salt in carbonized PAN fibres is calcined / converted to CuO nanoparticles with a diameter of 20 to 50 nm during the PAN carbonization process.
- LVD can be used to apply an even, thin CuO coating (less than 10 nm thick) onto the surface of electrospun PAN fibres.
- The addition of copper (II) chloride salts in increasing concentration gives fibres with decreasing diameter as the salt concentration increases.
- Copper salts give narrower diameter fibres than LiCl containing PAN electrospun fibres when the cation is at the same concentration relative to the nitrile group.
- It is difficult to obtain homogeneous dispersion of CuO nanoparticles in PAN fibres even after the use of sonication and surfactants.
- Copper (I) salts in ES PAN give ribbon like fibres with a relatively high diameter compared with copper (II) salts spun under identical conditions.
- A core-shell type structure is seen for both the electrospun PAN copolymer and the homopolymer, where the central region appears to have a lower density and is believed to be due to a solvent enriched core in the electrospun PAN fibres.
- The copper relative to the carbon was slightly consistently increased in the interior of the electrospun PAN fibre. The chlorine from the $CuCl_2$ salt is distributed homogeneously across the cross-sectioned samples, within the fibres.

4.7 NMR AND ESR SPECTROSCOPY STUDY OF ES PAN WITH SALTS: RESULTS, DISCUSSION AND CONCLUSIONS

4.7.1 Introduction to NMR and ESR

An analytical technique used to a small extent to obtain information on fibers is nuclear magnetic resonance spectroscopy, (NMR). Statton pioneered the use of wide-line NMR, which relates to the mobility of molecular segments within a fiber structure (Hearle 2002).

4.7.2 Equipment used and experimental procedure for NMR and ESR

All the ^{1}H-^{13}C cp-mas NMR and EPR results reported in this document were recorded on equipment at the Max Plank Institute for Polymers in Mainz, Germany with assistance from members of the working group of Prof HW Spies.

The NMR data was collected with assistance of Dr Ingo Schnell and Dr Anke Hoffmann. Dr Gunnar Jescke conducted the ESR and also assisted with the interpretation of the ESR data. The operating conditions for the NMR experiments are given in Table 4.21. The results were obtained using a Bruker 700 MHz NMR Spectrophotometer.

ESR spectra were recorded at ambient temperature on a Bruker Elexsys 680 spectrometer equipped with a 4103 TM rectangular cavity at a frequency of 9.775 GHz. The field range was 320±150 mT and field modulation with amplitude 0.5 mT and frequency of 100 kHz was used.

Spectra were averaged over 32 scans with a time constant of 20.48 ms and a conversion time of 81.92 ms. A microwave power of 2 mW was used without inducing any saturation effects in the signal.

4.7.3 NMR results on ES PAN fibres

The electrospun samples were analyzed by NMR in order to determine the effect of the spinning variables on the molecular orientation within the PAN fibres. Selected results from the numerous ^{1}H-^{13}C cp-mas NMR experiments are presented in Figure 4.46 and Figure 4.47.

4.7.4 Discussion and conclusions of the NMR results on ES PAN fibres

The NMR did not provide any useful data. The spectra of all the samples of each grade of PAN were identical irrespective of the spinning conditions. It was suggested by Dr Ingo Schnell at MPIP, Mainz, that the reason for this, at first unexpected result, was that the structure of the PAN fibre does not allow for molecular motion, resonance, in the amorphous domains of the fibre and thus one could not obtain information on the molecular orientation of PAN fibres.

A thorough literature search was conducted to try obtaining solid state, ^{1}H-^{13}C cp-mas NMR data on PAN fibres by other researchers but no references could be sourced.

It is known that the structure of the PAN fibre has been previously described as having “more” ordered and “less” ordered domains, as opposed to the crystalline and amorphous domains of most other polymeric fibres. The nitrile dipole bonding is believed to hinder possible molecular segmental motions in the PAN fibre making NMR not applicable for the molecular orientation measurement of PAN fibres.

Table 4.17 NMR description of ES 120k PAN with $CuCl_2$

Greyling

exp#	title	NS
1	sample #12; 1H 1D MAS at 30kHz	8
2	sample #12; 1H-13C CPMAS at 30kHz, 1.5ms contact time	512
3	sample #1; 1H 1D MAS at 30kHz	8
4	sample #1; 1H-13C CPMAS at 30kHz, 1.5ms contact time	1024
5	sample #22; 1H 1D MAS at 30kHz	8
6	sample #22: 1H-13C CPMAS at 30kHz; 1.5ms contact time	512
7	sample #23; 1H 1D MAS at 30kHz	8
8	sample #23; 1H-13C CPMAS at 30kHz	512
9	sample #10; 1H 1D MAS at 30kHz	8
10	sample #10; 1H-13C CPMAS at 30kHz	512
11	sample #14; 1H 1D MAS at 30kHz	8
12	sample #14; 1H-13C CPMAS at 30kHz	512
13	sample #15; 1H 1D MAS at 30kHz	8
14	sample #15; 1H-13C CPMAS at 30kHz	512
15	sample #4; 1H 1D MAS at 30kHz	8
16	sample #4; 1H-13C CPMAS at 30kHz (d1=0.5s)	512
17	sample #4; 1H-13C CPMAS at 30kHz (d1=0.1s)	512
18	Sample #4, 1H-13C REREDOR MAS at 30kHz, trcpl=4tR	512
19	sample #8; 1H 1D MAS at 30kHz	8
20	sample #8; 1H-13C CPMAS at 30kHz	512
21	sample #9; 1H 1D MAS at 30kHz	8
22	sample #9; 1H-13C CPMAS at 30kHz	512
23	sample #9; 1H-1H 1D DQF BaBa, texc = tR, MAS at 30kHz	16

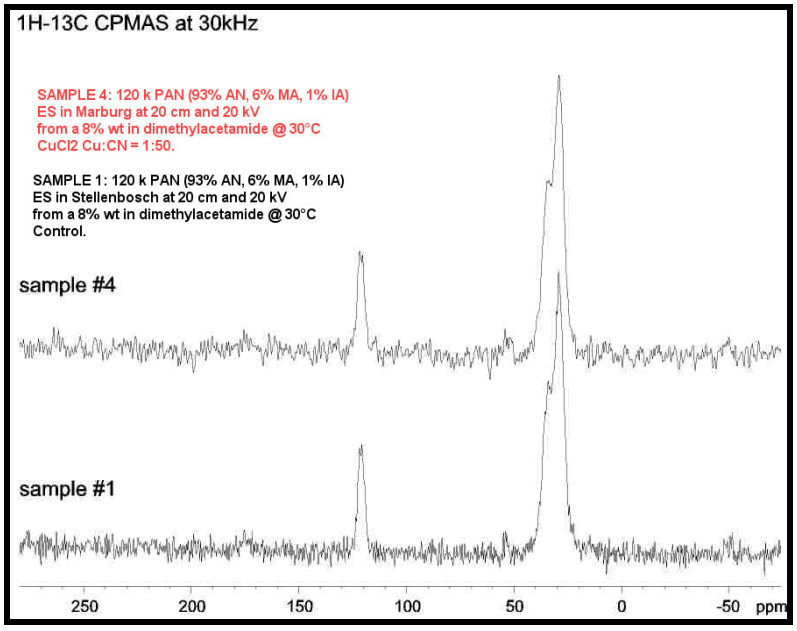

Figure 4.50 ^{1}H-^{13}C CPMAS NMR spectrum of ES 120 k PAN with $CuCl_2$.

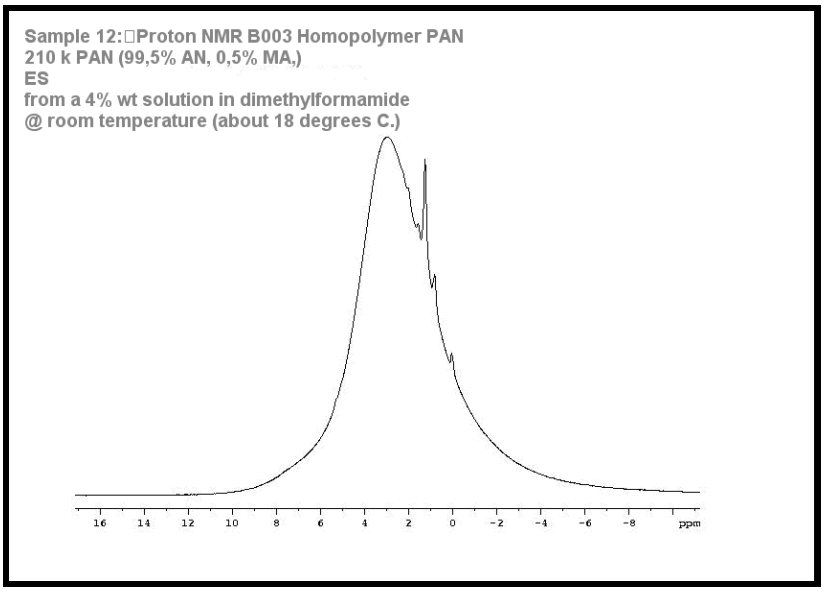

Figure 4.51 **^{1}H NMR spectrum of ES 210k PAN with $CuCl_2$.**

4.7.5 ESR results on ES PAN fibres

ESR data was collected for the PAN electrospun samples containing copper (II) salts. Structure on length scales between 0.3 and 10 nm and dynamics on time scales between approximately 10 µs and 1 µs can be characterized by ESR spectroscopy if a supramolecular system contains native paramagnetic centers such as free radicals or transition metal ions or if stable free radicals can be introduced as spin probes or labels.

Probe concentrations as low as 10 µmol.l^{-1} and sample volumes down to 5 µl are sufficient for recording continuous-wave (CW) EPR spectra at conventional frequencies of 9 - 35 GHz. Such experiments provide details on reorientation dynamics of small molecules or paramagnetic sidegroups that are in turn related to weak interactions between molecules (Jeschke 2002).

The ESR spectra of electrospun 120k PAN samples containing various concentrations of $CuCl_2$ salts are presented in Figure 4.48. The electrospinning procedure is described in Section 3.1 and the preparation of the copper containing samples in Section 4.1.

The ESR spectra of electrospun 120k PAN samples containing Li and Cu at a concentration such that Cu:CN and Li:CN = 1:50 are shown in Figure 4.49. The spectra of samples containing copper sulphate, copper nitrate and copper chloride are compared in Figure 4.50.

A composite view of all the ESR spectra recorded at MPIP is shown in Figure 4.51.

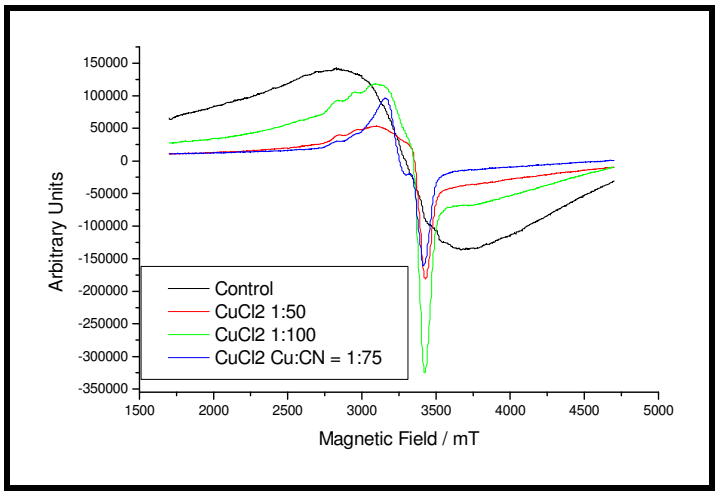

Figure 4.52 ESR spectra of ES 120k PAN with $CuCl_2$.

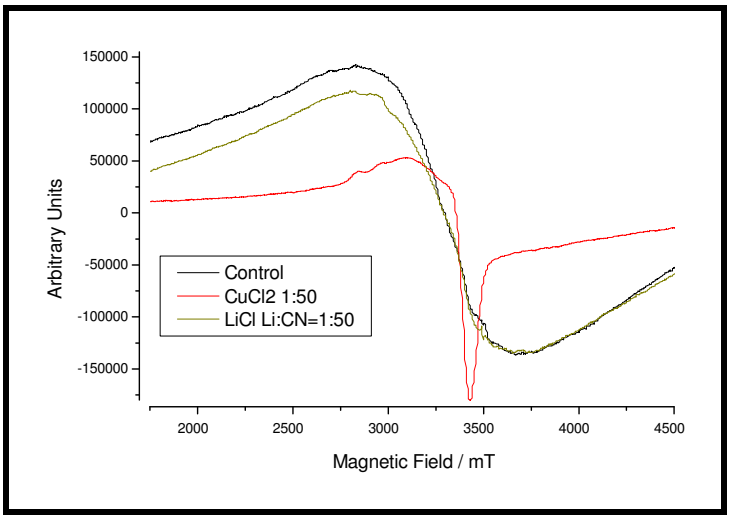

Figure 4.53 ESR spectra of ES 120k PAN with $CuCl_2$ and LiCl.

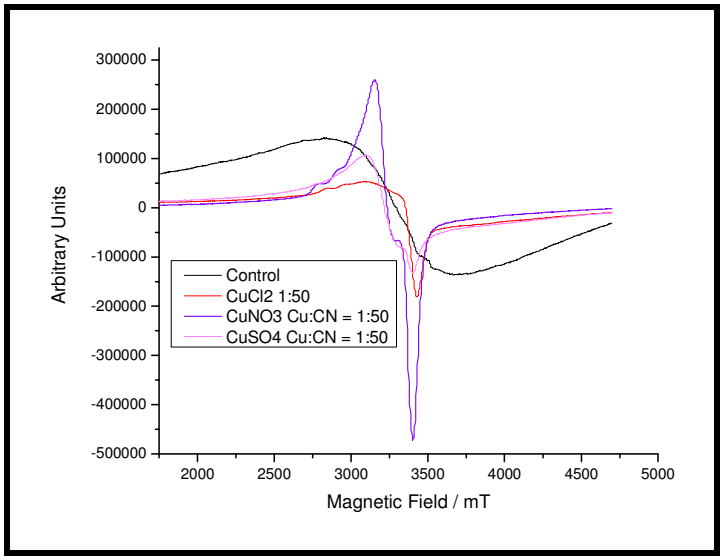

Figure 4.54 ESR spectra of ES 120k PAN with Cu-salts.

4.7.6 Discussion of the ESR results on ES PAN fibres

All of the ESR spectra have the basic structure of copper (typical of Cu^{2+} systems): the sharp "dip" near the centre of the spectrum, and 4 equally spaced peaks at lower magnetic field (hard to see in most of the spectra due to very broad line-widths. This structure is clearest in the $CuCl_2$, Cu:CN = 1:100 sample, and is due to an orientation-dependent g-tensor (which affects the magnetic field(s) at which resonance occurs). One component is the axial peak (due to the quartet and the other is the parallel orientation (the quartet is due to Cu having 3/2 spin).

All PAN samples exhibit a broad unstructured background signal (see control trace in all Figures) that is probably due to a small transition metal contamination introduced during electrospinning, perhaps from the copper wire electrode used in the process. Alternatively it may be due to the remnants of the iron redox catalyst used in the polymerization process.

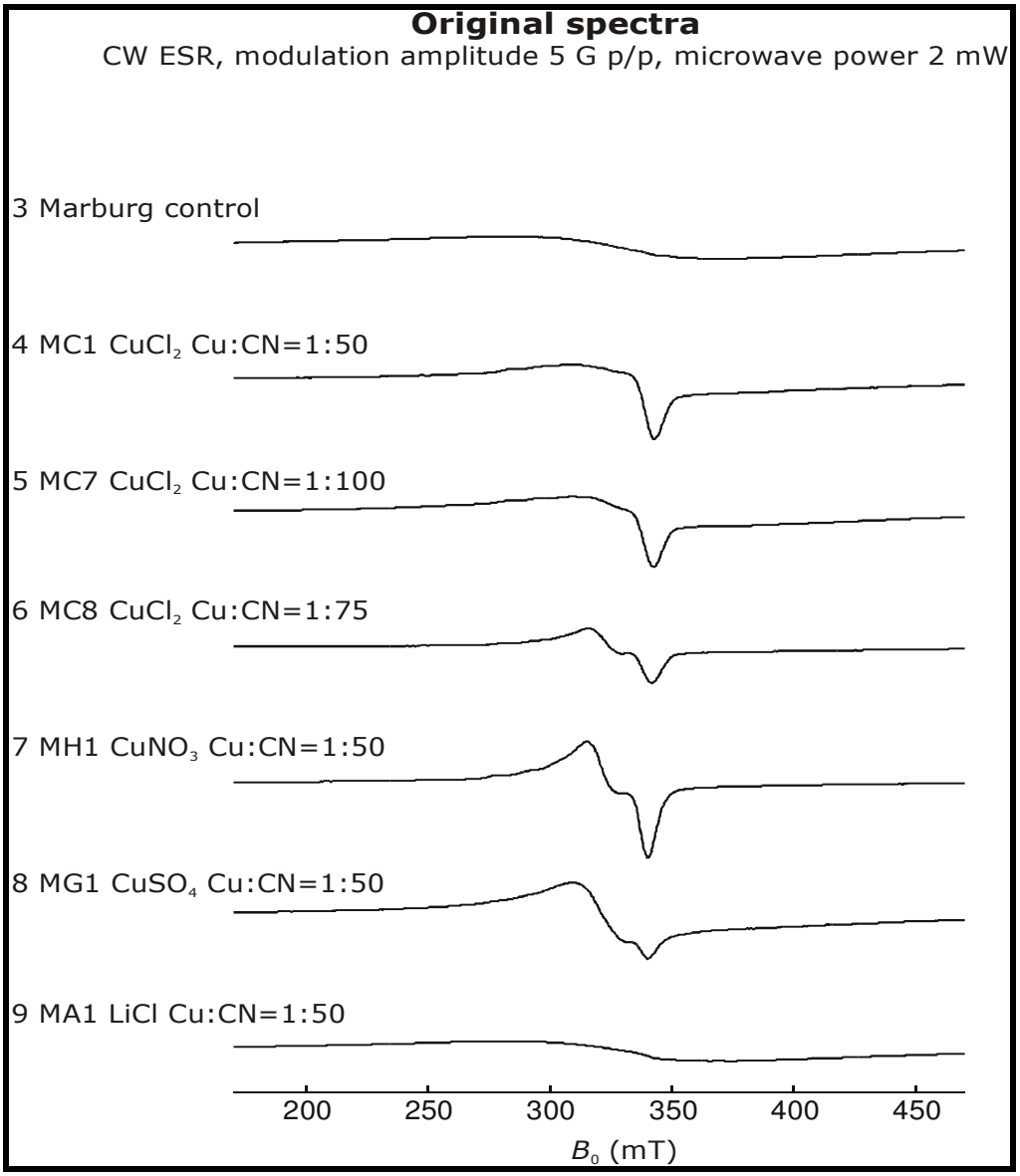

Figure 4.55 Composite of ESR spectra of ES 120 k PAN with Cu-salts.

The unresolved line suggests that these transition metal centers form clusters. In contrast, resolved and more intense spectra are observed in all samples that were prepared with addition of copper salts. These spectra demonstrate that copper is incorporated as Cu^{2+} ($3d^9$ electron configuration) with electron spin 1/2. The spectra observed for addition of $CuCl_2$ are typical for square planar coordination of copper (II) with a nearly axial *g* tensor and a resolved copper hyperfine splitting along g_z. The parameters are $g_x \approx g_y \approx 2.08$, $g_z \approx 2.32$, and $A_z = 11$ mT.

Within the errors that are caused by decreased resolution in such a polymeric sample, the principal g values agree with literature values for $CuCl_4^{2-}$ complexes with axially coordinated cations (Zanchini & Crispini 1990).

Curiously, at the intermediate copper concentration (Cu:CN = 1:75) the spectrum contains an additional component with lower *g* anisotropy and unresolved copper hyperfine coupling. The reason for this is unclear. If non-coordinating counterions such as nitrate or sulfate are used, the Cu(II) spectra are still resolved but do also exhibit features corresponding to lower *g* anisotropy. In the case of nitrate, a contribution with large *g* anisotropy and resolved hyperfine coupling is seen as well. This might be due to coordination by trace amounts of water.

The strong dependence of the line shape on the original counter-ion of the Cu^{2+} ion suggests that co-ordination by the nitrile groups of the polymer plays a minor role. This agrees with the observation that solvents like acetonitrile are rarely found to coordinate to one of the equatorial positions. However, such coordination cannot completely be ruled out. It is hard to prove either, as published examples invariably involve some other, stronger ligands in addition to nitriles, so that no parameters sets can be found that allow for reliable comparison. In the PAN samples, nitrile groups may be more likely to coordinate in the weakly interacting apical than in the strongly interacting equatorial positions of the coordination polyhedron, since under the given synthesis and sample preparation conditions stronger ligands such as water or alcohols are available (Pannier 2000).

For some of the samples (such as $CuSO_4$), it looks like there might be a further magnetic interaction (but could also be due to the superposition of 2 different spectra). Line-widths might also tell one something, and are most likely related to relative spin relaxation rates in the samples (although, again, other explanations are also possible), which are related to things like spin-spin interactions (a big factor in inorganic systems) and dynamics such as rotational mobility.

4.7.5 Conclusions from NMR and ESR analyses

- Solid state NMR cannot be applied to PAN fibres to assess the molecular orientation. The structure is too dense to allow magnetic resonance in even the less ordered “amorphous domains”.

- All of the ESR spectra on PAN containing copper salts have the basic structure of copper (typical of Cu^{2+} systems): the sharp "dip" near the centre of the spectrum, and 4 equally spaced peaks at lower magnetic field. This structure is clearest in the $CuCl_2$, Cu:CN = 1:100 sample, and is due to an orientation-dependent g-tensor (which affects the magnetic field(s) at which resonance occurs). One component is the axial peak (due to the quartet and the other is the parallel orientation (the quartet is due to Cu having 3/2 spin).
- All PAN samples exhibit a broad unstructured background signal that is probably due to a small transition metal contamination introduced during electrospinning, perhaps from the copper wire electrode used in the process. Alternatively it may be due to the remnants of the iron redox catalyst used in the polymerization process.
- The unresolved line suggests that these transition metal centers form clusters. In contrast, resolved and more intense spectra are observed in all samples that were prepared with addition of copper salts. These spectra demonstrate that copper is incorporated as Cu^{2+} ($3d^9$ electron configurations) with electron spin 1/2. The spectra observed for addition of $CuCl_2$ are typical for square planar coordination of copper(II) with a nearly axial *g* tensor and a resolved copper hyperfine splitting along *g*.
- The role of the anion (as a “spectator ion” in affecting the bonding of the copper salt in electrospun PAN with copper salts is highlighted in the ESR results.

4.8 XRD ANALYSIS OF ES PAN;

RESULTS AND DISCUSSION AND CONCLUSIONS

4.8.1 Introduction to XRD

One of the most useful techniques for studying polymeric fiber crystallinity and fibre molecular orientation is wide-angle X-ray diffraction, (WAXD or XRD). The related theory is discussed in depth in Section 2.3.5. In the case of PAN fibres, the width of only the primary equatorial peak around $2\Theta \approx 17°$ is regarded as a direct inverse correlation with the molecular orientation in the spun PAN fibre structure.

.4.8.2 XRD equipment and experimental procedure

This XRD data reported in this thesis was collected by Dr Remy Bucher at the NRF iThemba Material Laboratories in Faure, South Africa. The instrument is a BRUKER AXS (Germany) with a D8 Advance Diffractometer, and measurements are made with a locked Θ-Θ scan coupled mode. The X-ray tube uses Cu-K_α radiation (λ =1.5406Å) and a gas positron sensitive detector, PSD Vantec-1, with 1600 channels. Measurements were made at a 40kV tube voltage, 40mA tube current with variable slits at 0.28. The time was varied to obtain reasonable statistics.

4.8.3 XRD data processing and repeatability

The graphic below illustrates the data manipulation procedures.

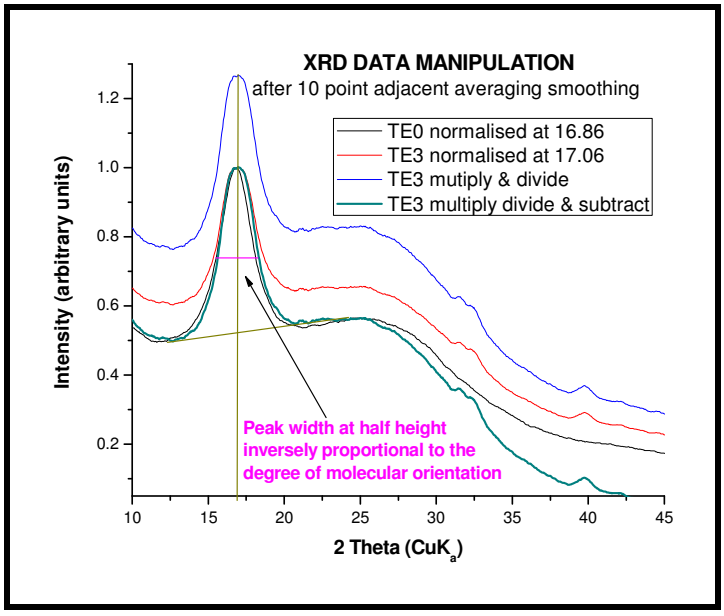

Figure 4.56 XRD data manipulation.

All the diffractograms were processed using Origin® software. Raw data was smoothed using a 10 point adjacent averaging and normalized on the 2Θ peak ≈ 17°. The height of the 2Θ peak for the samples with additives was then normalized with regards to the height of the 2Θ theta peak for

the electrospun control sample. The purpose of this procedure was to obtain data where the molecular orientation and coherence length, which in the case of PAN fibres is inversely related to the width at the half height could be easily visually evaluated.

The repeatability was evaluated on numerous wet spun and electrospun samples and the data is available on the attached DVD. The diffractograms were found to be repeatable as shown in Figure 4.57 for the electrospun homopolymer control sample which was mounted at different angles relative to the angle of the X-ray beam.

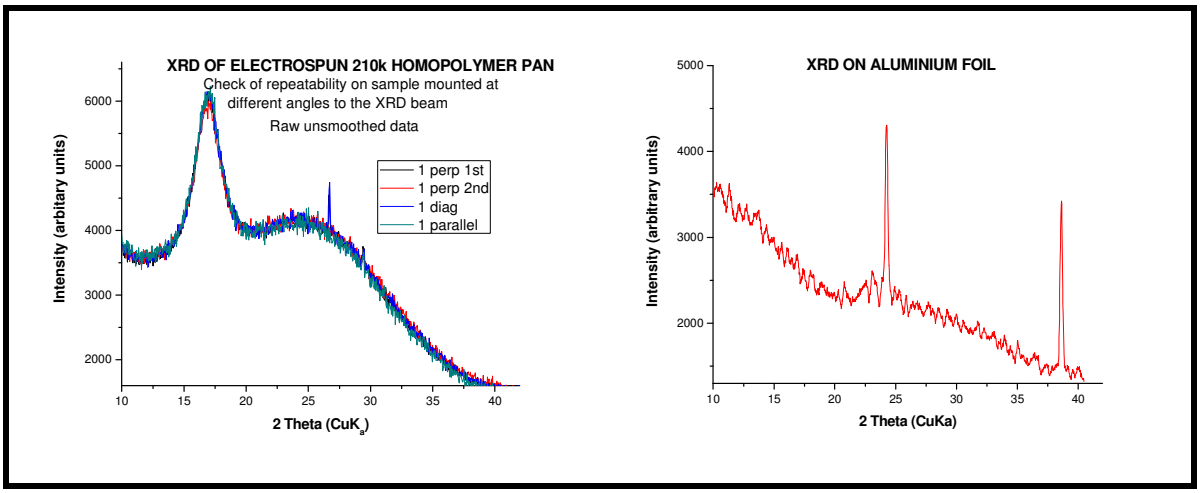

Figure 4.57 XRD data repeatability on electrospun homopolymer control and Al-foil.

The effect of fibre orientation on the repeatability of XRD was also evaluated with parallel fibres in a copolymer PAN crimped tow and it was found that irrespective of the angle at which samples were mounted relative to the X-ray beam direction, they gave comparable results.

Some data contains sharp spikes at different regions on the amorphous halo region of the diffractograms as seen at around 2Θ equals 26° in Figure 4.57. These peaks are not due to the backing aluminium foil which has a sharp peak at 2Θ equals 25°. Such peaks disappeared if the sample was rotated. These random sharp peaks are ignored in the following XRD discussion.

A difference in sample thickness of about 200 µm is known to affect the position of the equatorial peak by a shift of about 0.1° change in 2Θ. Peak shift values larger than 0.1° are viewed as significant and are attributed to the microstructure of the sample.

As a result of the type of data manipulation performed on all the diffractograms, in the cases where the intensity of the diffraction of the peak at 2Θ around 17° was weak, then data in the amorphous halo region sometimes becomes distorted such as seen for sample SC8 below.

4.8.4 XRD Results

Figures 4.58 to 4.66 show the effect of various sample preparation methods; electrospun and commercially wet spun, 210k homopolymer and 120k copolymer PAN with additives on the XRD diffractograms. All the electrospun samples were prepared from DMAc solvent and electrospun

into fibres at 20cm and 20 kV. Commercial wet spun fibres homopolymer and copolymer yarns and fabric were obtained at Lenzing Plastics, Germany and from BlueStar Fibres in Grimsby, UK.

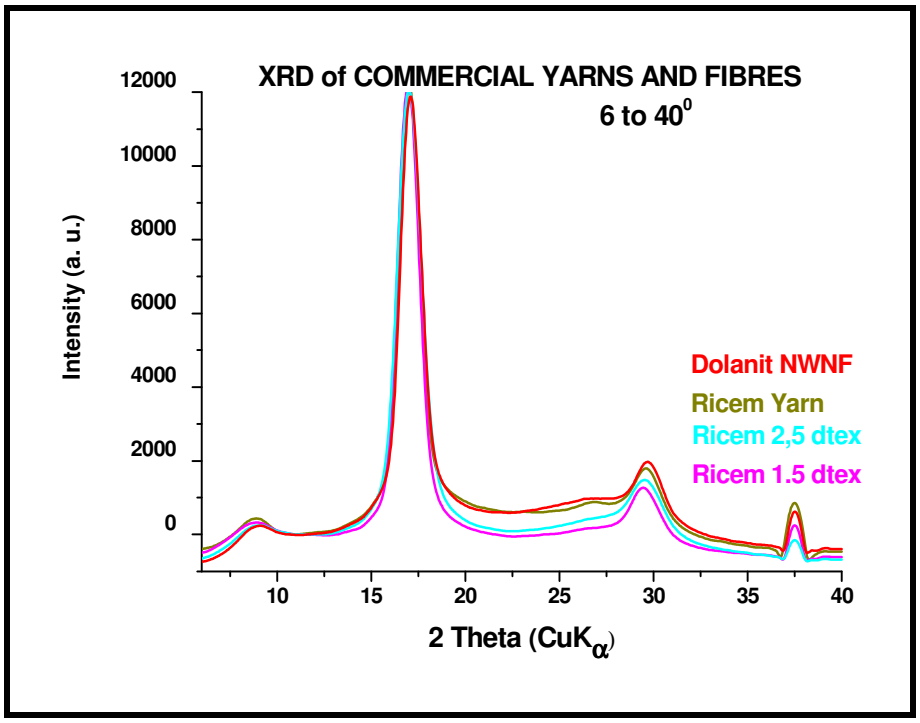

Figure 4.58 XRD of wet spun homopolymer PAN NWNF fabric, yarns and fibres.

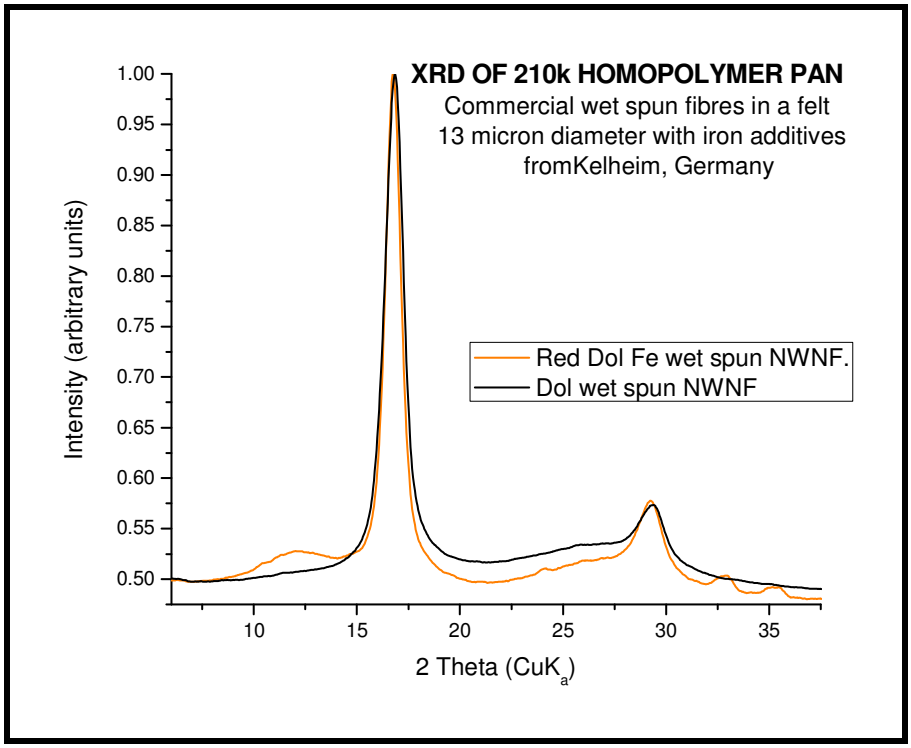

Figure 4.59 XRD of wet spun PAN fabric with iron oxide nanoparticles.

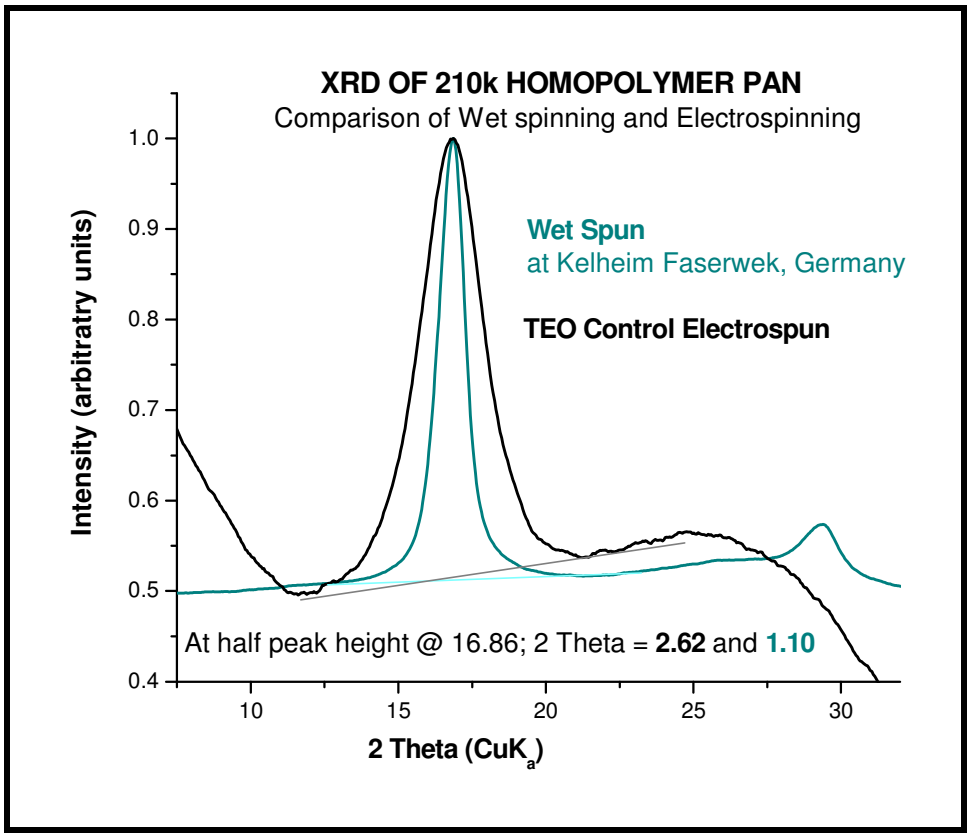

Figure 4.60 XRD of wet spun and electrospun homopolymer PAN.

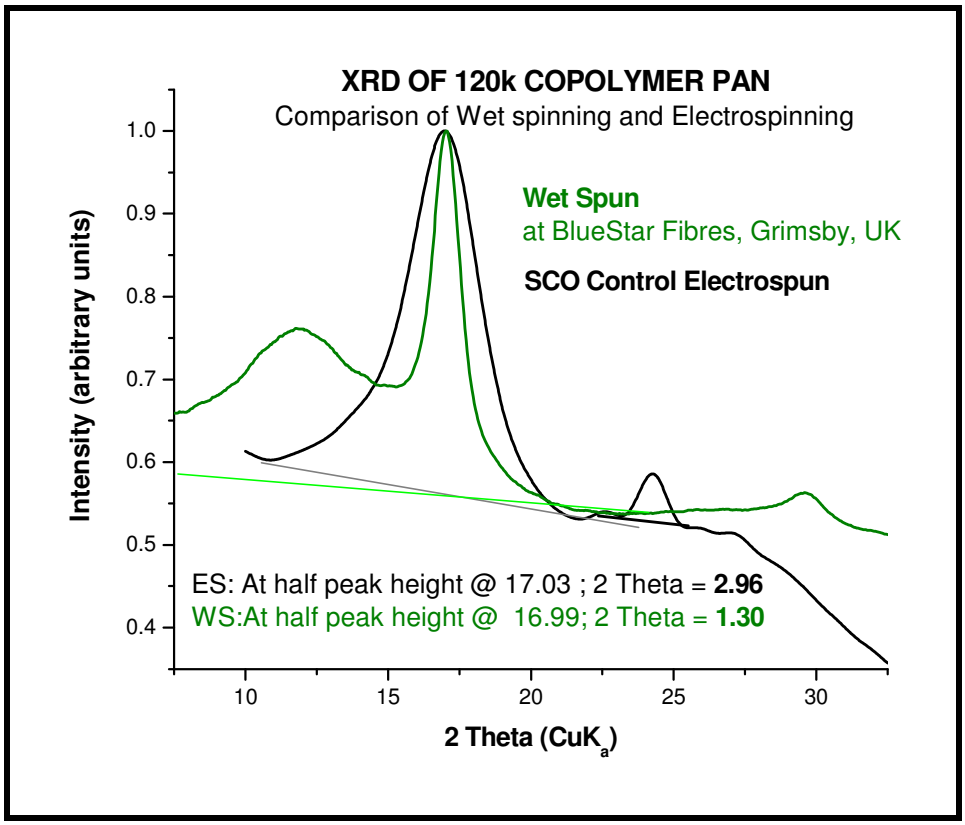

Figure 4.61 XRD of wet spun and electrospun copolymer PAN.

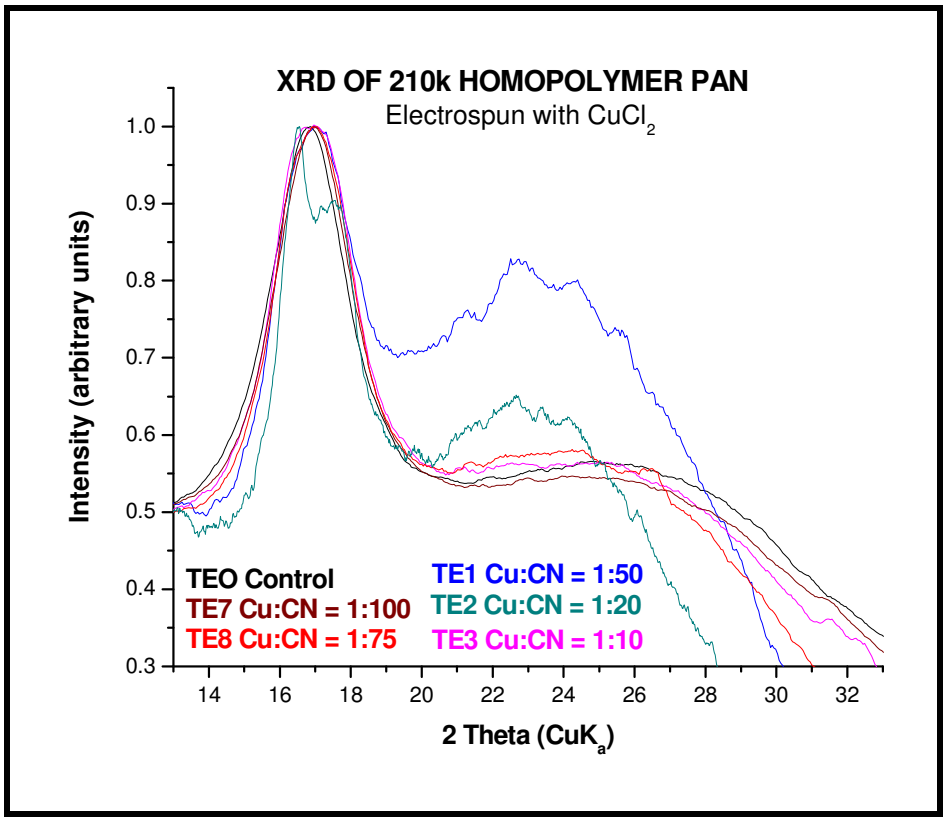

Figure 4.62 XRD of electrospun homopolymer PAN with $CuCl_2$ (13 to 33°).

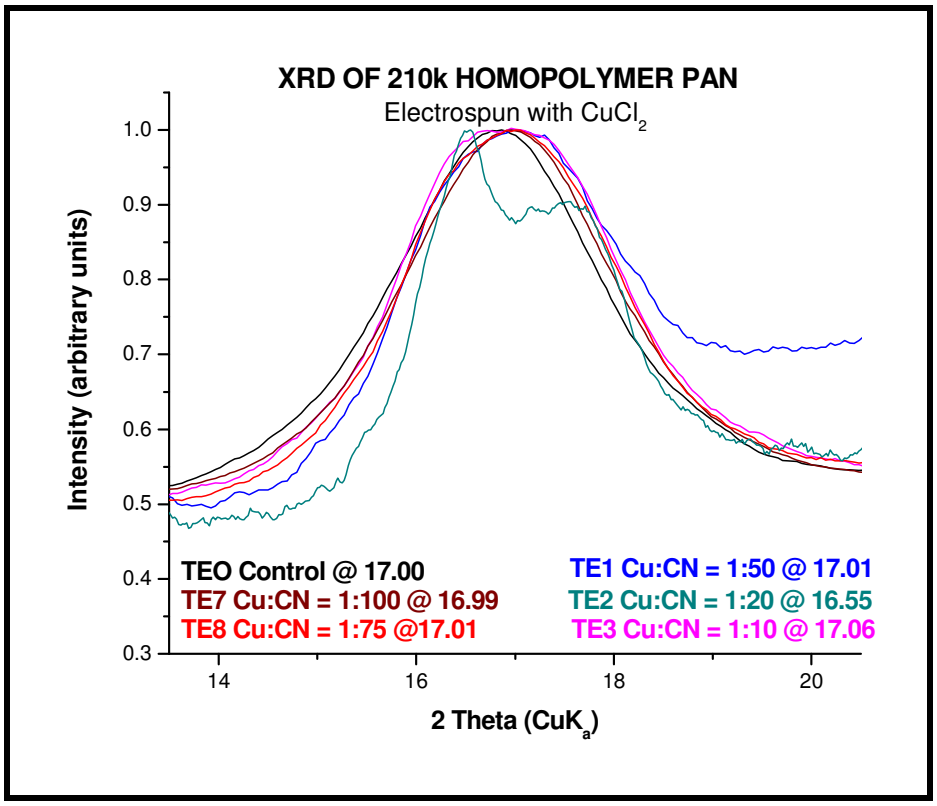

Figure 4.63 XRD of electrospun homopolymer PAN with $CuCl_2$ (13 to 20.5°).

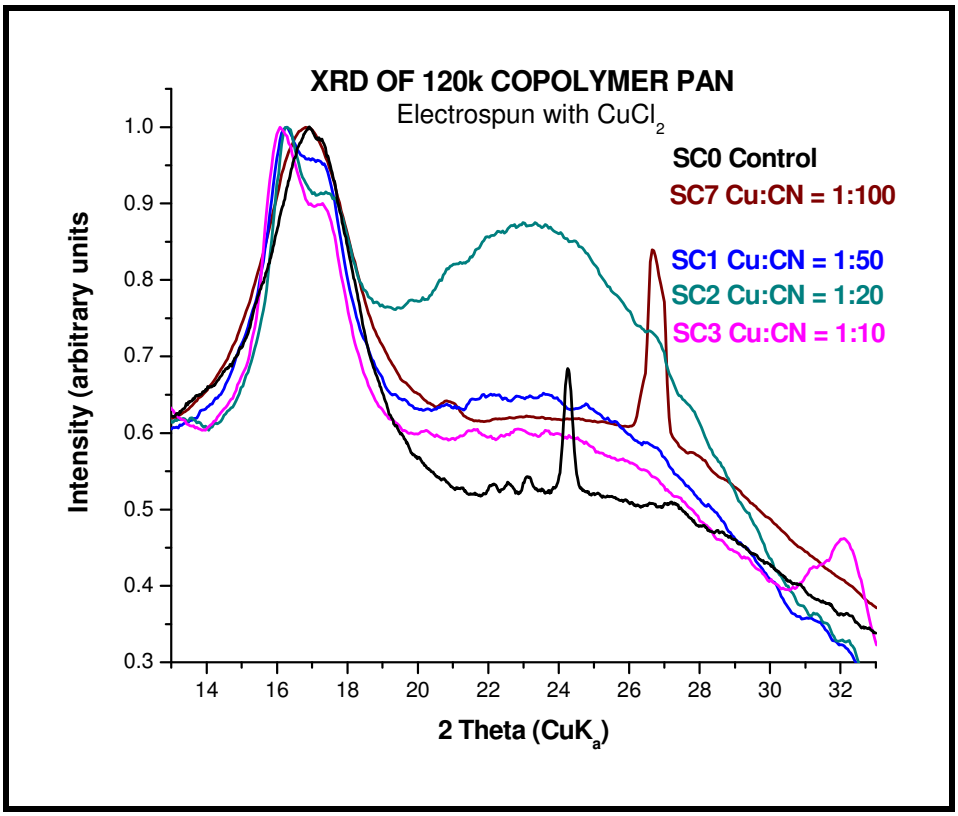

Figure 4.64 XRD of electrospun copolymer PAN with $CuCl_2$ (13 to 33°).

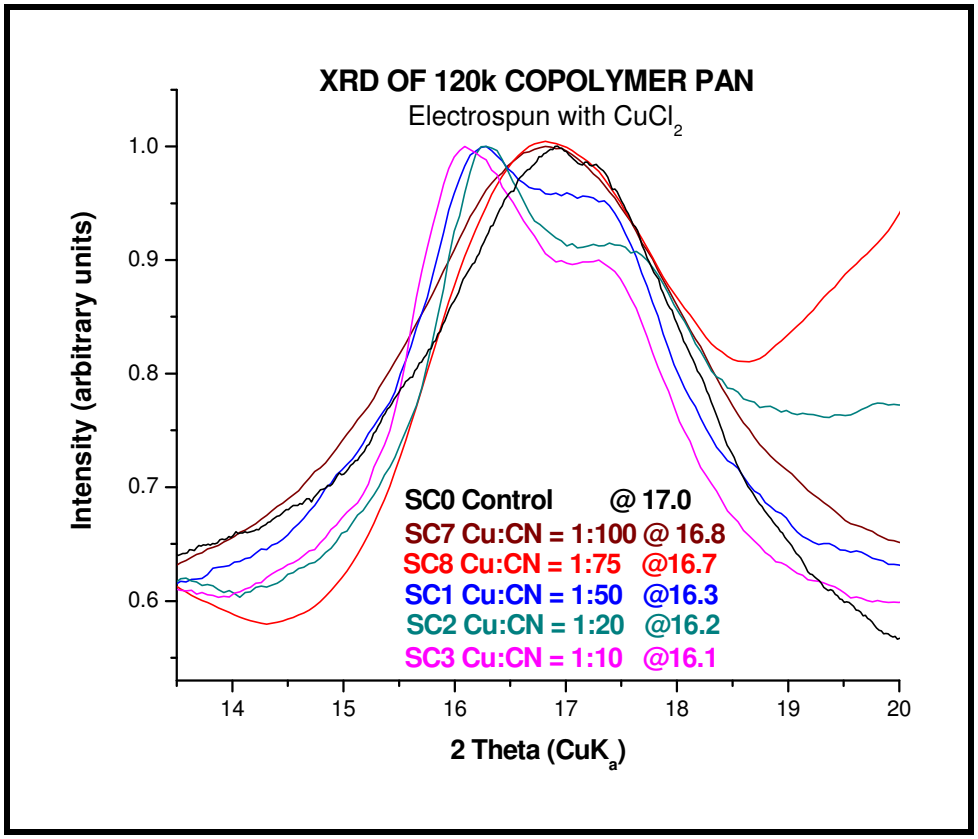

Figure 4.65 XRD of electrospun copolymer PAN with $CuCl_2$ (13 to 20°).

4.8.5 Discussion of XRD results

4.8.5.1 Introduction to the XRD discussion

The discussion on the results presented in Figures 4.59 to 4.66 is based mainly on the visibly significant reflection peaks in these graphics with some calculations of the d-spacing and the the coherence length as discussed in the subsections below. The most significant diffraction peaks in polyacrylonitrile are the two equatorial peaks at $2\theta = 17°$ and $2\theta = 29{,}5°$ and the meridonal peaks at $2\theta > 31°$. In quazi-crystalline PAN, peaks narrow and increase in intensity as a result of larger crystallite size and smaller lattice distortions. However, first a quick look at the effect of the experimental methodology on the results.

Figures 4.59 and 4.60 show the XRD diffractograms of commercial wet spun homopolymer PAN. In Figures 4.61 and 4.62 the primary equatorial peak of wet spun and electrospun homopolymer and copolymer fibres are compared. The effect of $CuCl_2$ salt addition in electrospun homopolymer and copolymer PAN fibres are compared in the XRD data in Figures 4.63 to 4.66.

With the data from measurements under the given experimental conditions, the calculated d-spacing (size and shape of the unit cell) and coherence lengths (crystallite stacking size) are difficult to determine accurately since the values would be based on subjective assumptions as to the actual peak shape. Reliable deconvolution of the data of the complex overlapping peaks using Origin® software was not successful. Yet, it will be shown that valuable data exists in these results which provide extra support for some of the less expected results presented in the preceding sub-sections of this chapter i.e. for FTIR, DSC and TGA.

4.8.5.2 Description of peaks, the *d*-spacing, conformation and relation to orientation

In PAN there are normally two equatorial peaks, of which the primary peak at $2\theta = 17°$ has a *d*-spacing of approximately 5.25 Å, and is a composite of orthorhombic (200) and hexagonal (110) reflections as shown in Figure 2.27 and the much weaker reflection at $2\theta = 29{,}5°$ which has a *d*-spacing of approximately 3.05 Å. The *d*-spacing is related to the lamella thickness of the crystallites and the inter-molecular distance of the PAN chains, and is affected by factors such as draw ratio, solvent residues, as well as temperature. These XRD results are in general accordance with these expected peak positions. Although, there are variations in the lattice parameter as a function of co-monomer ratio, the amount and type of salt added and fibre spinning conditions, the ratio of the *d*-spacing of the two peaks remains about $\sqrt{3} : 1$ within an experimental accuracy, indicating pseudo-hexagonal packing. It has been suggested by Rizzo et al. (1996) that *iso*-PAN takes a 3_1 helical chain conformation whereas *syn*-PAN prefers a planar zigzag conformation and that atactic PAN would be a combination, as shown by computer simulations. The diameter of the chain is: $(2 \times \sqrt{3})d_{(110)} = 6{,}1$ Å. With just two peaks, a definitive crystal-structure determination is not possible.

The primary equatorial peak(s) at 2θ ≈ 17° has been studied (Yamane et al. 1997) in UHMW-PAN at high draw ratios and found to actually be a composite peak as shown in Figure 2.27. This peak has been identified as an overlap of the (200) reflection at 2θ = 16.7° and the (110) reflection at 2θ = 17.1°. The separation of the double peaks becomes clearer with increasing draw ratio indicating the development of crystalline order. In a gel state film, the 2 peaks are about equivalent intensity but at intermediate draw ratios the (200) reflection has higher intensity and at an ultrahigh draw ratio for PAN the (110) reflection is more prominent.

4.8.5.4 Comparison of wet spun and electrospun homopolymer and copolymer PAN

The 2θ angle of the primary peak is seen to vary from 16,1° for the 120k copolymer PAN in Figure 4.66 to 17,1° for the electrospun 210k homopolymer PAN fibres shown in Figure 4.64.

From the Bragg equation presented in Section 2.3.5 one can deduce that higher values of 2θ result when the d-spacing is smaller and the crystal lattice is tighter. The improved packing in the homopolymer 500k Ricem™ (0,2 wt% VA) relative to the 210k Dolanit™ homopolymer (0,5 wt % MA) is again reflected in Figure 4.59 for the commercial wet spun fibres.

Most workers (Bohn et al. 1961, Siesler 1975) cite the arc width of the peak at 2θ ≈ 17° as a measure of molecular orientation in PAN. Broadening of diffraction peaks due to small crystallite size becomes a dominant effect and the breadth of the diffraction lines can be used to measure the crystalline packing perfection, using the Scherrer equation as discussed in Section 2.3.5.1.

The Scherrer constant, K used is 0,90 and the wavelength, λ, of the X-rays is 0,154 nm.

Table 4.18 Crystallite size in wet spun and electrospun homo- and co-PAN

	Spin type	**2 Θ position (°)**	**Width at ½ height** (2Θ in °)	**Width at ½ height** (Θ in °)	**Width at ½ height** (Θ in Radians)	**Cos Θ**	**Crystal size, L_c** nm
Homo-PAN	Wet	16.86	1.10	0.55	0.00968	0.95701	14.96
	Electro	16.86	2.62	1.31	0.02287	0.95701	6.26
Co-PAN	Wet	16.99	1.30	0.65	0.01135	0.95635	12.63
	Electro	17.03	2.96	1.48	0.02584	0.95615	5.55

This data is in agreement with similar data reported in literature by Zussman et al. (2005) where a coherence length, (L_c) of 5,314 nm was identified in an electrospun PAN nanofibre and 14,5 nm in a highly oriented PAN fiber containing 15% comonomer.

4.8.5.5 Comparison of electrospun homopolymer and copolymer PAN with $CuCl_2$

In Figure 4.64, where the XRD primary equatorial reflections of electrospun homopolymer 210k PAN with $CuCl_2$ are presented, the degree of orientation can be ranked as highest in the electrospun sample with **Cu:CN = 1:20** than in the electrospun control or at either lower Cu:CN (i.e Cu:CN = **1:50**, **1:75** and 1:100) or at higher Cu:CN (i.e. Cu:CN = **1:10**) based on the narrower peak profile. These results suggest that the crystallinity of the control electrospun 210k PAN homopolymer with a very broad peak at 2θ around 17° is low and the crystallites are randomly

oriented within the fibres of the spun mat. With increasing salt concentration, the (200), and (110), reflections became gradually sharper, Such changes indicate that the chains became progressively more oriented and crystallized along the draw direction.

In the case of the copolymer, as shown in Figure 4.66, where the XRD primary equatorial reflections of electrospun copolymer 120k PAN with $CuCl_2$ are presented, the degree of orientation can be ranked as (from highest to lowest) **Control @ 17°** > **Cu:CN = 1:100 @ 16.8°** > **Cu:CN = 1:75 @ 16.7°** > **Cu:CN = 1:50 @ 16.3°** > **Cu:CN = 1:20 @ 16.2°** > **Cu:CN 1:10 @ 16.1°** based on the narrower peak profile. The shift in the highest intensity of the peak is due to a shift from hexagonal packing to orthorhombic packing.

These results are summarized in Table 4.19, based on the position of the apex of the primary equatorial peak, the coherence length, the type of crystalline packing, the presence of a graphitic structure on the amorphous halo and off-equatorial, meridonal scattering indicative change from helical to a planar zig-zag conformation.

Table 4.19 XRD peak position and packing type

	Homopolymer PAN				Copolymer PAN			
Cu:CN	**Position**	**Lc**	**Type**	**Graphitic**	**Position**	**Lc**	**Type**	**Graphitic**
Wet	17.0	14.96	Hexag	No	17.0	12.63	Hexag	No
Control ES	17.0	6.26	Mixed	No	17.0	5.55	Mixed	No
1:100	17.0	ND	Mixed	No	16.8	ND	Mixed	No
1:75	17.0	ND	Mixed	No	16.7	5.43	Mixed	Yes
1:50	17.0	ND	Mixed	Yes - hi	16.3	ND	Ortho	Yes - hi
1:20	16.5	16.38	Ortho	Yes	16.2	ND	Ortho	Yes
1:10	17.1	ND	Mixed + meridonal	No	16.1	12.77	Ortho + meridonal	Yes

Notes: ND = not determined due to broad overlapping peak
hi = the highest indicator of a graphitic structure
Hexag – 2D hexagonal packing
Ortho – 3D orthorhombic packing
Mixed – mixed hexagonal and orthorhombic packing
Meridonal – planar zig-zag conformation down the length of the fibre

Coherence length calculations for the copolymer samples with Cu:CN = 1:75 and 1:10 and the homopolymer with Cu:CN = 1:20 are available in Appendix B. It is shown that copper at low concentrations decreases the coherence length, whilst at high concentration, a crystallite stacking size and molecular orientation comparable to wet spun fibres can be obtained, but the position of the primary peak shifts as the composite peak separates from the position of 2Θ characteristic for hexagonal packing (110) to a low angle characteristic of orthorhombic packing (200).

None of the electrospun samples show the secondary equatorial peak at 2Θ = 29.5°, (002 lattice plane), which is visible for both homopolymer and copolymer wet spun fibres as seen Figures 4.60 to 4.62.

The presence of 2 equatorial peaks in the XRD diffractograms of electrospun PAN was been reported by Zussman et al. (2005) however there were many differences in the spinning conditions (they spun onto a rotating manifold, with a syringe pump with an unknown grade of

PAN) to be able to draw conclusions from a direct comparison between this work and that of Zussman and co-workers. It is assumed most likely the post drawing on the rotating manifold is what accounts for their reporting of a secondary equatorial XRD peak at 2θ = 29,5°.

A discussion of a comparison of the findings from the XRD and correlation with the results collected using other analytical techniques is presented in Chapter 6, Conclusions.

4.8.6 Conclusions from the XRD analyses

- There is a significant difference between the XRD diffractograms for the commercial wet spun fibres and the electrospun fibres when using exactly the same grade of PAN. The electrospun fibres have a far lower crystallinity and show the presence of 3D crystallinity. The commercial wet spun fibres only have 2D crystallinity but the electrospun have 3D crystalinity.
- There is a sharp contrast in the shape of the XRD traces for copolymer and homopolymer PAN and the conditions under which transitions occur when copper salt is added. The electrospun homopolymer PAN fibres have higher orientation and larger crystallite sizes than the electrospun copolymer fibres. For the homopolymer, the values for the coherence length vary from 14.96 nm to 6.26 nm for the wet spun and electrospun fibres respectively. For the copolymer, the values for the coherence length vary from 12.63 nm to 5.55 nm for the wet spun and electrospun fibres respectively.
- The wet spun PAN fibres show characteristic 2D hexagonal packing as determined using the ratio of the equatorial peaks at 2θ = 17° which has a *d*-spacing of approximately 5.25 Å, and the much weaker reflection at 2θ = 29,5° which has a *d*-spacing of about 3.05 Å. The *d*-spacing is related to the inter-molecular distance of the PAN chains, and is affected by factors such as draw ratio, solvent residues, as well as temperature. The ratio of the *d*-spacing of the two peaks remains about $\sqrt{3}$: 1 within an experimental accuracy, indicating pseudo-hexagonal packing. The diameter of the chain is: $(2 \times \sqrt{3})d_{(110)}$ = 6,1 Å.
- The addition of salts to PAN fibres causes the 2θ value to decrease, indicating an increase in the d-spacing due to an increase in the inter-molecular distance between the chains assumed due to the packing of Cu ions in a columnar structure between the chains.
- The addition of salts to PAN fibres causes the primary equatorial peak(s) at 2θ ≈ 17° to split into 2 reflections at about 2θ = 16,7° and = 17.1°. The separation of the double peaks has been seen as a correlation with increasing draw ratio in wet spun PAN. The salts are thus acting as a plasticizer and effectively causing an increase in the draw ratio of the electrospinning process.

- None of the electrospun samples show the secondary equatorial peak at $2\Theta = 29.5^{o}$, (002 lattice plane), which is visible for both homopolymer and copolymer wet spun fibres.
- The XRD data provides support for some of the less expected results presented in the preceding sub-sections of this chapter i.e. for FTIR, DSC and TGA and comparisons are discussed in Chapter 6: Conclusions.

4.9 REFERENCES

Bahrami, S., Bajaj, P. & Sen, K., 2003. Thermal behavior of acrylonitrile carboxylic acid copolymers. *Jounal of Applied Polymer Science.* 88, p.685-98.

Bajaj, P., Paliwal, D. & Gupta, A., 1998. Influence of metal ions on structure and properties of acrylic fibers. *Jounal of Applied Polymer Science*. 67, p.1647-659.

Bartkowiak, A., Jezierska, J. & Spychaj, T., 1998. An EPR study of polysaccharide copper(II) complexes in composite dextran/epichlorohydrin gels. *Polymer Bulletin*. 41 (2), p.199-206.

Bashir, Z. The hexagonal mesophase in atactic polyacrylonitrile. A new interpretation of the phase transitions in the polymer. *Journal of Macromolecular Science, Part B: Physics*, 1525-609X, Volume 40, Issue 1, 2001, p. 41 – 67

Causin, V., 2005. A quantitative differentiation method for acrylic fibers by infrared spectroscopy. *Forensic Science International*. 151, p.125-31.

Dalton, S., 1999. Thermal stabilization of PAN fibres. *Polymer*, 40, p.5531-543.

Deng, S., Bai, R. & Chen, J., 2003. Behaviors and mechanisms of copper adsorption on hydrolyzed polyacrylonitrile fibers. *Journal of Colloid & Interface Science*. 260, p.265-72.

Deng, S. & Bai, R;, 2004. Removal of trivalent and hexavalent chromium with aminated polyacrylonitrile fibers: performance and mechanisms. *Water Research*. 38 (9), p. 2424-432

Drew, C., Liu, X. & Ziegler, D., 2003. Metal oxide-coated polymer nanofibres. *Nano Letters*. 3 (2), p.143-47.

Fennessey, S., 2004. Fabrication of aligned and molecularly oriented electrospun polyacrylonitrile nanofibers and the mechanical behavior of their twisted yarns. *Polymer.* 45, p.4217-225.

Hearle, J., 2002. Fibers, Structure. *Ullmann's Encyclopedia of Industrial Chemistry*. Wiley.

Hou X. 2009. Stretching-induced crystallinity and orientation to improve the mechanical properties of electrospun PAN nanocomposites. *Jnl of Material Design.* doi:10.1016/j.matdes.2009.01.051

Jeschke, G., 2002. Determination of the nanostructure of polymer materials by electron paramagnetic resonance spectroscopy. *Macromolecular Rapid Communications.* 23, p.227-46.

Jeschke, G., 2000. Structure characterization of the copper(II) complex of poly(4-vinylpyridine) by a combination of EPR, techniques. *Journal of Physical Chemistry B.* 104, p. 8382-390.

Kakudo, M. & Kasai, M., 1972. *X-ray Diffraction by Polymers.* Tokyo, Kodansha Ltd; 231-320.

Katii, K., 2003. Conductivity model and photoacoustic FTIR surface depth profiling of heterogeneous polymers. *Polymer.* 44, p.3319-325.

Kim, C., 2005. Electrochemical characterization of electrospun activated carbon nanofibres as an electrode in supercapacitors. *Journal of Power Sources.* 142, p.382-88.

Kirby, J., Brandrup, J. & Peebles L., 1968. On the chromophore of polyacrylonitrile II: The presence of ketonic groups in polyacrylonitrile. *Macromolecules*. 1 (1), p.53-58.

Masson J.C (ed). 1995. *Acrylic Fibre Technology and Applications*. NY, Marcel Dekker, 197-219.

McClelland, J.F., Jones, R.W., Luo, S & Seaverson, L.M, 1993. 'A Practical Guide to FT-IR Photoacoustic Spectroscopy' in "*Practical Sampling Techniques for Infrared Analysis"*, P.B. Coleman (Ed.), CRC Press, Boca Raton, FL, Chapter 5, p.107-44.

Minagawa, M., Yoshida, W., Kurita, S., Takada, S. & Yoshii, F., 1997. Solvent casting effect on the infrared characteristic absorption bands (1230/1250 cm^{-1}) of stereoregular isotactic poly(acrylonitrile) film. *Macromolecules.* 30, p.1782-786.

Minagawa, M., Taira, T., Yabuta, Y., Nozaki, K. & Yoshii, F., 2001. An anomalous tacticity-crystallinity relationship: a waxd study of stereoregular isotactic (83-25%) poly(acrylonitrile) powder prepared by urea clathrate polymerization. *Macromolecules.* 34, p.3679-683.

Minagawa, M., 2002. Conformational effect and FTIR diffuse reflection spectroscopy of stereoregular isotactic poly(acrylonitrile) prepared by urea clathrate polymerization. *Macromolecules.* 33 (12), p.1653-656.

Murthy, N.S., Reimschussel, A.C., & Kramer, V.J, 1990. Changes in void content and free-volume during heat setting. *Journal of Applied Polymer Science.* . 40, p. 249 – 265.

Pannier, M., Veit, S., Godt, A., Jeschke, G. & Spiess, H.W., 2001. Dead-time free measurement of dipole-dipole interactions between electron spin. *Journal of Magnetic Research.* 142, p.31-40.

Park, S.H., Jo, S.M., Kim, D.Y., Lee, W.S. & Kim, C., 2005. Effects of iron catalyst on the formation of crystalline domain during carbonization of electrospun acrylic nanofiber. *Synthetic Metals.* 150, p.265-270

Rizzo, P., Auriemma, F., Guerra, G., Petraccone, V. & Corradini, P., 1996. Conformational Disorder in the Pseudohexagonal Form of Atactic Polyacrylonitrile. *Macromolecules,* 29 (27), 8852-861.

Sawai, D., 1999. Uniaxial Drawing of Isotactic Poly(acrylonitrile): Development of Oriented Structure and Tensile Properties. *Macromolecules*. 32, p.5622-630.

Sen K., Bajaj, P. & Sreekumar, T., 2003. Thermal Behavior of Drawn Acrylic Fibers. *Journal of Polymer Science: Part B: Polymer Physics*. 41, p.2949-958.

Sergides, C.A., Chughtai, A.R., Smith, D.M. & Schissel, P, 1986. Relationship between the functional group concentrations and the infrared reflection-absorbance of polyacrylonitrile films. *Journal of Polymer Science: Polymer Physics Edition.* 23 (8), p.1573-584

Schmidt, P., Raab, M., Kolaric, J. & Eichorn, K., 2000. Comparison of two modern infrared spectroscopic methods for the determination of orientation. *Polymer Testing*. 19, p.205-12.

Shilton, S., Molecular orientation and performance of synthetic polymeric membranes for gas separation. *Polymer*. 38 (9), p2215-220.

Silverstein, S., 2004. Complex formation and degradation in poly(acrylonitrile co-vinyl acetate) containing copper nitrate. *Journal of Polymer Science: Polymer Physics Edition*. 42, p.1023-032.

Tachibana, M., Iwaizumi, M. & Tero-Kubota, S., 1987. EPR studies of copper(II) and cobalt(II) complexes of adriamycin. *Journal of Inorganic Biochemistry*. 2, p.133-40.

Tang, J., 1996. Electrochemical synthesis of polyacrylonitrile (PAN)-copper composite conductive film. *Journal of Applied Polymer Science*. 61, p.1773-779.

Tungol, M., Forensic analysis of acrylic copolymer fibers by infrared microscopy. *Applied Spectroscopy*. 47, p.1655-658.

Usami, T., Ohtani, I. & Tsuge, S., 1990. Structural study of polyacrylonitrile fibers during oxidative thermal degradation by pyrolysis-gas chromatography, solid-state ^{i3}C nuclear magnetic resonance and fourier transform infrared spectroscopy. *Macromolecules*. 23, p.2460-465.

Ward, I.M., 1982. *Developments in Orientated Polymers.* Applied Science Publishers, p.1-46.

Willmott, P.R. & Huber, J.R., 2000. Pulsed laser vaporization and deposition. *Reviews of Modern Physics*. 72 (1), p315-28.

Yamane, A. & Sawai, D., 1997. Development of ductility and tensile properties upon two-stage draw of ultrahigh molecular weight poly(acrylonitrile). *Macromolecules.* 30, p.4170-178.

Young, J.K. & Chong, R.P., 2005. The effect of the interaction between transition metal and precursor on the stabilization reaction of polyacrylonitrile (PAN). *Carbon,* 43 p. 2397-429.

Vaisman, L., Wachtel, E., Wagner, D & Marom, G., 2007. Polymer-nanoinclusion interactions in carbon nanotube based polyacrylonitrile extruded and electrospun fibers. *Polymer* 48 (2007) p.6843-54.

Zanchini, C. & Crispini, A. , 2002. The application of DFT and MM on kinetics and conformational studies". *Recent Research and Development in Chemical Physics*. 3, p. 35-55.

Zussman, E., Chen, X., Ding, W., Calabri, L., Dikin, D., Quintana, J. & Ruoff, R., 2005. Mechanical and structural characterization of electrospun PAN-derived carbon nanofibres. *Carbon*. 43, p.2175-185.

CHAPTER 5 – EXPERIMENTAL AND RESULTS

NANOFIBRE POTENTIAL APPLICATIONS – PROOF OF CONCEPT

As part of industrially funded academic research projects, three potential applications of electrospinning were evaluated for possible further development.

1. Composite layered dust filtration fabric with an electrospun membrane.
2. Modified electrospun PAN nanofibre fabric for heavy metal absorption.
3. Conductive blended electrospun fabric as an electrode material.

Applications 2, and 3 include additives in the electrospun fibres in the forms of a low molecular weight oligomer, (Chemisorb) and a polyaniline blend in PAN.

5.1 ELECTROSPUN NANOFIBRE PAN MATS ON PAN FILTER FABRICS

5.1.1 Introduction, background and aims

The aim of this screening research project of an industrial electrospinning application was to assess the effect of a thin membrane of electrospun PAN nanofibres on the surface of a filter fabric made from micron sized diameter PAN fibres from the same polymer grade. The aims were to improve the pressure drop characteristics and the filtration efficiency of very small particles (PM 2,5 and PM 1,0) of the filter fabric. This type of nonwoven needle-felt filter fabric is used in pulse-jet fabric filter plants to remove particulate matter from industrial boiler flue gas. The operating problems with these plants in South Africa and elsewhere i.e. fabric blinding and chemical degradation have been described previously in detail (Greyling et al.1996, Greyling 2000).

A company in the USA, Donaldson, commercially produces electrospun membranes onto the surface of spun-bonded, nonwoven polyester fabrics (not PAN needle-felts).

At the University of Akron, Prof D Reneker, one of the leading electrospinning researchers, conducted commercial electrospinning product development. The primary aim of these coated products was to serve as a coalescing filter for use in air conditioning systems (Hajra et al.2002). The technique for contacting polymer nanofibers (very long fibers) with glass fibers (short fibers) and preparing the filter media was developed in the laboratory of the University of Akron, Ohio, USA at the Coalescence Research Consortium. The patents for this particular invention have been filed (Chung et al 2004, 2006).

Statistical measures were developed for quality control as well as characterization of mass distribution in the fibrous substrates. Mass uniformity in fibrous structures, such as non-wovens, paper, or sprayed adhesives in non-woven film-based laminates, plays an important role in defining appearance, performance, and the processibility of such structures. For example, in filtration processes, web performance is largely dependent on the uniformity of the web. Thin spots in the fibrous sheet affect filtration performance by allowing large particles to pass through the filter.

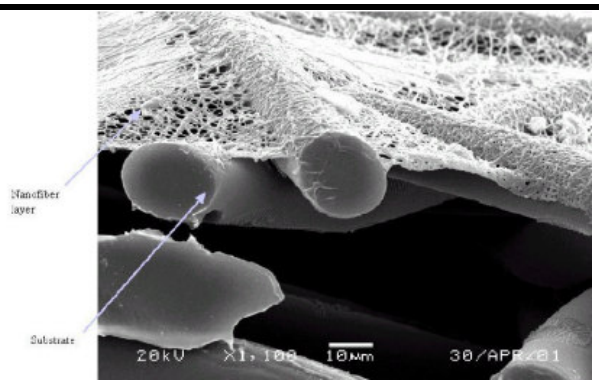

www.donaldson.com, Minneapolis, USA. Photomicrograph showing a cross-section of nanofibres electrospun onto a polyester spun-bond substrate. The substrate provides mechanical properties, while the web dominates coalescence and filtration performance.

Figure 5.1 Donaldson spun-bonded filter cloth with an ES membrane

Typically, non-woven webs are characterized in terms of basis weight, structure, and visual uniformity. A number of methods and techniques, both subjective and objective, are used in the nonwovens and paper industry to quantify web uniformity. These techniques range from expert-panels rating against benchmarks to using sophisticated image analysis techniques for quantifying mass uniformity in fibrous networks (Chhabra 2003, Aydilek 2002).

One way to improve the efficiency in filtering small particles (PM 2,5 and 1,0) in filter media is to use fibers of comparable or smaller diameter. Nanofibers due to their small diameter fit the situation perfectly. Nanofibers have a large surface area per unit mass of fiber and hence can be used as an efficient filtration medium to separate particles from gas or liquid streams. The electrospun nanofibre mats, however, have insufficient mechanical strength on their own and need to be attached to a more robust backing material.

Electrospinning can produce nanofibers in the desired range from 10 to 1000 nm. Two characteristics of electrospinning are relevant. Firstly that polymer fiber with a diameter smaller than one micron can be produced. The second feature is that electrospinning equipment is relatively simple and easy to operate. Potential problems include; delaminating of the electrospun membrane; inhomogeneous fibre distribution and thickness and mechanical damage of the fine fibres by abrasion of the filtration dust.

5.1.2 Experimental procedures

Sample preparation

Samples of a 600 $g.m^{-2}$ commercial, scrim reinforced, singed and calendared Dolanit® PAN non-woven needle-cloth were obtained from Andrew Textile Industries, (ATI), Bury, UK. The Dolanit® PAN surface fibres were 2,2 dtex (about 13 µm in diameter) and spun from a 210 000 $g.mol^{-1}$ molecular weight, 99,5% AN: 0,5% MA "homopolymer" PAN. The fabric was cut into 20 cm^2 sections and mounted on the sloping aluminium plate of the grounded aluminium electrode of the electrospinning apparatus using spray adhesive.

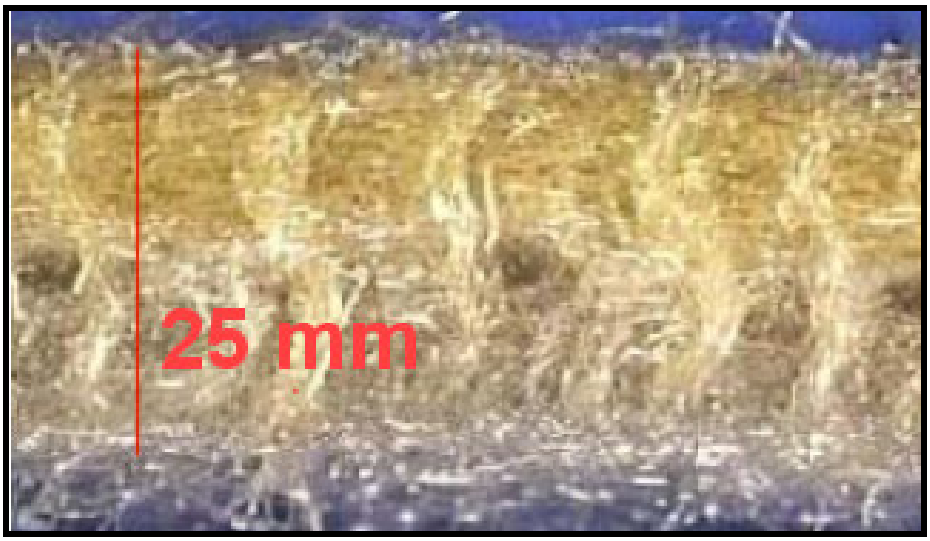

Figure 5.2 Microscope image of the cross-section of a typical PAN needle-felt.

Non-woven PAN needle-felt sections, were successfully covered by electrospun PAN nonwoven surface membranes. The electrospun polymer grade was exactly the same as the backing fabric and was obtained in powder form from Faserwerk Kelheim in Germany, the producers of Dolanit® fibres. The grounded electrode position was adjusted regularly manually to ensure uniform coverage by the nanofibres produced from a single pipette. The air-permeability of the final filter fabric samples was maintained at a level specified for usage in a conventional pulse-jet fabric filter plant. The applied spinning voltage was 20 kV at a spinning distance of 20 cm. The PAN fibres were spun from an 8% w/w solution in DMF at 30 °C.

Adhesion of the spun mat onto the backing felt required much method optimisation however, was completed successfully by spraying excess solvent onto the surface of the felt prior to application of the electrospun mat. The solvent spray was adjusted such that no fibre solvation occurred but only fibre swelling was observed by using a light microscope in reflection mode on the surface of the support fabric. After coating the samples were heat treated on a laboratory scale calendaring

machine under heated rollers at 70 °C between sheets of 100% Teflon® nonwoven cloth, also supplied by ATI.

Adhesion test procedure

The adhesion was evaluated visually after flexing the cloth for 50 cycles and also after rubbing with a finger. The mechanical flexing simulates the mechanical stress experienced during the pulse-cleaning process during filter operation and the rubbing simulates the effect of dust abrasion. The adhesion after these tests was compared to a commercial Gore-tex®, expanded polytetrafluoro-ethylene, PTFE membrane' coated PAN needlefelt.

SEM analysis procedure

The SEM analysis was performed by the University of Cape Town, Microscopy Unit on a fully analytical Leo S440 scanning electron microscope.

Air permeability test

Permeability tests on samples were conducted in the textile laboratory of Beier Albany, in Pinetown South Africa according to the ASTM Standard Test Methods for Felts, (ASTM D461-93).

Filtermedia comparison test on the basis of German Standard VDI 3926

This test was conducted by Dr Pieter Schulz in the laboratories of Tomas Josef Heimbach GmbH, fabric manufacturers in Düren, Germany.

The filtration capacity of filter materials can be judged by various methods and tests. A test under actual operating conditions, including post test laboratory analysis of the used bag still is the most representative method to test a filter material. Very often, a real test cannot be done, especially, if it is an installation, which is not yet in operation. Very often pilot plants are used to verify the filtration under practical conditions. However, the expenditures for pilot tests are almost as high as for real tests.

VDI guideline 3926 describes a test procedure to compare filter media samples. The procedure tries to make a simulation of the filtering process inside a pulse-jet filter. A filter media sample of 170 mm diameter is charged with a defined quantity of dust and a defined air-to-cloth-ratio. The cleaning of the sample with a pulse-jet impulse is either regulated by time or by differential pressure. Temperature, differential pressure, air volume and outlet emission are monitored and registered. VDI 3926 introduces two possible filter units. For this test filter unit type II, PALAS, Figure 5.3, was used.

Different from the real operating parameters in the real filter, the test application provides test results within a short period of time. The air-to-cloth-ratio, cleaning cycles, dust content or dust

character is selected to have a comparable charge of the filter media to the real expected lifetime. The results of the test are subject to interpretation according to the experience of the filter media manufacturer or Original Equipment Manufacturer, OEM, because practical results in the real application might differ from the test results. Theoretically, it would be possible to adjust the filtration parameter for the VDI test to the real application. But even then, the test results might differ from tests in the real application.

Air-to-cloth ratio	3,0 $m^3.m^2.h^{-1}$
Dust concentration	5,0 $g.m^3$
Tank pressure	5 bar
Cleaning	controlled by time
Duration of the filtration cycle	5 seconds
Number of pulses	2500
Impulse time of the pressure	100 ms

Figure 5.3 Test filter unit, Type II, PALAS at Tomas Josef Heimbach GmbH.

The choice of the test dust influences for the test results. The dust quality characteristics such as particle size distribution and particle shape must to be defined and must be reproducible. Even if the dust from the real application is used instead of test dust, the test results might be different from a test in the real application. The SEM micrograph and the dust specifications are given in Figure 5.4.

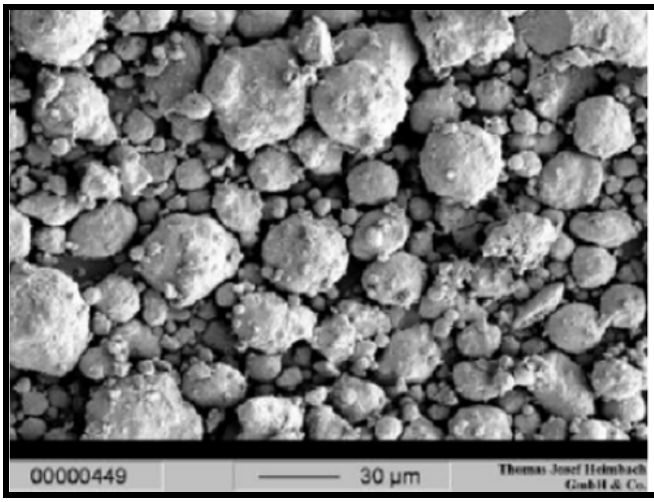

Designation: Al_2O_3, high purity alumina
Particle shape: round
Flow behavior: free flowing powder, not agglomerative
Dust behaviour: fine , free-flowing, good cleanability, penetrating
Particle Size: d_{10} = 8,2 µm;
d_{50} = 27,3 µm;
d_{90} = 52,8 µm

Figure 5.4 Pural® SB test dust from *Condea Chemie*, Hamburg.

The parameters have been chosen according to VDI 3926. The cleaning is controlled by time not by differential pressure. The filter media was cleaned every 5 seconds and therefore no filter cake was built up. This is the toughest test for a filter material and means maximum "aging".

5.1.3 Results on the electrospun PAN coated PAN filter fabric

The final products sent for further testing, showed no delaminating of the nanofibre coating. Samples with *Gore-tex®,* expanded polytetrafluoro-ethylene, (PTFE), membrane coated PAN filter fabrics showed delamination and discontinuities in the membrane structure after flexing and rubbing as a result of poor adhesion between the PTFE membrane and backing PAN fabric and in addition due to the soft nature of the expanded PTFE membrane.

A SEM micrograph of electrospun PAN nanofibres on the surface of a PAN needle-felt is shown in Figure 5.5.

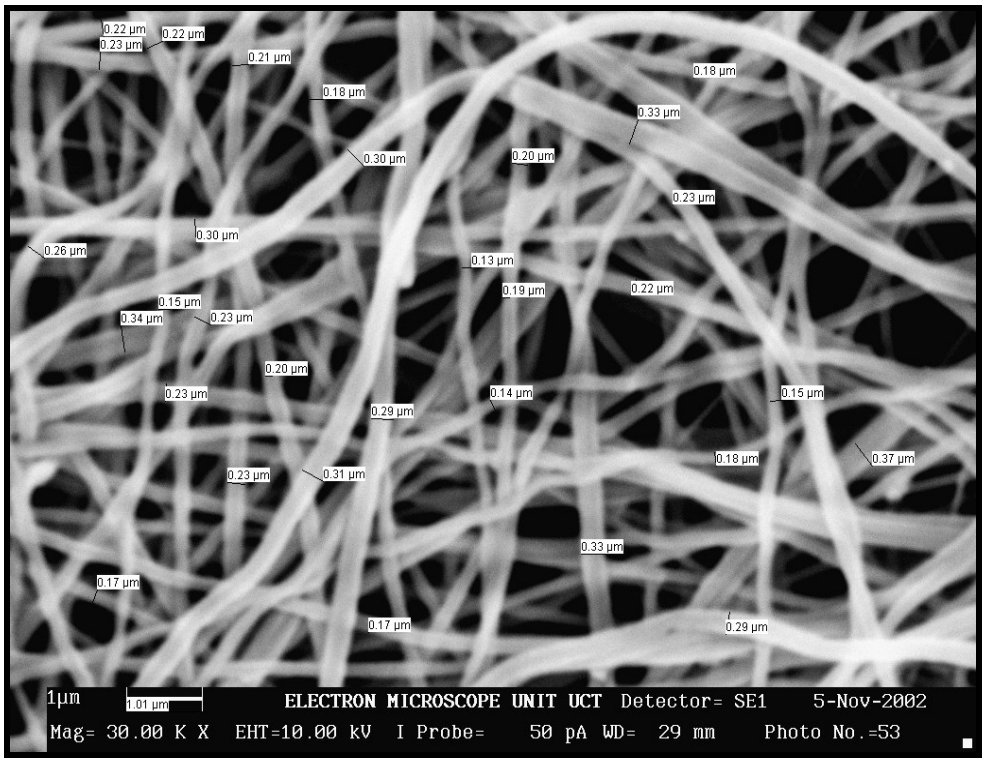

Figure 5.5 SEM micrograph of the surface of ES PAN coated on PAN filter felt.

The results of the air-permeability test conducted on the control sample and a sample coated for 10 minutes and 1 hour with electrospun nanofibres is presented in Table 5.1.

The results from the VDE filtration efficiency test conducted at Tomas Josef Heimbach Filter manufacturers are presented in Figure 5.6 and Figure 5,7. In the SEM micrograph in Figure 5.5 the backing 13 µm, 2.2 dtex, PAN fibres are not visible due to the focus depth of the SEM. The average

fibre diameter in the electrospun "membrane" is 200 nm. The fibre surface morphology in comparison to fibres spun under the same conditions, directly onto a grounded metal electrode, tends to be more ribbon-like, than round in cross-section.

Table 5.1 Air permeability results on coated and uncoated PAN needle-felts.

Identification	**Media 1**	**Media 2**	**Media 3**
Description	**Spun 20 cm, 20 kV for 1 hour**	**Uncoated ATI PAN Needle-felt**	**Spun 20cm, 20 kV for 10 min**
Air Permeability In $m^3.m^{-2}.min^{-1}$ at 125 Pa	0.56	7.7	1.72
	0.24	7.7	1.72
	0.43	8.1	1.76
	0.68	7.8	1.69
	0.54	8.3	1.66
	0.66	8.3	1.64
	0.37	7.9	1.70
	0.57	8.1	1.70
	0.33	8.5	1.67
	0.46	8.5	1.63
Average	**0.48**	**8.1**	**1.69**
Minimum	0.24	7.7	1.63
Maximum	0.66	8.5	1.76
Range	0.44	1.2	0.13

Figure 5.6 shows that the differential pressure climbed more rapidly for the uncoated filter cloth. The nanofibres on the surface prevent penetration of the test dust into the fabric and delay the onset of fabric blinding i.e dust becoming immobilised within the depth of the filter felt

Figure 5.7 shows that the thicker layer of nanofibres in media 1, coated for 1 hour, reduces the long-term emissions from the filter. The thin layer of nanofibres on media 3, coated for 10 minutes, has no effect on the level of emissions i.e. dust passing through the filter fabric.

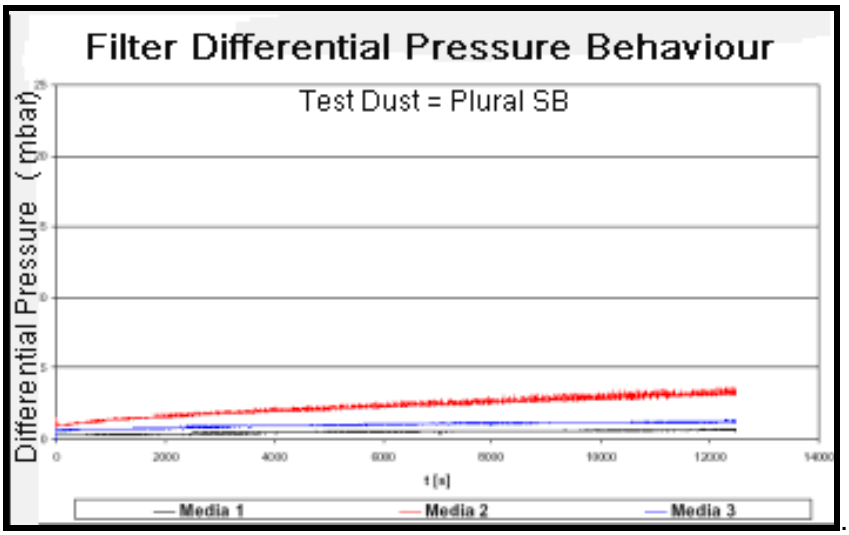

Figure 5.6 ES coated filters differential pressure comparison over time.

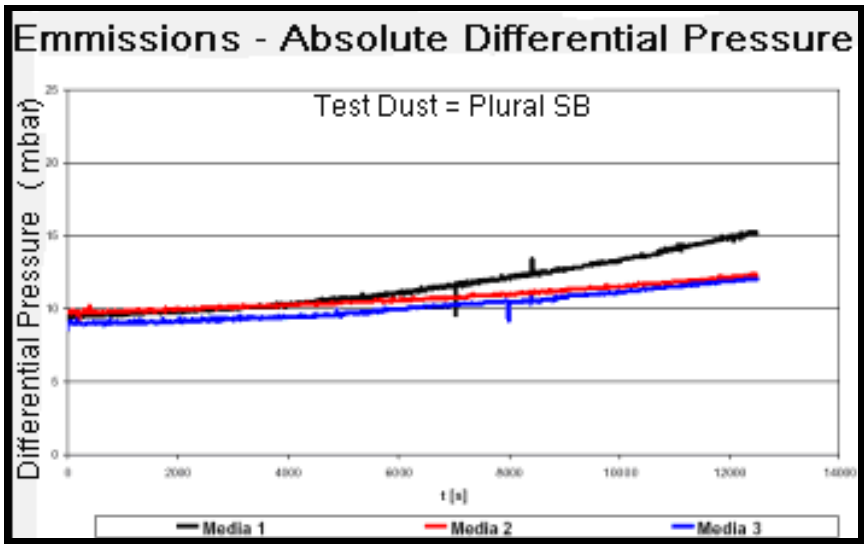

Figure 5.7 ES coated filters emissions comparison over time.

5.1.5 Conclusions of the electrospun coated filter fabric evaluation

The operational problem with uncoated media 2 is a result of fabric blinding and the emissions levels are acceptable. The application of a thin layer of electrospun nanofibres onto the surface of a standard filter felt should increase the filter service life due to the reduction in the rate of filter blinding.

5.1.6 Proposed future research

- Up-scaling to industrial scale with multiple pipettes in parallel across a standard 3 m width of needle-felt filter fabric. Similar development is currently underway at e-Spin Technologies in the USA.
- Trials of coated filters in an actual PJFF plant or pilot plant on site at the boiler.
- Application of polyvinylidene-fluoride, (PVDF), nanofibres onto PAN filters similar to Gore-tex® to give better dust cake removal and improved chemical resistance.
- Application of PAN / polyaniline nanofibres onto PAN or application of conductive polypyrolle or metalised nanofibres onto PAN filter fabrics to alter the triboelectric characteristics of the filter fabric (Ryne 2000).
- Investigate the use of hydroentanglement as opposed to needling to adhere the nanofibres onto the backing fabric.

Static electrification depends upon an excess or imbalance of electrical charge, which is produced by the transfer of charge when two materials are brought together and then separated/ rubbed together. This phenomenon is referred to as the triboelectric effect.

When particles conveyed in a pipe or duct collide, or come close to an electrically isolated and earth-grounded intrusive probe, a charge transfer results between the particles in the gas stream and the probe. It takes place on a continuous basis, because of the continuous stream of particles.

Gas breakdown can occur between two surfaces during separation. During this breakdown, charge can be transferred from one surface to the other via the path of the electrified air. In a fabric filter a triboelectric filter medium would aid in dust cake removal, preventing acid enrichment and thereby prolonging the filter service life.

References

ASTM D461-93. *Standard Test Methods for Felt*.

Adams C, 1987. *Nature's Electricity.* Tab Books; No. 2769; p.63.

Aydilek A.I, 2002. Digital image analysis to determine pore opening size distribution of nonwoven geotextiles. Journal of Computing in Civil Eng. p.280-290.

Chhabra, R, 2003; Nonwoven uniformity - Measurements using image analysis; Original Paper/Peer-Reviewed; 43; *INJ Spring;* (The Procter & Gamble Company, Cincinnati, USA)

Coalescence Research Consortium, Microscale Physiochemical Engineering Centre The University of Akron: Prof D Reneker, http://coel.ecgf.uakron.edu/~mpec/research.htm, accessed 31 Dec 2006.

e-Spin technologies; Dr. Jayesh Doshi. http://www.espintechnologies.com/, accessed 31 Dec 2006.

Greyling C.J., Sanderson R.D., Beeslaar M. & Hansen R., 1996. Pulse-jet fabric filters in the Southern Hemisphere; Monitoring methodology. *International Symposium of Filtration & Separation of Fine Dust*, Vienna, April 1996.

Greyling CJ; 2000. M.Sc thesis; Optimisation of the evaluation methods used on polymeric fibres and fabrics in bag filter plants, *University of Stellenbosch*.

Hajra M,, Mehta K., Chase G., 2003, Effects of humidity, temperature, and nanofibers on drop coalescence in glass fibre media; *Separation & Purification Technology.* 5, p.10-12.

Chung; Hoo Y. (Bloomington, MN) Hall; John R. B. (Burnsville, MN) Gogins; Mark A. (Roseville, MN) Crofoot; Douglas G. (Burnsville, MN) Weik; Thomas M. (Deephaven, MN), 2005. Process of

making fine fiber material, *US Patent* 6,955,775*,* assigned to Donaldson Company Inc., Minneapolis. October 18, 2005.

Chung, H., Hall, J.R.B., Gogins, M.A., Crofoot, D.G. & Weik, T.M., 2006. Polymer, polymer microfiber, polymer nanofiber and applications including filter structures, *US Patent 7,090,715,* assigned to Donaldson Company Inc., Minneapolis. August 15, 2006.

Ramsey, K., 1998. The emergence of triboelectric technology; Rust Report for the Institute for Polyacrylate Absorbents Inc. http://www.midwescofilter.com/pdf/triboflow%20technology.pdf accessed 31 December 2006.

Ryne C., 2000. Triboelectric generation: Getting charged; Desco Industries Inc. (DII); December 2000; Reproduced with Permission, EE-Evaluation Engineering, November, 2000.

5.2 ELECTROSPUN PAN CONTAINING OLIGOMER ABSORBENT ADDITIVES

5.2.1 Introduction, background and aims

Thie aim of this experiment was to measure the absorption characteristics of electrospun nanofibres. An oligomer Chemisorb® was blended with the PAN in the DMF spinning dope. The absorbtivity of the Chemisorb® is pH sensitive and it has been found to have the best absorbtivity for Hg in the pH range 3 to 6.

The mercury absorption experiment was conducted on a sample of ash dam leachate from Lethabo Power Station, near Vereeniging in Gauteng, South Africa.

Chemisorb® is a patented oligomer, developed by Prof. Klaus Koch of the University of Stellenbosch, originally for application as a powder for removal of platinum group chemical species from final platinum mine waste dams (Gie & Koch 2001, Koch & Bourne 1998).

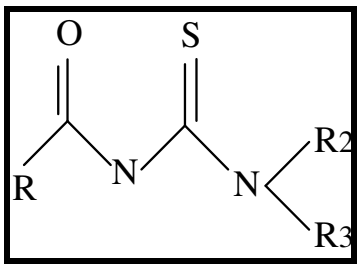

Figure 5.8 General structure of the oligomeric thiourea ligand, Chemisorb®.

The motivation for the development of these Chemisorb® complexing materials was as follows: Platinum Group metals never occur on their own in ores, but rather as complex mixtures of all the

precious metals and in very low concentrations. There was a need to develop a relatively cheap, robust on line method to effectively separate these metals from one another with good recovery.

The Environmental Protection Agency, definition of a leachate is as follows (http://www.epa.gov/ocepaterms/lterms.html)

Water that collects contaminants as it trickles through wastes, pesticides or fertilizers. Leaching may occur in farming areas, feedlots, and landfills, and may result in hazardous substances entering surface water, ground water, or soil.

In flue gas desulphurization, FGD sludge, leachate originates as water used in sludge / ash transport, water associated with or held in the sludge, precipitation, surface inflow, or underground inflow which has percolated through or permeated a body of ash. The resultant outflow from the side surfaces or bottom of a landfill or pond may contain soluble, suspended or colloidal species, which have been removed from the sludge.

Leachate from ash sludge has been a concern because of the potential for it either entering surface or groundwater and carrying heavy metal pollutants. There is concern that the leached specie may be deleterious to these waters, which in many cases are ingested by humans and animals and which may affect aquatic life. Pollution of groundwater by heavy metals species such as mercury, arsenic and cadmium is of particular concern. In many areas (including rural Mpumalanga) groundwater is a natural resource, which is widely consumed without testing or treatment.

The mercury concentration measured in a sample solution taken from the ash dam at Lethabo Power Station near Vereeniging was measured to be 50.29 ppm.

The EPA primary water standards stipulate a maximum level of mercury of 0,002 ppm. This concentration of mercury in the ash dam leachate liquor is 25 000 times greater than the recommended EPA water standard. The average mercury concentration measured in ash leachate at 4 FGD plants in the USA was <0,01 ppm

5.2.2 Experimental procedures

The granular *Chemisorb*® powdered oligomer was first ground to fine powder in a mortar with a pestle. The weighed aliquot (see Table 5.2 below was added to a 10 ml aliquot of a 10% 85k PAN copolymer in either DMF or DMAc and stirred overnight at 50 °C.

The lower molecular weight PAN 85k $g.mol^{-1}$ was used as it has a higher solubility than the 210k homopolymer and to allow maximum incorporation of the oligomer in the blend. The oligomer is soluble in both DMF and DMAc.

All samples were electrospun at a 20 cm spinning distance at 20 kV onto a flat aluminium foil covered grounded electrode at a spinning dope temperature of 30 °C. All samples were spun for 2 hours and are described in Table 5.2.

Previously in 2001, *Chemisorb*® / PAN blended mats were prepared at Drexel University in the USA. Samples were then spun at 20 °C but from a 1g oligomer per 10 g PAN polymer solution. The SEM micrographs of these fibres are shown in Figure 5.9 below.

Table 5.2 Sample description of PAN / *Chemisorb*® samples for electrospinning

CODE	MW (k)	%	cm	KV	Solvent and additive
N001	85	10	20	20	DMAc + 0.25g Chemisorb
N002	85	10	20	20	DMF + 0.25g Chemisorb
N003	85	10	20	20	DMF + 0.25 g Chemisorb
N004	85	10	20	20	DMAc + 0.25 g Chemisorb
N005	85	10	20	20	DMF + 0.25 g Chemisorb filtered (450 nm)
N006	85	10	20	20	DMF + 0.25 g Chemisorb filtered (450 nm)
N007	85	10	20	20	DMF + 0.50 g Chemisorb

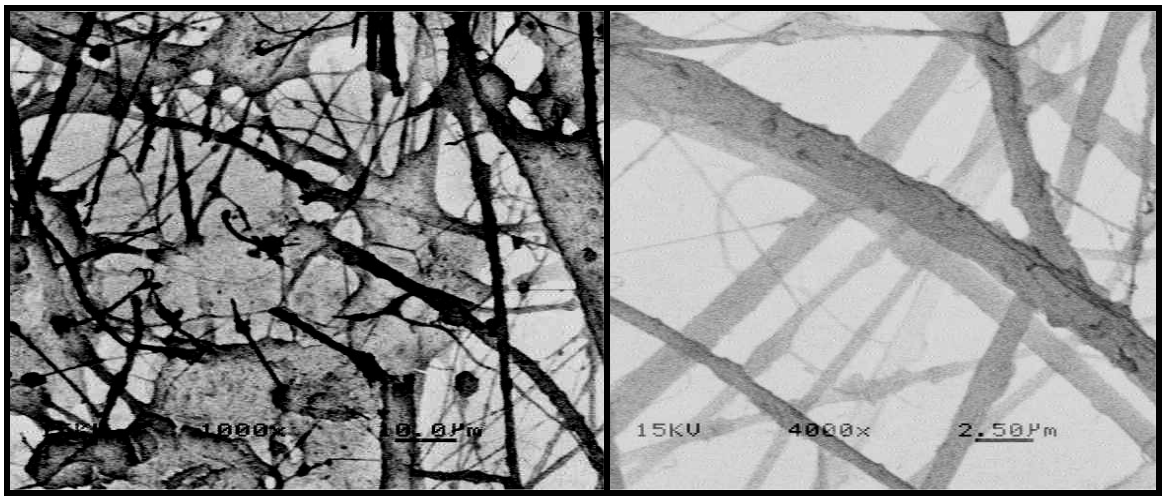

Figure 5.9 Micrographs of USA electrospun 10% Chemisorb® / PAN mats.

It can be seen that the fibres tended to be break during the spinning process. It can be clearly seen that the oligomer was not fully dissolved and there was a mutiimodal fibre diameter distribution.

The samples of PAN electrospun with the chemisorb oligomer at a lower weight concentration of 1:40 were later prepared. These samples were electrospun in preparation for the mercury removal experiments from both DMF and DMAc solvents. The SEM and EDAX results are shown in Figure 5.10 and Figure 5.11 respectively.

The solvent of choice for the spinning of PAN was DMF as the solubility of PAN and Chemisorb in DMF is higher. It can be seen in the micrographs above that the oligomer and polymer appear to be well blended in the sample spun from DMF. The fibre diameter under the given spinning conditions is about 200 nanometers.

A 5ppm solution of mercury ions was made by dissolving 1.1802 g of $HgCl_2$ in 1000 ml distilled water to give a 500ppm solution. This solution was than further diluted by taking 10 ml and diluting it to 1000ml, to give a 5ppm solution. The 5 ppm Hg control solution's was validated by BemLabs in the Strand using AES-ICP, and found to have a mercury concentration of 5.1 ppm. BemLabs in the Strand conducted all the water analyses.

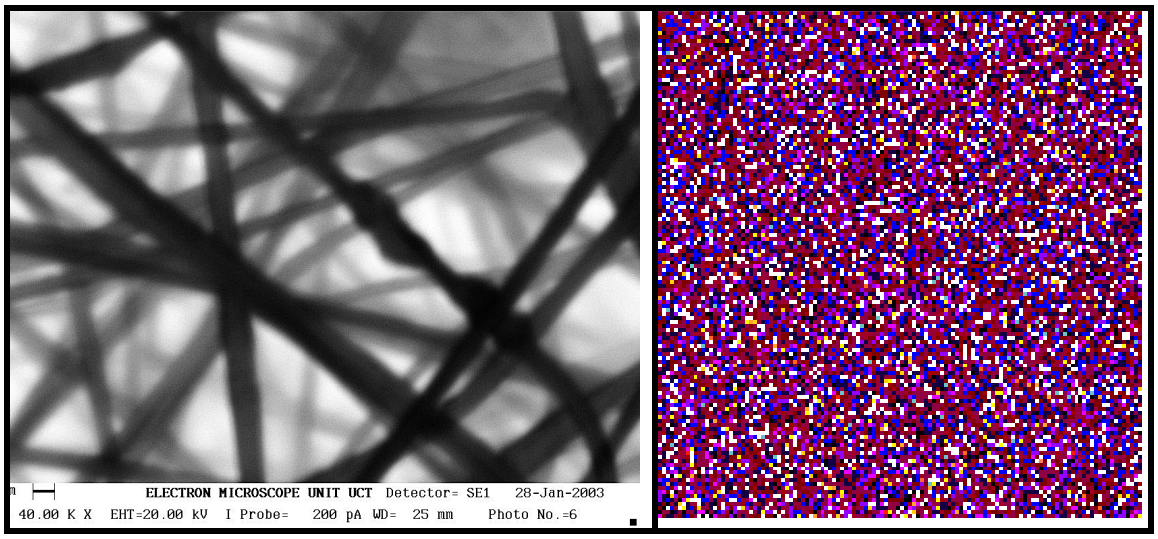

Figure 5.10 SEM and EDAX mapping of sulphur in sample N003 (from DMF).

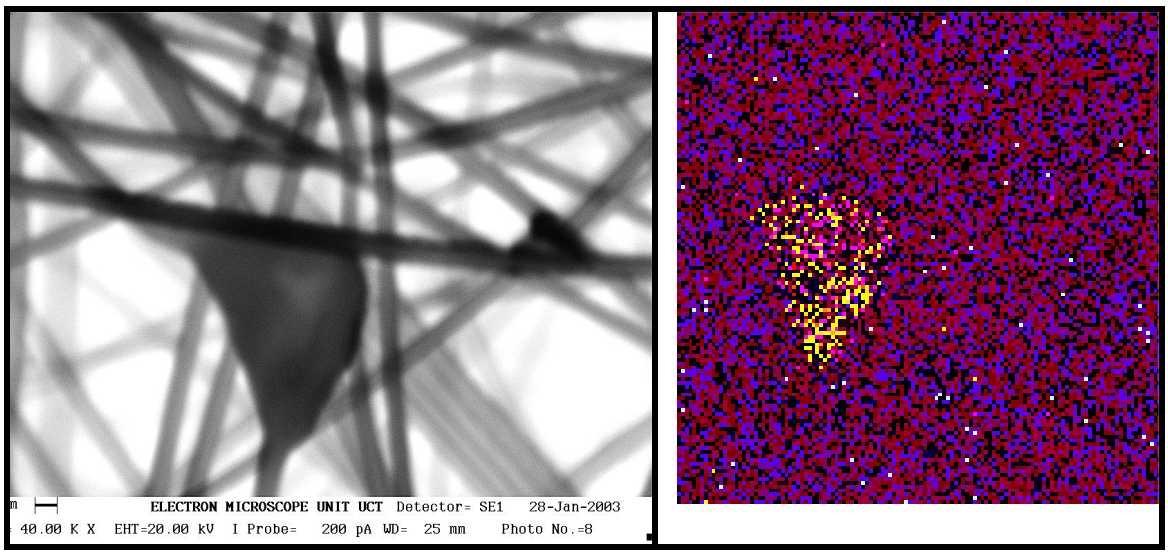

Figure 5.11 SEM and EDAX mapping of sulphur in sample N004 (from DMAc).

A 100ml sample was taken from each solution and the pH was adjusted to ±3.5, by adding 1drop of fuming HCl to the 5 ppm solutions and 2 drops to the leachate sample solutions. Table 5.3

presents the weight of the Chemisorb / PAN blended electrospun fibre mat placed with the 100 ml aqueous sample of the control or the ash dam leachate, for an hour. All solutions were reacted for 1 hour with the Chemisorb sample in the form of the electrospun PAN blended fibrous mats or the oligomer powder (C_{olig}), whilst stirred.

5.2.3 Results of the mercury absorption study

The water samples were analysed at Bemlabs using AES-ICP and are given in the Table 5.3 to5.5.

Table 5.3 Mercury removal chemical analysis results from Bemlabs

No	Description	Mass (g)	Hg Conc. Before	Hg Conc.
1	Sample solution N007	0.01511	50,29 ppm	4.960 ppm
2	Sample solution C_{olig}	0.01560		4.318 ppm
3	Sample solution N005	0.01438		5.430 ppm
4	Sample solution C_{mon}	0.01570		5.640 ppm
5	5ppm N007	0.01506	5,10 ppm	1.100 ppm
6	5ppm C_{olig}	0.01530		0.818 ppm
7	5ppm N005	0.01588		0.417 ppm
8	5ppm C_{mon}	0.01590		0.251 ppm

Table 5.4 Chemical analysis results for the leachate

Ref	Lab.	PH	EC	Na	K	Ca	Mg	SO_4	B	COD	Hg	Cd	TDS
No.	No.		mS/m	mg/l	mg/l	mg/l	mg/l	mg/l	mg/l	mg/l	mg/l	mg/l	mg/l
Lethabo	289	11.50	156.00	90.08	27.67	161.10	0.40	421.30	0.24	30.00	50.29	0.00	780.0

Table 5.5 Chemical analysis after treatment with powder and ES Chemisorb

Reference	Lab.	pH	EC	Na	K	Ca	Mg	Fe	SO_4	B	COD	Hg	TDS
No.	No.		mS/m	mg/l	mg/l	mg/l	mg/l	mg/l	mg/l	mg/l	mg/l	mg/l	mg/l
N007	489	2.60	85.90	1.76	0.76	9.00	1.82	0.12	5.30	0.33	44.0	4.96	454.0
C_{Olig}	490	3.10	24.40	1.43	0.75	0.38	0.27	0.04	5.24	0.32	43.0	4.31	122.0
N005	491	2.80	85.50	78.61	0.51	0.49	0.27	0.05	2.26	0.56	37.0	5.43	407.0
C_{Mon}	492	2.60	81.60	1.66	0.23	0.31	0.24	0.04	2.10	0.22	23.0	5.64	385.0
N007 5 ppm	493											1.10	
C_{Olig} 5 ppm	494											0.818	
N005 5 ppm	495											0.417	
C_{Mon} 5 ppm	496											0.251	

The results of the mercury removal investigation using the Chemisorb in both the immobilized fibre form and the powder form are presented in Table 5.3. A more comprehensive chemical characterization of the ash dam leachate is given in Table 5.4. The results after treatment with the Chemisorb are given in Table 5.5.

The one electrospun mat was dried after the treatment of the leachate and sent for SEM and EDAX Hg mapping analyses. The results are shown in Figure 5.12.

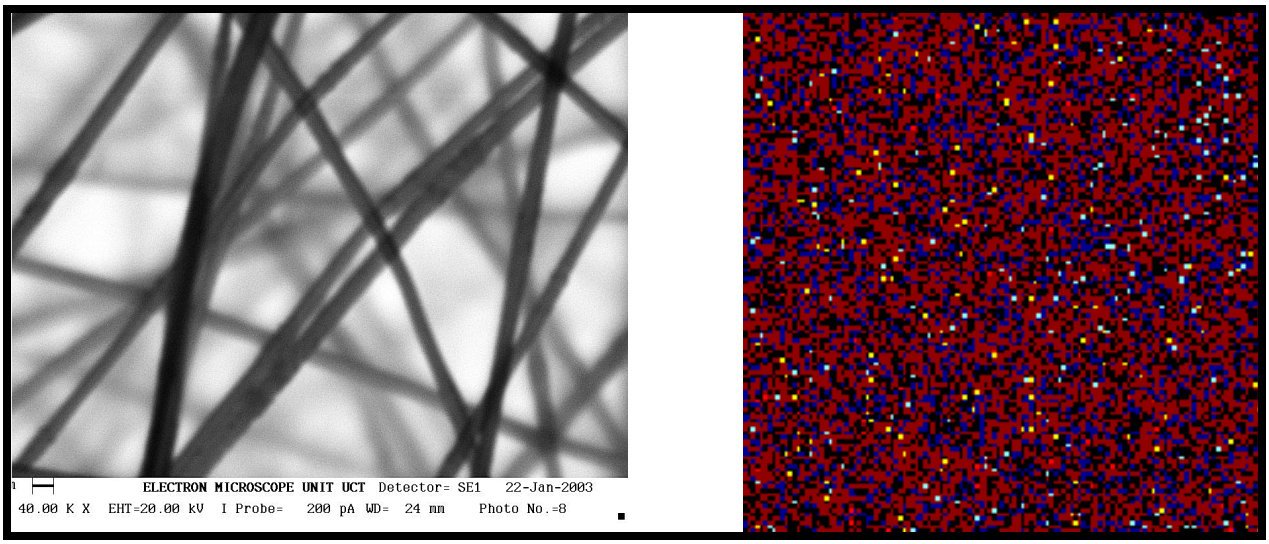

Figure 5.12 SEM and EDAX Hg mapping of sample N005 after treatment of Lethabo.

5.2.5 Conclusions

The electrospun Chemisorb® / PAN blended electrospun mats showed a high removal efficiency of mercury from the Lethabo ash dam leachate sample.

The sample with the higher loading of oligomer, NO07 showed a poorer absorbency than sample N005 with half the concentration of the blended oligomer. This could be due to the fact that the solubility of Chemisorb® is low in the PAN DMF solution and that at the higher concentration, the oligomer does not disperse well in the polymer fibres or agglomerates.

5.2.6 Recommended further development

Develop aligned fibre mats in order to achieve improved mechanical properties such that frames can be designed and engineered to immobilize the absorbent cloths for industrial application

Assess the absorption properties of specially modified PAN electrospun fabrics for Cr^{6+} and other heavy metal removal (Deng & Bai 2004).

Investigate the possibility of using surfactants to increase the solubility of Chemisorb in DMF and thus the efficiency of mercury removal.

In this research the absorbent was used to remove an environmental hazard. The same process could also be used in a mining process such as the mining removal of boric acid, vanadium or lithium chloride from seawater or mine ponds.

4.2.7 References

Deng S. & Bai R., 2004. Removal of trivalent and hexavalent chromium with aminated polyacrylonitrile fibers: performance and mechanisms. *Water Research.* 38, p.2424–432.

Gie I.E, & Koch K.R., 2001. RP-HPLC Analysis of Pt and Pd complexes with thiourea ligands and the role of ligand structure on separation and retention time. *Chemical Communications; Royal Society of Chemistry,* p.16-18.

Koch K.R &, Bourne S., 1998. Protonation mediated interchange between *mono*- and *bi*dentate coordination of *N*-benzoyl-*N*′,*N*′-dialkylthioureas: crystal structure of *trans*-bis(*N*-benzoyl-*N*′,*N*′-di(n-butyl)thiourea-*S*)-diiodoplatinum(II). *Journal of Molecular Structure.* 441 (1), p.11-16.

5.3 PRODUCTION OF PANi / PAN ELECTRODES BY ELECTROSPINNING

5.3.1 Introduction, background and aims

The aim of this experiment was to synthesize a high molecular weight polyaniline, then to blend it with PAN and electrospin potential high conductivity and high surface area electrodes.

Conductive nanofibers are expected to be used in the fabrication of tiny electronic devices or machines such as Schottky junctions, sensors and actuators. Due to the well-known fact that the rate of electrochemical reactions is proportional to the surface area of the electrode, conductive nanofibrous membranes are also quite suitable for use as porous electrodes in developing high performance batteries (Gua 2005, Huang et al. 2003a, Kim 2005). Electrospun PVDF has been used as a fibrous electrolyte in lithium batteries (Kim et al. 2004).

Since the initial discovery in 1977, that polyacetylene $(CH)_x$, now commonly known as the prototype conducting polymer, could be p- or n-doped either chemically or electronically to the metallic state, the development of the field of conducting polymers, "synthetic metals", has continued to accelerate at an unexpectedly rapid rate and a variety of other conducting polymers and their derivatives have been discovered.

Potential new technology has been developed by combining the now well-established field of electronic polymers (intrinsically conducting polymers, (synthetic metals), when doped with the emerging field of nanoscience (McDiarmid 2001).

According to literature, controlling the reaction temperature can control the molecular weight of polyaniline. In one article (Adams & Monkman 1997) the highest yield of polyaniline, (±162 000 Daltons), may be obtained if the reaction is carried out at –25ºC. This method was chosen since specific molecular weights were needed to match the molecular weights of the polyacrylonitrile in order to get an even blend distribution of the two polymers in the electro spun mats.

Polyaniline is a conducting polymer that has been widely studied for electronic and optical applications. Unlike other conjugated polymers, polyaniline has a simple and reversible acid / base doping / dedoping chemistry enabling control over properties such as free-volume, solubility, electrical conductivity, and optical activity. In recent years, one-dimensional (1-D) polyaniline nanostructures, including nanowires, rods, and tubes have been studied with the expectation that such materials will possess the advantages of both low-dimensional systems and organic conductors.

Physical methods, including electrospinning and mechanical stretching have been used to make polyaniline nanofibres. In earlier work, polyaniline fibrils of 100 nm in diameter, with a compact micro-spheroid under layer, were found on the surface of electrochemically-polymerized films. Interconnected network-like structures with polyaniline “nano-linkers” 10-50 nm wide have also been identified in polymer blends.

Despite the variety of current synthetic approaches to polyaniline nanostructures, there is a need for a practical synthetic method capable of making pure, uniform, and template-free polyaniline nanostructures with small diameters (sub-100 nm) in bulk quantities. Electrospun films of the polyaniline nanofibers possess much faster gas phase doping/ de-doping times compared with conventional cast films and therefore hold promise for sensor applications.

Pure PANi nanofibres have been electrospun into an acid bath. More often PANi is blended with another polymer most often PEO (Mueller 2002, Zhou et al. 2003) but also with polyamide (Hong 2005) and PAN (Pan & Yang 2005). For PANI–DBSA/PAN composite films obtained from solution casting, there may be interaction (hydrogen-bonding) between two components, which makes good compatibility and an nanolevel dispersion of PANI–DBSA in PAN.

The network structure of PANI–DBSA in PAN matrix should be responsible to low percolation threshold and high conductivity. Wet spun PAN / PANi composite fibres have also been studied (Jianming et al. 2005).

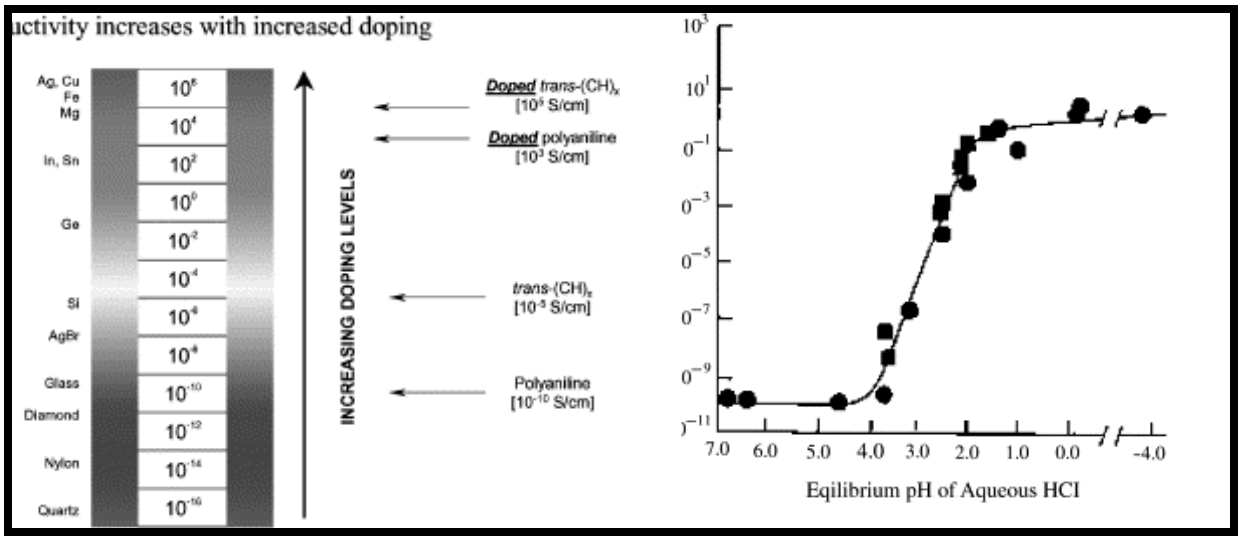

Figure 5.13 Conductivity of electronic polymers.

Figure 5.13 shows the conductivity of emeraldine base as a function of pH of HCl dopant solution as it undergoes protonic acid doping (and represent two independent series of experiments)

5.3.2 Experimental procedure

A 2.3 ml (0.25 mol) AnalaR Aniline and ±16 g LiCl salt (to prevent mixture freezing) were added to 24.5 ml of 1M HCl solution. A 7.132 g sample of $(NH_4)_2S_2O_8$ was made up to 20 g with distilled water and was added to the reaction mixture via a peristaltic pump at a rate of 5 ml per hour.

The reaction was contained in a jacketed reaction vessel with a magnetic stirrer, stirring at 700 rpm, and was cooled to –25 ℃ with an external circulating chiller. The reaction temperature did however not remain constant due to insufficient insulation on the piping of the chiller and the reaction vessel. After the addition of the oxidant the mixture was allowed to react for 46 hours at approximately –25 ℃. After which the reaction mixture was filtered and washed with 10 × 50 ml distilled water.

The precipitate was deprotonated with 25% NH_3 solutions over a 46 hour period. The new reaction mixture was then re-filtered, washed with 8 × 50 ml distilled water, followed by 2 × 50 ml isopropanol and than dried in a vacuum oven at 60 ℃ for 24 hours.

The mechanism of the polymerization reaction is presented below.

Initiation

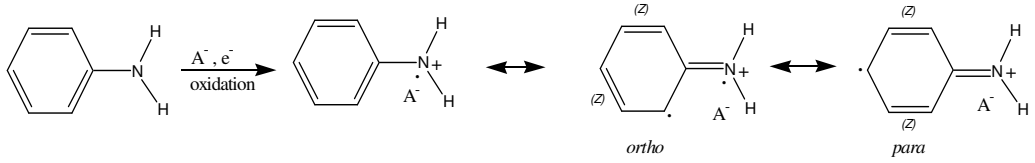

Coupling

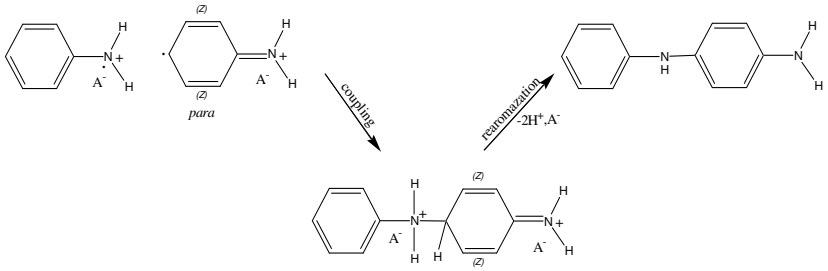

Chain propagation

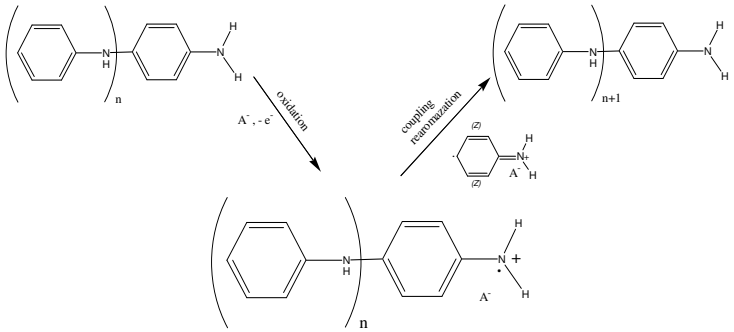

Deprotonation

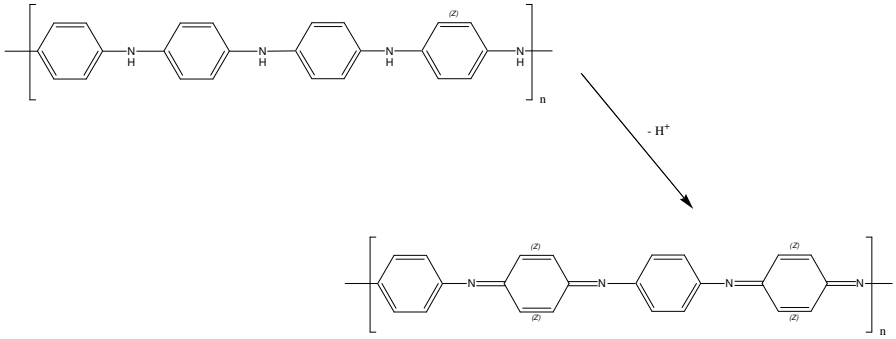

During the characterization process some solvent problems were experienced. Initially the polyaniline was completely insoluble in THF, it was then re-doped with 33% NH_3 solution for 24 hours at ambient temperature. This caused the polyaniline to become more soluble according to the Table below which contains the different solvents as well as the different solubilities of the polyaniline (after re-doping).

Table 5.6 PANi solubility in g.10 ml^{-1}

N-methylpyrollidone	Chloroform	Dimethylformamide
0.49	0.48	0.49

5.3.3 Characterization of the polyaniline

Attempts were made to measure the molecular mass of synthesized polyaniline. No usable results could be obtained from either GPC or MALDI-TOF MS. Similar to the problems encountered in

characterizing the molecular weight and polydispersity of PAN, the dipole interactions between the lone pair electron on the nitrogen atom cause problems in getting the sample into an extended chain conformation in solution and to fly properly to the target in the MALI-TOF MS experiment.

Samples of polyaniline with known molecular weight were obtained from Aldrich and dilute solution viscosity was used. The molecular weight of the synthesized polyaniline was estimated at 100 000 $mol.g^{-1}$.

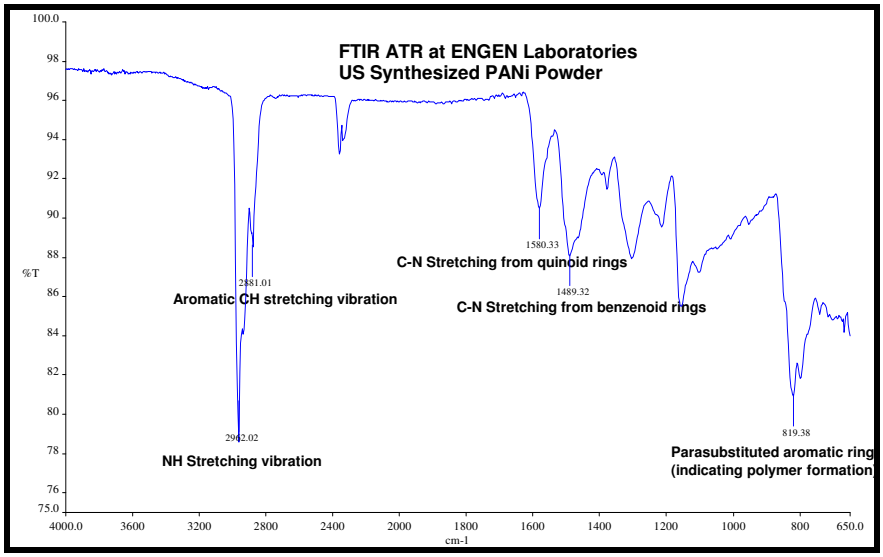

Figure 5.14 FTIR ATR of synthesized polyaniline.

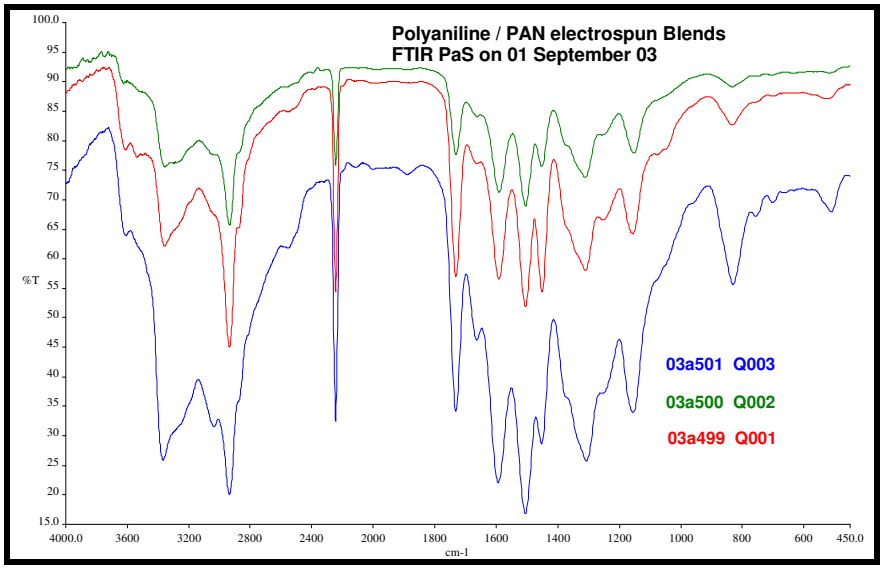

Figure 5.15 FTIR PAS of ES PAN / PANi blends.

The synthesized polyaniline was characterized by FTIR, ATR at the laboratories of Engen in Montague Gardens, South Africa. The sample was identified as being pure. The spectrum is presented in Figure 5.14. FTIR with photoaccoustic detection was also used to characterize the electrospun PAN / PANi blend fibres and the spectra are shown in Figure 5.15. This FTIR

technique could not be used on the synthesized polyaniline fibre due to the deep dark blue colour of the powder.

5.3.4 Characterization of the blended PANi / PAN electrospun mats

The majority of research into conducting polymer actuators to date has been carried out in aqueous electrolytes. However, several disadvantages associated with aqueous electrolytes (e.g. narrow electrochemical window) and conducting polymers in aqueous media (e.g. degradation at high potentials) have been confirmed to be the main factors limiting the lifetime of the conducting polymers (Lu et al. 2002).

Therefore, the use of non-aqueous electrolytes with a high boiling point, low vapour pressure and a wide electrochemical window would be advantageous for the fabrication of stable and durable conducting polymer materials.

Polyaniline has attracted considerable interest because of its conducting and electrochromic properties (Park & Park 2001). Polyaniline is recognised as one of the most promising organic conducting polymers for future development because of its high environmental stability, facile redox switching between differently coloured oxidation states and relatively high conductivity in its emeraldine salt form (Dominis et al. 2002).

The PAN / PANi blend samples are described in Table 5.7. All were spun at 30 °C from a DMF solution, according the procedure described in Section 3.1.

Table 5.7 PAN / PANi ES sample descriptions

Code	MW (k) PAN	% PAN	Distance	kV	Composition
Q001	**85k**	**10**	**20cm**	**20 Kv**	10g PAN + 0,25 g PANi
Q002	**85k**	**10**	**20cm**	**20 kV**	10g PAN + 0,50 g PANi
Q003	**85k**	**10**	**20cm**	**20 kV**	10g PAN + 0,75 g PANi

SEM, Figure 5.16, showed that as the PANi loading is increased from 0.25 g to 0.75 g, the surface morphology became rougher and the average fibre diameter also increased. The increased fibre diameter and networked structure is attributed to the electrochemical activity of the conductive polymer. These networked structure with increased average fibre diameter increased the surface area of the conductive polymer and these observations agree with the results obtained from cyclic voltammetry.

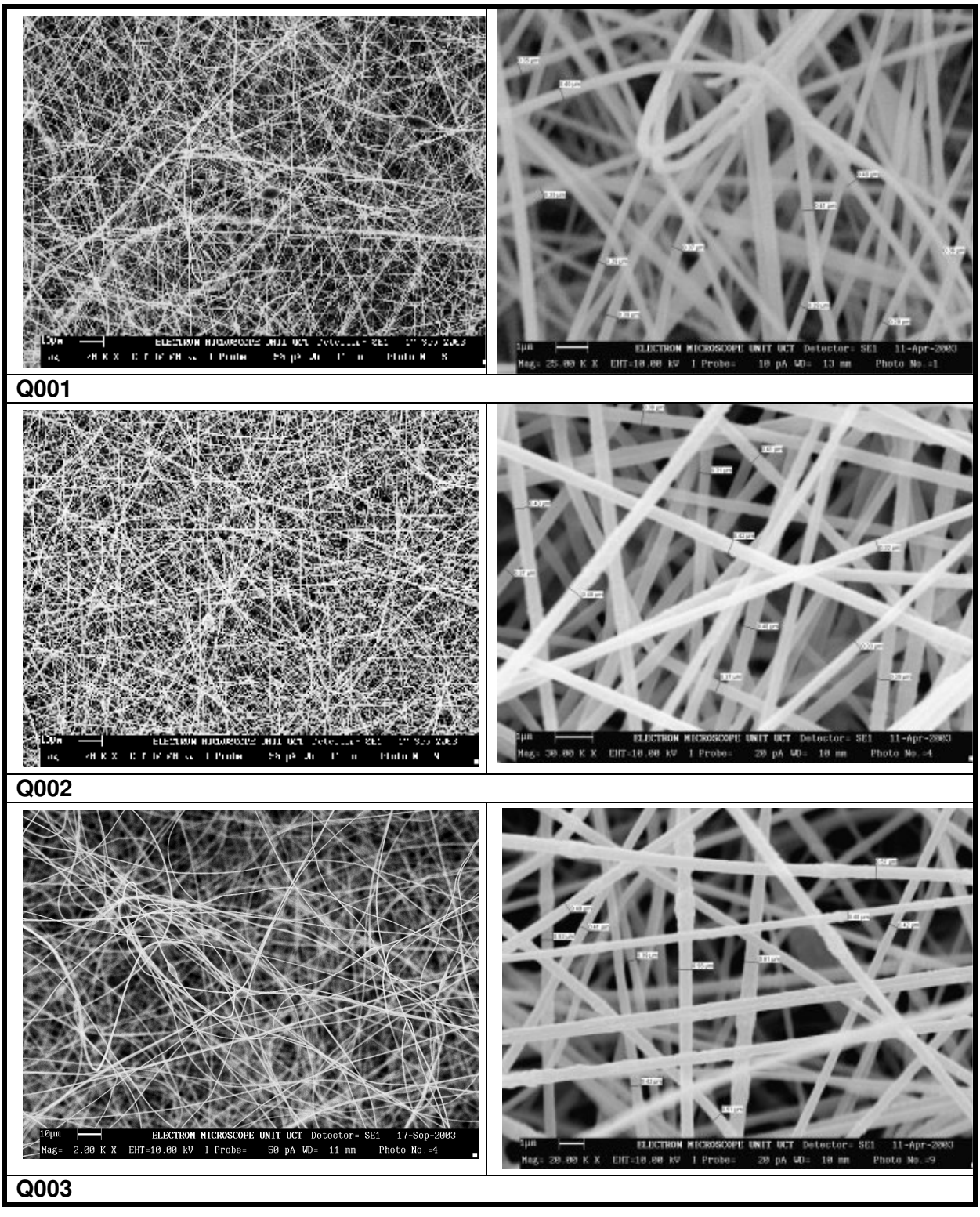

Figure 5.16 SEM low magnification to measure the ES electrode mat porosity.

A photograph of the electrospun PAN / PANi samples are shown in the Figure 5.17. The higher the concentration of the PANi, (sample Q003), the darker the colour. The highest concentration sample is on the foil in the middle of the stack in the photograph.

Figure 5.17 Photograph of the dark blue ES PANi / PAN mats on aluminium foil.

5.3.4 Cyclic voltammetric (CV) measurements of the PANi / PAN electrospun mats

CV is commonly used as the initial electrochemical technique to characterize a redox system (McDiarmid 2001). The redox couples are typically located by potential scans encompassing the entire accessible potential window. The scan range is narrowed for the study of a particular couple.

Many electrochemical reductions / oxidations generate an intermediate that rapidly reacts with components of the medium. One of the most useful aspects of CV is its application to the qualitative diagnoses of these homogeneous chemical reactions that are coupled to the electrode surface reactions

The CV experiments were carried out with an electrochemical analyzer, BAS 100, which is well equipped for this purpose. A three-electrode cell was used, comprising of a reference, counter and a working electrode. The reference electrode employed in this case is Ag/AgCl, the Pt electrode is the counter and the various loadings of PAN / PANi as the working electrode.

This PAN / PANi composite electrode has been evaluated in three different aqueous electrolytes, the basic medium, potassium hydroxide and acidic medium, sulphuric acid. The PAN / PANi composite electrode loadings were varied from 0.25 g, 0.5 g and 0.75 g (See Figure 5.18).

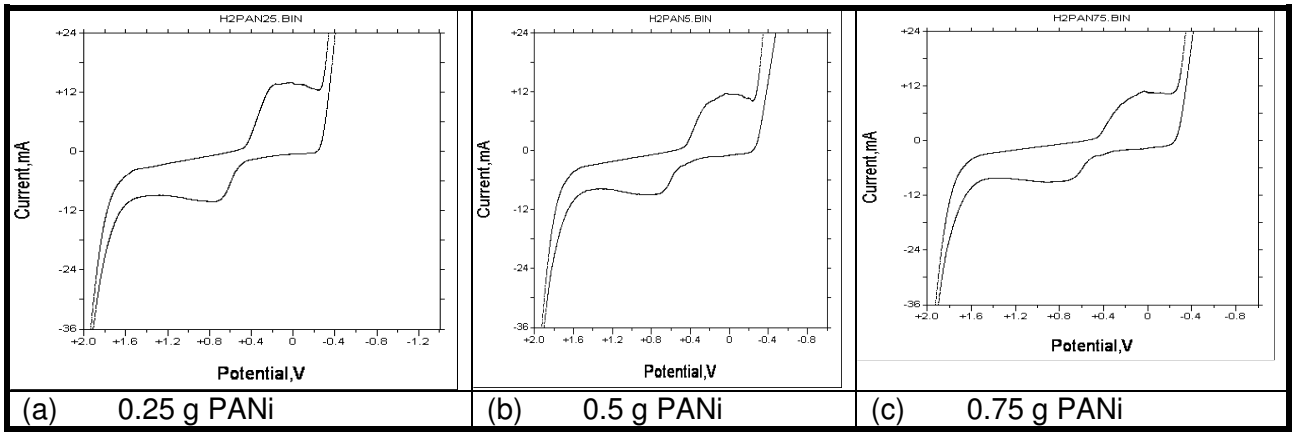

(a) 0.25 g PANi	(b) 0.5 g PANi	(c) 0.75 g PANi

Figure 5.18 Cyclic voltammograms of ES PAN / PANi in an acid medium.

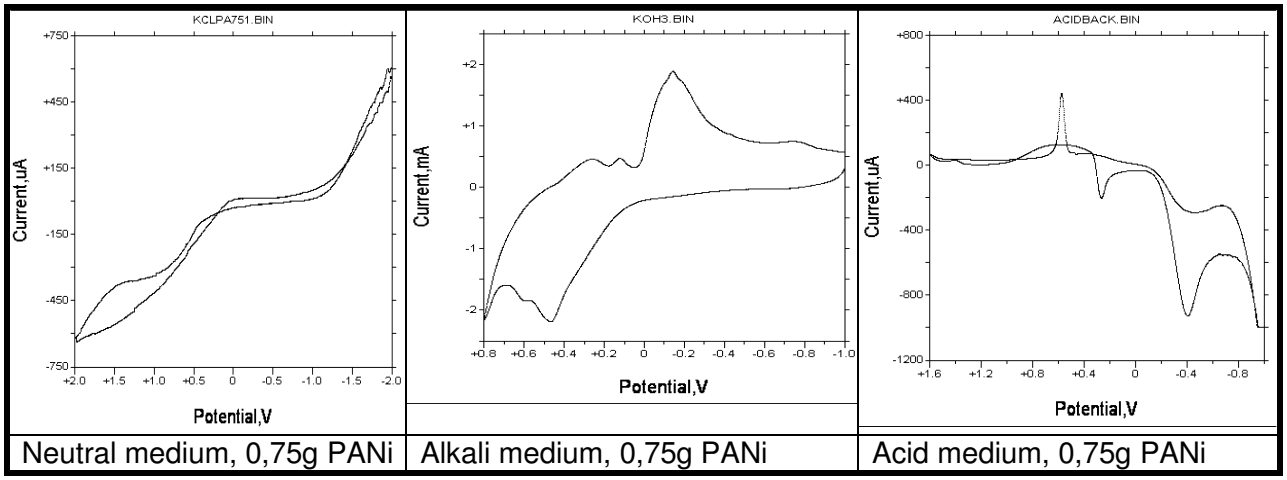

Neutral medium, 0,75g PANi	Alkali medium, 0,75g PANi	Acid medium, 0,75g PANi

Figure 5.19 Cyclic voltammograms of the ES mats in neutral, alkaline and acid solutions.

.

The reactivity of the redox couple was observed both in the acidic and in the basic media. In the acidic medium, one broad oxidation and reduction peaks were observed at the potential values of 0.75 V and 0.1 V respectively. Several oxidation and reduction peaks were observed in the basic medium. Throughout these experiments the trend has been that the higher the loading of the PANi composite, the better the performance.

5.3.5 Recommended further industrial development

Increase the loading of PANi in PAN for increased electrical conductivity in the 85k PAN but also the 120k PAN copolymer and the 210k PAN homopolymer. Assess applicability for use as battery electrodes in supercapacitators by evaluating the specific capacitance.

Place layers of PANi / PAN inside the batt of a fabric filter and use hydroentanglement to consolidate the fabric. Assess the ability of such a composite bag filter in changing the triboelectric properties, thus the dust cake structure and thereby the cleanability of a fabric filter.

5.3.6 References

Adams P.N & Monkman A.P, 1997. Characterization of high molecular weight polyaniline synthesized at –40 °C using a 0,25:1 mole ratio of persulfate oxidant to aniline. Synthetic Metals. 87, p.65-169.

Chang H., Tan Y., & Li Y., 2003. Conducting polyaniline nanofiber networks prepared by the doping induction of camphor sulfonic acid. *Journal of Applied Polymer Science.* 87, p.1537-540.

Dominis, A.J., Spinks, G.M., Kane-Maguire, L.A.P. & Wallace, G. 2002. A de-doping/re-doping study of organic soluble polyaniline. *Synthetic Metals.* 129, (2), p.165-172.

Gu S., 2005. Process optimization and empirical modeling for electrospun polyacrylonitrile (PAN) nanofiber precursor of carbon nanofibers. *European Polymer Journal*. 41, p.2559-568.

Hong K., 2005. Preparation of conducting Nylon-6 electrospun fiber webs by the *In Situ p*olymerization of polyaniline. *Journal of Applied Polymer Science.* 96, p.983-91.

Huang J., Virji S., Weiller B., & Kaner R., 2003. Polyaniline nanofibers: Facile synthesis and chemical sensors. *Jounal of the American Chemical Society,* 125, p.314-15.

Huang K, Zhang Y, Kotakic M, Ramakrishna S., 2003. A review on polymer nanofibers by electrospinning and their applications in nanocomposites. *Computational Science & Technology*, 63, p.2223-253.

Jianming J., Wei, P., Shenglin, Y.& Guang, L., 2005. Electrically conductive PANI-DBSA/Co-PAN composite fibers prepared by wet spinning. *Synthetic Metals.* 149, p.181-86.

Kim, C. & Yang K.S., 2003. Electrochemical properties of carbon nanofiber web as an electrode for supercapacitor prepared by electrospinning. *American Institute of Physics.* The Fiber Society Fall 2002 Technical Conference, Natick USA.

Kim, C., 2005. Electrochemical characterization of electrospun activated carbon nanofibres as an electrode in supercapacitors. *Journal of Power Sources* 142, p.382-88.

Kim, J. Won, S., 2004. Electrospun PVDF-based fibrous polymer electrolytes for lithium ion polymer batteries. *Electrochimica Acta*. 50, p.69-75.

Kulkarni M, & Athawale A., 2001. Poly(2,3-dimethylaniline) as a competent material for humidity sensor. *Jounal of Applied Polymer Science*. 81, p.1382-387.

Lu, W., Fadeev, A.G., Qi, B., Smela, E., Mattes, B., Ding, J., Spinks, G.M., Mazurkiewicz, J., Zhou, D., Wallace, G.G., MacFarlane, D.R., Forsyth, S.A. & Forsyth, M., 2002. Use of Ionic Liquids for π-Conjugated Polymer Electrochemical Devices. S*cience.* 297 (5583), p.983-987

MacDiarmid, A., 2001. Synthetic metals: A novel role for organic polymers. *Synthetic Metals.* 125 (1), p.11-22.

Mueller C 2002. Electrical characterization of polyaniline/polyethylene oxide nanofibers for field effect transistors. *NASA/TM-2002-212.* December 2002.

Pan W. & Yang S., 2005. Electrical and structural analysis of conductive polyaniline/polyacrylonitrile composites. *European Polymer Journal*. 41, p.2127-133.

Park, Y.H. & Park, C.R., 2001. Preparation of conducting polyacrylonitrile/polyaniline composite films by electrochemical synthesis and their electroactivity. *Synthetic Metals*. 118, (1-3), p187-192.

Wang X., Drew C., Lee S-H., Senecal K., Kumar J. & Samuelson L., 2002. Electrospun nanofibrous membranes for highly sensitive optical sensors. *Nano Letters*. 2 (11), p1273-275.

Zhou Y., Freitag, M., Hone, J., Staii, C., Johnson, A., Pinto, N & MacDiarmid, A.G., Fabrication and electrical characterization of polyaniline-based nanofibers with diameter below 30 nm. *Applied Physics Letters.* 83 (18), p.3800-802.

CHAPTER 6

CONCLUSIONS

6.1 INTRODUCTION TO THE CONCLUSIONS CHAPTER

The effect of the wet spinning and electrospinning process variables on the resultant molecular orientation and crystallinity of PAN fibres, is an “interesting” topic. Atactic polyacrylonitrile (PAN), is used to manufacture textile fibers and carbon fiber precursors which have been studied for more than 50 years. PAN remains a very intriguing polymer due to its unusual behavior, (two “Tg’s”, a thermoplastic which degrades before it melts, high overall crystallinity with highly disordered crystals and polymorphism). Dispute still prevails over the interpretation of the polymorphic condensed-phase structure and the thermal transitions PAN undergoes on heating. The effect of the electrospinning process variables and additives on the crystallinity and molecular orientation of electrospun polyacrylonitrile fibres is reported in this study and compared to commercial wet spun PAN, to try to explain the phase transitions of the PAN in fibrous form.

In this chapter the overall conclusions, as related to the aims are first presented, with the specific conclusions from each of the analytical areas of study. Thereafter, the conclusions are summarized and correlations are made between the findings from the different analytical techniques. These conclusions then provide the basis for a new theory, presented on the crystallinity and molecular orientation of electrospun PAN fibres, with and without additives.

The advantage of being able to electrospin small quantities of polymer into fibre form as a means to assess the effect of additives in the form of nanoparticles, conductive polymer blends, different grades of polyacrylonitrile, short chain oligomers and conductive mainly copper salts on the crystalline structure and thermal properties of the electrospun fibres is shown.

6.2 CONCLUSIONS AS RELATED TO AIMS

6.2.1 Study of the PAN electrospinning operation parameters

A study has been conducted and is presented to determine the effect of the electrospinning process variables such that the process of electrospinning PAN produces fibres with repeatable mat geometry and properties and to define the operating parameters of the electrospinning process for reproducible production of uniform, homogeneous PAN fibres and fabrics.

The specific conclusions in this regard from the research presented in Chapter 3 are;

- Novel image analysis methods to characterize elecrospun mat roughness and mat porosity have been developed.
- Under controlled conditions, there is a linear relationship between the electrospun applied voltage and the fibre diameter.
- There is not a linear relationship between the electrospun spinning distance (field strength) and the fibre diameter. There is generally an increase in the fibre diameter at the medium spinning distance in these series of PAN evaluated for this thesis.
- It appears that a viscosity of less than 1 Pa.s is required for electrospinning of PAN under the given electrospinning conditions of 20 cm and 20 kV in DMF at 30 °C under gravity feed.
- The relationship between the Berry Number, Be, and the electrospun fibre diameter for the PAN grades used is comparable with PLA only up to Be<5 but unique at higher Be for not only each type of polymer (PAN versus PLA) but also for the different PAN grades.
- A change in the solution concentration has a greater effect on the rate of change in electrospun fiber diameter for higher molecular weight PAN.
- The higher the take-up speed, the lower the fibre diameter. There is a linear relationship within the domain of the face velocities used in these experiments.
- The higher the concentration, the higher the fibre diameter for the same take-up speed. The fibres produced from 4% (w/w) solution had a greater reduction in diameter with increasing collector speed in comparison to fibres produced from 6% (w/w) solution.
- The mat morphology is dependant on the shape and conductivity of the grounded electrode.
- The nanofibres could be carbonized and showed a narrower fibre diameter than the diameter of the non-carbonized PAN fibres electrospun under the same conditions.

The ideal set of parameters for the further study of additives for electrospun PAN fibres of about 100nm and “bead-free” with the copolymer grade PAN was thus determined as, a voltage of 20kV at a spinning distance of 20cm from an 8% by weight solution of 120k PAN in DMAC, at 30 ºC and the homopolymer at 6% by weight in DMAc.

6.2.2 Study of the effect of variables on PAN crystallinity and molecular orientation

A study has been conducted which contributes to the understanding of the effect of various electrospinning variables on the degree of crystallinity and molecular orientation and resultant thermal properties of PAN fibres. Research has been conducted, using the advantage of being able

to electrospin small quantities of polymer into fibre form, to assess the effect of additives in the form of nanoparticles, polymer blends, different grades of PAN, short chain oligomers and conductive copper salts on the crystallinity and orientation and thermal properties of the electrospun fibres.

The nitrile-nitrile interactions are known to limit the ultimate draw ratio of PAN fibers and control the spinning dope viscosity. This thesis shows how, through the addition of a small quantity of salt to disrupt the nitrile interactions and also increase the conductivity of the PAN dope, that the effective draw ratio of the electrospun PAN fibres is increased such that fibres with 2D crystal structure and equivalent crystal morphology to wet spun fibres can be produced. The salts can act as a "plasticizer" and allow the formation of a 2D hexagonal crystal structure with closer packing than that in the 3D crystal structure identified in the electrospun fibres without additives or some additives can have the reverse effect of locking in additional "frozen-in" stress.

6.2.2.1 Specific conclusions from the FTIR results

- Cu complexation on the CN group in the FTIR spectra at 2242 cm^{-1} is seen for fibres electrospun from solutions where Cu:CN ≥ 1:2.
- Addition of LiCl salts at a concentration of Li:CN of ≤ 1:50 provides higher molecular orientation than electrospun PAN control fibres based on the FTIR derived "Orientation Factor", OF, results. However, the molecular orientation of electrospun PAN fibres even with LiCl addition is still much lower than the molecular orientation in commercial PAN fibres, produced via a wet spinning process.
- Cu complexation on the carboxylic acid group in the FTIR spectra at 1630 cm^{-1}; for electrospun samples the 1630 cm^{-1} peak shifts from 1632 cm^{-1} for Cu:CN ≤ 1:50 to 1600 cm^{-1} for Cu:CN ≥ 1:20. This has been shown to be due to residual solvent, which complexes the Cu-salt, and is "frozen-in" the electrospun fibre morphology.
- For annealed films; the shift from ±1630 to ±1600 cm^{-1} occurs at Cu:CN ≤ 1:20. Therefore the complexation is assumed to be time dependant during gelation. For complexation in the rapid electrospinning process, higher Cu concentration is required relative to a film.
- Addition of $CuCl_2$ salt to the spinning dope of the 120k PAN copolymer leads to a 74% reduction in the crystallinity relative to the control, whereas in the 210k homopolymer the salts yield an increase in the crystallinity by 29% as determined by the inverse relationship between the ratio of the heights of the peaks in FTIR at 1730 and 2240 cm^{-1} and the thus calculated degree of crystallinity.

6.2.2.2 Specific conclusions from the thermal analyses results

- The addition of copper chloride salt to electrospun PAN lowers the cyclisation exotherm and the onset temperature for cyclisation and will therefore be a beneficial addition in the carbon fibre production process. This is more pronounced in the homopolymer than the copolymer. In addition $CuCl_2$ disrupts the low temperature crystal-crystal transitions of the polymeric fibres. The disappearance of these crystal-crystal transition peaks is due to a tighter packing in the homopolymer PAN nanofibres with $CuCl_2$ which disallows the conversion between hexagonal and orthorhombic (and other) polymorphic crystal structures during heating.
- The effect of the salts on the glass transition temperature of the fibres is shown in Figure 4.24. It is shown in Figure 4.25 that the cyclisation enthalpy decreases as the conductivity of the spinning dope increases. However a 100% increase in the conductivity results in a 2% decrease in the peak enthalpy, indicating that the change in enthalpy is not dependant on the spinning conductivity but due to copper complexed inside the PAN fibres.
- All the Cu and Li salts added to PAN fibres in this research, increase the Tg of the resultant electrospun fibres.
- The effect of salts on the degree of "mass loss" during heating of the electrospun PAN has been evaluated. It is reported that the addition of Cu and Li salts to the copolymer PAN electrospun fibres and films, increases the weight % remaining on heating at 200 and 400 ºC.

6.2.2.3 Specific conclusions from the microscopy results

- Copper nitrate salt in carbonized copolymer PAN fibres is calcined / converted to CuO nanoparticles with a diameter of 20 to 50 nm during the PAN stabilization process (<200ºC) .
- LVD can be used to apply an even, thin CuO coating (less than 10 nm thick) onto the surface of electrospun PAN fibres.
- The addition of copper (II) chloride salts to PAN electrospinning dope in increasing concentration produces nanofibres fibres with decreasing diameter.
- Copper chloride salts give narrower diameter fibres than LiCl containing PAN electrospun fibres when the cation is at the same concentration relative to the nitrile group.
- It is difficult to obtain a homogeneous dispersion of CuO nanoparticles (40 to 70 nm) in PAN fibres even after the use of combinations of long-term ultra-sonication and surfactants.

- Copper (I) salts in electrospun PAN give ribbon-like fibres with a relatively higher diameter compared with copper (II) salts spun under identical conditions at the same Cu concentration.
- A core-shell type structure is seen for both the electrospun PAN copolymer and the homopolymer, where the internal region appears to have a lower density, believed to be due to a solvent enriched core in the electrospun PAN fibres.
- HRTEM showed that the concentration of copper relative to the carbon was slightly consistently increased in the interior of the electrospun PAN fibres. The chlorine from the $CuCl_2$ salt is distributed homogeneously across the cross-sectioned samples.

6.2.3.4 Specific conclusions from the NMR and ESR analyses results

- Solid state NMR cannot be applied to determine the molecular orientation in PAN fibres due to the tighter molecular packing than in other fibres such as polypropylene or PES.
- All of the ESR spectra on electrospun homopolymer and copolymer PAN containing copper salts have the basic structure of copper, typical of Cu^{2+} systems.
- All PAN samples exhibit a broad unstructured background signal that is probably due to a small transition metal contamination introduced during electrospinning, perhaps from the copper wire electrode used in the process. Alternatively it may be due to the remnants of the iron redox catalyst used in the PAN polymerization process.
- The role of the anion (as a "spectator ion" in affecting the bonding of the copper salt in electrospun PAN with copper salts is highlighted in the ESR results

6.2.3.5 Specific conclusions from the XRD results

- The addition of salts to electrospun PAN fibres causes the primary equatorial peak(s) at $2\theta \approx 17°$ to split into 2 reflections at about $2\theta = 16{,}7°$ and $= 17.1°$. The separation of the double peaks has been seen as a correlation with increasing draw ratio in wet spun PAN. The salts are thus acting as a plasticizer and effectively causing an increase in the draw ratio of the electrospinning process.
- The higher the salts concentration and thus the reduction in nitrile dipole interactions in the gel solution, the higher the extended chain conformation of the PAN molecules in the fibril during the electrospinning process giving, an effect comparable to an increase in draw ratio in wet spinning. The extent of this improvement with copper salts is dependant on the type of "spectator" anion.
- The addition of salts to PAN fibres causes the 2θ value to decrease, indicating an increase in the d-spacing due to an increase in the inter-molecular distance between the

chains assumed due to the packing of Cu ions and the anions in a columnar structure between the chains.

6.2.3 Comparison between electrospun and commercial PAN fibres

The internal morphology, crystallinity and orientation of solution electrospun PAN is compared with other commercial wet spun PAN fibres of the exact same polymer grades. It is found that the internal crystal structure and molecular orientation of electrospun PAN samples differ from that of wet spun PAN fibres for both the 120k PAN copolymer and the 85k and 210k PAN homopolymer.

The tightly packed 2D crystal structure of wet spun PAN fibres can be achieved via electrospinning, which normally produces 3-D crystallites, only by the addition of certain additives such as $Cu(NO_3)_2$ and at very high field strengths.

6.2.3.1 Specific conclusions from the FTIR results

- The degree of molecular orientation of homopolymer 85k PAN as determined by FTIR on electrospun PAN may be comparable to the orientation factor, OF, of wet spun PAN if the electrospinning field strength is $\geq 0{,}75$ kV.cm^{-1}.
- The crystallinity of the homopolymer electrospun PAN is significantly higher than the crystallinity of the electrospun 120k PAN copolymer.
- For all grades of PAN the peak at 1070 cm^{-1} broadens in the FTIR spectra of the electrospun fibres. In the electrospun 500k PAN, a peak appears at 1634 cm^{-1} and in the electrospun 210k PAN, a peak appears at 1666 cm^{-1}. In the electrospun 120k PAN, a peak appears at 1631 cm^{-1} whereas in the wet spun fibre a peak appears at 1585 cm^{-1}. This peak broadening on the eletrospun fibres indicates a less dense molecular packing with more room for stretching vibrations on the nitrile groups.
- There is residual solvent in the electrospun samples even after the samples are dried in a vacuum oven at 50°C for 12 hours and this impacts on the molecular orientation.

6.2.3.2 Specific conclusions from the thermal analyses results

- Wet spun PAN shows a slightly higher exotherm temperature, a higher enthalpy, and a broader temperature range at half peak height than the electrospun samples. These results indicate a higher degree of order and closer packing in the wet spun PAN fibres relative to the electrospun PAN fibres.
- The electrospun fibre has higher frozen-in stress than the wet spun fibres which go through an annealing stage during the commercial fibre production process.

- Wet spun PAN has a prominent thermal transition at 97,1 °C with a single large exotherm. The electrospun PAN has 2 distinct transitions, at 93,4 and 106,7 °C. This indicates the presence of different phases within the looser packed and less ordered "amorphous" regions allowing for molecular vibrations below the real Tg at 136 °C. Many researchers call the transition at around 90 to 100 °C a second actual Tg, named Tg_{11}. It has been argued that electrospinning has a plasticizing effect on the glass transition.

6.2.3.3 Specific conclusions from the NMR results

- Solid state cp-MAS NMR cannot be applied to either electrospun or wet-spun PAN fibres to assess the molecular orientation. The structure is too dense to allow magnetic resonance in even the less ordered "amorphous domains".

6.2.3.4 Specific conclusions from the XRD results

- There is a significant difference between the XRD diffractograms for the commercial wet spun fibres and the electrospun fibres when using exactly the same grade of PAN. The electrospun fibres have a far lower crystallinity and show the presence of 3D crystallinity. The commercial wet spun fibres only have 2D crystallinity but the electrospun have 3D crystallinity.
- There is a sharp contrast in the shape of the XRD traces for copolymer and homopolymer PAN and the conditions under which transitions occur. The electrospun homopolymer PAN fibres have higher orientation and larger crystallite sizes than the electrospun copolymer fibres. For the homopolymer, the values for the coherence lengths vary from 14.96 nm to 6.26 nm for the wet spun and electrospun fibres respectively. For the copolymer, the values for the coherence length vary from 12.63 nm to 5.55 nm for the wet spun and electrospun fibres respectively.
- The wet spun PAN fibres show characteristic 2D hexagonal packing as determined using the ratio of the equatorial peaks at $2\theta = 17°$, which has a *d*-spacing of approximately 5.25 Å, and the much weaker reflection at $2\theta = 29{,}5°$, which has a *d*-spacing of about 3.05 Å. The *d*-spacing is related to the inter-molecular distance of the PAN chains, and is affected by factors such as draw ratio, solvent residues, as well as temperature. The ratio of the *d*-spacing of the two peaks remains about $\sqrt{3} : 1$ within an experimental accuracy, indicating pseudo-hexagonal packing. The diameter of the chain is: $(2 \times \sqrt{3})d_{(110)} = 6{,}1$ Å.
- None of the electrospun samples show a prominent secondary equatorial peak at $2\Theta = 29.5°$, (002 lattice plane), which is clearly visible for both homopolymer and copolymer wet spun fibres.

- The XRD data provides support for some of the less expected results obtained in the FTIR, DSC and microscopy analyses.

6.2.4 Assessment of the potential use of electrospun membranes in industrial applications.

The potential application of electrospinning in some commercial niche areas is shown;

- PAN nanofibres on PAN fabric filters to retard the fabric filter blinding process.
- Blended polyaniline / polyacrylonitrile as potential electrode materials.
- Blended oligomers with polyacrylonitrile as adsorbents for water treatment.

6.3 GAPS IN EARLIER STUDIES AND KEY DIFFERENTIATORS OF THIS RESEARCH

Whilst in October 2009, as shown in Figure 2.2, according to the *Science Direct* Website, there were in excess of 2000 publications on the topic of electrospinning, more than 500 of these concern the electrospinning of PAN and of these about 100 which also contain the keyword orientation, the following gaps are noted in the reported research in Chapter 2;

- Most electrospinning publications are short two page documents looking at one type of polymer grade and the resultant fibres are analysed by only one analytical technique.
- The PAN grade is often not described in terms of co-monomer content and molecular weight.
- The analysis of the electrospun PAN fibres is conducted after heat treatment through the the stabilization and carbonization processes on carbon fibres.
- The publications on electrospun PAN fibres, generally do not contain additives. Two articles include studies to the inclusion of silver nitrate salt in electrospun PAN (Wang *et al*, 2005 and Chen *et al*, 2008), to investigate it's effect on the carbonization process and the formation of silver nanoparticles and one reference includes a study of the effect of lithium chloride addition at 2 concentrations in electrospun PAN (Qin, 2004) on only the fibre diameter. There are numerous reported studies on the inclusion of carbon nanotubes and other nanoparticles on electrospun carbon nanofibres, where specifically the effect of the electrical conductivity of the electrospun mat is studied.
- The keyword "orientation" in these publications refers to the macro-scale alignment of the fibres using different take-up devices in the electrospinning process .and not to the internal molecular orientation of the polymeric fibres.

The methodology used in this study of the effect of additives on electrospun versus wet spun fibre morphology differs from other studies in terms of the following criteria;

- This study assesses a broad range of variables changed systematically. Most publications give a "snap-shot" of the molecular structure of the electrospun fibres after changing one variable, as monitored by a single analytical method.
- Here the results from multiple analytical methodologies are compared simultaneously with wet and electrospun samples of both the homopolymer and the copolymer PAN grades.
- The molecular orientation within the electrospun and wet spun fibres are compared.
- Analysis of molecular interaction in solid state materials relies on the investigation of extremely small changes in the generated analytical data. In this investigation, in the case of the FTIR, DSC and XRD, small yet reproducibly persistent transitions are shown in expanded data, not normally reviewed in other publications i.e. the results analysed at far greater resolution, revealing new indicator peaks in the FTIR, DSC and XRD scans.
- Copper additives in electrospun PAN is studied for the first time. The copper salts are added over a wide range of concentration. The effect of the anion on the polymer crystallinity and molecular orientation is also investigated for the first time.
- FTIR and HRTEM are used to show that there is residual highly polar solvent remaining in all electrospun PAN samples and the HRTEM shows distinct different phases, with a less dense, solvent enriched phase in the centre of all the electrospun fibres and some lower density domains down the length of the electrospun homopolymer PAN fibres.
- The three dimensional orthorhombic crystal packing and planar zig-zag configuration of molecular chains in electrospun PAN fibres can be converted to a two-dimensional packing and a helical configuration, similar to that found in wet spun commercial fibres, through the addition of certain copper salts of which copper nitrate is shown in this study to have the most significant positive contribution to tighter and more ordered molecular packing.

6.4 PROPOSED THEORY ON MOLECULAR PACKING IN ELECTROSPUN PAN FIBRES

It is shown in the thermal analysis results that electrospun samples copolymer PAN samples have a double thermal endothermic transition whereas the wet spun samples with post treatment drawing have a single transition.

It is shown that electrospun samples of homopolymer PAN have a multiple thermal transitions between 90 and 150° whereas the wet spun sample has a single thermal transition.

The insertion of a salt can complex a fraction of the -C≡N groups radiated from the tight hexagonal packing, thereby interfering with the intramolecular interactions, and changing the helix diameter, which is related to the draw ratio. The SEM observations attest to the reduction in electrospun fiber diameter with addition of Cu-salts.

Electrospinning appears to effectively have a plasticizing effect on the glass transition temperature probably since the measurements are affected by the presence of residual solvent (DMSO, DMF or DMAc). The removal of these solvents, especially those having high dipole moments, is difficult / impossible in the case of polyacrylonitrile nanofibres and more difficult due to the complexation of Cu-salts on the solvents as shown in the FTIR results.

The influence of the salts in increasing the crystallinity and orientation is proven by the FTIR, DSC, microscopy and XRD results. It is surmised that the addition of salts impacts the electrospun fibres orientation via a few mechanisms, these being;

1. An increase in the solution conductivity, which is known to increase the effective field strength during electrospinning and thus, the repulsion of the jet instabilities, and thus, the effective draw ratio of the resultant electrospun fibres.
2. Complexation of the salts on the nitrile groups of the polymer and the solvent in the spinning dope which allows for an extended chain conformation in the dope and gel state between the pipette and the grounded electrode, thus allowing closer molecular packing with increased crystallinity and molecular orientation in the resultant dried fibres.
3. Complexation on the nitrile groups of the PAN which affects the packing density and crystal structure in the resultant nanofibres. One can decrease the dimensions of the unit cell, dependant on the spectator anion of the copper salt.
4. The formation of an additional ordered phase in the electrospun fibres due to complexation on the solvent which is “frozen-in” to the solidified nanofibres. This may act as a “plasticizer” during subsequent post drawing at elevated temperature on the electrospun nanofibres yielding ultra high strength nanofibres.

The presence of a third distinct phase is proposed within the structure of the electrospun samples with salts. Thus it is proposed that the quasi-crystalline fibre consists of ordered and less ordered domains and a third intermediary phase. The more ordered phase, when salts are present has a tighter packing than when the salts are not included in the spinning dope.

A possible explanation for the broader peaks in the XRD data of the electrospun samples, which result from lower molecular orientation, is that due to the rapid gelation during spinning that the molecules are frozen in to a by the addition of the copper salts, the strong dipole-nitrile interactions have been disrupted, enabling even the electrospun samples without post-drawing to achieve a similar highly orientated close hexagonal packing structure, as found in the commercial wet spun post-drawn fibres.

6.5 REFERENCES

Chen, R., Zhao, S & Han, G & Dong, J. (2008). Fabrication of the silver/polypyrrole/polyacrylonitrile composite nanofibrous mats. *Materials Letters*, 62. p.4031–4034.

Qin, X., 2004. The effect of LiCl on electrospinning of PAN polymer solution: theoretical analysis and experimental verification. *Polymer*; 45, p.6409-413.

Wang, Y., Aponte, M., Leon, N., Ramos, I., Furlan, R., Evoy, S. & Santiago-Avil´e, J., 2005. Preparation of silver nanoparticles dispersed in polyacrylonitrile nanofiber film spun by electrospinning. *Materials Letters*. 59, p.3046-049.

CHAPTER 7

RECOMMENDED FUTURE RESEARCH

7.1 INTRODUCTION

In Chapter 7, some additional fundamental research, beyond the scope off this thesis, is recommended. Some industrial research projects related to this thesis are mentioned in Appendix A.

Further investigations to elucidate the orientation and crystallinity of electrospun PAN fibres with additives are recommended. With PAN being the major industrial precursor for high tenacity carbon fibres, the ability to make aligned nanofibres with high molecular orientation and crystallinity and thus strength has potential vast industrial implications in terms of the production of reinforcement for strong, lightweight composite materials and also in the form of activated carbon as nanofilters for water treatment through the adsorption of toxic contaminants.

The specific recommended future research to further study and optimize the orientation and thus fibre strength, beyond that achieved in the research, is described in further detail below.

7.2 RECOMMENDED FURTHER FUNDAMENTAL RESEARCH

7.2.1 Electrospinning in an inert atmosphere at different ambient temperatures

Assess the structure and degradation of PAN with additives electrospun into an inert atmosphere at temperatures above and below the glass transition temperature.

7.2.2 Study the effect of forced alignment on fibre structure

Compare fibre chemical structure, orientation and crystallinity when electrospun by forced feed and onto a high speed take-up device and then also the structure of carbon fibres formed from the electrospun PAN

7.2.3 Study the effect of molecular weight distribution on fibre formation and structure

Electrospin polymers made by controlled living polymerization with well characterized molecular weight and molecular weight distribution. Study the effect of fewer short and long chain “impurities on the size of the amorphous domain and the resultant effect on fibre properties.

An investigation of the effect of remnant metal catalysts and other impurities on the fibre structure could also be of interest.

7.2.4 Density molecular orientation correlation

Conduct density measurements of electrospun PAN to try understand the XRD peaks.

Are the peaks at $2\theta \approx 22^{o}$ due to the amorphous halo or a different crystal structure to the one formed using conventional commercial wet spinning.

7.2.5 Effect of different salts and their concentration in PAN

The only salt evaluated in this study in the homopolymer was $CuCl_2$ and it would be of interest to expand this study to include the addition of other salts such as $CuSO_4$, $Cu(NO_3)_2$ LiCl and even other chlorides such as chromium, manganese, iron, cobalt and nickle into the homopolymer. As discussed below, the $CuSO_4$ salt had a greater influence on the resultant molecular orientation in the electrospun fibres than the $CuCl_2$ salt.

A study of the optimum salt concentration to achieve the highest molecular orientation in electrospun PAN homopolymer and copolymer fibres is recommended for future research. The only salt evaluated in this study in the homopolymer was $CuCl_2$ and it would be of interest to expand this study to include the addition of other salts such as $CuSO_4$, $Cu(NO_3)_2$ LiCl and even other cations such as chromium, manganese, iron, cobalt and nickel into the homopolymer.

7.2.6 XRD at different angles

The molecular orientation can be calculated from the distribution of intensity as a function of the azimuthal angle i.e. at a fixed distance from the center of the pattern. Second, azimuthal scans of the intensity of the (010) reflection can be used to measure the degree of molecular orientation in a PAN fiber. To observe the (002) reflection around $2\theta = 37°$ more clearly, XRD diffractograms should be recorded by tilting the samples relative to the incident beam.

Determination of the Hermann's orientation factor for the (110) plane of electrospun PAN additives should be determined. It was previously calculated to be 0.34 ± 0.03. Compared to the Herman's orientation factor of 0.6 for highly oriented melt-spun co-polymer fibers (85% acrylonitrile), and 0.66 for wet-spun copolymer fibers (90% acrylonitrile), the electrospun PAN shows somewhat lower orientation.

This is recommended as future research specifically with scanning the $2\theta = 17°$ region. Nearly perfect chain orientation has been measured at $f_c = 0.994\text{-}0.998$, which indicate nearly perfect chain orientation for highly drawn PAN samples. This must be conducted on highly orientated electrospun samples.

7.2.7 Collection of XRD Data with improved resolution

The re-collection of XRD data of all samples with improved resolution forms is recommended. The specific suggested alterations to the analytical methodology include measurements at a higher integration time but also measurements on aligned bundles of nanofibres over a broader range of 2θ (5° to 55°), including azimuthal scans at 2θ = 17° and with the step interval at 0,02° instead of the 0,05° step interval used here.

Polymorphism in PAN has been identified by other workers and it has been found that the orthorhombic form can be converted to the hexagonal form when the solvent is removed by drying, by extraction, or by drawing.

The optimum concentration of Cu:CN for $CuCl_2$ to increase orientation in electrospun PAN samples was not determined precisely from this study but lies around a ratio of 1:20. A study of the optimum salt concentration to achieve the highest molecular orientation in electrospun PAN fibres is recommended for future research.

7.2.8 Post treatment for increased orientation and mechanical strength correlation

Fibers with higher orientation can be obtained by the use of an in-line isothermal bath technique. Higher levels of orientation are also achieved as a result of post-drawing processes. In most cases, the drawn fibers are subsequently subjected to annealing by heating and cooling. The results for electrospun PAN fibres with copper based additives should be compared to the mechanical properties.

APPENDIX A

OTHER SCIENTIFIC ACTIVITIES BY THE AUTHOR DURING THIS PERIOD

This first list includes projects which are related to this thesis.

- Increasing the thermal and chemical resistance and resistance to shrinkage of PAN fibres used as fabric filters in hot gas filtration in collaboration with a PAN fibre producer in Europe.
- Investigating use of nanofibres to improve the "cleanability" of fabric filters.
- Compiled a research proposal for "Nanotechnologies for Water Treatment" which was accepted for funding by the National Research Foundation under the Nanotechnology Flagship Programme. Five of the 14 academic projects are related to electrospinning of PAN and natural polymers with various additives as related to this thesis, or functionalisation of PAN.
- Evaluation of nanofilter materials for application in water treatment in cholera outbreaks.
- Evaluation of nanofilter materials for the reduction of biofouling on power stations.
- Conducted research on the development of controlled release anti-tubercolosis drugs and assisted with the production of biodegradable nanofibres for artificial heart-leaflets.
- Evaluated commercial applications of electrospinning for the RSA Power Utility Eskom.
- Investigated the application of electrospun fibres as a support for DeSOx and DeNOx catalysts.

Non-related scientific activities

- Established a private research company doing research and product development, from fundamental academic research to industrialisation / commercialization in collaboration with industrial partners and private investors in South Africa and Internationally.
- Developed and patented a low cost high voltage insulator with a self-cleaning superhydrophobic surface based on nanotechnology.
- Co-authored 3 publications on the pollution performance of silicone rubber high voltage insulators and 2 technical publications on laboratory ageing of silicone rubber formulations.
- Wrote a testing procedure for the fingerprinting and accelerated ageing of high voltage non-ceramic insulating materials for Eskom and contributed to the writing of IEC standard test procedures through CIGRE.
- Assessment of the application of Zeolites as DeSOx /DeNOX catalysts and a CO_2 adsorbent.

Assisting the Department of Science and Technology with Nanotechnology Awareness in RSA.

APPENDIX B

Coherence length calculation on copolymer and homopolymer ES with $CuCl_2$

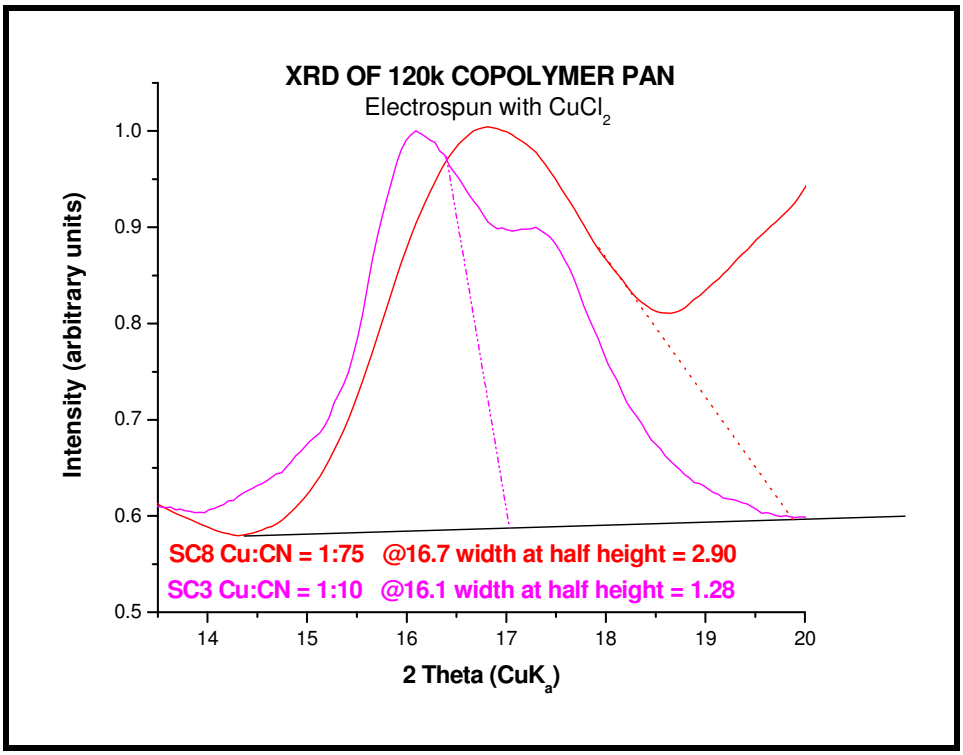

Figure 4.66* **XRD of electrospun copolymer PAN with $CuCl_2$ (13 to 20°).**

Table 4.18 **Crystallite Size of PAN Fibres**

	Spin type	2 Θ position °	Width at ½ height 2Θ in °	Width at ½ height Θ in °	Width at ½ height Θ in Radians	Cos Θ	Crystal size, L_c nm
Homo-PAN	Wet	16.86	1.10	0.55	0.00968	0.95701	14.96
	Electro	16.86	2.62	1.31	0.02287	0.95701	6.26
Co-PAN	Wet	16.99	1.30	0.65	0.01135	0.95635	12.63
	Electro	17.03	2.96	1.48	0.02584	0.95615	5.55
SC8 1:75	Electro	16.67	3.01	1.51	0.02636	0.95797	5.43
SC3 1:10	Electro	16.09	1.28	0.64	0.01117	0.96083	12.77
TE2 1:20	Electro	16.55	1.00	0.50	0.00873	0.95857	16.38

Note: for SC3 as per Figure 4.66* and TE2 as per Figure 4.64*, the L_c is calculated based on the (200) peak, whereas all other calculations based on the overlapping (200) and (110) peaks.

The Scherrer constant, K used is 0,90 and the wavelength, λ, of the X-rays is 0,154 nm.

Half height @ intensity = 0.55 therefore measure width at intensity 0.775

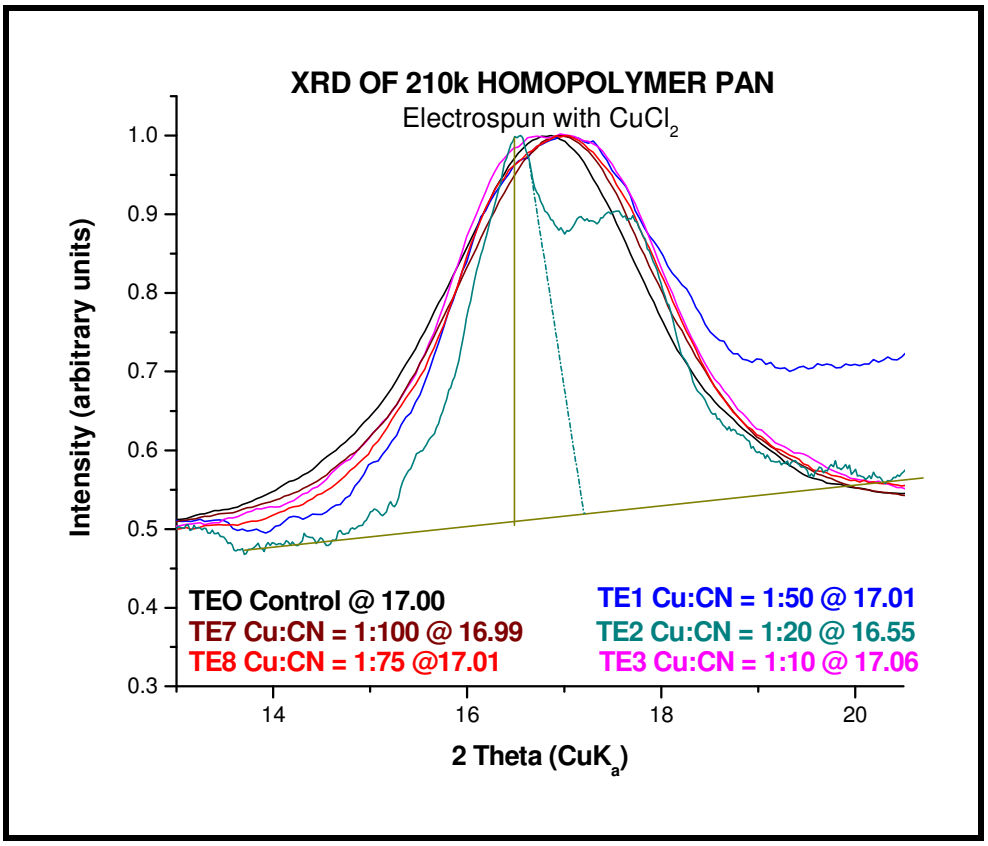

Figure 4.64* XRD of electrospun homopolymer PAN with $CuCl_2$ (13 to 20.5°).

At 2 theta = 6.55, half height @ intensity = 0.0.49, therefore measure width @ intensity = 0.745.